Detection of water and nutritional stress through clorophyll fluorescence and radiative transfer models from hyperspectral and thermal imagery

Doctoral Thesis.- Carlos Luis Camino González

TITULO: *Detection of water and nutritional stress through chlorophyll fluorescence and radiative transfer models from hyperspectral and thermal imagery*

AUTOR: *Carlos Luis Camino González*

Campus de Rabanales
Ctra. Nacional IV, Km. 396 A
14071 Córdoba

https://www.uco.es/ucopress/index.php/es/
ucopress@uco.es

UNIVERSIDAD DE CÓRDOBA

PROGRAMA DE DOCTORADO

INGENIERÍA AGRARIA, ALIMENTARIA, FORESTAL Y DEL DESARROLLO RURAL SOSTENIBLE

TESIS DOCTORAL

Detección de estrés hídrico y nutricional mediante fluorescencia clorofílica y modelos de transferencia radiativa a partir de imágenes hiperespectrales y térmicas

PhD THESIS

Detection of water and nutritional stress through chlorophyll fluorescence and radiative transfer models from hyperspectral and thermal imagery

PhD Candidate:

Carlos Luis Camino González

PhD Supervisors:

Dr. Pablo J. Zarco Tejada
(IAS, CSIC and MSE-FVAS, UoM)
Dra. Mª Victoria González Dugo
(IAS, CSIC)

UNIVERSIDAD DE CÓRDOBA

PROGRAMA DE DOCTORADO

INGENIERÍA AGRARIA, ALIMENTARIA, FORESTAL Y DEL DESARROLLO RURAL SOSTENIBLE

TESIS DOCTORAL

Detección de estrés hídrico y nutricional mediante fluorescencia clorofílica y modelos de transferencia radiativa a partir de imágenes hiperespectrales y térmicas

Presentado por **CARLOS LUIS CAMINO GONZÁLEZ** en satisfacción de los requisitos necesarios para la obtención del grado de **DOCTOR EN BIOLOGÍA**

Los directores,

Dr. Pablo J. Zarco Tejada

Investigador Científico
Instituto de Agricultura Sostenible (CSIC).
Profesor, School of Agriculture and Food, Faculty of Veterinary and Agricultural Sciences (FVAS), and Department of Infrastructure Engineering, School of Engineering (MSE), Universidad de Melbourne

Dra. María Victoria González Dugo

Investigadora Dpto. Agronomía
Instituto de Agricultura Sostenible (IAS)
Consejo Superior de Investigaciones Científicas (CSIC)

Córdoba, a 6 de Mayo de 2019

TÍTULO DE LA TESIS: Detección de estrés hídrico y nutricional mediante fluorescencia clorofílica y modelos de transferencia radiativa a partir de imágenes hiperespectrales y térmicas

DOCTORANDO/A: Carlos Luis Camino González

INFORME RAZONADO DEL/DE LOS DIRECTOR/ES DE LA TESIS

Dr. PABLO J. ZARCO TEJADA, Investigador Científico del Departamento de Agronomía, Instituto de Agricultura Sostenible, CSIC y la **Dra.** Mª **VICTORIA GONZÁLEZ DUGO**, Investigadora del Departamento de Agronomía, Instituto de Agricultura Sostenible, CSIC, directores de la presente tesis doctoral

INFORMAN:

Que la investigación sobre "Detección de estrés hídrico y nutricional mediante fluorescencia clorofílica y modelos de transferencia radiativa a partir de imágenes hiperespectrales y térmicas" que ha llevado a cabo **D. Carlos Luis Camino González**, bajo la dirección de los **Doctores Pablo J. Zarco Tejada y Mª Victoria González Dugo** y la tutoría del que subscribe, ha sido desarrollada con éxito y alcanzado los objetivos inicialmente propuestos.

Publicaciones científicas

1. **Camino C.,** Zarco-Tejada P. J. & González Dugo V. Effects of Heterogeneity within Tree Crowns on Airborne-Quantified SIF and the CWSI as Indicators of Water Stress in the Context of Precision Agriculture. Remote Sensing. 2018, 10(4), 604; https://doi.org/10.3390/rs10040604 .

   Datos de 2017 (JCR): índice de impacto 3.406, índice de impacto de los últimos 5 años 3.952 y 2º cuartil en el área temática de Remote Sensing.

2. **Camino C.,** González-Dugo V., Hernández P., Sillero J.C. & Zarco-Tejada P. J. Improved nitrogen retrievals with airborne-derived fluorescence and plant traits quantified from VNIR-SWIR hyperspectral imagery in the context of precision

agriculture. International Journal of Applied Earth Observation and Geoinformation. Volume 70, August 2018, Pages 105-117. https://doi.org/10.1016/j.jag.2018.04.013.

Datos de 2017 (JCR): índice de impacto 4.03, índice de impacto de los últimos 5 años 4.433 y 1º cuartil en el área temática de Remote Sensing.

3. **Camino C.,** González Dugo V., Hernández P. & Zarco-Tejada P. J. Radiative transfer Vcmax estimation from hyperspectral imagery and SIF retrievals to assess photosynthetic performance in rainfed and irrigated plant phenotyping trials. Accepted in Remote Sensing of Environment. 6 May 2019.

Datos de 2017 (JCR): índice de impacto 6.457, índice de impacto de los últimos 5 años 7.737 y 1º cuartil en el área temática de Remote Sensing.

Otras aportaciones destacables que han surgido de la presente tesis doctoral son tres contribuciones a congresos de ámbito internacional, dos publicaciones científicas adicionales en colaboración con otros grupos de investigación y una publicación en revistas de ámbito nacional.

Contribuciones a Congresos Internacionales

1. **C. Camino**, V. González-Dugo R. Mérida-García, P. Hernández and P. J. Zarco-Tejada. Retrieval of wheat nitrogen content using airborne hyperspectral VNIR-SWIR imagery through radiative transfer models and chlorophyll fluorescence quantification. 10th EARSeL SIG Imaging Spectroscopy Workshop, 19-21 April 2017, Zurich. Switzerland.

2. **C. Camino**, V. González-Dugo, M. López-López, P. J. Zarco-Tejada. Crown segmentation effects on the relation between field-measured assimilation and chlorophyll fluorescence quantified from high-spatial resolution hyperspectral imagery. 5th International Symposium Recent Advances in Quantitative Remote Sensing, 18-22 September 2017, Torrent (Valencia), Spain.

3. C. **Camino**, P. J. Zarco-Tejada and V. González-Dugo. Assessment of the spatial variability of CWSI within almond tree- crowns and its effects on the relationship with stomatal conductance. Geoscience and Remote Sensing (IGARSS), IEEE International Symposium, 22-25 July, 2018, Valencia Spain.

Publicaciones científicas en colaboración con otros grupos de investigación

1. S. Gálvez, R. Mérida-García, **C. Camino**, P. Borrill, M. Abrouk, R. H. Ramírez-González, S. Biyiklioglu, F. Amil-Ruiz, The IWGSC, G. Dorado, H. Budak,V. González-Dugo, P. J. Zarco-Tejada, R. Appels, Cristobal Uauy, Pilar Hernandez. Hotspots in the genomic architecture of field drought responses in wheat as breeding targets. *Funct. Integr. Genomics*.; doi:10.1007/s10142-018-0639-3

Datos de 2017 (JCR): índice de impacto 3.889, índice de impacto de los últimos 5 años 3.226, y 2º cuartil en el área temática de Genetic and Heredity Science.

2. P. J. Zarco-Tejada, **C. Camino**, P. S. A. Beck, R. Calderon, A. Hornero, R. Hernández-Clemente, T. Kattenborn, M. Montes-Borrego, L. Susca, M. Morelli, V. González-Dugo, P. R. J. North, B. B. Landa, D. Boscia, M. Saponari and J. A. Navas-Cortes. Previsual symptoms of *Xylella fastidiosa* infection revealed in spectral plant-trait alterations. *Nature Plants*, volume 4, pages 432–439 (2018). https://doi.org/10.1038/s41477-018-0189-7.

   Datos de 2017 (JCR): índice de impacto 11,471, índice de impacto de los últimos 5 años 11,471, y 1º cuartil en el área temática de Plant Sciences.

Publicaciones científicas en revistas de ámbito nacional

1. R. Calderon, **C. Camino**, P.S.A. Beck, A. Hornero, R. Hernández-Clemente, T. Kattenborn, M. Montes-Borrego, L. Susca, M. Morelli, V. Gonzalez-Dugo, P.R.J. North, B.B. Landa, D. Boscia, M. Saponari, P.J. Zarco-Tejada and J.A. Navas-Cortes. Detección pre-visual de la infección por *Xylella fastidiosa* en olivo a partir de imágenes hiperespectrales y térmicas. Phytoma, Diciembre 2018

Por todo ello, se autoriza la presentación de la tesis doctoral.

Córdoba, a 6 de Mayo de 2019

Firma de los directores

Fdo.: Dr. Pablo J. Zarco Tejada

Fdo.: Dra. María Victoria González Dugo

TÍTULO DE LA TESIS: Detección de estrés hídrico y nutricional mediante fluorescencia clorofílica y modelos de transferencia radiativa a partir de imágenes hiperespectrales y térmicas

DOCTORANDO/A: Carlos Luis Camino González

DR. ELÍAS FERERES CASTIEL, Catedrático de Producción Vegetal de la Escuela Técnica Superior de Ingenieros Agrónomos de la Universidad de Córdoba.

INFORMA:

Que la investigación sobre "Detección de estrés hídrico y nutricional mediante fluorescencia clorofílica y modelos de transferencia radiativa a partir de imágenes hiperespectrales y térmicas" que ha llevado a cabo D. Carlos Luis Camino González, bajo la dirección del Dr. Pablo J. Zarco Tejada y Dra. Mª Victoria González Dugo y la tutoría del que subscribe, ha sido desarrollada con éxito y alcanzado los objetivos inicialmente propuestos. Los resultados de la investigación realizada constituyen una aportación científica innovadora y relevante para el manejo del uso de sensores en la detección de estrés hídrico y nutricional, lo cual queda adecuadamente reflejado en los artículos publicados en revistas del JCR que satisfacen los requisitos de indicios de calidad. En consecuencia, como tutor de la tesis doctoral que comprende dicha investigación, considero que puede ser presentada para su exposición y defensa públicas en la Universidad de Córdoba y ratifico la consideración favorable emitida por los directores de la tesis doctoral a tal efecto.

Por todo ello, se autoriza la presentación de la tesis doctoral.

Córdoba, a 6 de Mayo de 2019

Firma del tutor y responsable de línea de investigación

Fdo.: Dr. Elías Fereres Castiel

Tesis doctoral por compendio de artículos

Esta tesis doctoral cumple el requisito establecido por la Universidad de Córdoba para su presentación como compendio de artículos, consistente en un mínimo de 3 artículos publicados o aceptados en revistas incluidas en los tres primeros cuartiles de la relación de revistas del ámbito de la especialidad y referenciadas en la última relación publicada por el Journal Citations Report (JCR):

1. **Camino C.,** Zarco-Tejada P. J. & González Dugo V. Effects of Heterogeneity within Tree Crowns on Airborne-Quantified SIF and the CWSI as Indicators of Water Stress in the Context of Precision Agriculture. Remote Sensing. 2018, 10(4), 604; https://doi.org/10.3390/rs10040604 .

   Datos de 2017 (JCR): índice de impacto 3.406, índice de impacto de los últimos 5 años 3.952 y 2º cuartil en el área temática de Remote Sensing.

2. **Camino C.,** González-Dugo V., Hernández P., Sillero J.C. & Zarco-Tejada P. J. Improved nitrogen retrievals with airborne-derived fluorescence and plant traits quantified from VNIR-SWIR hyperspectral imagery in the context of precision agriculture. International Journal of Applied Earth Observation and Geoinformation. Volume 70, August 2018, Pages 105-117. https://doi.org/10.1016/j.jag.2018.04.013.

   Datos de 2017 (JCR): índice de impacto 4.03, índice de impacto de los últimos 5 años 4.433 y 1º cuartil en el área temática de Remote Sensing.

3. **Camino C.,** González Dugo V., Hernández P. & Zarco-Tejada P. J. Radiative transfer Vcmax estimation from hyperspectral imagery and SIF retrievals to assess photosynthetic performance in rainfed and irrigated plant phenotyping trials. Accepted in Remote Sensing of Environment. 6 may 2019.

   Datos de 2017 (JCR): índice de impacto 6.457, índice de impacto de los últimos 5 años 7.737 y 1º cuartil en el área temática de Remote Sensing.

El Doctorando

Fdo.: Carlos Luis Camino González

Agradecimientos

Quisiera agradecer a tod@s las personas que me han ofrecido ayuda para poder acabar esta aventura tan entretenida que he realizado en el Instituto de Agricultura Sostenible (IAS), perteneciente al Consejo Superior de Investigación Científicas (CSIC).

En primer lugar me gustaría agradecer de forma especial al Dr. **Pablo J. Zarco Tejada**, maestro de grandes investigadores y ejemplo a seguir dentro del mundo de la investigación. Gracias por buscarme financiación, estar siempre pendiente de mí y darme la oportunidad de poder realizar mi Tesis doctoral dentro del laboratorio de Quantalab. Gracias también por enseñarme a establecer los cimientos para poder ser un buen investigador.

En segundo lugar, no menos importante, me gustaría agradecer de forma especial a Dra. **Victoria González Dugo**, que es para mí otro gran referente en el mundo de la investigación. Gracias por ayudarme a buscar financiación y apoyarme en todo, para que esta Tesis Doctoral haya podido salir adelante. También quiero agradecerte, lo bien que me acogiste a mi llegada al IAS, así como toda la ayuda recibida en descifrar los entresijos de las relaciones fisiológicas vs datos hiperespectrales y térmicos.

A la Dra. **Pilar Hernández Molina** por dejarme realizar mis experimentos y medidas de campo en los ensayos de trigo pertenecientes a tus proyectos. Gracias por las charlas, tus consejos y por querer que participe en tus proyectos. Quiero en especial darte las gracias, por facilitarme todo el material necesario para poder desarrollar mi Tesis Doctoral, así como otros proyectos de selección genómica en ensayos de trigos.

A la Dra. **Blanca Landa del Castillo** por todos tus consejos recibidos durante nuestras campañas de campo en Apulia, por permitirme participar en tus proyectos de investigación y por esa gestión de los botes de campo tan impresionante.

Al Dr. **Juan Antonio Navas Cortés** por compartir todos tus conocimientos en modelización en R, así como dejarme participar en tus proyectos de investigación y en todo lo que se tercie, aunque seas del Real Madrid, seguiremos colaborando juntos.

A la Dra. **Rosa M Mérida García**, por las charlas, los gritos y lo bien que lo hemos pasado en esta aventura tan entretenida mientras ha durado nuestra formación en el doctorado. Siempre nos quedará un Goiko!!!!. Además, quiero dar las gracias al padre de Rosa y familia al completo, sin vosotros no hubiera sido posible, muchas gracias por ese diseño tan fascinante y vuestra confianza infinita.

A la **Dra. Carmen Ortiz Bustos**, gracias por esos cafés, charlas, infinitos consejos y lo buenos momentos compartidos en le IAS y fuera. Dalo por seguro que seremos grandes amigos. A **Álvaro Calderón** ese pedazo estudiante de doctorando que tan buenos momentos hemos pasado desayunando, gracias infinitas por tu tiempo.

A los **chic@s** del laboratorio de Quantalab por haberme sufrido tantos días, escuchando mis infinitos suspiros durante mi doctorando, sin vuestra ayuda, hubiera sido imposible terminar mi Tesis Doctoral. A **Rafael Romero** por tu apoyo en térmico y siempre, repito siempre, querer ayudar, A **David Notario** por tus necesarias medidas de vuelo, ayuda en campo, procesamiento y tus calibraciones perfectas, a **Alberto Vera** por encargarte de todo lo referido a montaje de cámaras en el avión, tu ayuda en procesamiento de datos, y por dejarme volar en el avión, a **Alberto Hornero** por tú apoyo en las calibraciones, campañas de campo y colaboraciones científicas, y por último quisiera dar las gracias a mí mismo por aguantaros 😂

Al Dr. **Emilio Cuevas Agulló** por marcarme las líneas de lo que es investigar y lo que no, a dedicarme tu tiempo para que pudiera centrarme en lo importante y descartar lo superfluo. Muchas gracias por enseñarme a hacer ciencia. También gracias a todos los miembros del IARC-AEMET, en especial al Dr. **Alberto Berjón-Arrojo**, la Dra. **Natalia Prats Porta**, la Dr, **Rosa García Cabrera**, la Dra. **Iballa Hernández**, Dra. **Omaira García Rodríguez**, Dr. **Eliezer Sepúlveda, Enrique Reyes, Sergio, Juan de Bustos, Alberto Redondas, Pedro Romero, Rocío López, Ramón Ramos, Antonio Cruz, Concepción Sálamo, Marcos Damas…**. Y resto de grandes compañeros que me hicieron pasar muy buenos momentos en Tenerife. Esta tesis os la dedico !!.

A Dr. **Miguel Montes Borrego**, **Guillermo León Ropero**, **José Luis Trapero Casas** del grupo del Dr. **Juan Antonio Navas Cortés** y la Dra. **Blanca Landa del Castillo** por lo bien que lo pasamos en todas las campañas que hemos participado y lo refrescante que era charlar con una buena cervecita.

Al Dr. **José A. Jiménez Berni** por esas charlas de Hyper, Térmico y tus ganas de colaborar conmigo. Deseando poder empezar a colabora en materia machine learning.

Y nos menos importantes a mis **padres**, por vuestro apoyo incondicional. Así como a **Verónica**, **Arnau** y **Adriana** por darme vuestro infinito apoyo para poder hacer este sueño y no protestar viajando de un lado para otro, hasta dar con el grupo de investigación ideal. Gracias **Verónica de nuevo**, por tu apoyo incondicional y ser como eres, una gran madre y esposa.

CONTENTS

List of figures

Chapter 1

Chapter 3

Chapter 4

Chapter 5

List of tables

Chapter 3

Chapter 4

Chapter 5

Resumen

El nitrógeno (N) y el agua son los factores limitantes más importantes en la producción y crecimiento de un cultivo. Conocer el estado fisiológico de un cultivo durante sus etapas de crecimiento es crítico para la optimización de la aplicación de insumos agrícolas, la predicción del rendimiento y la vigilancia de enfermedades. Desde un punto nutricional, el N es un elemento esencial en la producción de clorofila, fundamental para el proceso de fotosíntesis, y otros componentes celulares de la planta (proteínas, ácidos nucleicos, aminoácidos). Por su parte, el déficit hídrico afecta los procesos de crecimiento, rasgos filogenéticos tales como estructura de la hoja y la forma, la eficiencia fotosintética, por lo que su detección temprana es sumamente importante.

En la última década, la estimación de parámetros fisiológicos a partir del uso de sensores hiperespectrales y térmicos se ha desarrollado ampliamente. A diferencia de los sensores multiespectrales de banda ancha, los sensores hiperespectrales se caracterizan por un elevado número de bandas estrechas y contiguas a lo largo del espectro electromagnético que permiten una mejor descripción de porciones específicas del espectro y, por tanto, una mejor cuantificación de rasgos bioquímicos y biofísicos a través de modelos físicos de transferencia radiativa. El uso de sensores de imagen de tipo hiperespectral y térmico permite cubrir grandes áreas y cuantificar la variabilidad espacial de parámetros relacionados con el estado fisiológico del cultivo, siendo una alternativa real a los métodos destructivos tradicionales de muestreo en campo con medidas foliares.

La presente tesis doctoral tiene como principal objetivo explorar la contribución que tiene la fluorescencia clorofílica (s*olar-induced fluorescence,* SIF) cuantificada mediante sensores hiperespectrales a bordo de plataformas aéreas en la cuantificación de N y en la estimación de la tasa máxima de carboxilación (Vcmax), como proxy de la actividad fotosintética. Para ello, se han utilizado sensores hiperespectrales y modelos de transferencia radiativa en ensayos de fenotipado de selección de variedades de trigo en condiciones de secano y regadío. En el estudio se evaluaron las relaciones fisiológicas obtenidas entre las medidas realizadas en campo con los rasgos bioquímicos, biofísicos y fotosintéticos obtenidos mediante inversión de modelos de transferencia radiativa (PROSPECT-SAILH y SCOPE), índices espectrales de

vegetación obtenidos con bandas situadas entre la región del visible y el infrarrojo de onda corta (400-1750 nm), la fluorescencia clorofílica cuantificada mediante el método de la profundidad de las líneas de Fraunhofer, e indicadores obtenidos con cámaras térmicas sensibles al rango espectral de 8-14 μm.

Dada la importancia de los efectos estructurales en la estimación de parámetros biofísicos y bioquímicos mediante sensores remotos de alta resolución, esta tesis doctoral ha estudiado los efectos de la heterogeneidad estructural dentro de las copas de los árboles. Para ello, se han desarrollado métodos automáticos de segmentación de las imágenes obtenidas con sensores aerotransportados hiperespectrales y térmicos de alta resolución. El objetivo de este primer trabajo, fue analizar la variabilidad estructural dentro del árbol, y su efecto en las relaciones obtenidas entre las medidas fisiológicas de fluorescencia clorofílica y los indicadores térmicos.

En la tesis doctoral se destaca el potencial que tienen las herramientas de detección remota para cuantificar la concentración de nitrógeno, detectar el estrés hídrico y estimar los rasgos de la fotosíntesis de la planta mediante el uso de imágenes hiperespectrales y térmicas combinadas con modelos de transferencia radiativa. Los resultados demuestran que la fluorescencia clorofílica natural mejora la estimación de la concentración de N y el parámetro Vcmax debido a la estrecha relación que tiene con la actividad fotosintética y la detección del estrés hídrico. Los resultados también resaltan la capacidad para estimar la tasa máxima de carboxilación utilizando inversiones con el modelo SCOPE y SIF cuantificado a partir de imágenes hiperespectrales de alta resolución en aplicaciones de fenotipado de alto rendimiento y agricultura de precisión.

Summary

Nitrogen (N) and water are the most important limiting factors in agricultural yield. Knowing the crop physiological status during the growth stages is critical for the optimization of resources use efficiency, yield predictions and the detection of diseases. Nitrogen is an essential element in the plant pigments (chlorophyll and carotenoids) and in the production of proteins, as well as in other plant cellular components such as nucleic acids. On the other hand, water deficit induces stomatal closure, affects growth rate and phylogenetic traits such as leaf structure and shape. Therefore, water stress decreases the photosynthetic rate and yield, and its early detection is critical.

In the last decade, physiological trait quantification and water stress detection methods carried out from hyperspectral and thermal sensors have been widely developed. In contrast to the broadband multispectral sensors, the hyperspectral technology is characterized by a high number of adjacent narrow bands along the electromagnetic spectrum that allow an accurate description of specific portions of the spectrum and, therefore, a better quantification of plant physiological traits retrieved through hyperspectral imagery. In fact, the use of high-resolution hyperspectral and thermal sensors allows covering large areas. This approach provides a reliable tool for monitoring the spatial variability of the crop status, being a real alternative to the traditional destructive methods of leaf sampling and leaf measurements in the field.

The main objective of this PhD thesis is to explore the contribution of the solar-induced chlorophyll fluorescence (SIF) to retrieve nitrogen status and maximum carboxylation rate (Vcmax), as a proxy of photosynthesis activity, through the use of high-resolution hyperspectral imagery onboard aerial platforms and the use of radiative transfer models. The work was carried out in phenotyping trials for wheat selection under rainfed and irrigated conditions. In the experimental trial sites, the physiological relationships obtained between the field physiological measurements and airborne-based remote sensing indicators were evaluated. In this regard, well-known thermal-based indicators acquired from high-resolution thermal sensors sensible to spectral range of 8-14 μm and the following indicators from high-resolution hyperspectral were used: i) vegetation spectral indices retrieved in the spectral region located at the visible and short-wave infrared domain (400-1750 nm); ii) plant traits derived by radiative transfer

model inversions (PROSPECT-SAILH, SCOPE) and iii) airborne-derived SIF retrievals by the Fraunhofer method.

Given the importance of the role played by the canopy structure in the retrieval of biophysical and biochemical traits using high-resolution remote sensors, the effects of the within tree-crown structural heterogeneity was assessed through the development of automatic segmentation algorithms. The objective was to explore the effects of the structure on the relationship between leaf physiological measurements and the chlorophyll fluorescence retrievals and thermal indicators acquired from the high-resolution hyperspectral and thermal imagery.

The PhD thesis highlights the potentials of innovative remote sensing tools for the quantification of nitrogen concentration, the detecting water stress and the retrieval of plant photosynthetic traits through the use of high-resolution hyperspectral and thermal airborne imagery combined with radiative transfer models. The results demonstrate that the airborne-quantified solar induced chlorophyll fluorescence improved the estimation of N concentration and Vcmax due to the strong relation it has with plant photosynthetic activity and water stress detection. Results also highlight the ability to estimate the maximum rate of carboxylation using SCOPE model inversions with airborne-quantified SIF derived from high-resolution hyperspectral imagers for high-throughput plant phenotyping and precision agriculture applications.

Chapter 1: Introduction

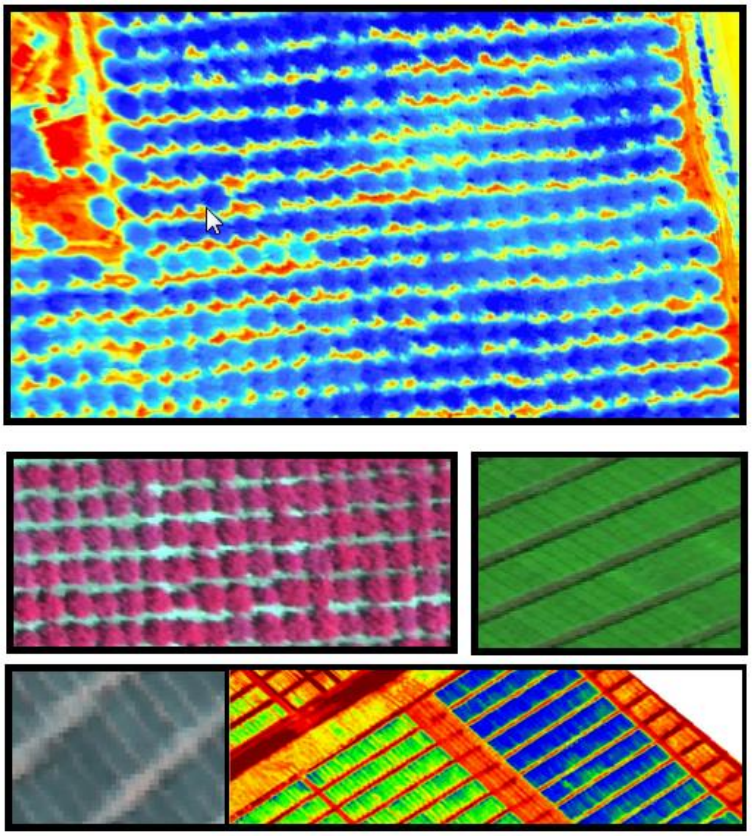

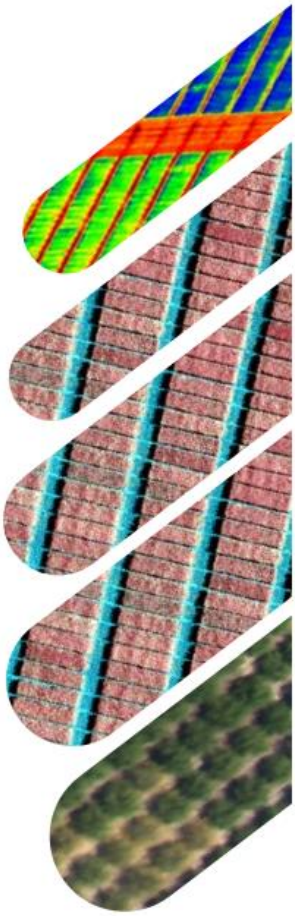

Chapter 1: Introduction

1.1 Photosynthesis: light absorption, regulation and its optical signal

The photosynthesis process starts with the light absorption of the incoming photosynthetically active radiation (PAR) captured in the chloroplasts and it involves light-dependent and light-independent biochemical reactions on the leaves (Fig. 1.1). On average, about 75% of visible irradiance is absorbed by leaves, but a very small fraction is converted to organic matter (Tremblay et al., 2011). In the absence of stress (e.g. water and N deficiency), the photosynthesis process transforms the electromagnetic energy into chemical energy (glucose) using atmospheric CO_2, water, ATP, NADPH and other molecules. For that, the Ribulose-1,5-biphosphate carboxylase/oxygenase (RuBisCO) uses the ATP and NADPH, which are generated into membranes of thylakoids, to synthesize RuBP, which reacts with CO_2 to reduce the 3-phosphoglyceric acid (3-PG) into glucose (Fig 1.1). The generation of ATP and NADPH used to regenerate RuBP is controlled by the maximum rate of electron transport (Jmax), while the latter biochemical reactions to produce glucose are constrained by the maximum rate of carboxylation (Vcmax).

The light energy conversion to chemical energy takes place in multiprotein complexes called photosystems. Two types of photosystem are found embedded in the thylakoid membrane, the photosystem II (PSII) and photosystem I (PSI). Both photosystems have the same basic structure; the light-harvesting complexes (LHC). It consists of multiple antenna proteins that contain chlorophyll a, chlorophyll b and carotenoids, which surround the reaction centre (RC), where the photochemistry occurs. Inside the thylakoid membrane, both PSII and PSI together with the cytochrome complex, form the photosynthetic electron transport chain (Figure 1.2). The LHC participates in the conversion of light absorbed PAR energy to chemical energy catalyzed by the RCs, while the cytochrome b_6f complex enables the transfer of electrons from PSII to PSI. That loss of energy is used to move hydrogen atoms from the stroma to the thylakoid lumen, generating a proton gradient across the thylakoid membrane. The proton gradient is used by ATP synthase during the process of ATP synthesis (Kramer et al., 2004).

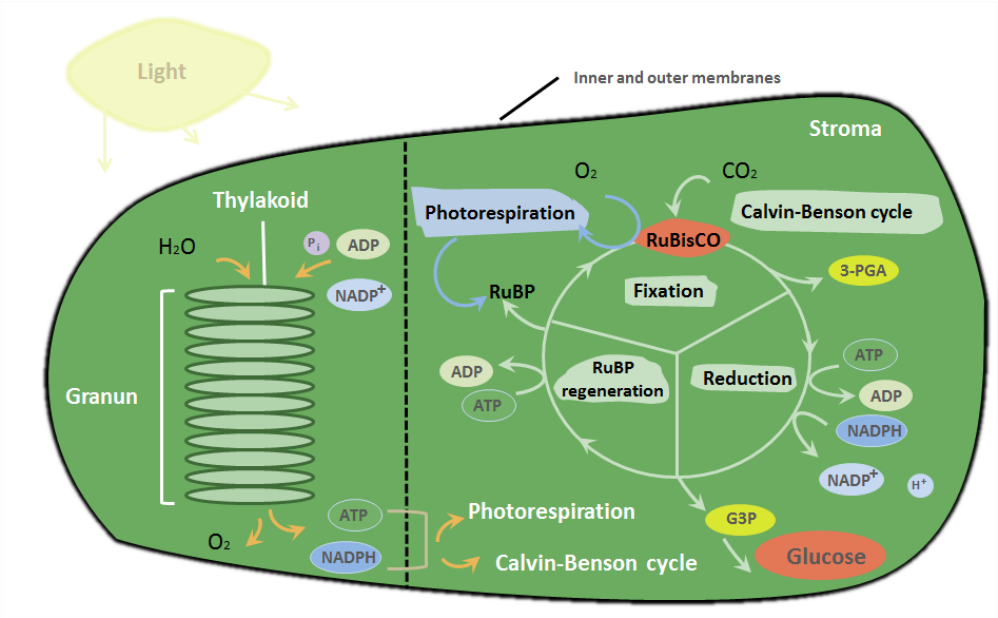

Fig. 1.1. The light and dark reactions in the chloroplast. The chloroplast is involved in both stages of photosynthesis. The light reaction takes place in the thylakoid discs where the H_20 is oxidized and O_2 is released. The electrons freed up from H_20 are transferred to ATP and NADPH molecules. The dark reaction occurs in the stroma and the cytoplasm. In the Calvin-Benson cycle, ATP and NADPH are used to fix CO_2.

The excess amount of energy absorbed by the light reactions is dissipated into in form of chlorophyll fluorescence and heat emission to prevent damages in the photosynthetic apparatus. Plants under N deficiency, water stress and other environmental constraints modify the relative proportions of absorbed PAR that is used for photosynthetic quantum conversion, chlorophyll fluorescence and heat emission. Nitrogen deficiency decreases the quantum yield of PSII electron transport, CO_2 assimilation of photosynthesis, the maximal efficiency of PSII photochemistry and increases the thermal energy dissipation activity (non-photochemical fluorescence quenching, NPQ) (Jin et al., 2015; Nunes et al., 1993). Flexas and Medrano (2002) showed that the decreased RuBP impaired the ATP synthesis in early drought phases, reducing the photochemistry and RuBisCO activity at severe water stress. At high radiance exposures, there is an increase in levels of the photosystem, cytochrome *b/f* complex, ATP synthase complex, and the amount of RuBisCO enzyme (Walter et al. 2015).

The plants have developed effective strategies to regulate the light absorption, one of them consist of adjusting the leaf chlorophyll pigment content (Porcar-Castell et al., 2014). Plants can also induce changes in the anthocyanins content, increasing the absorption in leaves and affecting the chlorophyll fluorescence emission and the

photosynthesis CO_2 assimilation (Hlavinka et al., 2013). Among others, plants adjust the internal distribution of chloroplast (Sarvikas et al., 2010), the movements to PSII photo-protection (Arena et al., 2008), and changes in surface structures such as pubescence in response to drought (Ehleringer et al., 1976; Galmés et al., 2007; Morales et al., 2002) for modulating the photosynthetic light absorption.

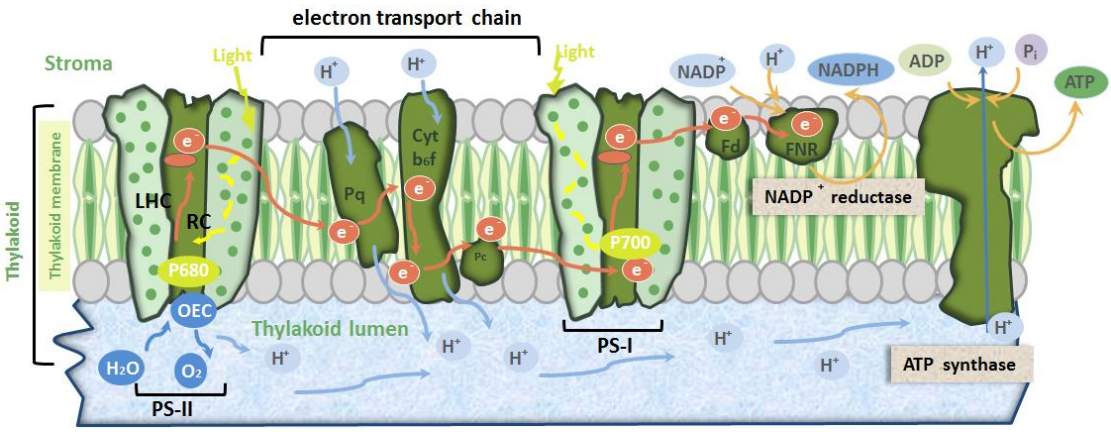

Fig. 1.2. Scheme of the photosynthetic electron transport chain. The excitation energy from absorbed photons in PSII (P680) is transferred to PSI via Cyt *b6f* complex. The energy from photons absorbed by PSI (P700) is used, via ferredoxin (F_d) to reduce the NADP+ into NADPH by the action of the ferredoxin-NADP reductase enzyme. Inside the thylakoid lumen, protons generated via Cyt *b6f* complex, plus the ones generated in the oxygen-evolving complex (OEC) into PSII, are transferred to chlorophyll stroma during ATP synthesis catalyzed by ATP synthase.

As described before, the CO_2 assimilation rate is determined by changes that occur during the biochemical and biophysical processes, which include CO_2 transport through the leaf and stomata, and the biochemical processes. In this regard, our understanding of the photosynthetic pathway is crucial to develop advanced methods that combine biochemical photosynthesis models and remote sensing tools for retrieving plant traits related to assimilation rate and nitrogen.

1.2 Drought stress on crops

The changing rainfall patterns and climate trends are causing the frequent onset of droughts around the world, reducing the yield of the main crops (Lobell et al., 2011). It is estimated that drought stress would be intensified with the global warming, affecting arable areas, especially in semi-arid and arid regions. By the end of this century, global surface average temperature will increase about 2.6-4.8ºC according to the fifth assessment report (AR5) published by the Intergovernmental Panel on Climate Change (IPCC, 2014). In addition, drought stress is a worldwide problem that adversely

constraint the global crop production, food security, infrastructure and agricultural incomes, as well as including shifts in the production areas of food and non-food crops around the world.

Drought stress is a complex physical-chemical process and one of the most important abiotic factors that cause a substantial decline in crop yields through negative impacts on plant growth, physiology, and reproduction (Barnabás et al., 2008). Under drought conditions, water deficits occur in crops when the evaporative demand exceeds the supply of soil water (Slatyer, 1967). Water stress is characterized by reduction of water content, turgor, water potential, wilting, closure of stomata, transpiration, CO_2 assimilation and decrease in cell enlargement and growth (Hsiao, 1973). Drought stress affects plant water status by decreasing the water potential and the water content in leaves. In addition, under severe water stress conditions, the plants halt the photosynthesis process, metabolism disturbance and finally, death occurs. The plant response to water stress occurs at several levels, according to the intensity and the duration of water stress, as well as on the growth stage of the crop. Water stress is accompanied by heat stress that causes changes at molecular, morphological, physiological and biochemical levels (Barnabás et al., 2008; Shao et al., 2008).

In water stress conditions, the stomatal closure limits water loss by evaporation, and reduces the CO_2 input from the atmospheric to the mesophyll, reducing the crop photosynthetic capacity and the synthesis of ribulose bisphosphate (RuBP) (Gimenez et al., 1992; Medrano et al., 1997). Under these conditions, the photorespiration increases due to the lower CO_2:O_2 ratio and the enzyme RuBisCO has a higher affinity for O_2 than CO_2. Therefore it inhibits the photosynthesis activity (Boyer, 1976).

The water deficiency in crops has a negative effect on photosystems, the electron transport system and CO_2 reduction pathways (Lamaoui et al., 2018) that may lead to a reduction in the overall photosynthetic performance. The stress-induced stomatal closure reduces the CO_2 availability into leaves, thereby decreasing CO_2 assimilation as well as inhibition of key photosynthetic enzymes and ATP synthases (Tezara et al., 1999; Zlatev and Cebola Lidon, 2012). The decrease in photosynthesis activity is also constrained by the inhibition of the processes in the Calvin cycle (Tezara et al., 1999), which occurs inside the chloroplasts. Under severe drought, the RuBisCO activity (Parry et al., 1993, 2002) and several non-stomatal effects are also affected (Medrano et

al., 1997; Reddy et al., 2004), such photophosphorylation process (Meyer and Genty, 1999), the RuBP regeneration (Lawlor and Cornic, 2002), and the ATP synthesis (Tezara et al., 1999). In addition, drought stress affects mesophyll metabolism (Lawlor and Cornic, 2002), becoming progressively more important with increasing water deficiency (Gimenez et al., 1992).

The water stress also inhibits the chlorophyll synthesis and increases the production of xanthophyll pigments, as a protective role within the leaves under severe water stress. The changes in photosynthesis activity associated with drought stress have also been related to changes in the de-epoxidation state of the xanthophyll cycle through non-photochemical quenching (Evain et al., 2004; Nichol et al., 2006). Water stress linked to other co-limiting factors (e.g. heat stress, high irradiance exposures and nutritional stress) modifies the relative proportions of absorbed light energy that are used for photosynthetic quantum conversion, chlorophyll fluorescence and heat emission. Under drought stress, the CO_2 assimilation is reduced, changing the solar-induced chlorophyll fluorescence (SIF) emission (Flexas et al., 2000, 1999; Flexas and Medrano, 2002) and heat dissipation.

1.3 Nitrogen deficiency in crops

Nitrogen (N) is the major limiting factor of crop yield and biomass after water deficiency. N is an essential element for plant growth, crop production, chlorophyll production and other plant cell components (Johnson, 2001; Bonfil et al., 2004; Zhu et al., 2008; Muñoz-Huerta et al., 2013) and it drives the canopy carbon assimilation (Li et al., 2014). An adequate N supply is crucial for the maintenance of plant biochemistry quality (Nobel, 2009) and enhances yield production and grain quality. In addition, N management has economic and environmental implications (Bonfil et al., 2004).Plants mainly absorb nitrogen from the soil in the form of ammonium (NH_4^+) and nitrate (NO_3^-). Insufficient application of N reduces plant growth and grain yield (Corp et al., 2003). On the other hand, nitrogen overfertilization is the primary reason for low N-use efficiency and negative environmental impacts on air and water quality as well as on biodiversity (Lu and Zhang, 2000). In particular, excessive nitrogen supply causes significant effects on the environment, such as NO_3^- leaching that greatly influence eutrophication and groundwater contamination (Inoue et al., 2012), as well as the nitrous oxide (N_2O) emissions, which contributes to global warming into greenhouse

gas emissions (Muñoz-Huerta et al., 2013; Chen, 2015) and can also damage human health through impacts on the air quality. In this regard, adequate N management is needed to improve the quality of life and reduce health care costs worldwide. In conclusion, optimized N fertilization programs are required to guide precision diagnosis of soil status and efficient crop management.

When crops face N deficiency, different plant strategies have been developed to optimize uptake nitrogen from the soil. The first crop strategy relies on an increase in gene expressions encoding nutrient-specific root transporters (Amtmann and Armengaud, 2009; Gojon et al., 2009; Masclaux-Daubresse et al., 2010; Maillard et al., 2015). This molecular response to nutritional deficiency is coupled with other plant strategies, such as growth and increased branching of roots for mineral nutrients uptakes (Giehl et al., 2014; Gruber et al., 2013), the root exudation of organic compounds for nutrient mobility (Maillard et al., 2015) and the remobilization of short or mid-term storage of N within the plant through the phloem, which occurs during vegetative and reproductive stages (Malagoli et al., 2005). N remobilization, which is correlated with foliar senescence, makes nutrients available for expanding leaves and younger organs, and contributes to increase the nitrogen use efficiency (Himelblau and Amasino, 2001). However, during the N remobilization, the photosynthesis activity is reduced due to the degradation of the enzyme RuBisCO, being the main N source of nitrogen for remobilization to other organs (e.g. seeds at the reproductive stage) during the senescence (Masclaux-Daubresse et al., 2010).

N deficiency induces changes in many physiological processes. Approximately the 75% of the total N content in leaves is contained in chloroplast proteins (Fig. 1.1), mainly in the RuBisCO and in chlorophyll binding proteins (Johnson, 2001; Rodriguez et al., 2006). Other studies found that in the chloroplast thylakoids about the 27% of total nitrogen is present in the RuBisCO (Makino et al., 1984) . Numerous works have shown a strong correlation between N and both RuBisCO (Evans, 1983) and chlorophyll content (Croft et al., 2017; Haboudane et al., 2002). N deficiency significantly induces a reduction in the photosynthetic capacity of leaves, because the chloroplast thylakoids and the Calvin-Benson cycle proteins represent the majority content of nitrogen in leaves. Evans and Terashima (1987) indicated that the amounts of thylakoid components per unit leaf are affected by nitrogen deficiency. However, as they showed the N deficiency does not alter the properties of the thylakoid membranes.

These and other studies have shown that chlorophyll content and RuBisCO content per unit leaf area decreased under N deficiency. Therefore, the partial electron transport rate through photosystem II (PSII) and the RuBisCO activity is affected by the N content per unit leaf area (Evans and Terashima, 1987; Seemann et al., 1987). Khamis et al. (1990) also demonstrated that the N deficiency had a small effect on photosynthetic quantum yield and a large effect on the light-saturated photosynthetic rate. In general, the nitrogen deficiency affects PSII photochemistry, lowering the quantum yield of PSII electron transport, the photochemical efficiency of PSII, and therefore the assimilation rate (Jin et al., 2015; Lu and Zhang, 2000).

1.4 Crop water stress and the infrared thermometry methodologies

Water scarcity is a major issue in many agricultural crops. The efficient use of water is a key requisite to decrease the share of freshwater diverted to agriculture and release water resources to food production, ecosystem function, and others society sectors, where demand is increasing (Jury and Vaux, 2007). Crop transpiration regulates the canopy energy and water balance, being the major cooling mechanism of crop canopies. It is well known that the crop transpiration is limited by the intercepted radiation, the air temperature, the crop-air vapour pressure deficit, soil water content and the stomatal conductance. Given that the canopy temperature and the transpiration process are closely related, measuring plant canopy temperature enables the assessment of crop water and transpiration status.

In recent years, water stress indicators have been successfully applied in many crops to monitor water status. In this regard, remote sensing technologies have been successfully demonstrated to have the capacity for monitoring water status and transpiration processes across entire fields (Meron et al., 2010; Gonzalez-Dugo et al., 2015; 2019). These studies and others have demonstrated that canopy temperature retrievals are reliable remote sensing tools and these retrievals have the advantage of being non-destructive as compared to traditional measures. Until the infrared thermometry devices became available, most plant temperature measurements were carried out with sensors on, or embedded in, leaves. Monteith and Szeicz (1962) and Tanne (1963) were among the first to estimate crop temperature using infrared thermometry technology. Ehrler (1973) using thermocouples embedded in cotton leaves, found that the relation found between leaf-air temperature and the air vapour

pressure deficit is linear. Idso et al. (1977) and Jackson et al. (1977) used the difference between canopy temperature (Tc) derived from infrared thermometry and air temperature (Ta) as an indicator of crops water status in wheat. These researches related the thermal-based indicator with yield and water requirements. Later, Idso et al. (1978) and Jackson et al. (1981) developed the concept of the crop water stress index (CWSI), as a thermal-based stress indicator using hand-held thermal infrared thermometers. The CWSI is based on the difference between canopy temperature and air temperature (Tc-Ta), normalized by the vapour pressure deficit (VPD), and is inversely related to transpiration and stomatal conductance (Jackson et al., 1981). The CWSI is calculated using two boundary conditions: i) when the transpiration is completely halted (referred as upper limit) and ii) when the canopy is transpiring at its potential rate (referred as non-water-stressed baseline or lower limit).

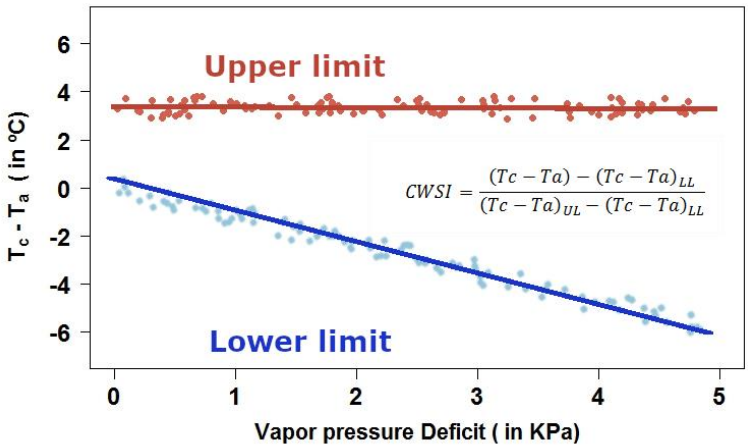

Fig. 1.3. Canopy-air temperature difference vs. air vapour pressure deficit (VPD). The upper and lower limits of the canopy-air temperature difference are represented in red and blue colours respectively.

These initial works that started in the 1970s and 1980s established the foundations for monitoring crop water stress using infrared thermometry technology. However, these works were site-specific and not useful for monitoring the spatial distribution of water status within a field, reducing decision-making procedures allowing farmers to maximize the water use efficiency.

In the context of thermal imaging for detecting water stress, the recent advance on remote sensing technologies offers the potential to retrieve thermal-based indicators from airborne thermal imaging and map spatial variability of water status. Sepulcre-Cantó et al. (2006) showed that water stress can be detected at the tree crown level and

at the orchard level using high spatial resolution airborne thermal imagers. In addition, Sepulcre-Cantó et al. (2007) demonstrated that remote sensing estimates of tree crown temperature were well correlated to yield and fruit quality indicators under different irrigation regimes of commercial orchards. Many studies have shown that high-resolution thermal imagery acquired from manned and unmanned aerial platforms enable the detection of water stress, showing accurate correlations with indicators of crop water status such as stomatal conductance and leaf water potential (e.g. Zarco-Tejada et al., 2013a; Gonzalez-Dugo et al., 2015; Bellvert et al., 2016). Other studies have showed that canopy temperature can be used to quantify the overall plant water status for low and moderately stressed crops (e.g. González-Dugo et al., 2006). Hence, thermal-based CWSI is a valuable tool to assess the crop water status and provides thermal mapping at high-resolution over the entire field (Taghvaeian et al., 2012; Gonzalez-Dugo et al., 2014).

1.5 Methods for sensing nitrogen status

Assessing crop N status at the field scale has become one critical goal to ensure more precise N application. Traditionally, the nitrogen content is estimated using tissue analysis such as Kjeldahl digestion and Dumas-combustion. However, those standard methods are expensive, time-consuming, need complex chemical analysis and require destructive crop sampling (Muñoz-Huerta et al., 2013). In fact, these analyses are not applicable for continuous monitoring of nitrogen status at the field scale. Therefore, finding alternative tools designed for the spatial monitoring of N status based on plant optical properties could be potentially used for large-scale assessment as an alternative to traditional time-consuming methods.

Remote sensing tools have received much attention as a fast and non-destructive method to estimate plant traits to determine plant constituents, including crop N status (Blackmer et al., 1994; Li et al., 2008; Silva-Perez et al., 2018). At leaf scale, the integrating spheres coupled with spectrometers have allowed characterizing the leaf optical properties (reflectance and transmittance). Subsequently, handheld proximal sensing systems have been designed to measure the reflectance and transmittance properties of leaves, and the emission of the chlorophyll fluorescence. The leaf reflectance devices, such as PolyPen RP-400 (Photon Systems Instruments, Brno, Czech Republic), designed to measure the leaf reflectance within the visible and near-infrared

(NIR) regions has been widely used to characterize optical plant traits and N deficiency using spectral indices. Other proximal sensing tools, such as SPAD-502 (Minolta Corp., Ramsey, NJ, USA), have been widely developed to measure the leaf chlorophyll content as a proxy for crop N status (Uddling et al., 2007; Cortazar et al., 2015). Other optical sensors designed to measure chlorophyll and polyphenols compound in leaves through chlorophyll fluorescence emission, such as the Dualex and Multiplex sensors (FORCE-A, Orsay, France) have been used to detect nutritional stress (Tremblay et al., 2012; Quemada et al., 2014) and disease symptoms (Zarco-Tejada et al., 2018). Thoren and Schmidhalter (2009) developed a laser optical sensor capable of measuring chlorophyll content as a proxy for N status, via the fluorescence ratio emission using 690 nm and 730 nm bands from near distances (3-4 meters). Other studies have used fluorometers to relate the chlorophyll fluorescence with photosynthesis plant traits (Flexas et al., 2000; Zarco-Tejada et al., 2016; Carmo-Silva et al., 2017).

At canopy scale, remote sensing methods have focused on measuring spectral reflectance for the quantification of nitrogen through green and particularly red-edge reflectance regions, due to the strong correlation between the N and chlorophyll content (Johnson, 2001; Gitelson et al., 2005; Zhu et al., 2008; Silva-Perez et al., 2018). By providing both spatial and temporal information, remote sensing sensors may serve as a cost-effective source of data for fertilizer N applications. Remote sensing has a proven ability to provide spatio-temporal measurements of canopy properties, and it has been recognized as a potential method for N estimation through plant trait retrievals related to physiology and biochemistry.

More advanced remote sensing technology relies on hyperspectral sensors onboard aerial platforms (unmanned/manned) to acquire canopy reflectance over a large number of narrow wavebands, generally with bandwidths less than 10 nm. With narrow bands, reflectance and absorption features of specific plant traits related to physiology and biochemistry can be retrieved, thus making progress on the quantification of nitrogen. Satellite sensors, such as QuickBird and Sentinel-2/3, have been proposed for the estimation of chlorophyll and N content using reflectance indices and the red-edge spectral bands (Bausch et al., 2008; Wong and He, 2013). However, the coarse spatial resolution of these satellite sensors, as well as the limited number of spectral bands hinders the independent retrieval of N in the context of precision agriculture and crop-monitoring studies.

Several methods have been applied to estimate N and other biophysical parameters at leaf and canopy scales from their optical properties. Simple empirical relationships using spectral indices calculated from high-resolution hyperspectral imagery are still the dominant method used to estimate nitrogen using the visible and near-infrared (NIR) (Stroppiana et al., 2009; Wang et al., 2012; Li et al., 2014) and the shortwave-infrared (SWIR) regions (Serrano et al., 2002; Ferwerda et al., 2005; Herrmann et al., 2010; Pimstein et al., 2011; Gnyp et al., 2014; Mahajan et al., 2016). However, the nitrogen estimation at canopy level from remote sensing requires appropriate modelling strategies using radiative transfer models (RTM) due to the large contribution of soil, structural and shadow effects in the canopy reflectance.

In recent years, chlorophyll fluorescence quantification has received increasing attention in the context of global monitoring of crop photosynthesis traits, potentially providing improvements for the estimation of nitrogen (Tremblay et al., 2012). The use of chlorophyll fluorescence emission retrievals at leaf and canopy scale has been widely demonstrated in numerous studies for detecting N deficiency (Schächtl et al., 2005; Corp et al., 2009; Tremblay et al., 2012) and effects of water stress (Flexas et al., 1999,2000, 2002; Zarco-Tejada et al., 2013b) and its use in the context of plant phenotyping is discussed in the next section.

1.6 Solar-induced chlorophyll fluorescence

Plant stress modifies the relative proportions of absorbed light energy that is used for photosynthetic quantum conversion, chlorophyll fluorescence and heat emission. Understanding processes that take over the energy partitioning in PSII is essential to assess photosynthetic CO_2 assimilation with chlorophyll fluorescence. The solar-induced chlorophyll fluorescence emission (SIF) occurs when the incoming light energy is absorbed by chlorophyll molecules in the antenna of PSII. In the absence of stress, the energy is effectively used by photochemistry, reducing the fluorescence yield; this de-excitation pathway is referred to photochemical quenching (PQ) of fluorescence. This initial level, called F_o, attesting the Q_A electron acceptor is fully oxidized. In contrast, when the reaction centres are fully occupied fluorescence is no longer quenched and shows its maximum level (F_m). Therefore, the Q_A is completely reduced and an increase in photochemical efficiency of PSII (F_v/F_m; where $Fv = F_m - F_o$) is yielded. This increase in fluorescence is associated with the decay of non-

photochemical quenching (NPQ). As the energy is dissipated at longer wavelengths within a very short time, the de-excitation of this energy is mainly attained through three competing processes: photochemistry, chlorophyll fluorescence emission, and non-radiative thermal energy dissipation (NPQ). These three energy dissipation mechanisms compete for excitation energy and are inter-dependent. In fact, the competing processes respond to changing physiological and environmental conditions. By measuring the chlorophyll fluorescence emission using remote sensing methods, we can retrieve information about changes in photochemistry efficiency and thermal dissipation.

The amplitude of SIF typically spans within the 650–800 nm range in the NIR spectral region depending on plant physiological traits, environmental stress and canopy structure. The chlorophyll fluorescence spectrum is composed of two peaks located at 685 nm and 740 nm (Fig. 1.4); the first one is mainly produced by the fluorescence emission of PSII, while the other maximum, located in the NIR region, is attributable to both PSI and PSII (Baker, 2008). In general, SIF is mainly driven by PSII because the contribution of fluorescence from PSI is generally weak, thus SIF at 685 nm is expected to yield a stronger relation with photosynthesis activity (Genty et al., 1989; Palombi et al., 2011).

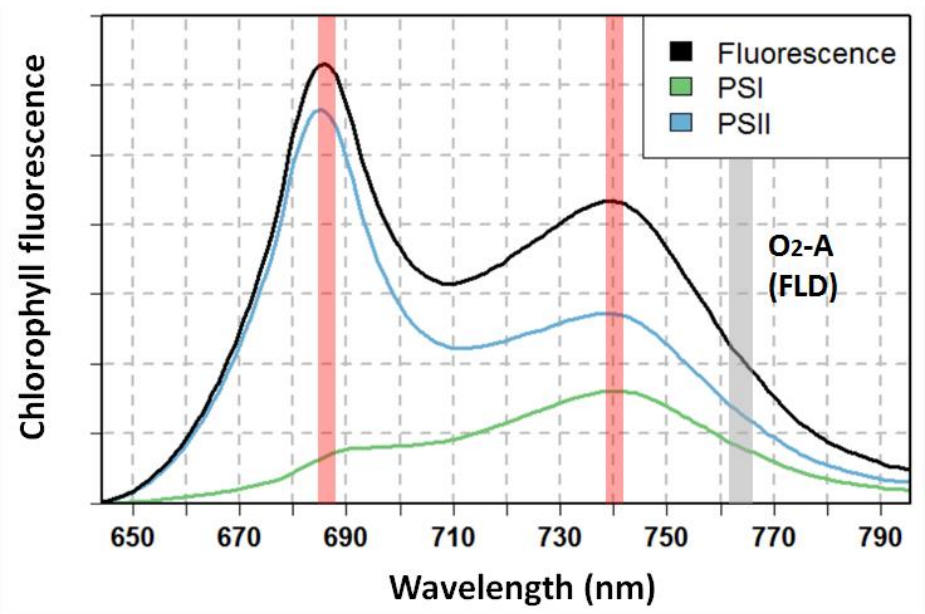

Fig. 1.4. Chlorophyll fluorescence signals with contributions from photosystem I (PSI) and photosystem II (PSII) simulated using the Soil-Canopy Observation of Photosynthesis and Energy (SCOPE) model. Blue and green lines indicate the PSI contribution of the photosystem I (PSI) and photosystem II (PSII), whereas the black lines indicate the total SIF (PSI + PSII contributions). The peak at 685 nm mostly

originates from PSII, while the peak at 740 nm originates from both PSI and PSII. The grey highlighted area is the absorption features due to oxygen in the O_2-A absorption region at 760 nm used for the Fraunhofer method to extract the chlorophyll fluorescence emission.

The total amount of chlorophyll fluorescence emission is relatively small compared to the incoming radiation (~1-2% of the total incoming light; Frankenberg and Berry 2018). Nevertheless, with the recent advance in imaging spectroscopy technology and remote sensing data processing, the chlorophyll fluorescence emission can be quantified at leaf and canopy scales.

The main methods used to measure chlorophyll fluorescence are based on i) pulse amplitude modulation (PAM) fluorometers systems or laser-induced fluorescence transient (LIFT) methods (active methods) and ii) the retrieval of SIF using passive methods. More generally, the active methods are applied at the leaf level, whereas passive methods are being commonly applied at the canopy level. The active methods allow the estimation of chlorophyll fluorescence yield parameters, such as F_o, F_m, F_v and steady-state chlorophyll fluorescence (F_s) through the use of an artificially modulated light to induce the leaf fluorescence signal. However, active sensors provide relative values of chlorophyll fluorescence yield that cannot be related to absolute radiometric values (Quick and Horton, 1984). In addition, active sensors have a limited application for monitoring at field scales, due to the spatial scale of operation which ranges from several centimetres to meters (Kolber et al., 2005; Amoros-Lopez et al., 2008). Alternatively, passive methods estimate SIF by combining solar irradiance and reflected radiance by vegetation through the use of atmospheric O_2 absorption features (Fig. 1.5). Drawing on the molecular oxygen absorption features on the solar spectrum, the European Space Agency (ESA) planned the FLuorescence EXplorer (FLEX) mission to tackle two main goals: i) to improve the methodologies for vegetation fluorescence retrievals from spaceborne high-resolution spectrometry and ii) to improve the current knowledge of vegetation chlorophyll fluorescence retrievals and its relation with the photosynthetic traits that drive the photosynthesis processes at global scales.

Most of the existing methods for retrieving SIF at ground-, airborne- and satellite levels are mainly based on the Fraunhofer Line Discrimination (FLD) principle (Plascyk and Gabriel, 1975). The FLD method is based on using the narrow dark lines present in the solar spectrum where the solar irradiance is attenuated by the effect of atmospheric O_2 absorption. Although, the solar irradiance exhibits several absorption features, the

O_2B and O_2A absorption bands located at 687.0 and 760.6 nm respectively, have been used to quantify chlorophyll fluorescence.

$$SIF_{retrieval} = \frac{L_{in}E_{out} - L_{out}E_{in}}{L_{in} - E_{out}} \quad 1.1$$

The FLD method estimates SIF by comparing the radiance (L) and irradiance (E) measured at a wavelength inside and outside the O_2 absorption feature (Eq. 1.1) according to the methods described (Moya et al., 2004; Meroni and Colombo, 2006; Damm et al., 2011). Recent studies have demonstrated that the FLD approach, used to quantify the chlorophyll fluorescence using two (FLD2) or three bands (FLD3) around the O_2A absorption features is suitable for hyperspectral imagery with large spectral oversampling (1.85 nm sampling interval) and wider spectral bandwidths (Damm et al., 2015; Zarco-Tejada et al., 2012; 2016).

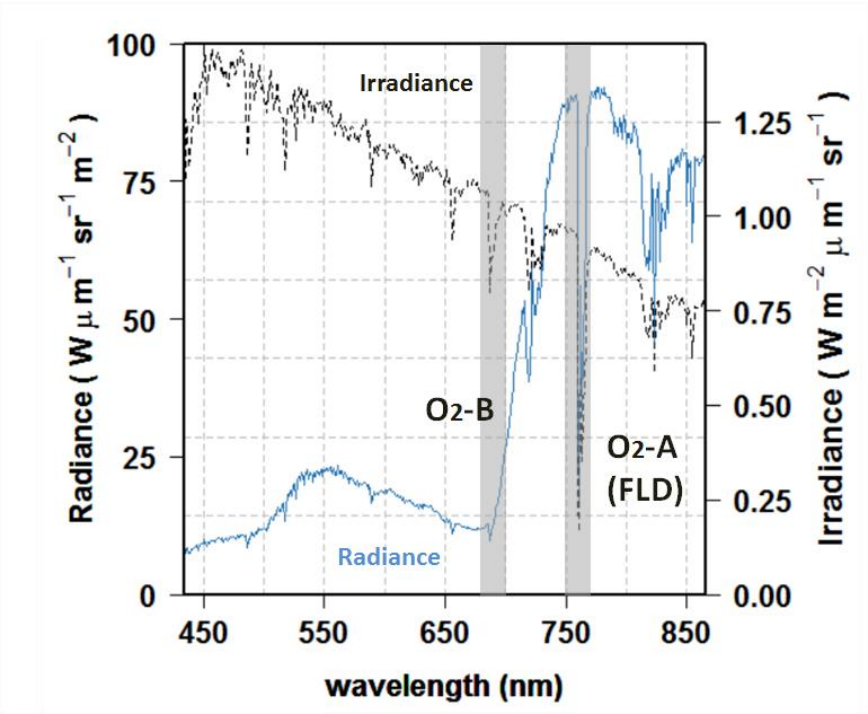

Fig. 1.5. The atmospheric irradiance (black) and the canopy radiance spectra (blue) used for fluorescence quantification with the 760 nm O_2-A FLD in-filling method. The O_2-A and O_2-B absorption features are marked with grey rectangles.

With the advent of imaging spectroscopy, SIF retrievals using remote sensing technologies have become a new area of research (Meroni et al., 2009, 2010) and opened a new perspective to assess photosynthesis at global (Frankenberg et al., 2011; Joiner et al., 2011; Koffi et al., 2015; Norton et al., 2017) and local scales (Pérez-Priego et al., 2005; Daumard et al., 2012). In fact, these advances in spectroscopy technology

opens up opportunities to use SIF emissions as an indicator of photosynthetic activity (Zhang et al., 2014; Zarco-Tejada et al., 2016), nutritional status (Tremblay et al., 2012; Quemada et al., 2014; Cendrero-Mateo et al., 2016) and gross primary productivity (Damm et al., 2015; Koffi et al., 2015; Yang et al., 2015; Norton et al., 2017; Smith et al., 2018). In addition, chlorophyll fluorescence is well-related to electron transport and is an indirect proxy with Vcmax through the accurate relationships found with chlorophyll content and net photosynthesis (Croft et al., 2017; Zarco-Tejada et al., 2016). Therefore, having robust and non-destructive tools derived from remote sensing for monitoring photosynthesis, as the underlying process for plant growth, remains a challenge in the agricultural context.

1.7 Radiative transfer modelling

There is a growing interest in developing approaches to quantify photosynthetic capacity, biochemical, structural, and physiological traits through satellite and airborne hyperspectral imagery. This increasing interest is due to recent advances in imaging spectroscopy, which offers the potential to retrieve plant traits linked to photosynthetic activity through leaf pigments and absorbed PAR radiation. The remote estimation of leaf biochemical traits from satellite, manned and unmanned platforms using multispectral and hyperspectral sensors have been the subject of recent efforts aiming at better monitoring of crop processes (e.g. photosynthesis, evapotranspiration, respiration) and ecosystem functioning. Previous efforts using remote sensing products to improve modelled estimates of carbon fluxes from terrestrial ecosystems have focused on using vegetation indices such as the structure-sensitive normalized difference vegetation index (NDVI) (Rouse et al., 1973) as an indicator of canopy greenness, and the photochemical reflectance index (PRI) (Gamon et al., 1992) related to the xanthophyll pigments cycle. Remote sensing reflectance has been used to establish relationships between photosynthetic status and plant traits, which shows that it is a useful tool for retrieving photosynthetic capacity due to its strong relation to chlorophyll content. In particular, non-parametric regression methods such as partial least squared regressions (PLSR) have been widely proposed for estimating chlorophyll content (Yu et al., 2015; Wang et al., 2017), and machine learning algorithms for estimating nitrogen concentration (Huang et al., 2004).

The development of statistical models between leaf reflectance and biochemical traits are still the dominant approach. Nonetheless, simple vegetation indices have been widely used to infer information about Vcmax (Houborg et al., 2013; Alton, 2017), canopy properties (Gamon et al., 1995) and plant traits related to plant physiology and leaf biochemistry: i) chlorophylls pigments (Haboudane et al., 2002; Zarco-Tejada et al., 2004); ii) carotenoids (Gitelson et al., 2002; Hernández-Clemente et al., 2012), iii) anthocyanins (Gitelson et al., 2006), iv) nitrogen content (Herrmann et al., 2010) and other macronutrients (Mahajan et al., 2014; Pimstein et al., 2011); v) water content (Clevers et al., 2010; Colombo et al., 2008) and vi) lignin and cellulose (Kokaly, 1999). However, these simple empirical methods are usually not effective due to the lack of robustness and transferability as they are usually specific in time, crop and field. Hence, the limitations of these empirical remote sensing approaches can be partly solved by physically-based radiative transfer models (RTM).

RTMs enable the simulation of the light absorption and scattering inside vegetation canopies accounting for leaf biochemical composition and canopy structural properties (Jacquemoud et al., 2009; Verhoef and Bach, 2007). Physical-based models enable a better understanding of the interaction of light with plants at both leaf and canopy levels. Physically based models offer advantages compared to statistical models built with narrow-band indices (Jacquemoud and Baret, 1990; Zarco-Tejada et al., 2004; Schlerf and Atzberger, 2006; Wang et al., 2015) and have been widely proposed for retrieving plant traits: i) chlorophyll and nitrogen content (Clevers and Kooistra, 2012; Wang et al., 2015); ii) carotenoid content (Hernández-Clemente et al., 2012), iv) water and dry matter content (Jacquemoud and Baret, 1990), v) structural parameters, such as leaf area index (Koetz et al., 2005; Sehgal et al., 2016), and vi) photosynthesis-related traits (Dechant et al., 2017; Zhang et al., 2014; Silva-Perez et al., 2018). In recent years, the combination of both approaches has successfully begun to develop through the use of hybrid methods (Verrelst et al., 2015a; Upreti et al., 2019). These methods exploit the RTM and non-linear non-parametric regression algorithms for the retrieval of biophysical traits using machine learning regression algorithm, PLSR or Gaussian processes regression (GPR).

At the leaf level, PROSPECT (Jacquemoud and Baret, 1990) is one of the most widely used RTMs for retrieving leaf biophysical traits and simulating leaf directional hemispherical reflectance and transmittance. PROSPECT is a radiative transfer model

based on Allen's generalized "'plate model" (Allen et al., 1969, 1970), that represents the optical properties of plant leaves over the solar spectrum from 400 nm to 2500 nm. PROSPECT is based on the representation of the leaf as one or several absorbing plates with rough surfaces giving rise to isotropic scattering. The biochemical parameters included in PROSPECT model are the chlorophyll content (C_{ab}), carotenoid content, dry matter (C_m), water content (C_w) and the leaf internal structure parameter (N). The PROSPECT model estimates the scattering process using the leaf structure parameter N and the spectral refractive index (n). Whilst, the absorption process is modeled using leaf chlorophyll concentration, water content, and the corresponding specific spectral absorption coefficients (K_{Cab} and K_w). In addition, PROSPECT assumes that the major light absorption is entirely caused by chlorophylls, although carotenoids (including xanthophyll pigments) and anthocyanins may be significant in greening or senescing leaves.

Several versions of PROSPECT model have been released since 1990. The PROSPECT-5 model (Feret et al., 2008) included separation between chlorophyll and carotenoids. This pigments separation performed in PROSPECT-5 can significantly improve the remote sensing capacity to retrieve photosynthetic rates and more accurate monitoring of vegetation stress (Jacquemoud et al., 2009). The latest version of PROSPECT model, PROSPECT-D (Féret et al., 2017) enables the simulation of leaf optical properties using the three main pigments (chlorophylls, carotenoids, and anthocyanins) that control the leaf optical properties, taking into account the plant lifecycle (leaf emergence, anthocyanin response to stress responses and leaf senescence).

The optical plant canopy properties largely depend on the optical properties of leaves, canopy scattering, and soil background. The simulation of reflectance at canopy level is the result of coupling different optical simulation models that take into account the leaf optical biochemical properties and the structure and composition of the canopy. One of the earliest canopy reflectance model was the scattering by arbitrary inclined leaves (SAIL) model (Verhoef, 1984, 1985). The SAIL model is an extension of the 1-D model developed by (Suits, 1971) to simulate the bidirectional reflectance at plant canopies, by solving the scattering and absorption of upward-downward radiative fluxes. The main biophysical variables included in SAIL model are the leaf area index (LAI), leaf inclination distribution function (LIDF), hot spot parameter, soil reflectance

and the viewing and solar zenith angles. Since the SAIL model was proposed, subsequent models have been developed to describe the vertically heterogeneity of the canopies, including multi-layer and multi-element one-dimensional models such as GeoSAIL (Verhoef and Bach, 2003). Advances in numerical approaches have allowed developing optimized versions of the SAIL model, such as 4SAIL (Verhoef et al., 2007). Other investigations coupled SAIL and geometric models to simulate discontinuous tree canopies using the shadowed and illuminated components, incorporating crown clumping, such as GeoSail (Huemmrich 2001). Besides this increase of complexity and new developments, SAIL has been adapted to include the fluorescence emission, such as in FLSAIL (Rosema et al., 1991), FluorSAIL (Miller et al., 2005), and the thermal emission in 4SAIL (Verhoef et al., 2007).

SAILH has been coupled with PROSPECT to derive PROSAIL (Baret et al., 1992) to reduce the dimensionality of the inverse problems and to assess the retrievals of plant traits at leaf and canopy levels. Later, PROSPECT has been widely coupled with most subsequent versions of SAIL that have been developed to characterize the heterogeneity within the canopy such as GeoSAIL (Verhoef and Bach, 2003), 2M-SAIL (le Maire et al., 2008), and 4SAIL2 (Verhoef and Bach, 2007). It has been also integrated into other canopy reflectance models such as i) DART (Discrete Anisotropic Radiative Transfer) for simulations in heterogeneous 3D-scenes (Gastellu-Etchegorry et al., 1996), ii) SPRINT (Spreading of Photons for Radiation INTerception) developed by Goel and Thompson (2000) and it has been used for chlorophyll content estimation through Monte Carlo model (Zarco-Tejada et al., 2004), iii) coupled FluorMODleaf+ FluorSAIL (FLIM; Forest Light Interaction Model) for assessment of tree-crowns components on the quantification of the fluorescence signal (Zarco-Tejada et al., 2013), iv) FLIGHT model (three-dimensional Forest LIGHT interaction) for estimation of forest fire fuel properties (Kötz et al., 2004), v) FluorWPS model (Fluorescence model with Weighted Photon Spread method) to compute sun-induced chlorophyll fluorescence at 3-D canopy (Zhao et al., 2016) and the vi) FluorFLIGHT 3-D to account for forest structure (Hernández-Clemente et al., 2017).

The retrieval of plant traits related (Vcmax, Jmax) to photosynthetic capacity derived from satellite and hyperspectral data combined with terrestrial biosphere models (TBMs) simulations are increasingly emerging. TBMs are the principal approach for providing accurately estimation of terrestrial carbon uptake at local and global scales

(Beer et al., 2010). In recent years, progress has been made to quantify photosynthetic capacity from hyperspectral and satellite imagery, enabling the development of TBMs at new spatial scales for estimating gross primary productivity by combining satellite-based SIF retrievals with the Soil Canopy Observation, Photochemistry and Energy fluxes (SCOPE) model developed by van der Tol et al. (2009) (Koffi et al., 2015; Zhang et al., 2018, 2014).

Traditionally, Vcmax and Jmax are estimated by fitting the photosynthesis biochemical model to gas-exchange measurements (Sharkey et al., 2007; Walker et al., 2014). Progress in TBMs has allowed to successfully estimate top-canopy photosynthetic capacity (Vcmax and Jmax) through chlorophyll fluorescence emission retrieved from satellites (Alton, 2017; Koffi et al., 2015; Zhang et al., 2018), imaging spectroscopy (Serbin et al., 2015) and spectrometers (Dechant et al., 2017). TBMs typically include a photosynthesis scheme coupled with leaf and canopy RTMs and balance energy models. In particular, SCOPE simulates reflectance and fluorescence emission of homogeneous vegetation canopies taking into account the leaf biochemical and biophysical traits, the photosynthesis process, vegetation structure, and micro meteorological conditions.

New advances in SCOPE have enabled to simulate spectral and bidirectional reflectance, fluorescence, and photosynthesis on vertically heterogeneous vegetation canopies, such as the subsequent mSCOPE model (Yang et al., 2017). The inclusion of vertical heterogeneity of leaf properties in SCOPE promise a better understanding of the relations between remote sensing data and plant functional traits. For photosynthesis, SCOPE uses the biochemical photosynthesis models based on the Farquhar–von Caemmerer–Berry (FvCB) model (Farquhar et al., 1980) for C_3, the Caemmerer model for C_4 (Caemmerer, 2000) and the coupled photosynthesis-stomatal model for C_3 (Collatz et al., 1991) and C_4 (Collatz, G., Ribas-Carbo, M., and Berry, 1992). At the leaf level, SCOPE model uses the Fluspect model (Vilfan et al., 2016), as an extension of PROSPECT, to simulates leaf reflectance, transmittance and fluorescence. At the canopy level, RTMo and RMTf (Van der Tol et al., 2016), which are based on 1-D SAIL model, compute the incident light radiation and emitted fluorescence.

The integration of the main biochemical photosynthesis models into TBMs enables the estimation of CO_2 assimilation across scales from leaf biochemistry to crop level. In

particular, RTMs coupled with biochemical photosynthesis models and balance energy models offer a physical-tool to investigate the effects of canopy structure and plant traits on the retrieval of chlorophyll fluorescence at the top of the canopy. They provide an estimation of canopy scattering of SIF by simulating the light-canopy interaction. Future works should address the development of spatial continuous maps of key photosynthetic traits at broad scales using TBMs and hyperspectral imagers. With this regard, this thesis is carried out for showing suitable methodologies for retrieving physiological traits using SIF derived from hyperspectral imagery and plant traits simulated by RMTs and TMBs.

References

Allen, W.A., Gausman, H.W., Richardson, A.J., 1970. Mean Effective Optical Constants of Cotton Leaves*. J. Opt. Soc. Am. 60, 542–547. https://doi.org/10.1364/JOSA.60.000542

Allen, W.A., Gausman, H.W., Richardson, A.J., Thomas, J.R., 1969. Interaction of Isotropic Light with a Compact Plant Leaf*. J. Opt. Soc. Am. 59, 1376–1379. https://doi.org/10.1364/JOSA.59.001376

Alton, P.B., 2017. Retrieval of seasonal Rubisco-limited photosynthetic capacity at global FLUXNET sites from hyperspectral satellite remote sensing: Impact on carbon modelling. Agric. For. Meteorol. 232, 74–88. https://doi.org/10.1016/j.agrformet.2016.08.001

Amoros-Lopez, J., Gomez-Chova, L., Vila-Frances, J., Alonso, L., Calpe, J., Moreno, J., Del Valle-Tascon, S., 2008. Evaluation of remote sensing of vegetation fluorescence by the analysis of diurnal cycles. Int. J. Remote Sens. 29, 5423–5436. https://doi.org/10.1080/01431160802036391

Amtmann, A., Armengaud, P., 2009. Effects of N, P, K and S on metabolism: new knowledge gained from multi-level analysis. Curr. Opin. Plant Biol. 12, 275–283. https://doi.org/10.1016/j.pbi.2009.04.014

Arena, C., Vitale, L., De Santo, A.V., 2008. Paraheliotropism in Robinia pseudoacacia L.: An efficient strategy to optimise photosynthetic performance under natural environmental conditions. Plant Biol. 10, 194–201. https://doi.org/10.1111/j.1438-8677.2008.00032.x

Baker, N.R., 2008. Chlorophyll Fluorescence: A Probe of Photosynthesis In Vivo. Annu. Rev. Plant Biol. 59, 89–113. https://doi.org/10.1146/annurev.arplant.59.032607.092759

Baret, F., Fourty, T., 1997. Estimation of leaf water content and specific leaf weight from reflectance and transmittance measurements. Agronomie 17, 455–464. https://doi.org/10.1051/agro:19970903

Baret, F., Jacquemoud, S., Guyot, G., Leprieur, C., 1992. Modeled analysis of the biophysical nature of spectral shifts and comparison with information content of broad bands. Remote Sens. Environ. 41, 133–142. https://doi.org/10.1016/0034-4257(92)90073-S

Barnabás, B., Jäger, K., Fehér, A., 2008. The effect of drought and heat stress on reproductive processes in cereals. Plant, Cell Environ. 31, 11–38. https://doi.org/10.1111/j.1365-3040.2007.01727.x

Bausch, W.C., Halvorson, A.D., Cipra, J., 2008. Quickbird satellite and ground-based multispectral data correlations with agronomic parameters of irrigated maize grown in small plots. Biosyst. Eng. 101, 306–315. https://doi.org/10.1016/j.biosystemseng.2008.09.011

Beer, C., Reichstein, M., Tomelleri, E., Ciais, P., Jung, M., Carvalhais, N., Rödenbeck, C., Arain, M.A., Baldocchi, D., Bonan, G.B., Bondeau, A., Cescatti, A., Lasslop, G., Lindroth, A., Lomas, M., Luyssaert, S., Margolis, H., Oleson, K.W., Roupsard, O., Veenendaal, E., Viovy, N., Williams, C., Woodward, F.I., Papale, D., 2010. Terrestrial Gross Carbon Dioxide Uptake: Global Distribution and Covariation with Climate. Science (80). 329, 834–838. https://doi.org/10.1126/science.1184984

Bellvert, J., Marsal, J., Girona, J., Gonzalez-Dugo, V., Fereres, E., Ustin, S.L., Zarco-Tejada, P.J., 2016. Airborne thermal imagery to detect the seasonal evolution of crop water status in peach, nectarine and Saturn peach orchards. Remote Sens. 8, 1–17. https://doi.org/10.3390/rs8010039

Blackmer, T.M., Schepers, J.S., Varvel, G.E., 1994. Light reflectance compared with other nitrogen stress measurements in corn leaves. Agron. J. 86, 934–938. https://doi.org/10.2134/agronj1994.00021962008600060002x

Bonfil, D.J., Karnieli, A., Raz, M., Mufradi, I., Asido, S., Egozi, H., Hoffman, A., Schmilovitch, Z., 2004. Decision support system for improving wheat grain quality in the Mediterranean area of Israel. F. Crop. Res. 89, 153–163. https://doi.org/10.1016/j.fcr.2004.01.017

Boyer, J.S., 1976. Photosynthesis at Low Water Potentials. Philos. Trans. R. Soc. Lond. B. Biol. Sci. 273, 501–512.

Caemmerer von, S., 2000. Biochemical models of leaf photosynthesis. Tech. Plant Sci. 53, 1689–1699. https://doi.org/10.1017/CBO9781107415324.004

Carmo-Silva, E., Andralojc, P.J., Scales, J.C., Driever, S.M., Mead, A., Lawson, T., Raines, C.A., Parry, M.A.J., 2017. Phenotyping of field-grown wheat in the UK highlights contribution of light response of photosynthesis and flag leaf longevity to grain yield. J. Exp. Bot. 68, 3473–3486. https://doi.org/10.1093/jxb/erx169

Cendrero-Mateo, M.P., Moran, M.S., Papuga, S.A., Thorp, K.R., Alonso, L., Moreno, J., Ponce-Campos, G., Rascher, U., Wang, G., 2016. Plant chlorophyll fluorescence: Active and passive measurements at canopy and leaf scales with

different nitrogen treatments. J. Exp. Bot. 67, 275–286. https://doi.org/10.1093/jxb/erv456

Chen, P., 2015. A Comparison of Two Approaches for Estimating the Wheat Nitrogen Nutrition Index Using Remote Sensing. Remote Sens. 7, 4527–4548. https://doi.org/10.3390/rs70404527

Clevers, J.G.P.W., Kooistra, L., 2012. Using hyperspectral remote sensing data for retrieving canopy chlorophyll and nitrogen content. IEEE J. Sel. Top. Appl. Earth Obs. Remote Sens. 5, 574–583. https://doi.org/10.1109/JSTARS.2011.2176468

Clevers, J.G.P.W., Kooistra, L., Schaepman, M.E., 2010. Estimating canopy water content using hyperspectral remote sensing data. Int. J. Appl. Earth Obs. Geoinf. 12, 119–125. https://doi.org/10.1016/j.jag.2010.01.007

Collatz, G., Ribas-Carbo, M., and Berry, J.A., 1992. Coupled photosynthesis-stomatal conductance model for leaves of C4 plants. Aus. J. Plant Physiol., 1 9, 519–538.

Collatz, G.J., Ball, J.T., Grivet, C., Berry, J.A., 1991. Physiological and environmental regulation of stomatal conductance, photosynthesis and transpiration: a model that includes a laminar boundary layer. Agric. For. Meteorol. 54, 107–136. https://doi.org/10.1016/0168-1923(91)90002-8

Colombo, R., Meroni, M., Marchesi, A., Busetto, L., Rossini, M., Giardino, C., Panigada, C., 2008. Estimation of leaf and canopy water content in poplar plantations by means of hyperspectral indices and inverse modeling. Remote Sens. Environ. 112, 1820–1834. https://doi.org/10.1016/j.rse.2007.09.005

Corp, L.A., McMurtrey, J.E., Middleton, E.M., Mulchi, C.L., Chappelle, E.W., Daughtry, C.S.T., 2003. Fluorescence sensing systems: In vivo detection of biophysical variations in field corn due to nitrogen supply. Remote Sens. Environ. 86, 470–479. https://doi.org/10.1016/S0034-4257(03)00125-1

Corp, L.A., Middleton, E.M., Campbell, P.K.E., Huemmrich, K.F., Cheng, Y.-B., Daughtry, C.S.T., 2009. Remote sensing techniques to monitor nitrogen-driven carbon dynamics in field corn. Proc. SPIE - Int. Soc. Opt. Eng. 7454, 1–11. https://doi.org/10.1117/12.825508

Cortazar, B., Koydemir, H.C., Tseng, D., Feng, S., Ozcan, A., 2015. Quantification of plant chlorophyll content using Google Glass. Lab Chip 15, 1708–16. https://doi.org/10.1039/c4lc01279h

Croft, H., Chen, J.M., Luo, X., Bartlett, P., Chen, B., Staebler, R.M., 2017. Leaf chlorophyll content as a proxy for leaf photosynthetic capacity. Glob. Chang. Biol. 23, 3513–3524. https://doi.org/10.1111/gcb.13599

Damm, A., Erler, A., Hillen, W., Meroni, M., Schaepman, M.E., Verhoef, W., Rascher, U., 2011. Modeling the impact of spectral sensor configurations on the FLD retrieval accuracy of sun-induced chlorophyll fluorescence. Remote Sens. Environ. 115, 1882–1892. https://doi.org/10.1016/j.rse.2011.03.011

Damm, A., Guanter, L., Paul-Limoges, E., van der Tol, C., Hueni, A., Buchmann, N., Eugster, W., Ammann, C., Schaepman, M.E., 2015. Far-red sun-induced chlorophyll fluorescence shows ecosystem-specific relationships to gross primary production: An assessment based on observational and modeling approaches. Remote Sens. Environ. 166, 91–105. https://doi.org/10.1016/j.rse.2015.06.004

Daumard, F., Goulas, Y., Champagne, S., Fournier, A., Ounis, A., Olioso, A., Moya, I., 2012. Continuous monitoring of canopy level sun-induced chlorophyll fluorescence during the growth of a sorghum field. IEEE Trans. Geosci. Remote Sens. 50, 4292–4300. https://doi.org/10.1109/TGRS.2012.2193131

Dechant, B., Cuntz, M., Vohland, M., Schulz, E., Doktor, D., 2017. Estimation of photosynthesis traits from leaf reflectance spectra: Correlation to nitrogen content as the dominant mechanism. Remote Sens. Environ. 196, 279–292. https://doi.org/10.1016/j.rse.2017.05.019

Ehleringer, J., Bjorkman, O., Mooney, H.A., 1976. Leaf Pubescence: Effects on Absorptance and Photosynthesis in a Desert Shrub. Science (80). 192, 376–377. https://doi.org/10.1126/science.192.4237.376

Ehrler, W.L., 1973. Cotton Leaf Temperatures as Related to Soil Water Depletion and Meteorological Factors1. Agron. J. 65, 404–409. https://doi.org/10.2134/agronj1973.00021962006500030016x

Evain, S., Flexas, J., Moya, I., 2004. A new instrument for passive remote sensing: 2. Measurement of leaf and canopy reflectance changes at 531 nm and their relationship with photosynthesis and chlorophyll fluorescence. Remote Sens. Environ. 91, 175–185. https://doi.org/10.1016/j.rse.2004.03.012

Evans, J., Terashima, I., 1987. Effects of Nitrogen Nutrition on Electron Transport Components and Photosynthesis in Spinach. Aust. J. Plant Physiol. 14, 59. https://doi.org/10.1071/PP9870059

Evans, J.R., 1983. Nitrogen and Photosynthesis in the Flag Leaf of Wheat (Triticum aestivum L.). Plant Physiol. 72, 297–302. https://doi.org/10.1104/pp.72.2.297

Evans, J.R., Sharkey, T.D., Berry, J.A., Farquhar, G.D., 1986. Carbon Isotope Discrimination measured Concurrently with Gas Exchange to Investigate CO2 Diffusion in Leaves of Higher Plants. Funct. Plant Biol. 13, 281–292.

Farquhar, G.D., von Caemmerer, S., Berry, J.A., 1980. A biochemical model of photosynthetic CO2 assimilation in leaves of C3 species. Planta 149, 78–90. https://doi.org/10.1007/BF00386231

Feret, J.B., François, C., Asner, G.P., Gitelson, A.A., Martin, R.E., Bidel, L.P.R., Ustin, S.L., le Maire, G., Jacquemoud, S., 2008. PROSPECT-4 and 5: Advances in the leaf optical properties model separating photosynthetic pigments. Remote Sens. Environ. 112, 3030–3043. https://doi.org/10.1016/j.rse.2008.02.012

Féret, J.B., Gitelson, A.A., Noble, S.D., Jacquemoud, S., 2017. PROSPECT-D: Towards modeling leaf optical properties through a complete lifecycle. Remote Sens. Environ. 193, 204–215. https://doi.org/10.1016/j.rse.2017.03.004

Ferwerda, J.G., Skidmore, A.K., Mutanga, O., 2005. Nitrogen detection with hyperspectral normalized ratio indices across multiple plant species. Int. J. Remote Sens. 26, 4083–4095. https://doi.org/10.1080/01431160500181044

Flexas, J., Briantais, J.M., Cerovic, Z., Medrano, H., Moya, I., 2000. Steady-state and maximum chlorophyll fluorescence responses to water stress in grapevine leaves: A new remote sensing system. Remote Sens. Environ. 73, 283–297. https://doi.org/10.1016/S0034-4257(00)00104-8

Flexas, J., Escalona, J.M., Evain, S., Gulías, J., Moya, I., Osmond, C.B., Medrano, H., 2002. Steady-state chlorophyll fluorescence (Fs) measurements as a tool to follow variations of net CO2 assimilation and stomatal conductance during water-stress in C3 plants. Eur. Sp. Agency, (Special Publ. ESA SP 26–29. https://doi.org/10.1034/j.1399-3054.2002.1140209.x

Flexas, J., Escalona, J.M., Medrano, H., 1999. Water stress induces different levels of photosynthesis and electron transport rate regulation in grapevines. Plant, Cell Environ. 22, 39–48. https://doi.org/10.1046/j.1365-3040.1999.00371.x

Flexas, J., Medrano, H., 2002. Drought-inhibition of photosynthesis in C3plants: Stomatal and non-stomatal limitations revisited. Ann. Bot. 89, 183–189. https://doi.org/10.1093/aob/mcf027

Frankenberg, C., Berry, J., 2018. Solar Induced Chlorophyll Fluorescence: Origins, Relation to Photosynthesis and Retrieval, Comprehensive Remote Sensing. Elsevier. https://doi.org/10.1016/B978-0-12-409548-9.10632-3

Frankenberg, C., Butz, A., Toon, G.C., 2011. Disentangling chlorophyll fluorescence from atmospheric scattering effects in O2 A-band spectra of reflected sun-light. Geophys. Res. Lett. 38, 1–5. https://doi.org/10.1029/2010GL045896

Galmés, J., Medrano, H., Flexas, J., 2007. Photosynthesis and photoinhibition in response to drought in a pubescent (var. minor) and a glabrous (var. palaui) variety of Digitalis minor. Environ. Exp. Bot. 60, 105–111. https://doi.org/10.1016/j.envexpbot.2006.08.001

Gamon, J.A., Field, C.B., Goulden, M.L., Griffin, K.L., Hartley, A.E., Joel, G., Penuelas, J., Valentini, R., 1995. Relationships between NDVI, canopy structure, and photosynthesis in three Californian vegetation types. Ecol. Appl. 5, 28–41. https://doi.org/10.2307/1942049

Gamon, J.A., Peñuelas, J., Field, C.B., 1992. A narrow-waveband spectral index that tracks diurnal changes in photosynthetic efficiency. Remote Sens. Environ. https://doi.org/10.1016/0034-4257(92)90059-S

Gastellu-Etchegorry, J.P., Demarez, V., Pinel, V., Zagolski, F., 1996. Modeling Radiative Transfer in Heterogeneous 3-D Vegetation Canopies 156, 131–156.

Genty, B., Briantais, J.M., Baker, N.R., 1989. The relationship between the quantum yield of photosynthetic electron transport and quenching of chlorophyll fluorescence. Biochim. Biophys. Acta - Gen. Subj. 990, 87–92. https://doi.org/10.1016/S0304-4165(89)80016-9

Giehl, R.F.H., Gruber, B.D., Von Wirén, N., 2014. It's time to make changes: Modulation of root system architecture by nutrient signals. J. Exp. Bot. 65, 769–778. https://doi.org/10.1093/jxb/ert421

Gimenez, C., Mitchell, V.J., Lawlor, D.W., 1992. Regulation of Photosynthetic Rate of Two Sunflower Hybrids under Water Stress. Plant Physiol. 98, 516–524. https://doi.org/10.1104/pp.98.2.516

Gitelson, A.A., Keydan, G.P., Merzlyak, M.N., 2006. Three-band model for noninvasive estimation of chlorophyll, carotenoids, and anthocyanin contents in higher plant leaves. Geophys. Res. Lett. 33. https://doi.org/10.1029/2006GL026457

Gitelson, A.A., Zur, Y., Chivkunova, O.B., Merzlyak, M.N., 2002. Assessing Carotenoid Content in Plant Leaves with Reflectance Spectroscopy. Photochem. Photobiol. 75, 272c

Gnyp, M.L., Bareth, G., Li, F., Lenz-Wiedemann, V.I.S., Koppe, W., Miao, Y., Hennig, S.D., Jia, L., Laudien, R., Chen, X., Zhang, F., 2014. Development and implementation of a multiscale biomass model using hyperspectral vegetation indices for winter wheat in the North China Plain. Int. J. Appl. Earth Obs. Geoinf. 33, 232–242. https://doi.org/10.1016/j.jag.2014.05.006

Goel, N.S., Thompson, R.L., 2000. A snapshot of canopy reflectance models and a universal nodel for the radiation regime. Remote Sens. Rev. 18, 197–225. https://doi.org/10.1080/02757250009532390

Gojon, A., Nacry, P., Davidian, J.C., 2009. Root uptake regulation: a central process for NPS homeostasis in plants. Curr. Opin. Plant Biol. 12, 328–338. https://doi.org/10.1016/j.pbi.2009.04.015

González-Dugo, M.P., Moran, M.S., Mateos, L., Bryant, R., 2006. Canopy temperature variability as an indicator of crop water stress severity. Irrig. Sci. 24, 233–240. https://doi.org/10.1007/s00271-005-0022-8

Gonzalez-Dugo, V., Goldhamer, D., Zarco-Tejada, P.J., Fereres, E., 2015. Improving the precision of irrigation in a pistachio farm using an unmanned airborne thermal system. Irrig. Sci. 33, 43–52. https://doi.org/10.1007/s00271-014-0447-z

Gonzalez-Dugo, Victoria, Hernandez, P., Solis, I., Zarco-Tejada, P.J., 2015. Using high-resolution hyperspectral and thermal airborne imagery to assess physiological

condition in the context of wheat phenotyping. Remote Sens. 7, 13586–13605. https://doi.org/10.3390/rs71013586

Gonzalez-Dugo, V., Lopez-Lopez, M., Espadafor, M., Orgaz, F., Testi, L., Zarco-Tejada, P., Lorite, I.J., Fereres, E., 2019. Transpiration from canopy temperature: Implications for the assessment of crop yield in almond orchards. Eur. J. Agron. 105, 78–85. https://doi.org/10.1016/j.eja.2019.01.010

Gonzalez-Dugo, V., Zarco-Tejada, P.J., Fereres, E., 2014. Applicability and limitations of using the crop water stress index as an indicator of water deficits in citrus orchards. Agric. For. Meteorol. 198–199, 94–104. https://doi.org/10.1016/j.agrformet.2014.08.003

Gruber, B.D., Giehl, R.F.H., Friedel, S., von Wiren, N., 2013. Plasticity of the Arabidopsis Root System under Nutrient Deficiencies. Plant Physiol. 163, 161–179. https://doi.org/10.1104/pp.113.218453

Haboudane, D., Miller, J.R., Tremblay, N., Zarco-Tejada, P.J., Dextraze, L., 2002. Integrated narrow-band vegetation indices for prediction of crop chlorophyll content for application to precision agriculture. Remote Sens. Environ. 81, 416–426. https://doi.org/10.1016/S0034-4257(02)00018-4

Hernández-Clemente, R., Navarro-Cerrillo, R.M., Zarco-Tejada, P.J., 2012. Carotenoid content estimation in a heterogeneous conifer forest using narrow-band indices and PROSPECT+DART simulations. Remote Sens. Environ. 127, 298–315. https://doi.org/10.1016/j.rse.2012.09.014

Hernández-Clemente, R., North, P.R.J., Hornero, A., Zarco-Tejada, P.J., 2017. Assessing the effects of forest health on sun-induced chlorophyll fluorescence using the FluorFLIGHT 3-D radiative transfer model to account for forest structure. Remote Sens. Environ. 193, 165–179. https://doi.org/10.1016/j.rse.2017.02.012

Herrmann, I., Karnieli, A., Bonfil, D.J., Cohen, Y., Alchanatis, V., 2010. SWIR-based spectral indices for assessing nitrogen content in potato fields. Int. J. Remote Sens. 31, 5127–5143. https://doi.org/10.1080/01431160903283892

Himelblau, E., Amasino, R.M., 2001. Nutrients mobilized from leaves of Arabidopsis thaliana during leaf senescence. J. Plant Physiol. 158, 1317–1323. https://doi.org/10.1078/0176-1617-00608

Hlavinka, J., Nauš, J., Špundová, M., 2013. Anthocyanin contribution to chlorophyll meter readings and its correction. Photosynth. Res. 118, 277–295. https://doi.org/10.1007/s11120-013-9934-y

Houborg, R., Cescatti, A., Migliavacca, M., Kustas, W.P., Yang, X., Tang, J., Mustard, J.F., Lee, J., Rossini, M., Rascher, U., Alonso, L., Burkart, A., Cilia, C., Cogliati, S., Colombo, R., Damm, A., Drusch, M., Guanter, L., Hanus, J., Hyvärinen, T., Julitta, T., Jussila, J., Kataja, K., Kokkalis, P., Kraft, S., Kraska, T., Matveeva, M., Moreno, J., Muller, O., Panigada, C., Pikl, M., Pinto, F., Prey, L., Pude, R.,

Rossini, M., Schickling, A., Schurr, U., Schüttemeyer, D., Verrelst, J., Zemek, F., Houborg, R., Cescatti, A., Migliavacca, M., Kustas, W.P., Genty, B., Briantais, J.M., Baker, N.R., 2013. Satellite retrievals of leaf chlorophyll and photosynthetic capacity for improved modeling of GPP. Agric. For. Meteorol. 117, 10–23. https://doi.org/10.1016/j.agrformet.2013.04.006

Hsiao, T.C., 1973. Plant Responses to Water Stress. Annu. Rev. Plant Physiol. 24, 519–570. https://doi.org/10.1146/annurev.pp.24.060173.002511

Huang, Z., Turner, B.J., Dury, S.J., Wallis, I.R., Foley, W.J., 2004. Estimating foliage nitrogen concentration from HYMAP data using continuum removal analysis. Remote Sens. Environ. 93, 18–29. https://doi.org/10.1016/j.rse.2004.06.008

Huemmrich, K.F., 2001. The GeoSail model: a simple addition to the SAIL model to describe discontinuous canopy reflectance. Remote Sens. Environ. 75, 423–431.

Idso, S.B., Jackson, R.D., Reginato, R.J., 1978. Extending the "Degree Day" Concept of Plant Phenological Development to Include Water Stress Effects. Ecology 59, 431–433. https://doi.org/10.2307/1936570

Idso, S.B., Jackson, R.D., Reginato, R.J., 1977. Remote-sensing of crop yields. Science (80). 196, 19–25. https://doi.org/10.1126/science.196.4285.19

Inoue, Y., Sakaiya, E., Zhu, Y., Takahashi, W., 2012. Diagnostic mapping of canopy nitrogen content in rice based on hyperspectral measurements. Remote Sens. Environ. 126, 210–221. https://doi.org/10.1016/j.rse.2012.08.026

IPCC, 2014. Climate change 2014. Synthesis report. Versión inglés, Climate Change 2014: Synthesis Report. Contribution of Working Groups I, II and III to the Fifth Assessment Report of the Intergovernmental Panel on Climate Change. https://doi.org/10.1017/CBO9781107415324

Jackson, R.D., Idso, S.B., Reginato, R.J., Pinter, J.P.J., 1981. Canopy temperature as a crop water stress indicator. Water Resour. Res. 17, 1133–1138. https://doi.org/10.1029/WR017i004p01133

Jackson, R.D., Reginato, R.J., Idso, S.B., 1977. Wheat canopy temperature: A practical tool for evaluating water requirements. Water Resour. Res. 13, 651–656. https://doi.org/10.1029/WR013i003p00651

Jacquemoud, S., Baret, F., 1990. PROSPECT: A model of leaf optical properties spectra. Remote Sens. Environ. 34, 75–91. https://doi.org/10.1016/0034-4257(90)90100-Z

Jacquemoud, S., Verhoef, W., Baret, F., Bacour, C., Zarco-Tejada, P.J., Asner, G.P., François, C., Ustin, S.L., 2009. PROSPECT + SAIL models: A review of use for vegetation characterization. Remote Sens. Environ. 113, S56–S66. https://doi.org/10.1016/j.rse.2008.01.026

Jin, X., Yang, G., Tan, C., Zhao, C., 2015. Effects of nitrogen stress on the photosynthetic CO2 assimilation, chlorophyll fluorescence, and sugar-nitrogen ratio in corn. Sci. Rep. 5, 9311. https://doi.org/10.1038/srep09311

Johnson, L.F., 2001. Nitrogen influence on fresh-leaf NIR spectra. Remote Sens. Environ. 78, 314–320. https://doi.org/10.1016/S0034-4257(01)00226-7

Joiner, J., Yoshida, Y., Vasilkov, A.P., Yoshida, Y., Corp, L.A., Middleton, E.M., 2011. First observations of global and seasonal terrestrial chlorophyll fluorescence from space. Biogeosciences 8, 637–651. https://doi.org/10.5194/bg-8-637-2011

Jury, W.A., Vaux, H.J., 2007. The Emerging Global Water Crisis: Managing Scarcity and Conflict Between Water Users. Adv. Agron. 95, 1–76. https://doi.org/10.1016/S0065-2113(07)95001-4

Khamis, S., Lamaze, T., Lemoine, Y., Foyer, C., 1990. Adaptation of the Photosynthetic Apparatus in Maize Leaves as a Result of Nitrogen Limitation : Relationships between Electron Transport and Carbon Assimilation. Plant Physiol. 94, 1436–1443. https://doi.org/10.1104/pp.94.3.1436

Koetz, B., Baret, F., Poilvé, H., Hill, J., 2005. Use of coupled canopy structure dynamic and radiative transfer models to estimate biophysical canopy characteristics. Remote Sens. Environ. 95, 115–124. https://doi.org/10.1016/j.rse.2004.11.017

Koffi, E.N., Rayner, P.J., Norton, A.J., Frankenberg, C., Scholze, M., 2015. Investigating the usefulness of satellite-derived fluorescence data in inferring gross primary productivity within the carbon cycle data assimilation system. Biogeosciences 12, 4067–4084. https://doi.org/10.5194/bg-12-4067-2015

Kokaly, R., 1999. Spectroscopic Determination of Leaf Biochemistry Using Band-Depth Analysis of Absorption Features and Stepwise Multiple Linear Regression. Remote Sens. Environ. 67, 267–287. https://doi.org/10.1016/S0034-4257(98)00084-4

Kolber, Z., Klimov, D., Ananyev, G., Rascher, U., Berry, J., Osmond, B., 2005. Measuring photosynthetic parameters at a distance: laser induced fluorescence transient (LIFT) method for remote measurements of photosynthesis in terrestrial vegetation. Photosynth. Res. 84, 121–129. https://doi.org/10.1007/s11120-005-5092-1

Kötz, B., Schaepman, M., Morsdorf, F., Bowyer, P., Itten, K., Allgöwer, B., 2004. Radiative transfer modeling within a heterogeneous canopy for estimation of forest fire fuel properties. Remote Sens. Environ. 92, 332–344. https://doi.org/10.1016/j.rse.2004.05.015

Kramer, D.M., Avenson, T.J., Edwards, G.E., 2004. Dynamic flexibility in the light reactions of photosynthesis governed by both electron and proton transfer reactions. Trends Plant Sci. 9, 349–357. https://doi.org/https://doi.org/10.1016/j.tplants.2004.05.001

Lamaoui, M., Jemo, M., Datla, R., Bekkaoui, F., 2018. Heat and Drought Stresses in Crops and Approaches for Their Mitigation. Front. Chem. 6, 1–14. https://doi.org/10.3389/fchem.2018.00026

Lawlor, D.W., Cornic, G., 2002. Photosynthetic carbon assimilation and associated metabolism in relation to water deficits in higher plants. Plant, Cell Environ. 25, 275–294. https://doi.org/10.1046/j.0016-8025.2001.00814.x

le Maire, G., François, C., Soudani, K., Berveiller, D., Pontailler, J.Y., Bréda, N., Genet, H., Davi, H., Dufrêne, E., 2008. Calibration and validation of hyperspectral indices for the estimation of broadleaved forest leaf chlorophyll content, leaf mass per area, leaf area index and leaf canopy biomass. Remote Sens. Environ. 112, 3846–3864. https://doi.org/10.1016/j.rse.2008.06.005

Li, F., Gnyp, M.L., Jia, L., Miao, Y., Yu, Z., Koppe, W., Bareth, G., Chen, X., Zhang, F., 2008. Estimating N status of winter wheat using a handheld spectrometer in the North China Plain. F. Crop. Res. 106, 77–85. https://doi.org/10.1016/j.fcr.2007.11.001

Li, F., Mistele, B., Hu, Y., Chen, X., Schmidhalter, U., 2014. Reflectance estimation of canopy nitrogen content in winter wheat using optimised hyperspectral spectral indices and partial least squares regression. Eur. J. Agron. 52, 198–209. https://doi.org/10.1016/j.eja.2013.09.006

Lobell, D.B., Schlenker, W., Costa-Roberts, J., 2011. Climate Trends and Global Crop Production Since 1980. Science (80). 333, 616–620. https://doi.org/10.1126/science.1204531

Lu, C., Zhang, J., 2000. Photosynthetic CO2 assimilation, chlorophyl fluorescence and photoinhibition as affected by nitrogen deficiency in maize plants. Plant Sci. 151, 135–143.

Mahajan, G.R., Pandey, R.N., Sahoo, R.N., Gupta, V.K., Datta, S.C., Kumar, D., 2016. Monitoring nitrogen, phosphorus and sulphur in hybrid rice (Oryza sativa L.) using hyperspectral remote sensing. Precis. Agric. 1–26. https://doi.org/10.1007/s11119-016-9485-2

Mahajan, G.R., Sahoo, R.N., Pandey, R.N., Gupta, V.K., Kumar, D., 2014. Using hyperspectral remote sensing techniques to monitor nitrogen, phosphorus, sulphur and potassium in wheat (Triticum aestivum L.). Precis. Agric. 15, 499–522. https://doi.org/10.1007/s11119-014-9348-7

Maillard, A., Diquélou, S., Billard, V., Laîné P., Garnica, M., Prudent, M., Garcia-Mina, J.-M., Yvin, J.-C., Ourry, A., 2015. Leaf mineral nutrient remobilization during leaf senescence and modulation by nutrient deficiency. Front. Plant Sci. 6, 1–15. https://doi.org/10.3389/fpls.2015.00317

Makino, A., Mae, T., Ohira, K., 1984. Relation between Nitrogen and Ribulose-1,5-bisphosphate Carboxylase in Rice Leaves from Emergence through Senescence.

Plant Cell Physiol. 25, 429–437. https://doi.org/10.1093/oxfordjournals.pcp.a076730

Malagoli, P., Laine, P., Rossato, L., Ourry, A., 2005. Dynamics of nitrogen uptake and mobilization in field-grown winter oilseed rape (Brassica napus) from stem extension to harvest: I. Global N flows between vegetative and reproductive tissues in relation to leaf fall and their residual N. Ann. Bot. 95, 853–861. https://doi.org/10.1093/aob/mci091

Masclaux-Daubresse, C., Daniel-Vedele, F., Dechorgnat, J., Chardon, F., Gaufichon, L., Suzuki, A., 2010. Nitrogen uptake, assimilation and remobilization in plants: Challenges for sustainable and productive agriculture. Ann. Bot. 105, 1141–1157. https://doi.org/10.1093/aob/mcq028

Medrano, H., Parry, M.A.J., Socias, X., Lawlor, D.W., 1997. Long term water stress inactivates Rubisco in subterranean clover. Ann. Appl. Biol. 131, 491–501. https://doi.org/10.1111/j.1744-7348.1997.tb05176.x

Meron, M., Tsipris, J., Orlov, V., Alchanatis, V., Cohen, Y., 2010. Crop water stress mapping for site-specific irrigation by thermal imagery and artificial reference surfaces. Precis. Agric. 11, 148–162. https://doi.org/10.1007/s11119-009-9153-x

Meroni, M., Busetto, L., Colombo, R., Guanter, L., Moreno, J., Verhoef, W., 2010. Performance of Spectral Fitting Methods for vegetation fluorescence quantification. Remote Sens. Environ. 114, 363–374. https://doi.org/10.1016/j.rse.2009.09.010

Meroni, M., Colombo, R., 2006. Leaf level detection of solar induced chlorophyll fluorescence by means of a subnanometer resolution spectroradiometer. Remote Sens. Environ. 103, 438–448. https://doi.org/10.1016/j.rse.2006.03.016

Meroni, M., Rossini, M., Guanter, L., Alonso, L., Rascher, U., Colombo, R., Moreno, J., 2009. Remote sensing of solar-induced chlorophyll fluorescence: Review of methods and applications. Remote Sens. Environ. 113, 2037–2051. https://doi.org/10.1016/j.rse.2009.05.003

Meyer, S., Genty, B., 1999. Heterogeneous inhibition of photosynthesis over the leaf surface of Rosa rubiginosa L. during water stress and abscisic acid treatment: induction of a metabolic component by limitation of CO 2 diffusion. Planta 210, 126–131.

Monteith, J.L., Szeicz, G., 1962. Radiative temperature in the heat balance of natural surfaces. Q. J. R. Meteorol. Soc. 88, 496–507. https://doi.org/10.1002/qj.4970883781

Morales, F., Abadía, A., Abadía, J., Montserrat, G., Gil-Pelegrín, E., 2002. Trichomes and photosynthetic pigment composition changes: Responses of Quercus ilex subsp. ballota (Desf.) Samp. and Quercus coccifera L. to Mediterranean stress conditions. Trees - Struct. Funct. 16, 504–510. https://doi.org/10.1007/s00468-002-0195-1

Miller, J., Berger, M., Goulas, Y., Jacquemoud, S., Louis, J., Mohammed, G., et al. (2005). Development ofa Vegetation Fluorescence Canopy Model, ESTEC Contract No. 16365/ 02/NL/FF. 138 pp. (http://www.ias.csic.es/fluormod/

Moya, I., Camenen, L., Evain, S., Goulas, Y., Cerovic, Z.G., Latouche, G., Flexas, J., Ounis, A., 2004. A new instrument for passive remote sensing: 1. Measurements of sunlight-induced chlorophyll fluorescence. Remote Sens. Environ. 91, 186–197. https://doi.org/10.1016/j.rse.2004.02.012

Muñoz-Huerta, R.F., Guevara-Gonzalez, R.G., Contreras-Medina, L.M., Torres-Pacheco, I., Prado-Olivarez, J., Ocampo-Velazquez, R. V., 2013. A review of methods for sensing the nitrogen status in plants: advantages, disadvantages and recent advances. Sensors (Basel). 13, 10823–10843. https://doi.org/10.3390/s130810823

Nichol, C.J., Rascher, U., Matsubara, S., Osmond, B., 2006. Assessing photosynthetic efficiency in an experimental mangrove canopy using remote sensing and chlorophyll fluorescence. Trees - Struct. Funct. 20, 9–15. https://doi.org/10.1007/s00468-005-0005-7

Nobel, P.S., 2009. Conversion Factors and Definitions. Physicochem. Environ. plant Physiol. 553–556. https://doi.org/10.1016/B978-0-12-374143-1.00014-4

Norton, A.J., Rayner, P.J., Koffi, E.N., Scholze, M., 2017. Assimilating solar-induced chlorophyll fluorescence into the terrestrial biosphere model BETHY-SCOPE: Model description and information content. Geosci. Model Dev. Discuss. 1–26. https://doi.org/10.5194/gmd-2017-34

Nunes, M.A., Ramalho, J.D.C., Dias, M.A., 1993. Effect of nitrogen supply on the photosynthetic performance of leaves from coffee plants exposed to bright light. J. Exp. Bot. 44, 893–899. https://doi.org/10.1093/jxb/44.5.893

Palombi, L., Cecchi, G., Lognoli, D., Raimondi, V., Toci, G., Agati, G., 2011. A retrieval algorithm to evaluate the Photosystem i and Photosystem II spectral contributions to leaf chlorophyll fluorescence at physiological temperatures. Photosynth. Res. 108, 225–239. https://doi.org/10.1007/s11120-011-9678-5

Parry, M., Delgado, E., Vadell, J., Keys, A., Lawlor, D., Medrano, H., 1993. stress and the diurnal activity of ribulose-1, 5-bisphosphate carboxylase in field grown Nicotiana tabacum genotypes selected for survival at low CO2 concentrations. Plant Physiol. Biochem. 31, 113–120.

Parry, M.A.J., Andralojc, P.J., Khan, S., Lea, P.J., Keys, A.J., 2002. Rubisco activity: Effects of drought stress. Ann. Bot. 89, 833–839. https://doi.org/10.1093/aob/mcf103

Pérez-Priego, O., Zarco-Tejada, P.J., Miller, J.R., Sepulcre-Cantó, G., Fereres, E., 2005. Detection of water stress in orchard trees with a high-resolution spectrometer

through chlorophyll fluorescence In-Filling of the O2-A band. IEEE Trans. Geosci. Remote Sens. 43, 2860–2868. https://doi.org/10.1109/TGRS.2005.857906

Pimstein, A., Karnieli, A., Bansal, S.K., Bonfil, D.J., 2011. Exploring remotely sensed technologies for monitoring wheat potassium and phosphorus using field spectroscopy. F. Crop. Res. 121, 125–135. https://doi.org/10.1016/j.fcr.2010.12.001

Plascyk, J.A., Gabriel, F.C., 1975. The Fraunhofer line discriminator MKII an airborne instrument for precise and standardized ecological luminescence measurement. IEEE Trans. Instrum. Meas. 24, 306–313. https://doi.org/10.1109/TIM.1975.4314448

Porcar-Castell, A., Tyystjärvi, E., Atherton, J., Van Der Tol, C., Flexas, J., Pfündel, E.E., Moreno, J., Frankenberg, C., Berry, J.A., 2014. Linking chlorophyll a fluorescence to photosynthesis for remote sensing applications: Mechanisms and challenges. J. Exp. Bot. 65, 4065–4095. https://doi.org/10.1093/jxb/eru191

Quemada, M., Gabriel, J.L., Zarco-Tejada, P., 2014. Airborne hyperspectral images and ground-level optical sensors as assessment tools for maize nitrogen fertilization. Remote Sens. 6, 2940–2962. https://doi.org/10.3390/rs6042940

Quick, W.P., Horton, P., 1984. Studies on the Induction of Chlorophyll Fluorescence in Barley Protoplasts. II. Resolution of Fluorescence Quenching by Redox State and the Transthylakoid pH Gradient. Proc. R. Soc. B Biol. Sci. 220, 371–382. https://doi.org/10.1098/rspb.1984.0007

Reddy, A.R., Chaitanya, K.V., Vivekanandan, M., 2004. Drought-induced responses of photosynthesis and antioxidant metabolism in higher plants. J. Plant Physiol. 161, 1189–1202. https://doi.org/10.1016/j.jplph.2004.01.013

Rodriguez, D., Fitzgerald, G.J., Belford, R., Christensen, L.K., 2006. Detection of nitrogen deficiency in wheat from spectral reflectance indices and basic crop eco-physiological concepts. Aust. J. Agric. Res. 57, 781–789. https://doi.org/10.1071/AR05361

Rosema, A., Verhoef, W., Schroote, J., Snel, J.F.H., 1991. Simulating fluorescence light-canopy interaction in support of laser-induced fluorescence measurements. Remote Sens. Environ. 37, 117–130. https://doi.org/10.1016/0034-4257(91)90023-Y

Rouse, J.W., Hass, R.H., Schell, J.A., Deering, D.W., 1973. Monitoring vegetation systems in the great plains with ERTS. Third Earth Resour. Technol. Satell. Symp. 1, 309–317. https://doi.org/citeulike-article-id:12009708

Sarvikas, P., Hakala-Yatkin, M., Dönmez, S., Tyystjärvi, E., 2010. Short flashes and continuous light have similar photoinhibitory efficiency in intact leaves. J. Exp. Bot. 61, 4239–4247. https://doi.org/10.1093/jxb/erq224

Schächtl, J., Huber, G., Maidl, F.-X., Sticksel, E., Schulz, J., Haschberger, P., 2005. Laser-Induced Chlorophyll Fluorescence Measurements for Detecting the Nitrogen Status of Wheat (Triticum aestivum L.) Canopies. Precis. Agric. 6, 143–156. https://doi.org/10.1007/s11119-004-1031-y

Schlerf, M., Atzberger, C., 2006. Inversion of a forest reflectance model to estimate structural canopy variables from hyperspectral remote sensing data. Remote Sens. Environ. 100, 281–294. https://doi.org/10.1016/j.rse.2005.10.006

Seemann, J.R., Sharkey, T.D., Wang, J.L., Osmond, C.B., 1987. Environmental effects on photosynthesis, nitrogen-use efficiency, and metabolite pools in leaves of sun and shade plants. Plant Physiol. 84, 796–802. https://doi.org/10.1104/pp.84.3.796

Sehgal, V.K., Chakraborty, D., Sahoo, R.N., 2016. Inversion of radiative transfer model for retrieval of wheat biophysical parameters from broadband reflectance measurements. Inf. Process. Agric. 3, 107–118. https://doi.org/10.1016/j.inpa.2016.04.001

Sepulcre-Cantó, G., Zarco-Tejada, P.J., Jiménez-Muñoz, J.C., Sobrino, J.A., Miguel, E. De, Villalobos, F.J., 2006. Detection of water stress in an olive orchard with thermal remote sensing imagery. Agric. For. Meteorol. 136, 31–44. https://doi.org/10.1016/j.agrformet.2006.01.008

Sepulcre-Cantó, G., Zarco-Tejada, P.J., Jiménez-Muñoz, J.C., Sobrino, J.A., Soriano, M.A., Fereres, E., Vega, V., Pastor, M., 2007. Monitoring yield and fruit quality parameters in open-canopy tree crops under water stress. Implications for ASTER. Remote Sens. Environ. 107, 455–470. https://doi.org/10.1016/j.rse.2006.09.014

Serbin, S.P., Singh, A., Desai, A.R., Dubois, S.G., Jablonski, A.D., Kingdon, C.C., Kruger, E.L., Townsend, P.A., 2015. Remotely estimating photosynthetic capacity, and its response to temperature, in vegetation canopies using imaging spectroscopy. Remote Sens. Environ. 167, 78–87. https://doi.org/10.1016/j.rse.2015.05.024

Serrano, L., Penuelas, J., Ustin, S.L., 2002. Remote sensing of nitrogen and lignin in Mediterranean vegetation\rfrom AVIRIS data:\rDecomposing biochemical from structural signals. Remote Sens. Environ. 81, 355–364.

Shao, H.B., Chu, L.Y., Jaleel, C.A., Zhao, C.X., 2008. Water-deficit stress-induced anatomical changes in higher plants. Comptes Rendus - Biol. 331, 215–225. https://doi.org/10.1016/j.crvi.2008.01.002

Sharkey, T.D., Bernacchi, C.J., Farquhar, G.D., Singsaas, E.L., 2007. Fitting photosynthetic carbon dioxide response curves for C3 leaves. Plant, Cell Environ. 30, 1035–1040. https://doi.org/10.1111/j.1365-3040.2007.01710.x

Silva-Perez, V., Molero, G., Serbin, S.P., Condon, A.G., Reynolds, M.P., Furbank, R.T., Evans, J.R., 2018. Hyperspectral reflectance as a tool to measure biochemical and physiological traits in wheat. J. Exp. Bot. 69, 483–496. https://doi.org/10.1093/jxb/erx421

Slatyer R. O, 1967. Plant-water relationships. Academic Press.

Smith, W.K., Biederman, J.A., Scott, R.L., Moore, D.J.P., He, M., Kimball, J.S., Yan, D., Hudson, A., Barnes, M.L., Macbean, N., Fox, A.M., Litvak, M.E., 2018. Chlorophyll Fluorescence Better Captures Seasonal and Interannual Gross Primary Productivity Dynamics Across Dryland Ecosystems of Southwestern North America. Geophys. Res. Lett. 748–757. https://doi.org/10.1002/2017GL075922

Stroppiana, D., Boschetti, M., Brivio, P.A., Bocchi, S., 2009. Plant nitrogen concentration in paddy rice from field canopy hyperspectral radiometry. F. Crop. Res. 111, 119–129. https://doi.org/10.1016/j.fcr.2008.11.004

Suits, G.H., 1971. The calculation of the directional reflectance of a vegetative canopy. Remote Sens. Environ. 2, 117–125. https://doi.org/https://doi.org/10.1016/0034-4257(71)90085-X

Taghvaeian, S., Chávez, J.L., Hansen, N.C., 2012. Infrared thermometry to estimate crop water stress index and water use of irrigated maize in northeastern colorado. Remote Sens. 4, 3619–3637. https://doi.org/10.3390/rs4113619

Tanner, C. B., Plant temperatures, Agron. J., 55, 210-211, 1963

Tezara, W., Mitchell, V.J., Driscoll, S.D., Lawlor, D.W., 1999. Water stress inhibits plant photosynthesis by decreasing coupling factor and ATP. Nature 401, 914–917. https://doi.org/10.1038/44842

Thoren, D., Schmidhalter, U., 2009. Nitrogen status and biomass determination of oilseed rape by laser-induced chlorophyll fluorescence. Eur. J. Agron. 30, 238–242. https://doi.org/10.1016/j.eja.2008.12.001

Tremblay, N., Fallon, E., Ziadi, N., 2011. Sensing of crop nitrogen status: Opportunities, tools, limitations, and supporting information requirements. Horttechnology 21, 274–281.

Tremblay, N., Wang, Z., Cerovic, Z.G., 2012. Sensing crop nitrogen status with fluorescence indicators. A review. Agron. Sustain. Dev. 32, 451–464. https://doi.org/10.1007/s13593-011-0041-1

Uddling, J., Gelang-Alfredsson, J., Piikki, K., Pleijel, H., 2007. Evaluating the relationship between leaf chlorophyll concentration and SPAD-502 chlorophyll meter readings. Photosynth. Res. 91, 37–46. https://doi.org/10.1007/s11120-006-9077-5

Upreti, D., Huang, W., Kong, W., Pascucci, S., Pignatti, S., Zhou, X., Ye, H., Casa, R., 2019. A Comparison of Hybrid Machine Learning Algorithms for the Retrieval of Wheat Biophysical Variables from Sentinel-2. Remote Sens. 11, 481. https://doi.org/10.3390/rs11050481

van der Tol, C., Rossini, M., Cogliati, S., Verhoef, W., Colombo, R., Rascher, U., Mohammed, G., 2016. A model and measurement comparison of diurnal cycles of sun-induced chlorophyll fluorescence of crops. Remote Sens. Environ. 186, 663–677. https://doi.org/10.1016/j.rse.2016.09.021

van der Tol, C., Verhoef, W., Timmermans, J., Verhoef, A., Su, Z., 2009. An integrated model of soil-canopy spectral radiances, photosynthesis, fluorescence, temperature and energy balance. Biogeosciences 6, 3109–3129. https://doi.org/10.5194/bg-6-3109-2009

Verhoef, W., 1985. Earth observation modeling based on layer scattering matrices. Remote Sens. Environ. 17, 165–178. https://doi.org/https://doi.org/10.1016/0034-4257(85)90072-0

Verhoef, W., 1984. Light scattering by leaf layers with application to canopy reflectance modeling: The SAIL model. Remote Sens. Environ. 16, 125–141. https://doi.org/10.1016/0034-4257(84)90057-9

Verhoef, W., Bach, H., 2007. Coupled soil-leaf-canopy and atmosphere radiative transfer modeling to simulate hyperspectral multi-angular surface reflectance and TOA radiance data. Remote Sens. Environ. 109, 166–182. https://doi.org/10.1016/j.rse.2006.12.013

Verhoef, W., Bach, H., 2003. Remote sensing data assimilation using coupled radiative transfer models. Phys. Chem. Earth 28, 3–13. https://doi.org/10.1016/S1474-7065(03)00003-2

Verhoef, W., Jia, L., Xiao, Q., Su, Z., 2007. Unified Optical-Thermal Four-Stream Radiative Transfer Theory for Homogeneous Vegetation Canopies. IEEE Trans. Geosci. Remote Sens. 45, 1808–1822. https://doi.org/10.1109/TGRS.2007.895844

Verrelst, J., Camps-Valls, G., Muñoz-Marí, J., Rivera, J.P., Veroustraete, F., Clevers, J.G.P.W., Moreno, J., 2015. Optical remote sensing and the retrieval of terrestrial vegetation bio-geophysical properties - A review. ISPRS J. Photogramm. Remote Sens. 108, 273–290. https://doi.org/10.1016/j.isprsjprs.2015.05.005

Vilfan, N., van der Tol, C., Muller, O., Rascher, U., Verhoef, W., 2016. Fluspect-B: A model for leaf fluorescence, reflectance and transmittance spectra. Remote Sens. Environ. 186, 596–615. https://doi.org/10.1016/j.rse.2016.09.017

Walker, A.P., Beckerman, A.P., Gu, L., Kattge, J., Cernusak, L.A., Domingues, T.F., Scales, J.C., Wohlfahrt, G., Wullschleger, S.D., Woodward, F.I., 2014. The relationship of leaf photosynthetic traits - Vcmax and Jmax - to leaf nitrogen, leaf phosphorus, and specific leaf area: A meta-analysis and modeling study. Ecol. Evol. 4, 3218–3235. https://doi.org/10.1002/ece3.1173

Wang, W., Yao, Xia, Yao, XinFeng, Tian, Y., Liu, X., Ni, J., Cao, W., Zhu, Y., 2012. Estimating leaf nitrogen concentration with three-band vegetation indices in rice and wheat. F. Crop. Res. 129, 90–98. https://doi.org/10.1016/j.fcr.2012.01.014

Wang, Z., Kawamura, K., Sakuno, Y., Fan, X., Gong, Z., Lim, J., 2017. Retrieval of chlorophyll-a and total suspended solids using iterative stepwise elimination partial

least squares (ISE-PLS) regression based on field hyperspectral measurements in irrigation ponds in Higashihiroshima, Japan. Remote Sens. 9, 1–14. https://doi.org/10.3390/rs9030264

Wang, Z., Skidmore, A.K., Wang, T., Darvishzadeh, R., Hearne, J., 2015. Applicability of the PROSPECT model for estimating protein and cellulose + lignin in fresh leaves. Remote Sens. Environ. 168, 205–218. https://doi.org/10.1016/j.rse.2015.07.007

Wong, K., He, Y., 2013. Estimating grassland chlorophyll content using remote sensing data at leaf, canopy, and landscape scales. Can. J. Remote Sens. 39, 155–166. https://doi.org/10.5589/m13-021

Yang, P., Verhoef, W., van der Tol, C., 2017. The mSCOPE model: A simple adaptation to the SCOPE model to describe reflectance, fluorescence and photosynthesis of vertically heterogeneous canopies. Remote Sens. Environ. 201, 1–11. https://doi.org/10.1016/j.rse.2017.08.029

Yang, X., Tang, J., Mustard, J.F., Lee, J., Rossini, M., Rascher, U., Alonso, L., Burkart, A., Cilia, C., Cogliati, S., Colombo, R., Damm, A., Drusch, M., Guanter, L., Hanus, J., Hyvärinen, T., Julitta, T., Jussila, J., Kataja, K., Kokkalis, P., Kraft, S., Kraska, T., Matveeva, M., Moreno, J., Muller, O., Panigada, C., Pikl, M., Pinto, F., Prey, L., Pude, R., Rossini, M., Schickling, A., Schurr, U., Schüttemeyer, D., Verrelst, J., Zemek, F., Houborg, R., Cescatti, A., Migliavacca, M., Kustas, W.P., Genty, B., Briantais, J.M., Baker, N.R., 2015. Satellite retrievals of leaf chlorophyll and photosynthetic capacity for improved modeling of GPP. Agric. For. Meteorol. 990, 10–23. https://doi.org/10.1111/gcb.13017

Yu, K., Gnyp, M.L., Gao, L., Miao, Y., Chen, X., Bareth, G., 2015. Estimate Leaf Chlorophyll of Rice Using Reflectance Indices and Partial Least Squares. Photogramm. - Fernerkundung - Geoinf. 2015, 45–54. https://doi.org/10.1127/pfg/2015/0253

Zarco-Tejada, P.J., Camino, C., Beck, P.S.A.A., Calderon, R., Hornero, A., Hernández-Clemente, R., Kattenborn, T., Montes-Borrego, M., Susca, L., Morelli, M., Gonzalez-Dugo, V., North, P.R.J.J., Landa, B.B., Boscia, D., Saponari, M., Navas-Cortes, J.A., 2018. Previsual symptoms of Xylella fastidiosa infection revealed in spectral plant-trait alterations. Nat. Plants 4, 432–439. https://doi.org/10.1038/s41477-018-0189-7

Zarco-Tejada, P.J., González-Dugo, V., Berni, J.A.J., 2012. Fluorescence, temperature and narrow-band indices acquired from a UAV platform for water stress detection using a micro-hyperspectral imager and a thermal camera. Remote Sens. Environ. 117, 322–337. https://doi.org/10.1016/j.rse.2011.10.007

Zarco-Tejada, P.J., González-Dugo, M. V., Fereres, E., 2016. Seasonal stability of chlorophyll fluorescence quantified from airborne hyperspectral imagery as an indicator of net photosynthesis in the context of precision agriculture. Remote Sens. Environ. 179, 89–103. https://doi.org/10.1016/j.rse.2016.03.024

Zarco-Tejada, P. J., González-Dugo, V., Williams, L.E., Suárez, L., Berni, J.A.J., Goldhamer, D., Fereres, E., 2013a. A PRI-based water stress index combining structural and chlorophyll effects: Assessment using diurnal narrow-band airborne imagery and the CWSI thermal index. Remote Sens. Environ. 138, 38–50. https://doi.org/10.1016/j.rse.2013.07.024

Zarco-Tejada, P. J., González-Dugo, V., Williams, L.E., Suárez, L., Berni, J.A.J.J., Goldhamer, D., Fereres, E., 2013b. A PRI-based water stress index combining structural and chlorophyll effects: Assessment using diurnal narrow-band airborne imagery and the CWSI thermal index. Remote Sens. Environ. 138, 38–50. https://doi.org/10.1016/j.rse.2013.07.024

Zarco-Tejada, Pablo J., Miller, J.R., Harron, J., Hu, B., Noland, T.L., Goel, N., Mohammed, G.H., Sampson, P., 2004. Needle chlorophyll content estimation through model inversion using hyperspectral data from boreal conifer forest canopies. Remote Sens. Environ. 89, 189–199. https://doi.org/10.1016/j.rse.2002.06.002

Zarco-Tejada, P. J., Miller, J.R., Morales, A., Berjón, A., Agüera, J., 2004. Hyperspectral indices and model simulation for chlorophyll estimation in open-canopy tree crops. Remote Sens. Environ. 90, 463–476. https://doi.org/10.1016/j.rse.2004.01.017

Zarco-Tejada, Pablo J., Suarez, L., Gonzalez-Dugo, V., 2013. Spatial resolution effects on chlorophyll fluorescence retrieval in a heterogeneous canopy using hyperspectral imagery and radiative transfer simulation. IEEE Geosci. Remote Sens. Lett. 10, 937–941. https://doi.org/10.1109/LGRS.2013.2252877

Zhang, Y., Guanter, L., Berry, J.A., Joiner, J., van der Tol, C., Huete, A., Gitelson, A., Voigt, M., Köhler, P., 2014. Estimation of vegetation photosynthetic capacity from space-based measurements of chlorophyll fluorescence for terrestrial biosphere models. Glob. Chang. Biol. 20, 3727–3742. https://doi.org/10.1111/gcb.12664

Zhang, Y., Guanter, L., Joiner, J., Song, L., Guan, K., 2018. Spatially-explicit monitoring of crop photosynthetic capacity through the use of space-based chlorophyll fluorescence data. Remote Sens. Environ. 210, 362–374. https://doi.org/10.1016/j.rse.2018.03.031

Zhao, F., Dai, X., Verhoef, W., Guo, Y., van der Tol, C., Li, Y., Huang, Y., 2016. FluorWPS: A Monte Carlo ray-tracing model to compute sun-induced chlorophyll fluorescence of three-dimensional canopy. Remote Sens. Environ. 187, 385–399. https://doi.org/10.1016/j.rse.2016.10.036

Zhu, Y., Yao, X., Tian, Y., Liu, X., Cao, W., 2008. Analysis of common canopy vegetation indices for indicating leaf nitrogen accumulations in wheat and rice. Int. J. Appl. Earth Obs. Geoinf. 10, 1–10. https://doi.org/10.1016/j.jag.2007.02.006

Zlatev, Z., Cebola Lidon, F., 2012. An overview on drought induced changes in plant growth, water relations and photosynthesis. Emirates J. Food Agric. 24, 57–72.

Chapter 2: Objectives

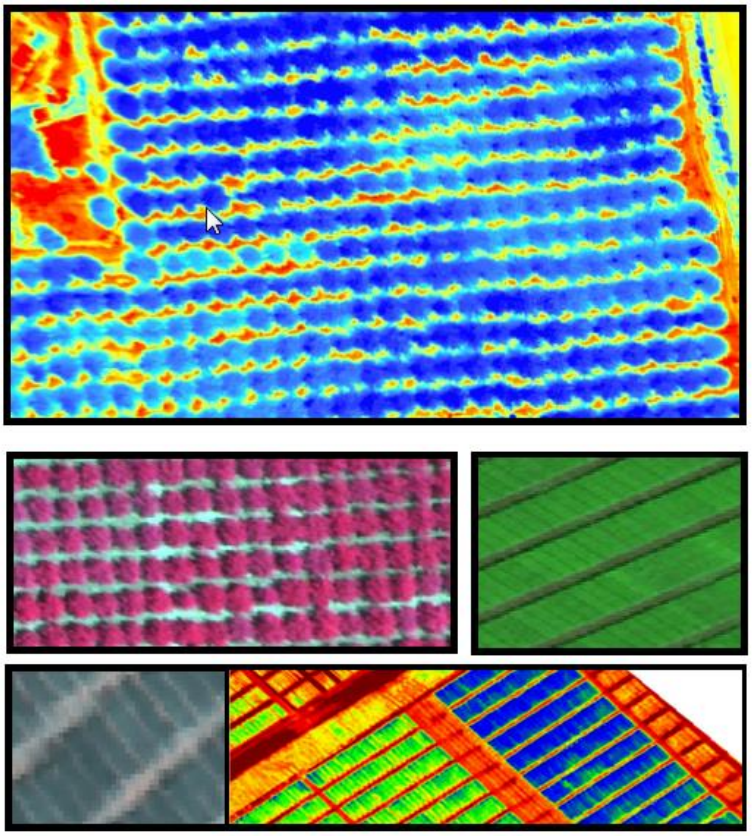

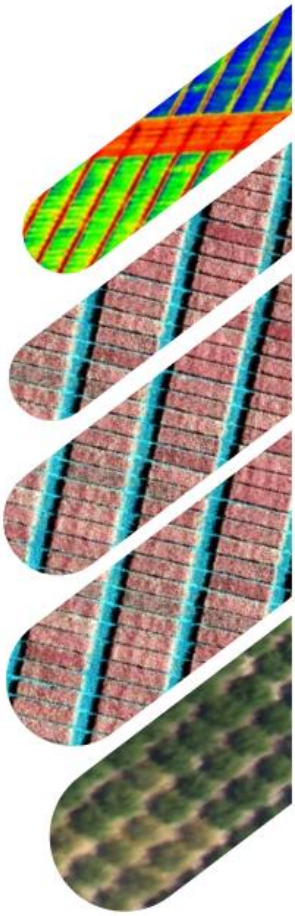

Chapter 2: Objectives

The main objective of the PhD thesis is to assess the contribution played by airborne-retrieved solar-induced chlorophyll fluorescence (SIF) in the quantification of nitrogen and Vcmax under irrigated and rainfed Mediterranean conditions. In order to reach this specific objective, the thesis explores advanced remote sensing methods linking radiative transfer model inversions (RTM, e.g. PROSPECT-SAILH, SCOPE models) and photosynthetic traits quantified from high-resolution airborne hyperspectral imagery. In particular, nitrogen concentration, structural parameters and leaf biochemical constituents were assessed from hyperspectral remote sensing images as an alternative to traditional leaf-destructive and time-consuming methods.

The first study conducted during the thesis aimed at exploring the airborne hyperspectral-derived SIF and thermal-based CWSI on the relationships with water stress indicator and photosynthetic traits in orchard crops. These results enabled to establish an accurate methodology for retrieving plant physiological traits through the use of automatic object-based tree-crown detection algorithm based on quartile breaks applied to the high-resolution hyperspectral and thermal imagery.

From the crop nutritional point of view, the results reached during the thesis addressed the ability of regression models combining airborne-derived SIF and plant traits retrieved from VNIR-SWIR hyperspectral imagery and RTM inversions to predict N concentration under semi-arid conditions.

Regarding the remote assessment of the photosynthesis capacity Vcmax, the thesis investigated the feasibility of the high-resolution airborne hyperspectral imagery combined with SCOPE model inversion to detect plant traits related to Vcmax and physiological changes induced by irrigation regimes and wheat varieties. Thus, the following specific objectives were identified:

1. To assess the effects caused by the within-tree structural variability and background on the airborne-derived SIF and thermal-based CWSI physiological indicators for water stress detection.

2. To assess the retrieval of nitrogen using airborne-derived fluorescence and plant traits quantified from VNIR-SWIR hyperspectral imagery under irrigated and rainfed Mediterranean conditions.

3. To evaluate the remote detection of the photosynthetic capacity in rainfed and irrigated plant phenotyping trials through radiative transfer Vcmax estimation from hyperspectral imagery and SIF.

2.1 Outline of the Doctoral Thesis

This Doctoral Thesis is presented as chapters, each one dealing with the objectives previously described.

Chapter 3 addresses the Objective 1 and proposes methodologies for the automatic object-based tree crown detection algorithm based on watershed segmentation on high-resolution hyperspectral and thermal airborne imagery. The method is applied at the tree-crown scale in an almond orchard under two irrigation regimes. This chapter highlights the importance of taking into account the structural and soil-background effects on the quantification of airborne solar-induced chlorophyll fluorescence (SIF) retrievals, the image-based spectral traits and thermal indicators derived from high-resolution hyperspectral and thermal airborne imagery. This work demonstrates the large effects caused by the within-tree structural variability and background effects on the relations with assimilation rate and stomatal conductance by the airborne-derived SIF and CWSI physiological indicators used for water stress detection. This work was published in *Remote Sensing*:

Camino C., Zarco-Tejada P. J. & González Dugo V. *Effects of Heterogeneity within Tree Crowns on Airborne-Quantified SIF and the CWSI as Indicators of Water Stress in the Context of Precision Agriculture*. Remote Sensing, 2018, 10(4), 604; https://doi.org/10.3390/rs10040604.

Chapter 4 addresses the objective 2. The research presented here assesses the contribution played by airborne-retrieved solar-induced chlorophyll fluorescence on the retrieval of leaf nitrogen, comparing to traditional physiological indices (structural and chlorophyll *a*+*b*) and nitrogen indices calculated using the 400-1750 nm spectral domain under two water regimes in the context of wheat phenotyping. The work focuses on the use of the stepwise multiple regression analysis using biophysical parameters derived from radiative transfer models, narrow-band spectral indices and

chlorophyll fluorescence quantified from the high-resolution hyperspectral imagery over the VNIR and SWIR spectral range. This work was published in the *International Journal of Applied Earth Observation and Geoinformation*:

Camino C., González-Dugo V., Hernández P., Sillero J.C. & Zarco-Tejada P. J. *Improved nitrogen retrievals with airborne-derived fluorescence and plant traits quantified from VNIR-SWIR hyperspectral imagery in the context of precision agriculture*. International Journal of Applied Earth Observation and Geoinformation, Volume 70, August 2018, Pages 105-117. https://doi.org/10.1016/j.jag.2018.04.013.

Chapter 5 addresses the objective 3. The work completed the study conducted in Chapter 3, demonstrating the ability to estimate the maximum rate of carboxylation (Vcmax) using SCOPE model inversions with airborne-quantified SIF retrieved from high-resolution hyperspectral imagery. This work demonstrates that SIF is a reliable indicator of photosynthetic activity and could be estimated by airborne remote sensing for high-throughput plant phenotyping and precision agriculture applications. This work was accepted for publication in *Remote Sensing of Environment* (6 May 2019):

Camino C., González Dugo V., Hernández P. & Zarco-Tejada P. J. *Radiative transfer Vcmax estimation from hyperspectral imagery and SIF retrievals to assess photosynthetic performance in rainfed and irrigated plant phenotyping trials*. Accepted in Remote Sensing of Environment, 6 May 2019.

Chapter 6 summarizes the conclusions of each chapter and the general conclusions of this doctoral thesis. The main findings are synthesized including a general discussion that links the three main chapters developed in this work. In addition, this chapter summed up the further research work that needs to be carried out in the future.

Chapter 3

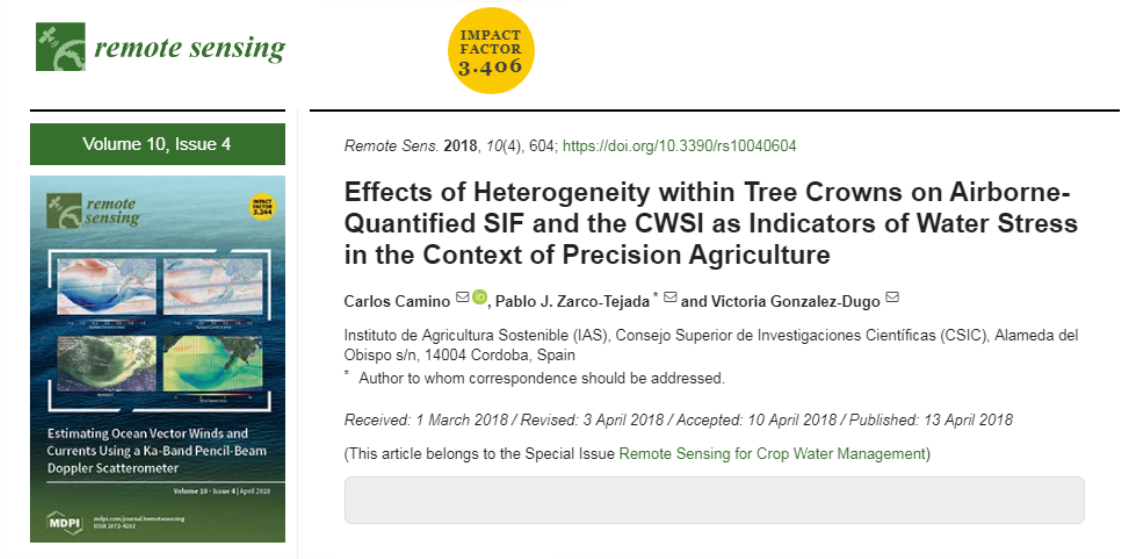
remote sensing

IMPACT FACTOR 3.406

Volume 10, Issue 4

Estimating Ocean Vector Winds and Currents Using a Ka-Band Pencil-Beam Doppler Scatterometer

Remote Sens. **2018**, *10*(4), 604; https://doi.org/10.3390/rs10040604

Effects of Heterogeneity within Tree Crowns on Airborne-Quantified SIF and the CWSI as Indicators of Water Stress in the Context of Precision Agriculture

Carlos Camino, Pablo J. Zarco-Tejada * and Victoria Gonzalez-Dugo

Instituto de Agricultura Sostenible (IAS), Consejo Superior de Investigaciones Científicas (CSIC), Alameda del Obispo s/n, 14004 Cordoba, Spain

* Author to whom correspondence should be addressed.

Received: 1 March 2018 / Revised: 3 April 2018 / Accepted: 10 April 2018 / Published: 13 April 2018

(This article belongs to the Special Issue Remote Sensing for Crop Water Management)

Published in Remote Sensing, 2018, 10(4), 604 https://doi.org/10.3390/rs10040604

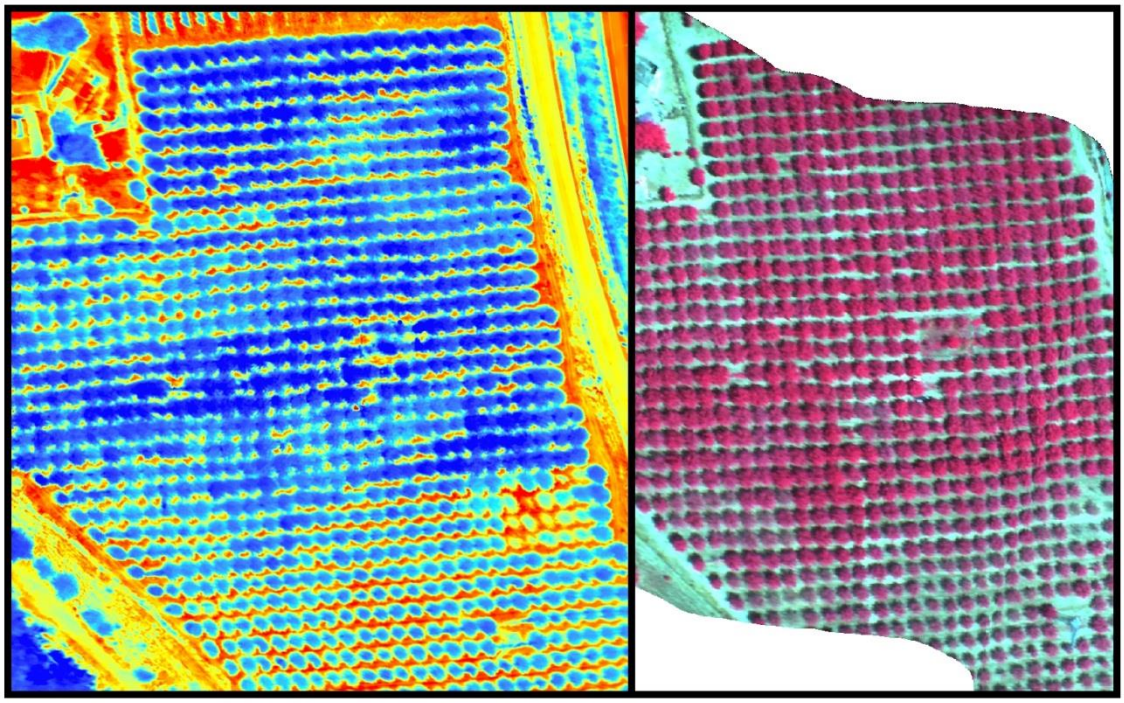

Chapter 3: Effects of heterogeneity within tree-crowns on airborne-quantified SIF and the CWSI as indicators of water stress in the context of precision agriculture

Resumen

Esta investigación se centró en comprender los efectos de la heterogeneidad estructural dentro de las copas de los árboles en la estimación de la fluorescencia clorofílica inducida por el sol (SIF) y un índice de estrés hídrico, denominado Crop Water Stress Index (CWSI). En este trabajo, exploramos la variabilidad de SIF y CWSI observada en copas de árboles sometidos a diferentes regímenes de estrés hídrico, así como sus efectos en las relaciones con las medidas fisiológicas realizadas a escala foliar. Para ello, se adquirieron imágenes hiperespectrales de alta resolución (20 cm) para evaluar la cuantificación de la fluorescencia en las partes de las copas iluminadas por el sol y en copas completas aplicando el método de las líneas de Fraunhofer (FLD) y métodos automáticos de detección de objetos sobre copas de árboles. También medimos la distribución de la temperatura del dosel dentro de las copas de árboles utilizando algoritmos de segmentación basados en percentiles de temperatura aplicados a las imágenes térmicas de alta resolución (25 cm). El estudio se realizó en un huerto de almendros cultivado bajo tres regímenes de riego ubicado en Córdoba. Se realizaron tres campañas aerotransportadas con cámaras hiperespectrales y térmicas de alta resolución a bordo de un avión tripulado durante el verano de 2015. Las relaciones entre SIF y la tasa de asimilación mejoraron significativamente cuando se utilizaron los píxeles de las partes de copa iluminados por el sol en todas las fechas de vuelo. Por el contrario, la señal SIF extraída de las copas completas de los árboles se degradó considerablemente debido a la heterogeneidad del dosel observada dentro de las copas. Las segmentaciones mediante cuartiles aplicadas a las imágenes térmicas mostraron que los valores de CWSI obtenidos estaban dentro del rango teóricamente esperado de CWSI sólo cuando los píxeles pertenecían a las clases del percentil 50. Sin embargo, los valores de CWSI se sesgaron en el cuartil superior (Q_{75}) para todos los regímenes de riego, debido a los efectos del suelo que afectan a la temperatura media calculada en la copa. La relación entre CWSI y Gs se vio muy afectada por los niveles de segmentación de copa aplicados, mejorando notablemente cuando los valores de CWSI se calcularon a partir de la segmentación de la copa del cuartil medio (Q_{50}), correspondiente a los píxeles de vegetación con temperaturas más frías y más puros (r^2=0.78 en píxeles de vegetación

pura frente a r^2=0.52 en píxeles con temperaturas más altas). Este estudio destaca la importancia de utilizar imágenes hiperespectrales y térmicas de alta resolución para extracciones de las componentes puras de copas de árboles mediante segmentación en el contexto de la agricultura de precisión y la detección de estrés hídrico.

Abstract

This research focused on understanding the effects of structural heterogeneity within tree-crowns on the airborne retrieval of solar-induced chlorophyll fluorescence (SIF) and the Crop Water Stress Index (CWSI). We explored the SIF and CWSI variability observed within crowns of trees subjected to different water stress regimes and its effect on the relationships with leaf physiological measurements. High-resolution (20 cm) hyperspectral imagery was acquired to assess fluorescence retrieval from sunlit portions of the tree crowns using the Fraunhofer line depth method, and from entire crowns using automatic object-based tree crown detection methods. We also measured the canopy temperature distribution within tree-crowns using segmentation algorithms based on temperature percentiles applied to high-resolution (25 cm) thermal imagery. The study was conducted in an almond orchard cultivated under three watering regimes in Cordoba, in southern Spain. Three airborne campaigns took place during the summer of 2015 using high-resolution hyperspectral and thermal cameras on board a manned aircraft. Relationships between SIF and the assimilation rate improved significantly when the sunlit tree crown pixels extracted through segmentation were used for all flight dates. By contrast, the SIF signal extracted from the entire tree crowns was highly degraded due to the canopy heterogeneity observed within tree crowns. The quartile crown segmentations applied to the thermal images showed that the CWSI values obtained were within the theoretically expected CWSI range only when the pixels were extracted from the 50th percentile class.

However, the CWSI values were biased in the upper quartile (Q_{75}) for all watering regimes due to the soil background effects on the calculated mean crown temperature. The relationship between the CWSI and Gs was heavily affected by the crown segmentation levels applied and improved remarkably when the CWSI values were calculated from the middle quartile crown segmentation (Q_{50}), corresponding to the coldest and purest vegetation pixels (r^2 = 0.78 in pure vegetation pixels vs. r^2 = 0.52 with the warmer pixels included in the upper quartile). This study highlights the importance of using high-resolution hyperspectral and thermal imagery for pure-object segmentation extractions from tree crowns in the context of precision agriculture and water stress detection.

3.1 Introduction

Water deficits occur in crops when the evaporative demand exceeds the supply of soil water (Slatyer, 1967). As a result, plant growth and its physiological processes are affected (Hsiao, 1973). Particularly, water stress reduces photosynthetic activity and induces stomatal closure. Consequently, evaporative cooling is reduced and canopy temperature increases. Besides the increase of temperature experienced by plants under water stress, the steady-state chlorophyll fluorescence emission (i.e., solar-induced fluorescence, SIF) is also affected due to the reduction of photosynthesis (Schreiber and Bilger, 1987, Lichtenthaler and Rinderle, 1988; Lichtenthaler et al., 1996). At the leaf scale, relationships between SIF and the assimilation rate vary due to the stress conditions (Flexas et al., 1999, 2000, 2002) but also due to irradiance levels, temperature, nutritional status, and other environmental factors. For the purpose of characterizing plant water status, various field-level physiological measurements such as leaf water potential, stomatal conductance and net assimilation are currently used. However, these leaf-level measurements are time-consuming and therefore very restricted for operational purposes, especially when the aim is to characterize the spatial patterns of the physiological processes and within-field water status variability across an entire orchard. Therefore, finding adequate strategies for monitoring the within-field variability of physiological conditions is critical in the context of precision agriculture and for precision irrigation purposes. In this regard, image-based remote sensing methods based on innovative indicators directly linked to plant functioning are considered useful for the adequate monitoring of photosynthetic status and water stress in crops.

Recent studies have successfully demonstrated that image-based remote quantification of SIF is directly associated with the photosynthetic rate for detecting vegetation stress (Pérez-Priego et al., 2005; Meroni and Colombo, 2006; Porcar-Castell et al., 2014; Rascher et al., 2015). Although the use of narrow bands has been proposed for accurate retrieval of SIF in absolute terms (i.e., below 1 nm FWHM), recent studies have demonstrated that airborne hyperspectral imagery acquired with broader bandwidths (5–7 nm) still captures the fluorescence signal, which makes it possible to monitor photosynthesis over time (Damm et al., 2010, 2011).

The high heterogeneity observed within tree-crowns and the large effects caused by soil background and sunlit/shaded areas must be considered due to their influence on the SIF signal quantified from remote sensing imagery. The acquisition of very high-resolution hyperspectral imagery enables the extraction of the SIF signal from each crown component, assessing the large effects caused by the canopy structure. In fact, the effects of canopy architecture have been the focus of several studies using hybrid models (Zarco-Tejada et al., 2013) and 3D simulation (Hernández-Clemente et al., 2017). The use of three-dimensional (3D) information on a canopy structure based on airborne full-waveform Light Detection and Ranging (LiDAR) to characterize canopy structure (Dandois and Ellis, 2013; Hernández-Clemente et al., 2014) is a promising field of research that may provide valuable information about the canopy architecture and the high heterogeneity observed within tree-crowns. Nevertheless, no studies have explored the effects of within-crown structure on SIF quantification or the relationship of such effects with photosynthesis.

In the context of thermal imaging for detecting water stress, several studies have shown that high-resolution thermal imagery acquired from manned and unmanned aerial platforms enables the detection of water stress, showing accurate relationships with stomatal conductance (Jones et al., 2009; Bendig et al., 2015; V. Gonzalez-Dugo et al., 2015; Zarco-Tejada et al., 2013) and water potential (Bellvert, 2014; Gonzalez-Dugo et al., 2014; Bellvert et al., 2016). Yet, within crown structure also plays a critical role in the quantification of crown temperature and in the relationships obtained with physiological measures. In fact, some studies have demonstrated that crown heterogeneity is a reliable tool for the early detection of plant water stress (Fuchs, 1990; Gardner et al., 1981). The variability of within-tree temperature and its relationship with water status can be due to several factors. At the individual tree level, stomatal closure related to water stress increases the overall canopy temperature and is affected by the water supply. In addition, it is well known that changes in leaf angle distribution, radiation exposure, leaf area density, and canopy architecture affect the variability of canopy temperature within crowns. Other factors, such as soil water and nutritional deficit (Rodriguez et al., 2005) as well as the effect of diseases (Calderón et al., 2013) also lead to differences in crown canopy temperature. As crown temperature is affected by the tree structure, the thermal-based indicator known as the Crop Water Stress Index (CWSI) (Idso et al., 1981; Jackson et al., 1981) is also affected. The CWSI is based on

the difference between canopy temperature and air temperature (Tc-Ta), normalized by the vapour pressure deficit (VPD), and is inversely related to transpiration and stomatal conductance (Jackson et al., 1981). Thus, within-tree structural variability plays a role in the relationships between the CWSI and stomatal conductance used to detect water stress. Moreover, external effects due to the surrounding non-vegetation targets may play a role in the quantified tree-level CWSI and its relationship with physiological measures.

The research presented in this manuscript was carried out in an almond orchard subjected to different water stress regimes due to the regulated deficit irrigation levels imposed. The goal of this study was to assess within-tree structural effects on chlorophyll fluorescence and on the mean temperature quantified from high-resolution hyperspectral and thermal images in the context of water stress detection and precision irrigation. In addition, we explored the influence of tree structure and the background on the relationships between SIF and the field-measured assimilation rate, and the CWSI and stomatal conductance.

3.2 Material and Methods

3.2.1 Study site and field data collection

The experiment was performed in July and August 2015 in an almond orchard subjected to regulated deficit irrigation treatments and a plot under rainfed (RF) conditions. The experimental site was located in Cordoba, in southern Spain, at the Alameda del Obispo Research Station (37°52′N, 4°49′W). The climate is Mediterranean with mild winters and warm and dry summers. A weather station located at 300 m from the experimental site collected an average of air temperature of 18.6 °C and relative humidity of 62% along the 2015 year. Annual rainfall and reference evapotranspiration (ETo; Penman-Monteith) were 330 and 1250 mm, respectively. In this research, three watering regimes were analyzed: a rainfed plot was compared to plots subjected to two irrigated treatments, a fully irrigated control (FI), where irrigation fulfilled crop water requirements, and a severely regulated deficit irrigation treatment (RDI, which received 20% ETc during the period comprised in this study. The irrigated treatments were replicated four times using a randomized block design (Fig. 3.1). The orchard was drip irrigated with two lateral pipes per almond tree row and kept free of weeds, pests, and

diseases. For more information about the experimental design and the irrigation levels, see López-López et al. (López-López et al., 2018).

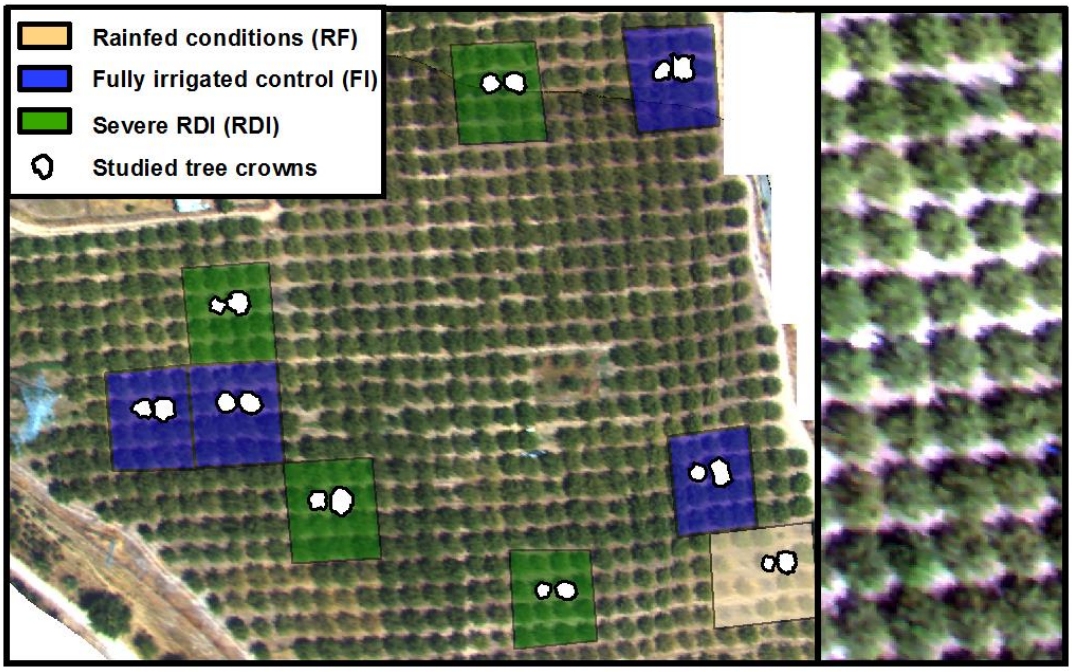

Fig. 3.1. Overview of the almond orchard experimental site imaged by the hyperspectral sensor, showing the four replicates of the irrigated treatments and the rainfed condition plot (a). The central almond trees (in white) used to collect leaf measurements are shown. A detail view is displayed in (b).

3.2.2 Airborne campaigns Study

Three airborne campaigns were performed on July 1st (day of the year DOY 182), August 5th (DOY 217) and August 25th (DOY 237) in 2015. We used a micro-hyperspectral imager (Micro-Hyperspec VNIR model, Headwall Photonics, Fitchburg, MA, USA) and a thermal infrared camera (FLIR SC655, FLIR Systems, Wilsonville, OR, USA) set in tandem on board a Cessna aircraft operated at 200 m altitude by the Laboratory for Research Methods in Quantitative Remote Sensing (QuantaLab) of the Spanish Council for Scientific Research (Consejo Superior de Investigaciones Científicas; IAS-CSIC, Córdoba, Spain). After each flight, the thermal and hyperspectral imagery was processed in the QuantaLab-IAS-CSIC laboratory.

The Micro-Hyperspec VNIR was set up with a configuration of 260 spectral bands acquired at 1.85 nm/pixel and 12-bit radiometric resolution in the 400–885 nm spectral region, yielding a 6.4 nm full width at half maximum (FWHM) with a 25-µm slit. The acquisition and storage module achieved 50 frames per second at 25 ms integration

time. The 8-mm focal length lens yielded an IFOV of 0.93 mrad and an angular FOV of 50° with a spatial resolution of 20 cm (Fig. 3.2a). The radiometric calibration was performed in the laboratory using coefficients derived from an integrating sphere (CSTM-USS-2000C LabSphere, North Sutton, NH, USA) at four levels of illumination and six integration times. The hyperspectral imagery was atmospherically corrected using the irradiance (E) measured at the time of the flight by means of an ASD Field Spectrometer (FieldSpec Handheld Pro, ASD Inc., Longmont, Colorado, USA) with 3 nm bandwidth and a cosine corrector-diffuser probe. The spectral resolution of the airborne imagery was matched with irradiance through a Gaussian convolution. The orthorectification of the hyperspectral imagery was performed using PARGE software (ReSe Applications Schläpfer, Wil, Switzerland) with input data acquired with an inertial measuring unit (IMU) installed on board and synchronized with the hyperspectral camera.

The thermal camera (FLIR SC655, FLIR Systems, Wilsonville, OR, USA) used in this study had a resolution of 640 × 480 pixels with a 13.1 mm focal length and 16 bit radiometric resolution, providing an angular FOV of 45 × 33.7°, which yielded a ground resolution of 25 cm at the altitude of the flights (Fig. 3.2c). The thermal imagery was calibrated using ground temperature data collected with a handheld infrared thermometer (LaserSight, Optris, Germany) on each flight date. The thermal imagery was processed and atmospherically corrected in the QuantaLab-IAS-CSIC laboratory (Berni et al., 2009; Zarco-Tejada et al., 2012).

3.2.3 Within-crown segmentation methods

Each individual tree crown was segmented based on quartile breaks applied to the high-resolution hyperspectral and thermal imagery. The image segmentation was automatically conducted using in R software (R Core Team, 2018). The methods to handle hyperspectral and thermal imagery and vector files were based on the “raster”, “maptools”, and “sp” packages (Bivand and Lewin-Koh, 2017; Bivand et al., 2013; Hijmans, 2017; Pebesma and Bivand, 2005) in R. An automatic object-based tree crown detection algorithm based on watershed segmentation (i.e., thresholds) using the “ClassInt” package (Bivand, 2017) in R was applied to the hyperspectral imagery to separate almond crowns from the soil background. For each tree crown, the next step focused on separating the sunlit crown from the mixed crown area (i.e., the remaining

tree crown, composed of soil contaminated pixels, shadows, and canopy background components) through spectral contrast analysis between sunlit/mixed pixels and background pixels. Tree crown hyperspectral reflectance (ρ) was segmented through the following steps: (1) the normalized difference vegetation index (NDVI) (Rouse et al., 1973) was used as a structural index to discriminate between sunlit vegetation and non-vegetation pixels (Xiao et al., 2004). Next, a NDVI threshold ≥0.55 was used (Fig. 3.2a); (2) taking advantage of the strong absorption of chlorophyll in the 677 nm band and the high reflectance at 800 nm produced by pure vegetation pixels, we normalized the difference between both regions using Equation (1). The normalized difference between the red and infrared regions using an automatic quartile break using the classIntervals function from "ClassInt" package was introduced to separate the mixed and sunlit areas within each tree crown (Fig. 3.2b). This segmentation enabled us to identify the sunlit areas within entire crowns, separating them from shaded areas and pixels affected by background soil (due to low leaf area density).

$$\frac{(\rho_{800}-\rho_{677})-Min(\rho_{800}-\rho_{677})}{Max(\rho_{800}-\rho_{677})-Min(\rho_{800}-\rho_{677})}[0-1] \qquad (5.1)$$

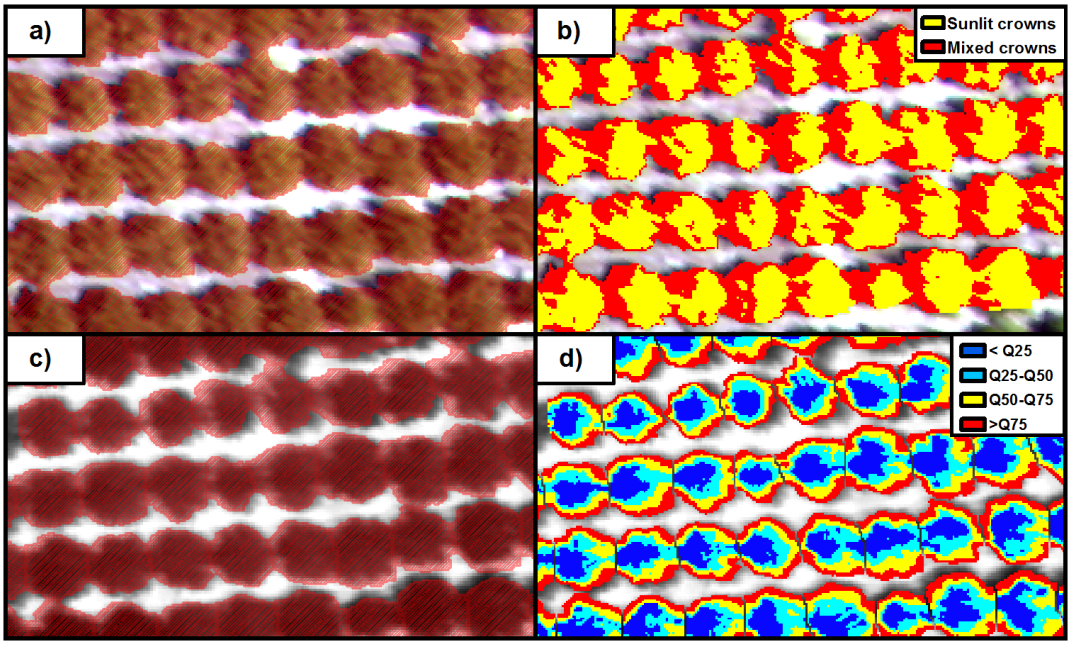

Fig. 3.2.View of the entire crowns (in red with stripes) retrieved using automatic object-based crown detection applied to the imagery acquired with the Hyperspec VNIR (a) and thermal FLIR SC655 (c) cameras. The sunlit crowns (in yellow) and mixed crowns (in red) extracted from the hyperspectral imagery are shown in (b). The temperature segmentations based on quartile methods using thermal imagery are shown in (d).

Individual tree crown temperature was extracted from the high-resolution thermal imagery through image segmentation via automatic quartile breaks based on the temperature gradient. Using the same scheme as for the hyperspectral imagery, the watershed segmentation method was applied to separate the tree crown from the soil background. However, the watershed segmentation in the thermal imagery was applied using the Sauvola's thresholding method (Sauvola and Pietikäinen, 2000) based on the standard deviation and average from the entire image. Next, each tree crown was divided into four quartiles by automatic object-based crown detection using the classIntervals function from "ClassInt" package in R. The pixels of individual tree crowns were divided into four classes using the 25th, 50th, and 75th percentiles (Fig. 3.3d). The proposed four classes comprised (i) pixels below the first quartile (Q_{25}), associated with the coldest and purest vegetation areas without soil background; (ii) pixels within quartile Q_{25} and the middle quartile (Q_{50}); (iii) pixels within Q_{50} and the upper quartile (Q_{75}); and (iv) pixels above the upper quartile (Q_{75}), associated with the warmest areas mainly affected by the background soil.

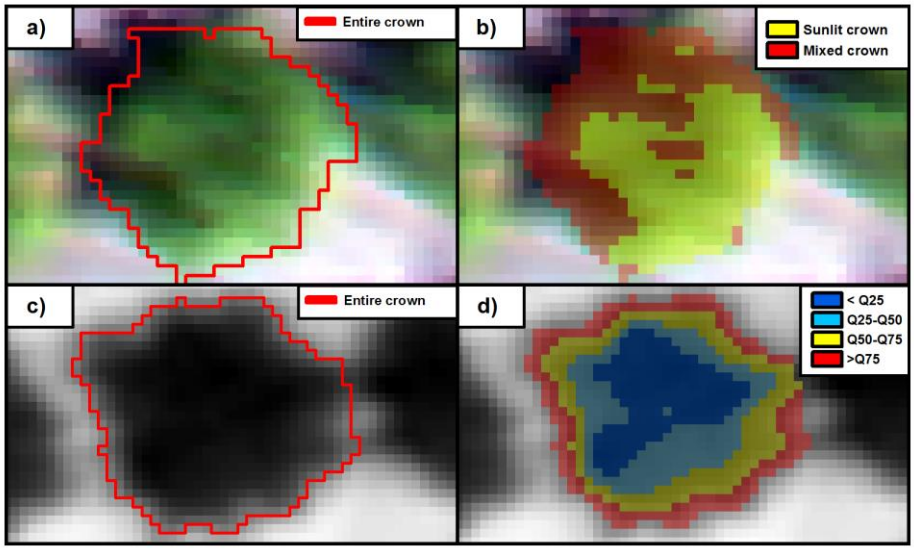

Fig. 3.3. View of an entire tree crown acquired with the hyperspectral (a) and the thermal camera (c). Identification of the sunlit crown and the mixed crown components in the hyperspectral (b) and the thermal imagery (d).

3.2.4 Sub-crown SIF and CWSI retrieval calculated from the high-resolution imagery

Single-tree crown radiance and reflectance spectra were extracted from the high-resolution hyperspectral imagery. The solar-induced chlorophyll fluorescence (SIF) signal was retrieved using the Fraunhofer line depth (FLD) principle (Plascyk and Gabriel, 1975). According to the method described in (Moya et al., 2004; Meroni and

Colombo, 2006; Damm et al., 2011), the mean object-based radiance (L) for each tree crown calculated from the hyperspectral data and the irradiance obtained by the field ASD spectrometer at the time of the flight were used to quantify SIF. The retrieval method was based on two spectral bands located inside (762 nm) and outside (750 nm) of the O_2–A absorption feature (Moya et al., 2004; Meroni et al., 2010) (see Fig. 3.5.4a). SIF was extracted from the entire tree crowns and the sunlit areas within each tree crown (Fig. 3.3b). SIF quantified from the trees of the experiment was compared to the leaf-level measurements of net photosynthesis acquired at the time of the flight for each date. In addition, following a similar methodology to that proposed by Zarco-Tejada et al. (Zarco-Tejada et al., 2016), a normalization scheme was applied to all trees and dates to compare the relationship between SIF and assimilation rates for water stress detection on the flight dates. The normalized SIF was calculated by dividing each within-tree object-level SIF value by the maximum value of FI (i.e., non-stressed trees) for each single date.

Based on the temperature quartile segmentation (Fig. 3.3d), the CWSI was retrieved from the thermal imagery as a water stress indicator of the almond tree crowns. The average canopy tree crown temperature (Tc) extracted from the thermal imagery, air temperature (Ta), and relative humidity was used to calculate the CWSI according to the methodology proposed by Idso et al. (1981). Theoretical CWSI boundaries are 0 (no water stress) and 1 (maximum water stress). The CWSI was compared with the field measurements of stomatal conductance acquired at the time of the flight on the various dates.

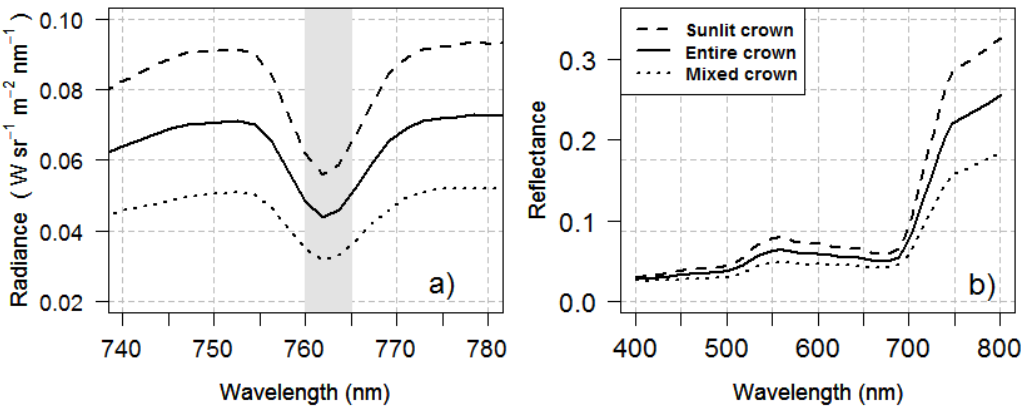

Fig. 3.4. Radiance spectra in W·sr^{-1}·m^{-2}·nm^{-1} (a) and reflectance spectra (b) retrieved from high-resolution hyperspectral imagery during the second flight. The spectra shown correspond to a tree crown under severe RDI. The vertical grey region in a) shows the O_2-A atmospheric oxygen absorption band.

3.3 Results

3.3.1 Field physiological measurements

Fig. 3.5 shows the relationship between the assimilation rate (A; in µmol·m^{-2}·s^{-1}) and stomatal conductance (Gs; in mmol·m^{-2}·s^{-1}) as well as the temporal changes experienced by each physiological indicator as a function of the water stress treatments. Table 3.1 shows the separability between treatments for A and Gs using an analysis of variance (ANOVA) F test followed by Tukey's HSD (honest significant difference) test. This table summarizes the basic statistics for the physiological measurements. As shown in Fig. 3.5a, the assimilation rate was linearly related to the stomatal conductance for the three flight dates. In general, for all flight dates, the physiological status showed higher values for FI than for RDI and RF treatments (Figure 3.5b, c). At the time of the three flights, the field physiological measurements taken at the leaf level from almond trees under RF conditions were kept below 1.8 µmol·m^{-2}·s^{-1} for A and 106 mmol·m^{-2}·s^{-1} for Gs, indicating that these trees were severely affected by water stress. Meanwhile, trees subjected to the FI treatment yielded the highest average stomatal conductance and assimilation rate on all flight dates.

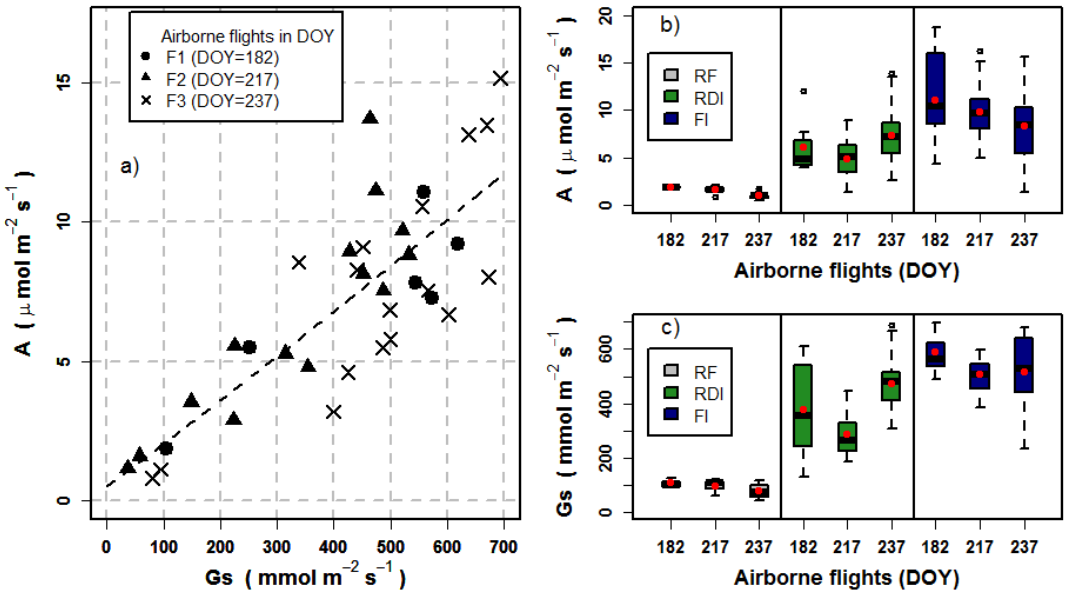

Fig. 3.5. Scatter plot obtained between field assimilation rate (A; µmol·m^{-2}·s^{-1}) and stomatal conductance (Gs; in·mmol·m^{-2}·s^{-1}) for each flight date (F1–F3) (a). The boxplots show the A (b) and Gs (c) variability registered on rainfed (RF), severe regulated deficit irrigation (RDI) and full irrigation (FI) for each flight date (F1–F3). In the boxplots, the average values are shown with a red point. The black line within the box is the median, and the top and bottom of the box is the 75th and 25th quartile, respectively. The whiskers represent the upper and the lower limits based on the difference with the interquartile ranges (Q ± 1.5 × IQR). The outliers represented as asterisk correspond to values out of upper and lower limits.

The results of the ANOVA showed significant differences in Gs and A between all irrigation treatments for each flight date; these differences were greater in the flight performed on DOY 217 (F-value = 65.37 and 68.33 for A and Gs, respectively; both with p-values $\leq 2.82\times10^{-12}$). Tukey's HSD post-hoc analysis showed statistically significant differences in Gs between almond trees subjected to rainfed and irrigated treatments for each flight date (p-value < 0.05). However, there were no differences in assimilation rate between the two irrigated treatments on DOY 237.

Table 3.1. Average assimilation rate and stomatal conductance measured for each water regime and flight date. F statistic and p-value obtained from the standard analysis of variance (ANOVA).

	Mean ± SD			ANOVA		Tukey
A	**RF**	**RDI**	**FI**	**F-value**	**p-value**	**p-value**
Flight 1 (DOY=182)	1.87 $_{a}$	6.05 $_{b}$ ±2.7	11.1 $_{c}$ ±5.0	4.762	0.0238	<0.05
Flight 2 (DOY=217)	1.60 $_{a}$ ±0.3	5.04 $_{b}$ ±1.6	9.82 $_{c}$ ±2.7	65.37	<2e-16	<0.001
Flight 3 (DOY=237)	1.0 $_{a}$ ±0.4	7.40 $_{b}$ ±2.5	8.30 $_{b}$ ±3.9	20.15	8.48e-08	<0.001*
Gs						
Flight 1 (DOY=182)	105.6 $_{a}$ ±18.2	377.4 $_{b}$ ±159.2	587.7 $_{c}$ ±82.1	22.53	1.06e-06	<0.001
Flight 2 (DOY=217)	96.0 $_{a}$ ±31.4	285.1 $_{b}$ ±78.0	504.5 $_{c}$ ±60.2	68.33	2.82e-12	<0.001
Flight 3 (DOY=237)	76.6 $_{a}$ ±27.7	473.3 $_{b}$ ±93.5	523.6 $_{c}$ ±202.4	28.18	9.11e-10	<0.05

Notes: RF, RDI and FI correspond to rainfed, severe regulated deficit irrigation and full irrigation, respectively. Treatments sharing the same letter are not significantly different in Tukey's honest significant difference (HSD) post-hoc test. SD = standard deviation. The * indicates significant differences between RF and the irrigated treatments. Letters (a, b and c) represent the results of Tukey's post-hoc comparisons of group means.

3.3.2 Within-crown SIF and CWSI variability as a function of water stress

The object-based crown segmentation methods applied to the hyperspectral imagery to separate sunlit from mixed regions within tree-crowns (Fig. 3.3b and 3.4) made it possible to assess the coefficient of variation (CV; Table 3.2) as a function of water stress levels. These results indicated that the sunlit crown portions showed more homogeneity in pixel variability for all water stress regimes on each flight date. By contrast, entire crowns had more heterogeneity due to the mixture of sub-crown components such as pure vegetation, shaded areas, and soil effects. As a result of within-crown variability, SIF yielded a higher CV for entire crowns than for sunlit crowns, as expected (Table 3.2). It is interesting to note that the CV for sunlit crowns was higher in RDI than in FI and RF treatments. By contrast, the CV for entire crowns increased with higher values of water stress. Overall, SIF showed higher average values in sunlit crowns than in entire crowns. Moreover, SIF differences between treatments increased when the sunlit areas were considered. In general terms, the average SIF

signal was higher in the FI treatment, followed by the RDI and finally the RF treatment for both entire and sunlit crown segmentations. However, the mean fluorescence signal calculated from pixels of entire tree crowns was highly degraded compared to the SIF of sunlit crowns due to the effects of the mixed fractional canopy on each pixel (Table 3.2). In these situations, the SIF emission caused a decrease in radiance values in the range close to the O2-A absorption peak (Fig. 3.4a), compared to the SIF signal when the sunlit crown segmentations were conducted. Moreover, as shown on Table 3.2, the SIF signal was more affected by the atmospheric conditions on each flight date for all studied water stress regimes than it was by the canopy temperature extracted from thermal imagery. Regarding the reflectance profiles, the pixels from sunlit crowns showed reflectance values higher in the near infrared region (Fig. 3.4b) as compared to pixels from mixed crowns (shaded areas, branches and soil background). However, entire crowns, which correspond to the aggregation of pixels from sunlit and mixed crowns, are displayed between sunlit crown and mixed crown radiance and reflectance (Fig. 3.4).

Table 3.2. Average values and coefficient of variation (CV) of solar-induced chlorophyll fluorescence (SIF) and canopy temperature (Tc) retrieved from tree crown segmentation for each water stress regime and flight date. RF, RDI and FI correspond to rainfed, severe regulated deficit irrigation and full irrigation, respectively. The Tc value is divided into four quartile classes based on the 25th, 50th, and 75th quartiles (Q).

Average values (CV, coefficient of variation)						
	SIF		**Temperature (Tc in K)**			
	Entire crowns	**Pure veg. pixels**	**<Q25**	**Q25-Q50**	**Q50-Q75**	**>Q75**
Flight 1 (DOY=182)						
RF	2.43 (0.17)	2.67 (0.08)	308.1 (0.01)	308.7 (0.02)	309.8 (0.05)	315.1 (0.03)
RDI	**2.73 (0.20)**	**3.11 (0.17)**	**304.7 (0.05)**	**305.2 (0.05)**	**306.0 (0.07)**	**311.1 (0.06)**
FI	3.06 (0.26)	3.55 (0.11)	303.1 (0.03)	303.5 (0.03)	304.1 (0.04)	309.1 (0.06)
Flight 2 (DOY=217)						
RF	2.94 (0.11)	2.99 (0.09)	309.5 (0.01)	310.4 (0.01)	311.8 (0.01)	314.1 (0.02)
RDI	**3.85 (0.15)**	**4.22 (0.11)**	**304.9 (0.04)**	**306.0 (0.04)**	**307.4 (0.03)**	**310.2 (0.04)**
FI	4.21 (0.16)	4.71 (0.08)	303.3 (0.03)	304.1 (0.02)	305.2 (0.03)	308.0 (0.05)
Flight 3 (DOY=237)						
RF	1.25 (0.22)	1.41 (0.15)	308.9 (0.01)	311.0 (0.01)	313.6 (0.02)	316.8 (0.02)
RDI	**1.88 (0.34)**	**2.25 (0.21)**	**305.3 (0.04)**	**306.5 (0.04)**	**308.8 (0.05)**	**313.0 (0.05)**
FI	1.86 (0.36)	2.32 (0.20)	304.3 (0.03)	305.4 (0.03)	307.0 (0.04)	311.2 (0.06)

The mean Tc values increased from <Q_{25} to >Q_{75}. In addition, when average values for the four classes were compared for each flight and treatment, the difference between Q_{50}–Q_{75} and Q_{75} was higher than between the other pairs of ranges, indicating that Q_{75} was substantially different (Table 3.2). Looking at the spatial pattern of the range obtained within each tree crown (located on the crown edges, Fig. 3.3d), it can be observed that the effects of background and soil pixels on the average value were the main drivers of these differences. Overall, the average canopy temperature was greater in the RF treatment than in the RDI treatment, which was in turn higher than in FI. Similarly to what was observed for the CV of SIF values obtained from sunlit crowns, the variability of canopy temperature for all classes (except for >Q_{75}) displayed an increasing value between FI and RDI treatments and then decreased for RF trees.

These quartile segmentation methods enabled the characterization of the temperature distribution within individual tree crowns but also of its effects on the CWSI. The assessment of the CWSI, as a normalized indicator, enabled the comparison of the canopy temperature between dates and also between ranges. In the almond trees of the experiment, the rainfed treatment resulted in increased stomatal closure, smaller crowns, and lower leaf density caused by the long-term water stress imposed. As a consequence, the CWSI values obtained were close to the theoretical maximum value of 1 (Fig. 3.6), even for Q_{25}. Considering the overall high temperature retrieved in all quartiles, it seems that the CWSI values recorded for RF trees were more affected by soil background compared to severe RDI and FI trees (Table 3.2). The NDVI values retrieved for these trees agreed with this observation (data not shown). The quartile crown segmentations also showed that CWSI values were biased in the Q_{50}–Q_{75} range and upper quartile (>Q_{75}) for all watering regimes, as consequence of soil background effects (Fig. 3.6). As a result, mean CWSI values were shifted beyond the maximum of the theoretical CWSI limit (i.e., CWSI > 1), even for trees subjected to RF conditions in the Q_{25}–Q_{50} quartile classes with smaller crowns. Overall, CWSI values retrieved from the two lower classes (≤50th percentile) were within the theoretical CWSI range for the irrigated regimes. The aggregation of pixels of the two classes below the 50th percentile resulted in values that may explain the observation and physiological measurements: the average values remained within the expected 0–1 range, indicating that pure vegetation pixels were targeted with little contamination from the soil background. The CWSI obtained from RF trees displayed an average value of 1.05, slightly above the

maximum. In trees subjected to the FI and RDI treatments, the CWSI values obtained were 0 and 0.30, respectively.

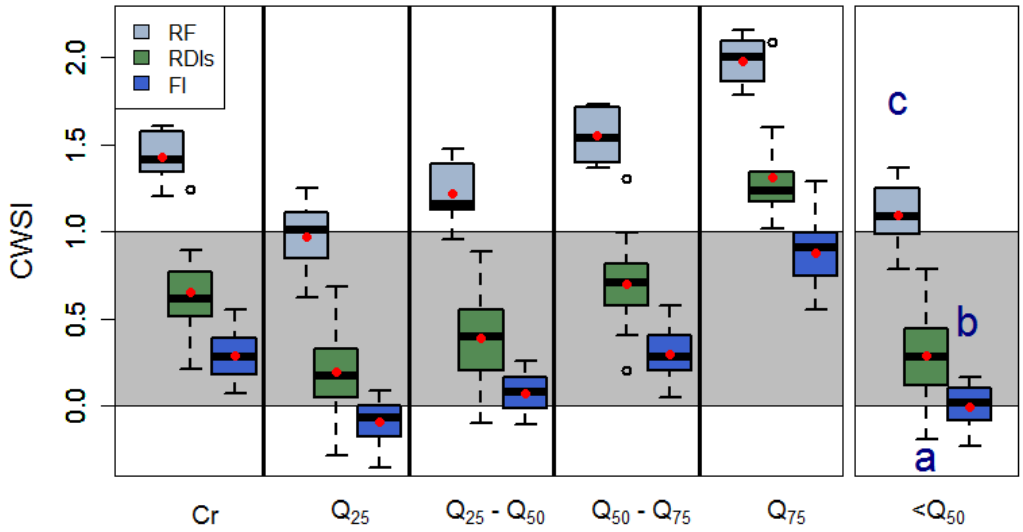

Fig. 3.6. Box plot showing the airborne-quantified Crop Water Stress Index (CWSI) from entire crowns (Cr), the quartile classes separated using the 25th, 50th and 75th percentiles and the aggregated quartile classes (Q_{25} and Q_{25}–Q_{50}) for the water regimes of the experiment. RF, RDI and FI correspond to rainfed, severe regulated deficit irrigation and full irrigation, respectively. The grey shading corresponds to the theoretical CWSI limits between 0 and 1. Average values are shown with a red point. In the box plots, the black line within the box is the median, the top and bottom of the box is the 75th and 25th quartile respectively. The whiskers represent the upper and lower limits based on the difference with the interquartile ranges (Q ± 1.5 × IQR). The outliers represented as circles, correspond to values out of upper and lower limits. Treatments sharing the same letter were not significantly different in Tukey's HSD post-hoc test (p-value < 0.0005).

3.3.3 Effects of crown segmentation on relationships between SIF and assimilation

The average SIF quantified from each tree crown was correlated with the mean assimilation rate across all dates for the entire crown and for the sunlit crown pixel selection. Results were statistically significant (r^2 > 0.66, p-value <0.005) across all dates for both crown segmentation levels (Fig. 3.7). Results slightly improved when the sunlit crown segmentations were used (Fig. 3.7b). The range of variation for the SIF values extracted from entire crowns became narrower and shifted towards lower SIF levels (Fig. 3.7c), as a consequence of the mixture of soil background and shaded areas. The changes observed in SIF retrieval were related to the contribution of shaded areas and background effects to the overall SIF signal quantified from the entire crown.

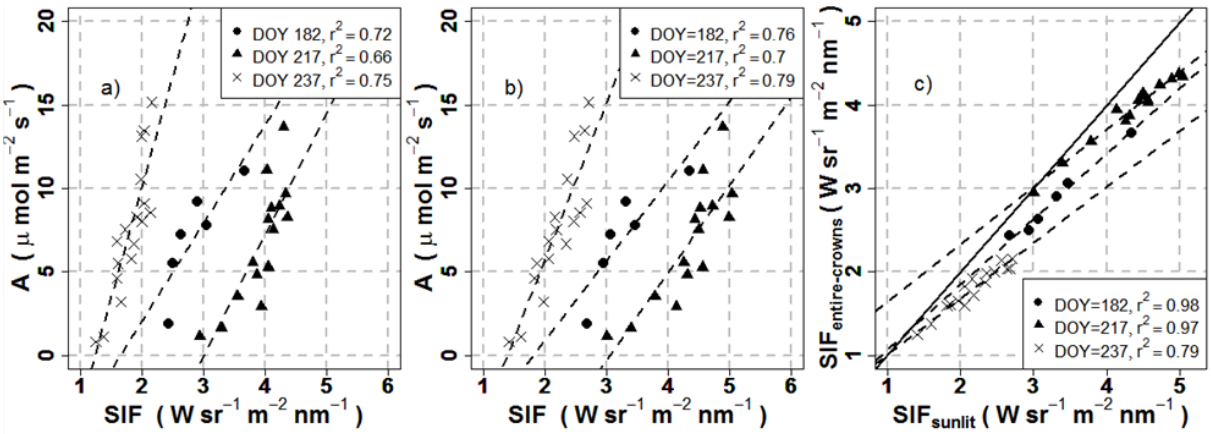

Fig. 3.7. Relationships found on single dates between leaf net assimilation rate and airborne chlorophyll fluorescence (SIF) for entire tree crowns (a) and sunlit tree crowns (b). Relationships between SIF extracted from entire tree crowns and sunlit tree crowns (c) for single dates.

The relationship between the fluorescence signal and the net assimilation for entire and sunlit crowns was different for each flight date (Fig. 3.7). A method based on the normalization of SIF for each tree to the non-water stressed SIF value for each date yielded a single relationship between SIF and A on the three flights conducted throughout the season (Fig. 3.8a). The normalized SIF extracted from the sunlit crown segmentations yielded a slight better relationship with A (r^2 = 0.66; p-value < 0.0005 and residual standard error = 2.17) than that of entire crowns (r^2 = 0.56; p-value < 0.0005, residual standard error = 2.45). These results demonstrated the improved sensitivity to A when the sunlit pixel component was used both on individual dates and normalizing across the entire season.

The separability among water stress treatments according to the seasonally-normalized SIF assessed via an ANOVA and Tukey's post-hoc analysis (Table 3.3) showed a statistically significant difference between the means of the water stress regimes. Tukey's post-hoc analysis showed statistically significant differences between FI and RDI (p-value < 0.05) for sunlit crown segmentations, while the seasonally-normalized SIF extracted from entire crowns did not show any differences between them. In particular, Figure 3.8b shows that differences between treatments in the median and the average of the normalized SIF were greater when it was extracted from sunlit crown segmentations than when it was derived from entire crowns. As a result, the SIF signal extracted from sunlit pixels was able to track the physiological changes due to the water stress regimes imposed.

Table 3.3. ANOVA and Tukey's HSD post-hoc analysis of normalized solar-induced chlorophyll fluorescence values extracted from pure sunlit crowns and entire crowns for each water stress treatment. RF, RDI an d FI correspond to rainfed, severe regulated deficit irrigation and full irrigation, respectively.

	ANOVA		Tukey's test	
	F-value	p-value	T-value	p-value
Entire crowns	16.39	9.55e-03		
FI-RF	…	…	5.720	< 1e-04
FI-RDI	…	…	-2.030	0.1169
RF-RDI	…	…	4.225	0.000468
Pure sunlit crowns	20.25	1.44e-06		
FI-RF	…	…	6.338	<0.001
FI-RDI	…	…	-2.534	0.0399
RF-RDI	…	…	4.489	<0.001

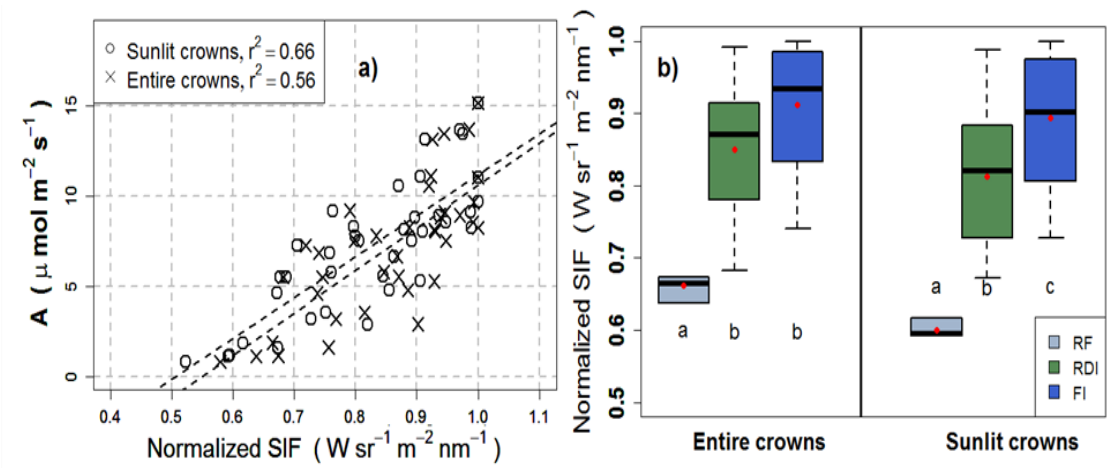

Fig. 3.8. Relationships found between leaf assimilation and normalized airborne-quantified chlorophyll fluorescence for entire and pure sunlit crowns (a). Box plot of normalized SIF retrieved from entire crowns and pure sunlit crowns for the water stress regimes explored (b). The mean value is represented with a red point. For each segmentation, treatments sharing the same letter were not significantly different in Tukey's HSD post-hoc test (p-value < 0.05).

3.3.4 Effects of crown segmentation on the relationships between the CWSI and stomatal conductance

The average CWSI quantified from each tree crown was compared to mean stomatal conductance across all dates for all crown segmentation levels based on temperature quartile thresholds. The results in Fig. 3.9a show that the CWSI was linearly and inversely correlated with stomatal conductance. The relationships showed large effects due to the quartile-crown segmentations applied: CWSI values extracted from the upper quartile (>Q_{75}) shifted towards high values of the CWSI due to the soil background effects; by contrast, in the lower half (<Q_{50}) and entire crown pixels, CWSI values were lower than 1 for the irrigated regimes. Relationships with Gs improved

remarkably when CWSI values corresponded to the coldest and purest vegetation areas associated to the first quartile (<Q_{25}) and pixels from the lower half quartile (<Q_{50}), yielding an r^2 = 0.77 and r^2 = 0.78, respectively. However, the agreement with field-measured stomatal conductance yielded a weaker coefficient of determination for >Q_{75} (r^2 < 0.52, p-value < 0.005). Fig. 3.9b shows the displacement between quartile classes in the lower half (<Q_{50}), which obtained the best results with Gs. Quartile-crown segmentations with a greater mixture of shaded and background pixels within tree-crowns were placed above the 1:1 line, compared to segmentations associated with the coldest and purest vegetation areas, which were close to the 1:1 line.

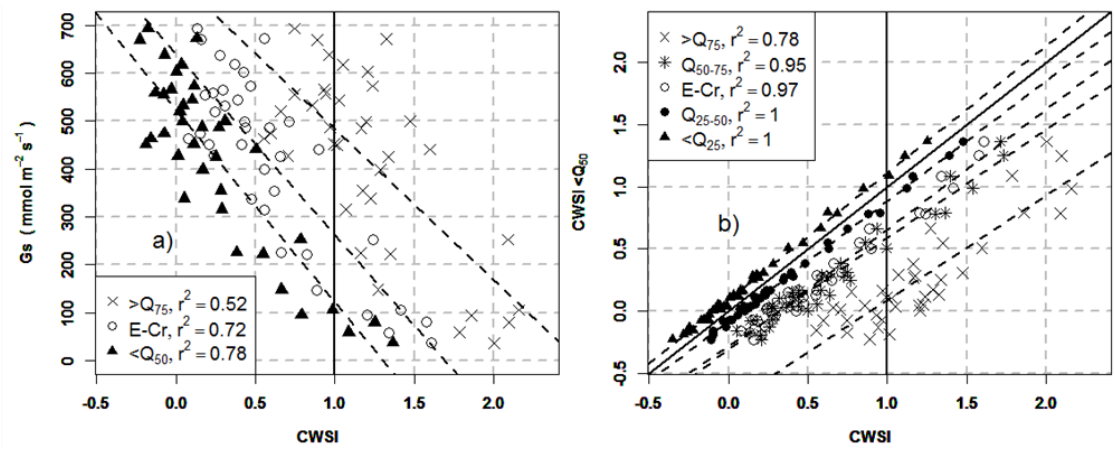

Fig. 3.9. Relationships found between leaf stomatal conductance (Gs) and the CWSI by extracting pixels from entire crowns (E-Cr), pixels below the middle quartile (<Q_{50}), and pixels in the upper quartile (>Q_{75}) for all flight dates (a). Relationships between CWSI pixels extracted from the middle quartile class (<Q_{50}) and all quartile-crown and entire tree crown segmentations explored (b). Solid black line represents the line 1:1, and dashed lines are fit lines for the studied quartile masks and entire crown mask.

The separability among water stress treatments via the ANOVA F-test and Tukey's HSD test (Table 3.4) showed statistically significant differences in the CWSI (p-value < 0.0005) between all the treatments explored, indicating that CWSI derived from high-resolution thermal imagery was able to separate between almond trees under different water regimes.

Table 3.4. ANOVA and Tukey's HSD post-hoc analysis of the CWSI extracted from quartile segmentations for each water stress treatment.

	ANOVA		Tukey's test	
	F-value	**p-value**	**T-value**	**p-value**
<Q50	60.28	4.6e-12	60.28	4.6e-12
FI-RF	…	…	-10.944	< 1e-04
FI-RDI	…	…	4.283	0.000383
RF-RDI	…	…	-7.814	< 1e-04

3.4 Discussion

This study explored the effects of within-tree crown variability on airborne-based fluorescence retrievals and the CWSI as indicators of water stress. The range of variation in water status observed in this experiment, ranging from well-watered to rainfed conditions, enabled the assessment of stress detection performance of the remote sensing indicators when different segmentation methods were applied to high-spatial resolution hyperspectral and thermal images. This methodology made it possible to assess the effects caused by shadows and background on the fluorescence and thermal indicators used for water stress detection. Sunlit vegetation and entire crowns were used to quantify the fluorescence signal, while temperature quartiles were used as a segmentation method for the canopy thermal imagery. It is important to note that the segmentation methods were applied automatically, minimizing the influence of the operator to identify the regions of interest.

Previous studies have demonstrated that the SIF signal and its relationship with the assimilation rate is reduced under complex canopy structures and with background soil effects (Zarco-Tejada et al., 2013). In this study, SIF retrievals extracted from entire crowns were affected by shadows, structural, and background soil effects, masking changes in fluorescence amplitude caused by the physiological condition. The results presented here show that chlorophyll fluorescence retrieval was highly degraded due to the effects of structure, leaf density, sunlit/shaded areas, and soil background. As shown in Fig. 3.4a, when the entire crown was used, the radiance magnitude was reduced in the range close to the O_2-A absorption peak, compared to sunlit pixels within the tree crowns. This result is in agreement with Hernández-Clemente et al. (2017), who demonstrated that SIF emission extracted from sunlit crown pixel radiance was greatly affected by the increasing contribution of shaded and background pixels. In this study, within-tree crown heterogeneity was confirmed by the higher coefficient of variation

observed in the SIF retrievals extracted from entire crowns (Table 3.2) for all watering regimes. By contrast, lower CV values of SIF were obtained from the sunlit crown segmentation areas, which are associated to vegetation pixels without soil contamination. The heterogeneity of the shaded and sunlit areas within almond tree crowns modulated the relationship between airborne fluorescence and assimilation rates. As shown in Fig. 3.7, the relationships between fluorescence and assimilation varied as a function of stress level and atmospheric conditions on each flight date. However, as shown on Table 3.2, water stress reduced airborne SIF retrievals, yielding a relative mean SIF that was lower in crowns of trees subjected to RF conditions than in those irrigated trees. This result is consistent with (Lee et al., 2013; Pérez-Priego et al., 2005), who demonstrated that the SIF signal is sensitive to plant water stress.

Daumard et al. (2012) showed that atmospheric impacts on SIF retrievals should be taken into account. This issue was observed in Fig. 3.7, which shows a changing relationship between the assimilation rate and the SIF quantified on different dates. The changes in the slope and amplitude of the relationships with the assimilation rate that are shown in the figure were due to several reasons: (i) the SIF emission was affected by atmospheric scattering effects (i.e., aerosol optical depth, aerosol height, surface albedo, and surface pressure) when the O_2-A absorption band at 760 nm was used to estimate the fluorescence emission (Frankenberg et al., 2011). Although the Fraunhofer method reduced the atmospheric scattering effects using bands close to the oxygen absorption band, these scattering effects were still present; (ii) the fluorescence signal was modulated not only by the irradiance levels but also by the water stress and ambient conditions imposed during the different flight dates; and (iii) the inherent offsets of the SIF approach created when it was calculated from broader bandwidth hyperspectral imagery (i.e., 5–7 nm FWHM), which generated absolute errors in the quantification of the SIF signal. For these reasons, specific strategies are required for the proper use of chlorophyll fluorescence measurements in precision agriculture.

Following a normalization SIF scheme, fluorescence emission was normalized by the maximum fluorescence signal emitted by the control well-watered almond trees, which served as a reference. The relationship obtained between the normalized fluorescence emission and the field-measured assimilation rate was linear and yielded better results when the sunlit crown segmentation was applied (r^2 = 0.66). Our approach confirmed the feasibility of using the normalized fluorescence signal as an indicator of

photosynthetic activity throughout the season. In this research, we also showed that normalized SIF retrieval was lower under rainfed conditions than under irrigated regimes in both tree crown segmentations explored (Fig. 3.8b). This result is consistent with previous studies (Flexas et al., 1999, 2002,; Zarco-Tejada et al., 2013b) that have shown that water stress induces changes in chlorophyll fluorescence emission. In this study, the ANOVA and Tukey's HSD post-hoc test (Table 3.3) confirmed that the normalized SIF retrieval extracted from sunlit areas within tree-crowns was able to separate the three water stress regimes analyzed (as was observed with the physiological measurements); by contrast, the normalized SIF extracted from entire crowns showed no differences between the irrigated treatments. These results highlight the need for high-resolution hyperspectral imagery to extract the SIF signal from sunlit vegetation within tree-crowns.

Other studies have shown that thermal imaging reveals spatial heterogeneity within tree-crowns (Agam et al., 2014; Gonzalez-Dugo et al., 2012) or between plant canopies (González-Dugo et al., 2006; Grant et al., 2007), which can be used as an indicator to monitor stress conditions. These studies have reported that the heterogeneity of canopy temperature is a reliable tool for tracking the water status using thermal airborne imagery. However, few studies have focused on the assessment of the variability of thermal airborne indicators within tree-crowns, probably due to the high resolution needed to accomplish this task. In this regard, Gonzalez-Dugo et al. (Gonzalez-Dugo et al., 2012) demonstrated that the mean canopy temperature in almond trees affects the relationship between intra-crown temperature variability and water potential. In fact, they demonstrated that the variability of crown temperature was higher in almond trees subjected to intermediate irrigation levels compared to well-watered ones and to trees subjected to the most water-stressed treatments. In that case, canopy architecture and soil background temperature had an influence as the temperature was extracted for entire tree crowns. However, in the present study, we extracted pure pixels. We analyzed CWSI variability between different crown areas and its relationship with stomatal conductance measured at the leaf level. The central part of the crowns displayed lower temperature values, which were associated with pure vegetation without soil contamination. However, in some cases, the pattern of the temperature distribution associated to pure vegetation may shift towards other crown areas due to changes caused by the density of vegetation canopy, crown structural effects, leaf angle

distribution, leaf area index, and the solar angle at the time of flight. The assessment of the CWSI as a temperature-derived normalized index allowed us to account for the environmental conditions at the time of acquisition and also to assess the thermal information from the three flight dates. Moreover, the calculation of the CWSI enabled the assessment of the area that better described overall plant performance, avoiding the contamination of soil background.

This study shows that pixels contained in crown areas below the 50th percentile ($<Q_{25}$ and Q_{25}–Q_{50}) corresponded to pure vegetation pixels without soil background effects (Figure 3.3d), compared to pixels included into the Q_{50}–Q_{75} and Q_{75} quartile classes associated with pixels with soil contamination and with low leaf densities. These results explained the high average CWSI values displayed when pixels extracted from Q_{50}– Q_{75} and Q_{75} segmentations were used (Fig. 3.6), an effect observed in all treatments (Table 3.2). As a result, the mean CWSI values reached the upper out-of-range limit. Overall, the CWSI retrieved from the lower half quartile ($<Q_{50}$) was within the theoretical CWSI range for the irrigated treatments and rainfed regime. However, the mean CWSI value recorded in RF trees for Q_{25}–Q_{50} was slightly above the maximum theoretical CWSI value. This bias was due to the effect of soil background related to the low leaf area density. According to the ANOVA F-test followed by Tukey's HSD post-hoc analysis (Table 3.4), the aggregated quartile classes ($<Q_{50}$) displayed the required accuracy to identify the differences under different water regimes.

The relationships obtained between the CWSI and field-measured stomatal conductance were statistically significant (p-value < 0.005) and well correlated, yielding weaker relationships with stomatal conductance for the upper quartile-crown segmentations (Q_{75}) (r^2 = 0.62). This inverse relationship with Gs yielded robust statistical results when the CWSI was extracted from pixels below the middle quartile (r^2 = 0.78 and p-value < 0.005). The good agreement with stomatal conductance confirms that the CWSI can be used as a stress indicator in precision agriculture applications. In agreement with recent studies (Meron et al., 2010;Gonzalez-Dugo et al., 2015), this research also showed that the CWSI is a reliable tool for monitoring the spatial variability of water stress using high-resolution thermal imagery. Furthermore, our results provide a detailed quantification of the spatial variability of the crown

temperature within almond tree crowns and identify an automatic procedure for improving the accuracy for monitoring water status in orchard tree crops.

3.5 Conclusion

This study demonstrates the large effects caused by within-tree structural variability and background on the airborne-derived SIF and CWSI physiological indicators used for water stress detection. Results highlight the importance of collecting high-resolution hyperspectral and thermal imagery in orchard crops to enable targeting pure crown-level vegetation pixels. The crown segmentation methods applied to extract sunlit vegetation crown areas improved the relationships between SIF and field-measured leaf assimilation rate. The SIF retrievals carried out using sunlit vegetation pixels minimized the impact of canopy structure and reduced the soil background effects, enabling a better detection of water stress. In the thermal imagery, the crown segmentation methods demonstrated that within-crown shadows and the background affected CWSI. When entire tree crowns were used, the CWSI values obtained fell outside the expected theoretical range of variation, affecting the relationship with stomatal conductance.

References

Agam, N., Segal, E., Peeters, A., Levi, A., Dag, A., Yermiyahu, U., Ben-Gal, A., 2014. Spatial distribution of water status in irrigated olive orchards by thermal imaging. Precis. Agric. 15, 346–359. https://doi.org/10.1007/s11119-013-9331-8

Bellvert, J., 2014. El uso de la teledetección de alta resolución como herramienta para realizar un manejo eficiente del riego en viñedos. Univ. Cordoba.

Bellvert, J., Marsal, J., Girona, J., Gonzalez-Dugo, V., Fereres, E., Ustin, S.L., Zarco-Tejada, P.J., 2016. Airborne thermal imagery to detect the seasonal evolution of crop water status in peach, nectarine and Saturn peach orchards. Remote Sens. 8, 1–17. https://doi.org/10.3390/rs8010039

Bendig, J., Yu, K., Aasen, H., Bolten, A., Bennertz, S., Broscheit, J., Gnyp, M.L., Bareth, G., 2015. Combining UAV-based plant height from crop surface models, visible, and near infrared vegetation indices for biomass monitoring in barley. Int. J. Appl. Earth Obs. Geoinf. 39, 79–87. https://doi.org/10.1016/j.jag.2015.02.012

Berni, J., Zarco-Tejada, P.J., Suarez, L., Fereres, E., 2009. Thermal and Narrowband Multispectral Remote Sensing for Vegetation Monitoring From an Unmanned Aerial Vehicle. IEEE Trans. Geosci. Remote Sens. 47, 722–738. https://doi.org/10.1109/TGRS.2008.2010457

Bivand, R., 2017. classInt: Choose Univariate Class Intervals.

Bivand, R., Lewin-Koh, N., 2017. maptools: Tools for Reading and Handling Spatial Objects.

Bivand, R.S., Pebesma, E., Gomez-Rubio, V., 2013. Applied spatial data analysis with R, Second edition. Springer, NY.

Calderón, R., Navas-Cortés, J.A., Lucena, C., Zarco-Tejada, P.J., 2013. High-resolution airborne hyperspectral and thermal imagery for early detection of Verticillium wilt of olive using fluorescence, temperature and narrow-band spectral indices. Remote Sens. Environ. 139, 231–245. https://doi.org/10.1016/j.rse.2013.07.031

Damm, A., Elber, J., Erler, A., Gioli, B., Hamdi, K., Hutjes, R., Kosvancova, M., Meroni, M., Miglietta, F., Moersch, A., Moreno, J., Schickling, A., Sonnenschein, R., Udelhoven, T., van der Linden, S., Hostert, P., Rascher, U., 2010. Remote sensing of sun-induced fluorescence to improve modeling of diurnal courses of gross primary production (GPP). Glob. Chang. Biol. 16, 171–186. https://doi.org/10.1111/j.1365-2486.2009.01908.x

Damm, A., Erler, A., Hillen, W., Meroni, M., Schaepman, M.E., Verhoef, W., Rascher, U., 2011. Modeling the impact of spectral sensor configurations on the FLD retrieval accuracy of sun-induced chlorophyll fluorescence. Remote Sens. Environ. 115, 1882–1892. https://doi.org/10.1016/j.rse.2011.03.011

Dandois, J.P., Ellis, E.C., 2013. High spatial resolution three-dimensional mapping of vegetation spectral dynamics using computer vision. Remote Sens. Environ. 136, 259–276. https://doi.org/10.1016/j.rse.2013.04.005

Daumard, F., Goulas, Y., Champagne, S., Fournier, A., Ounis, A., Olioso, A., Moya, I., 2012. Continuous monitoring of canopy level sun-induced chlorophyll fluorescence during the growth of a sorghum field. IEEE Trans. Geosci. Remote Sens. 50, 4292–4300. https://doi.org/10.1109/TGRS.2012.2193131

Flexas, J., Briantais, J.M., Cerovic, Z., Medrano, H., Moya, I., 2000. Steady-state and maximum chlorophyll fluorescence responses to water stress in grapevine leaves: A new remote sensing system. Remote Sens. Environ. 73, 283–297. https://doi.org/10.1016/S0034-4257(00)00104-8

Flexas, J., Escalona, J.M., Evain, S., Gulías, J., Moya, I., Osmond, C.B., Medrano, H., 2002. Steady-state chlorophyll fluorescence (Fs) measurements as a tool to follow variations of net CO2 assimilation and stomatal conductance during water-stress in C3 plants. Eur. Sp. Agency, (Special Publ. ESA SP 26–29. https://doi.org/10.1034/j.1399-3054.2002.1140209.x

Flexas, J., Escalona, J.M., Medrano, H., 1999. Water stress induces different levels of photosynthesis and electron transport rate regulation in grapevines. Plant, Cell Environ. 22, 39–48. https://doi.org/10.1046/j.1365-3040.1999.00371.x

Frankenberg, C., Butz, A., Toon, G.C., 2011. Disentangling chlorophyll fluorescence from atmospheric scattering effects in O_2 A-band spectra of reflected sun-light. Geophys. Res. Lett. 38, 1–5. https://doi.org/10.1029/2010GL045896

Fuchs, M., 1990. Infrared measurement of canopy temperature and detection of plant water stress. Theor. Appl. Climatol. 42, 253–261. https://doi.org/10.1007/BF00865986

Gardner, B.R., Blad, B.L., Watts, D.G., 1981. Plant and air temperatures in differentially-irrigated corn. Agric. Meteorol. 25, 207–217. https://doi.org/10.1016/0002-1571(81)90073-X

González-Dugo, M.P., Moran, M.S., Mateos, L., Bryant, R., 2006. Canopy temperature variability as an indicator of crop water stress severity. Irrig. Sci. 24, 233–240. https://doi.org/10.1007/s00271-005-0022-8

Gonzalez-Dugo, V., Goldhamer, D., Zarco-Tejada, P.J., Fereres, E., 2015. Improving the precision of irrigation in a pistachio farm using an unmanned airborne thermal system. Irrig. Sci. 33, 43–52. https://doi.org/10.1007/s00271-014-0447-z

Gonzalez-Dugo, V., Hernandez, P., Solis, I., Zarco-Tejada, P.J., 2015. Using high-resolution hyperspectral and thermal airborne imagery to assess physiological condition in the context of wheat phenotyping. Remote Sens. 7, 13586–13605. https://doi.org/10.3390/rs71013586

Gonzalez-Dugo, V., Zarco-Tejada, P., Berni, J.A.J., Suárez, L., Goldhamer, D., Fereres, E., 2012. Almond tree canopy temperature reveals intra-crown variability that is water stress-dependent. Agric. For. Meteorol. 154–155, 156–165. https://doi.org/10.1016/j.agrformet.2011.11.004

Gonzalez-Dugo, V., Zarco-Tejada, P.J., Fereres, E., 2014. Applicability and limitations of using the crop water stress index as an indicator of water deficits in citrus orchards. Agric. For. Meteorol. 198–199, 94–104. https://doi.org/10.1016/j.agrformet.2014.08.003

Grant, O.M., Tronina, Ł., Jones, H.G., Chaves, M.M., 2007. Exploring thermal imaging variables for the detection of stress responses in grapevine under different irrigation regimes. J. Exp. Bot. 58, 815–825. https://doi.org/10.1093/jxb/erl153

Hernández-Clemente, R., Navarro-Cerrillo, R.M., Romero Ramírez, F.J., Hornero, A., Zarco-Tejada, P.J., Ramírez, F.J.R., Hornero, A., Zarco-Tejada, P.J., 2014. A novel methodology to estimate single-tree biophysical parameters from 3D digital imagery compared to aerial laser scanner data. Remote Sens. 6, 11627–11648. https://doi.org/10.3390/rs61111627

Hernández-Clemente, R., North, P.R.J., Hornero, A., Zarco-Tejada, P.J., 2017. Assessing the effects of forest health on sun-induced chlorophyll fluorescence using the FluorFLIGHT 3-D radiative transfer model to account for forest structure. Remote Sens. Environ. 193, 165–179. https://doi.org/10.1016/j.rse.2017.02.012

Hijmans, R.J., 2017. raster: Geographic Data Analysis and Modeling.

Hsiao, T.C., 1973. Plant Responses to Water Stress. Annu. Rev. Plant Physiol. 24, 519–570. https://doi.org/10.1146/annurev.pp.24.060173.002511

Idso, S.B., Jackson, R.D., Pinter, P.J., Reginato, R.J., Hatfield, J.L., 1981. Normalizing the stress-degree-day parameter for environmental variability. Agric. Meteorol. 24, 45–55. https://doi.org/10.1016/0002-1571(81)90032-7

Jackson, R.D., Idso, S.B., Reginato, R.J., Pinter, J.P.J., 1981. Canopy temperature as a crop water stress indicator. Water Resour. Res. 17, 1133–1138. https://doi.org/10.1029/WR017i004p01133

Jones, H.G., Serraj, R., Loveys, B.R., Xiong, L., Wheaton, A., Price, A.H., 2009. Thermal infrared imaging of crop canopies for the remote diagnosis and quantification of plant responses to water stress in the field. Funct. Plant Biol. 36, 978–989. https://doi.org/10.1071/FP09123

Lee, J.-E., Frankenberg, C., van der Tol, C., Berry, J.A., Guanter, L., Boyce, C.K., Fisher, J.B., Morrow, E., Worden, J.R., Asefi, S., Badgley, G., Saatchi, S., 2013. Forest productivity and water stress in Amazonia: observations from GOSAT chlorophyll fluorescence. Proc. R. Soc. B Biol. Sci. 280, 20130171–20130171. https://doi.org/10.1098/rspb.2013.0171

Lichtenthaler, H.K., Lang, M., Sowinska, M., Heisel, F., Miehé, J.A., 1996. Detection of Vegetation Stress Via a New High Resolution Fluorescence Imaging System. J. Plant Physiol. 148, 599–612. https://doi.org/10.1016/S0176-1617(96)80081-2

Lichtenthaler, H.K., Rinderle, U., 1988. The Role of Chlorophyll Fluorescence in The Detection of Stress Conditions in Plants. C R C Crit. Rev. Anal. Chem. 19, S29–S85. https://doi.org/10.1080/15476510.1988.10401466

López-López, M., Espadador, M., Testi, L., Lorite, I.J., Orgaz, F., Fereres, E., 2018. Water use of irrigated almond trees when subjected to water deficits. Agric. Water Manag. 195, 84–93. https://doi.org/10.1016/j.agwat.2017.10.001

Meron, M., Tsipris, J., Orlov, V., Alchanatis, V., Cohen, Y., 2010. Crop water stress mapping for site-specific irrigation by thermal imagery and artificial reference surfaces. Precis. Agric. 11, 148–162. https://doi.org/10.1007/s11119-009-9153-x

Meroni, M., Busetto, L., Colombo, R., Guanter, L., Moreno, J., Verhoef, W., 2010. Performance of Spectral Fitting Methods for vegetation fluorescence quantification. Remote Sens. Environ. 114, 363–374. https://doi.org/10.1016/j.rse.2009.09.010

Meroni, M., Colombo, R., 2006. Leaf level detection of solar induced chlorophyll fluorescence by means of a subnanometer resolution spectroradiometer. Remote Sens. Environ. 103, 438–448. https://doi.org/10.1016/j.rse.2006.03.016

Moya, I., Camenen, L., Evain, S., Goulas, Y., Cerovic, Z.G., Latouche, G., Flexas, J., Ounis, A., 2004. A new instrument for passive remote sensing: 1. Measurements of sunlight-induced chlorophyll fluorescence. Remote Sens. Environ. 91, 186–197.

https://doi.org/10.1016/j.rse.2004.02.012

Pebesma, E.J., Bivand, R.S., 2005. Classes and methods for spatial data in R. R News 5, 9–13.

Pérez-Priego, O., Zarco-Tejada, P.J., Miller, J.R., Sepulcre-Cantó, G., Fereres, E., 2005. Detection of water stress in orchard trees with a high-resolution spectrometer through chlorophyll fluorescence In-Filling of the O2-A band. IEEE Trans. Geosci. Remote Sens. 43, 2860–2868. https://doi.org/10.1109/TGRS.2005.857906

Plascyk, J.A., Gabriel, F.C., 1975. The Fraunhofer line discriminator MKII an airborne instrument for precise and standardized ecological luminescence measurement. IEEE Trans. Instrum. Meas. 24, 306–313. https://doi.org/10.1109/TIM.1975.4314448

Porcar-Castell, A., Tyystjärvi, E., Atherton, J., Van Der Tol, C., Flexas, J., Pfündel, E.E., Moreno, J., Frankenberg, C., Berry, J.A., 2014. Linking chlorophyll a fluorescence to photosynthesis for remote sensing applications: Mechanisms and challenges. J. Exp. Bot. 65, 4065–4095. https://doi.org/10.1093/jxb/eru191

R Core Team, 2018. R: A Language and Environment for Statistical Computing.

Rascher, U., Alonso, L., Burkart, A., Cilia, C., Cogliati, S., Colombo, R., Damm, A., Drusch, M., Guanter, L., Hanus, J., Hyvärinen, T., Julitta, T., Jussila, J., Kataja, K., Kokkalis, P., Kraft, S., Kraska, T., Matveeva, M., Moreno, J., Muller, O., Panigada, C., Pikl, M., Pinto, F., Prey, L., Pude, R., Rossini, M., Schickling, A., Schurr, U., Schüttemeyer, D., Verrelst, J., Zemek, F., 2015. Sun-induced fluorescence - a new probe of photosynthesis: First maps from the imaging spectrometer HyPlant. Glob. Chang. Biol. 21, 4673–4684. https://doi.org/10.1111/gcb.13017

Rodriguez, D., Sadras, V.O., Christensen, L.K., Belford, R., 2005. Spatial assessment of the physiological status of wheat crops as affected by water and nitrogen supply using infrared thermal imagery. Aust. J. Agric. Res. 56, 983–993. https://doi.org/10.1071/AR05035

Rouse, J.W., Hass, R.H., Schell, J.A., Deering, D.W., 1973. Monitoring vegetation systems in the great plains with ERTS. Third Earth Resour. Technol. Satell. Symp. 1, 309–317. https://doi.org/citeulike-article-id:12009708

Sauvola, J., Pietikäinen, M., 2000. Adaptive document image binarization. Pattern Recognit. 33, 225–236. https://doi.org/10.1016/S0031-3203(99)00055-2

Schreiber, U., Bilger, W., 1987. Rapid assessment of stress effects on plant leaves by chlorophyll fluorescence measurements, in: Tenhunen, J.D., Catarino, F.M., Lange, O.L., Oechel, W.C. (Eds.), Plant Response to Stress: Functional Analysis in Mediterranean Ecosystems. Springer Berlin Heidelberg, Berlin, Heidelberg, pp. 27–53. https://doi.org/10.1007/978-3-642-70868-8_2

Slatyer R. O, 1967. Plant-water relationships. Academic Press.

Xiao, Q., Ustin, S.L., McPherson, E.G., 2004. Using AVIRIS data and multiple-masking techniques to map urban forest tree species. Int. J. Remote Sens. 25, 5637–5654. https://doi.org/10.1080/01431160412331291224

Zarco-Tejada, P.J., González-Dugo, V., Berni, J.A.J., 2012. Fluorescence, temperature and narrow-band indices acquired from a UAV platform for water stress detection using a micro-hyperspectral imager and a thermal camera. Remote Sens. Environ. 117, 322–337. https://doi.org/10.1016/j.rse.2011.10.007

Zarco-Tejada, P.J., González-Dugo, M. V., Fereres, E., 2016. Seasonal stability of chlorophyll fluorescence quantified from airborne hyperspectral imagery as an indicator of net photosynthesis in the context of precision agriculture. Remote Sens. Environ. 179, 89–103. https://doi.org/10.1016/j.rse.2016.03.024

Zarco-Tejada, P.J., González-Dugo, V., Williams, L.E., Suárez, L., Berni, J.A.J.J., Goldhamer, D., Fereres, E., 2013a. A PRI-based water stress index combining structural and chlorophyll effects: Assessment using diurnal narrow-band airborne imagery and the CWSI thermal index. Remote Sens. Environ. 138, 38–50. https://doi.org/10.1016/j.rse.2013.07.024

Zarco-Tejada, P.J., Morales, A., Testi, L., Villalobos, F.J., 2013b. Spatio-temporal patterns of chlorophyll fluorescence and physiological and structural indices acquired from hyperspectral imagery as compared with carbon fluxes measured with eddy covariance. Remote Sens. Environ. 133, 102–115. https://doi.org/10.1016/j.rse.2013.02.003

Zarco-Tejada, P.J., Suarez, L., Gonzalez-Dugo, V., 2013. Spatial resolution effects on chlorophyll fluorescence retrieval in a heterogeneous canopy using hyperspectral imagery and radiative transfer simulation. IEEE Geosci. Remote Sens. Lett. 10, 937–941. https://doi.org/10.1109/LGRS.2013.2252877

Chapter 4

International Journal of Applied Earth Observation and Geoinformation
Volume 70, August 2018, Pages 105-117

Improved nitrogen retrievals with airborne-derived fluorescence and plant traits quantified from VNIR-SWIR hyperspectral imagery in the context of precision agriculture

Journal Metrics
CiteScore: 4.46
Impact Factor: 4.003
5-Year Impact Factor: 4.433

Carlos Camino [a], Victoria González-Dugo [a], Pilar Hernández [a], J.C. Sillero [b], Pablo J. Zarco-Tejada [a]

[a] Instituto de Agricultura Sostenible (IAS), Consejo Superior de Investigaciones Científicas (CSIC), Alameda del Obispo s/n, 14004, Córdoba, Spain

[b] Instituto Andaluz de Investigación y Formación Agraria, Pesquera, Alimentaria y de la Producción Ecológica (IFAPA), Centro Alameda del Obispo, s/n, 14004, Córdoba, Spain

https://doi.org/10.1016/j.jag.2018.04.013

Published in International Journal of Applied Earth Observation and Geoinformation. Volume 70, August 2018, Pages 105-117. https://doi.org/10.1016/j.jag.2018.04.013

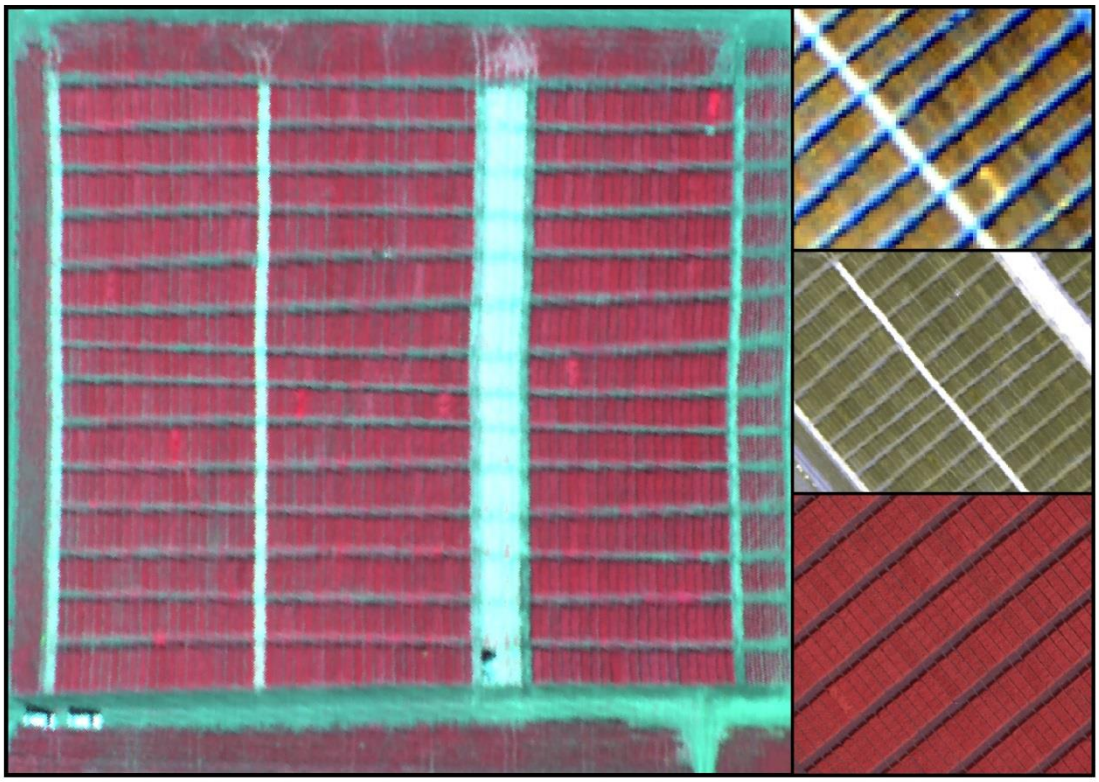

Chapter 4: Improved nitrogen retrievals with airborne-derived fluorescence and plant traits quantified from VNIR-SWIR hyperspectral imagery in the context of precision agriculture

Resumen

En condiciones semiáridas, el nitrógeno (N) es, después del agua, el principal factor limitante del rendimiento del cultivo, y su cuantificación con precisión es esencial. Estudios recientes han demostrado que la fluorescencia clorofílica inducida por el sol (SIF) cuantificada a partir de imágenes hiperespectrales es un indicador fiable de la actividad fotosintética en el contexto de la agricultura de precisión y en la detección temprana de estrés del cultivo. En condiciones de estrés, el papel de la fluorescencia puede ser crítico para nuestra comprensión de los niveles de nitrógeno debido a su relación con la fotosíntesis y la tasa máxima de carboxilación (Vcmax). La investigación llevada a cabo en este estudio tiene como objetivo evaluar la contribución desempeñada por la fluorescencia clorofílica obtenida mediante sensores aerotransportados hiperespectrales en la cuantificación de N en condiciones mediterráneas de regadío y de secano. El estudio se llevó a cabo en tres ensayos de selección fenotípica de trigo localizados en el sur de España durante las campañas 2015 y 2016. Las campañas aerotransportadas adquirieron imágenes con dos cámaras hiperespectrales que cubrían las regiones espectrales de 400–850 nm (20 cm de resolución) y 950-1750 nm (70 cm de resolución). Para cuantificar N, se construyeron modelos de regresión múltiple con y sin SIF a partir de caracteres de la planta estimados por inversión del modelo de transferencia radiativa (RTM) y mediante la utilización de índices espectrales. Los resultados mostraron que la precisión de los modelos para la estimación de N aumentó tras incluir la fluorescencia clorofílica ($r^2_{LOOCV} \geq 0.92$; $p < 0.0005$) en comparación con los modelos construidos sólo con constituyentes bioquímicos como clorofila *a* + *b* (C_{ab}), materia seca (C_m) y espesor de agua equivalente (C_w) (r^2_{LOOCV} varió de 0,68 a 0,77; $p < 0{,}005$). Además, los índices de nitrógeno (NI) centrados en 1510 nm obtuvieron mejores relaciones con la concentración de N (r^2 = 0,69) que los índices de clorofila tradicionales (TCARI / OSAVI r^2= 0,45) y los índices estructurales (NDVI r^2= 0,57) calculados en la región VNIR. Este trabajo demuestra que, en condiciones de riego y secano, los indicadores directamente relacionados con la fotosíntesis, como la fluorescencia clorofílica, mejoran las predicciones de la concentración de N.

Abstract

In semi-arid conditions, nitrogen (N) is the main limiting factor of crop yield after water, and its accurate quantification remains essential. Recent studies have demonstrated that solar-induced chlorophyll fluorescence (SIF) quantified from hyperspectral imagery is a reliable indicator of photosynthetic activity in the context of precision agriculture and for early stress detection purposes. The role of fluorescence might be critical to our understanding of N levels due to its link with photosynthesis and the maximum rate of carboxylation (Vcmax) under stress. The research presented here aimed to assess the contribution played by airborne-retrieved solar-induced chlorophyll fluorescence to the retrieval of N under irrigated and rainfed Mediterranean conditions. The study was carried out at three field sites used for wheat phenotyping purposes in Southern Spain during the 2015 and 2016 growing seasons. Airborne campaigns acquired imagery with two hyperspectral cameras covering the 400–850 nm (20 cm resolution) and 950-1750 nm (70 cm resolution) spectral regions. The performance of multiple regression models built for N quantification with and without including the airborne-retrieved SIF was compared with the performance of models built with plant traits estimated by model inversion, and also with standard approaches based on single spectral indices. Results showed that the accuracy of the models for N retrieval increased when chlorophyll fluorescence was included ($r^2_{LOOCV} \geq 0.92$; $p<0.0005$) as compared to models only built with chlorophyll a+b (C_{ab}), dry matter (C_m) and equivalent water thickness (C_w) plant traits (r^2_{LOOCV} ranged from 0.68 to 0.77; $p< 0.005$). Moreover, nitrogen indices (NIs) centered at 1510 nm yielded more reliable agreements with N concentration ($r^2=0.69$) than traditional chlorophyll indices (TCARI/OSAVI $r^2=0.45$) and structural indices (NDVI $r^2=0.57$) calculated in the VNIR region. This work demonstrates that under irrigated and non-irrigated conditions, indicators directly linked with photosynthesis such as chlorophyll fluorescence improves predictions of N concentration.

4.1 Introduction

Nitrogen (N) content plays an important role in the plant life cycle. In the most situations, N is the major limiting factor of crop yield after water deficiency, and it is an essential element in plant growth (Lemaire et al., 2008). It is well documented that an adequate N supply is crucial for the maintenance of plant biochemistry quality (Nobel, 2009), and that N deficiency greatly changes the photosynthetic capacity, leading to a decrease in photosynthetic quantum yield and light-saturated photosynthetic rate (Khamis et al., 1990). N management of crops has important economic impacts and environmental implications, although nitrogen overfertilization is widely used by farmers as a form of insurance against uncertain soil fertility (Tremblay et al., 2012). In particular, a higher N supply causes significant effects on the environment. Hence, an adequate N management strategy is needed to guide precision diagnosis of soil status and efficient crop management.

Traditionally, the N concentration is estimated using chemical analyses based on leaf tissue, such as Kjeldahl-digestion and Dumas-combustion, due to their reliability in organic N determination. However, these methods are destructive, time consuming, and need complex analysis. Moreover, traditional N estimates provide only limited information, as sampling is based on only a limited number of sites in a given field; they are therefore not suitable for the continuous monitoring of N content in the entire field. For these reasons, remote sensing and, in particular, hyperspectral imagery, can be useful for monitoring spatial and temporal variations in crop N content over large areas (Quemada et al., 2014).

The use of simple empirical models that incorporate hyperspectral reflectance indices is still the dominant method used to estimate N (Ferwerda et al., 2005; Stroppiana et al., 2009; Herrmann et al., 2010; Wang et al., 2012; Li et al., 2014; Mahajan et al., 2016). Several studies have shown improvements in canopy N quantifications using reflectance bands in the near infrared (NIR) and in the short-wave infrared (SWIR) regions (Kokaly, 1999; Ferwerda et al., 2005; Herrmann et al., 2010; Pimstein et al., 2011; Gnyp et al., 2014; Mahajan et al., 2014), especially when indices calculated from wavelengths centered at 850 and 1510 nm are used, as described in detail by Herrmann et al. (2010). Serrano et al. (2002) also showed that the combination of the 1510 nm and 1680 nm spectral regions was sensitive to N concentration in green

biomass. Nevertheless, and despite the successful empirical relationships, nitrogen estimation at the canopy level from remote sensing requires appropriate modeling strategies due to the large contribution of structural and shadow effects to canopy reflectance (Zarco-Tejada et al., 2005). On the other hand, radiative transfer models offer advantages compared to index-based empirical models regarding robustness and transferability (Jacquemoud and Baret, 1990; Zarco-Tejada et al., 2004; Schlerf and Atzberger, 2006; Wang et al., 2015), and these have been widely proposed as a method for retrieving chlorophyll content, dry matter, and water content from remote sensing data (Clevers and Kooistra, 2012; Jacquemoud and Baret, 1990; Zarco-Tejada et al., 2004). In this context, recent studies have evaluated the estimation of leaf N content using models built with leaf and canopy biophysical parameters retrieved by inversion (e.g. Wang et al., 2015), and these have yielded reasonable success (r^2= 0.58).

In recent years, the quantification of chlorophyll fluorescence has attracted increasing attention in the context of global monitoring of crop physiology and vegetation functioning, and this method can offer improvements on the estimation of N status (Tremblay et al., 2012). Chlorophyll fluorescence is generally considered as a direct proxy for electron transport rate and hence photosynthetic activity (Genty et al., 1989; Weis and Berry, 1987). The leaf-level maximum carboxylation rate (Vcmax; µmol·CO2·m-2·s-1) is closely related to the chlorophyll content at leaf scale (Croft et al., 2017; Houborg et al., 2013) and with solar-induced chlorophyll fluorescence (SIF) (Rascher et al., 2015; Yang et al., 2015). In this regard, SIF can be considered as a direct link with Vcmax through its strong connexion to chlorophyll content and photosynthetic activity (Walker et al., 2014). In fact, recent studies have demonstrated the link between chlorophyll fluorescence and photosynthetic activity at leaf and canopy levels (see e.g. Zarco-Tejada et al., 2013, 2016; Cendrero-Mateo et al., 2016). The rationale is based on the dependence of chlorophyll fluorescence emissions on chlorophyll concentration and photosystem I (PSI) and II (PSII) efficiency (Lichtenthaler et al., 1996). It is well documented that N deficiency affects PSII photochemistry, lowering the quantum yield electron transport, the photochemical efficiency, and therefore the assimilation rate (Lu and Zhang, 2000; Jin et al., 2015).

Crop water status may alter N balance: crop N demand is reduced under drought conditions, as growth rate diminishes (Gonzalez-Dugo et al. 2010). In arid and semi-arid environments, the co-limitation between nitrogen and water often reduces crop production which therefore must be considered together (Sadras, 2004). For these reasons, spectral indicators related to the leaf functioning, as chlorophyll fluorescence, is a potentially important candidate for improving the quantification of N concentration using passive remote sensing techniques. The present study aimed to explore the contribution of airborne-retrieved chlorophyll fluorescence to the quantification of N concentration using hyperspectral imagery. Specifically, we evaluated the fluorescence quantification in spring wheat (early sowing) grown under rainfed and irrigated conditions to assess whether they contributed significantly to the retrieval of N concentration in the context of precision agriculture and plant phenotyping experiments.

4.2 Material and Methods

4.2.1 Study area

The study was carried out in 2015 and 2016 at three field trial sites for durum wheat (*Triticum turgidum L. var. durum)* and bread wheat (*Triticum aestivum L.)* selection in Southern Spain. The sowing date for all sites was mid-November in the previous year. Regarding fertilization, pest and disease management, all the plots received the same treatment at all trial sites. Fertilization with diammonium phosphate and urea was carried out in early November, while similar amounts of fungicides and pesticides were applied at the early and middle growth stages at all trial sites.

The first trial site was located in Ecija (EC), near Seville, Southern Spain (*37°32'17"N, 5°06'57"W*), which was managed under rainfed conditions in 2015. The experiment was designed with a balanced square lattice design using 300 individual plots (6 x 1.25 meters) separated in four blocks, with 150 varieties of durum wheat and 150 of bread wheat. Each cultivar was replicated three times per block (Fig. 4.1a).

The second site trial was in Carmona (CA), also close to Seville, Southern Spain (*37°30'29"N, 5°34'42"W*) in 2015. The experiment comprised 882 individual plots (7.5x1.25 meters) divided into two blocks managed under rainfed conditions and one block under irrigated conditions. Each block contained a mixture of varieties of durum and bread wheat, each cultivar replicated three times per block (Fig. 4.1b).

The third trial site was managed by IFAPA in Santaella (SA), near Cordoba, Southern Spain (*37°31'34"N, 4°50'40"W*) in 2016, where 20 varieties of durum wheat and 20 varieties of bread wheat were replicated three times under irrigated and rainfed conditions (Fig. 4.1c). The plot size was 15 m^2 (10 x 1.5 meters).

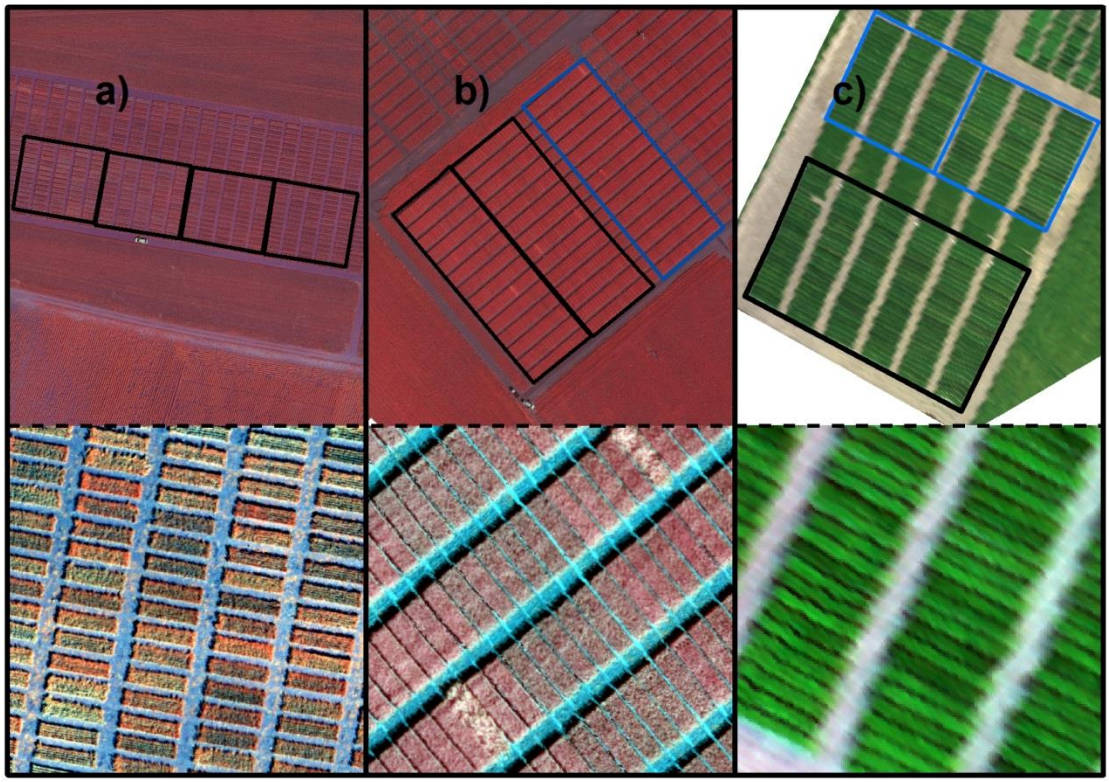

Fig. 4.1. Scene of the field trial sites at EC (a), CA (b) and Santaella (c) obtained with a color infrared camera (CIR; a and b, not used for analysis in this study) and the hyperspectral imagery (c) on board the aircraft. Black rectangles indicate plots under rainfed conditions and blue rectangles indicate plot under irrigated conditions.

4.2.2 Field data

In order to assess the physiology and the leaf optical properties of the wheat, a series of leaf-level measurements were made concurrently with the airborne flights at midday (12:00 to 13:00 h local time) at all the trial sites. A summary of field measurements and airborne campaigns at each trial site is shown in Table 4.1. The wheat growth stage during the flight campaigns refers to the stem length at the time of the first flight in Santaella (SA-1) and grain filling (milking stage) at the time of the flights in EC, CA and the second flight in Santaella (SA-2).

Leaf water potential (ψ_L; MPa) was measured using a pressure chamber (Model 600 Pressure Chamber Instrument, PMI Instrument Company, Albany, NY, USA) on two sunlit leaves per plot. Assimilation rate (A; $\mu mol \cdot m^{-2} \cdot s^{-1}$) and stomatal conductance (Gs; $mmol \cdot m^{-2} \cdot s^{-1}$) were measured using a photosynthesis measurement system (LCDpro-SD, ADC Bioscientific Ltd., Herts, UK) on two sunlit leaves per plot. Steady-state leaf fluorescence yield (Ft) and a SPAD chlorophyll content indicator were measured on 10 to 15 leaves per plot using a FluorPen FP100 (Photon Systems Instruments, Brno, Czech Republic) and a chlorophyll meter (SPAD-502, Minolta Corp., Ramsey, NJ, USA), respectively. The relationship between chlorophyll concentration and SPAD readings for wheat found by Uddling *et al*. (2007) was applied to convert SPAD data into chlorophyll content ($\mu g \cdot cm^{-2}$). Total N concentration was determined by the Kjeldhal method (Kjeldahl, 1883) on 20-25 sunlit leaves sampled per plot. As in the rest of the physiological measurements, a random selection of the sunlit leaves was carried out from the central area of each plot.

Table 4.1. Field measurements and flight dates during the 2015 and 2016 campaigns.

Year	Site	Flight dates	Type of flight (a)	Field measurements	Plots with field data
2015	EC	28/05	Noon (T+VNIR +SWIR)	ψ_L, A, Gs, Ft, SPAD, N	12 (b)
	CA	30/05	Noon (T+VNIR +SWIR)	ψ_L, A, Gs, Ft, SPAD, N	18 (b)
2016	SA-1	17/03	Noon (T+VNIR +SWIR)	ψ_L, A, Gs, Ft, SPAD, N	24 (b) and 45(c)
	SA-2	26/04	Noon (T+VNIR +SWIR)	ψ_L, A, Gs, Ft, SPAD, N	24 (b) and 50(c)

a T= thermal camera, VNIR = hyperspectral visible and infrared camera (400-885 nm), SW NIR = hyperspectral near-infrared and short-wave infrared camera (950-1750 nm).
b number of plots with all leaf measurements
c number of plots with only measurements of SPAD and total leaf nitrogen.

4.2.3 Airborne hyperspectral imagery

A hyperspectral imager covering the visible and near-infrared region (Micro-Hyperspec VNIR, Headwall Photonics, Fitchburg, MA, USA) and a second hyperspectral imager covering the NIR and the SWIR regions (Micro-Hyperspec NIR-100, Headwall Photonics) were installed in tandem on a Cessna aircraft operated by the Laboratory for Research Methods in Quantitative Remote Sensing (QuantaLab), Consejo Superior de Investigaciones Científicas (IAS-CSIC, Spain). Imagery was acquired at 250 m above ground level with the aircraft flying on the solar plane during the flight campaigns of 2015 and 2016. The campaigns were flown at midday (local time) to minimize differences due to sun angle effects between flights.

The micro-hyperspec VNIR was set up with a configuration of 260 spectral bands acquired at 8 nm/pixel and 12-bit radiometric resolution in the 400–885 nm spectral region, thus yielding a 6.4 nm Full Width at Half Maximum (FWHM) with a 25-µm slit. The acquisition and storage module had a 50 fps frame rate with an integration time of 25 ms. The 8-mm focal length lens yielded an IFOV of 0.93 mrad and an angular FOV of 50° with a spatial resolution of 20 cm (Fig. 4.2a) (further information regarding the setup of micro-hyperspec VNIR can be obtained from Zarco-Tejada *et al*., 2016).

The micro-hyperspec NIR-100 camera was flown with a configuration of 165 spectral bands and 16-bit radiometric resolution in the spectral region of 950 to 1750 nm, yielding 6.05 nm FWHM with a 25-µm slit and an optical aperture of f/1.4. The FWHM and the center wavelength for each spectral band were derived after spectral calibration using a Cornerstone 260 1/4m Monochromator (model 74100; Oriel Instruments, USA) and the XE-1 Xenon Calibration Light Source (Oceanic Optics, USA). The frame rate on board the aircraft was set to 50 fps with an integration time of 40 ms. The 12.5-mm focal length lens yielded an angular FOV of 38.6º with a spatial resolution of 70 cm (Fig. 4.2b).

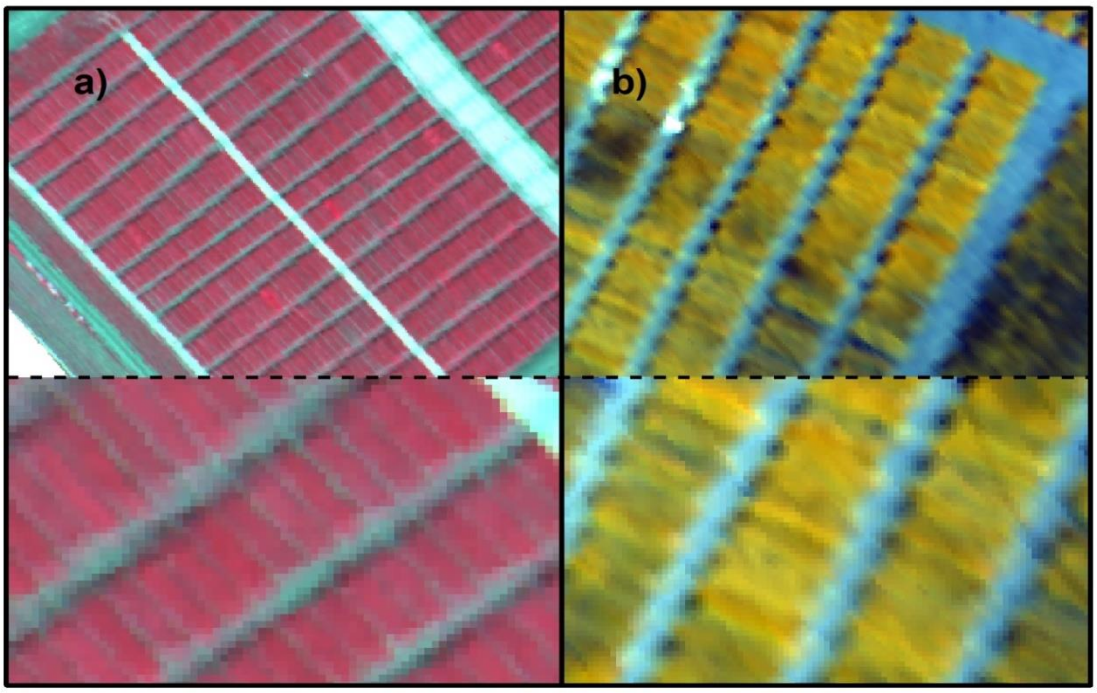

Fig. 4.2. Sample hyperspectral VNIR (400-800 nm region) (a) and hyperspectral NIR (900-1700 nm region) (b) imagery acquired during the 2015 and 2016 airborne campaigns performed at the trial sites at CA and SA-1, respectively.

Radiometric calibration of the hyperspectral cameras and ortho-rectification of the imagery were carried out as described by Zarco-Tejada *et al*. (2016). Atmospheric correction of the imagery was performed using aerosol optical depth (AOD) and weather data to simulate the incoming irradiance using the SMARTS model (Gueymard, 1995; Gueymard *et al*., 2002), measured in the field concurrently with the airborne flights. The SMARTS model has been used in previous studies to calculate reflectance from both multispectral and hyperspectral imagery (Berni *et al*., 2009; Zarco-Tejada *et al*., 2012, 2016; Calderón *et al*., 2013, 2015). A further step was carried out to apply an empirical line calibration (Smith and Milton, 1999) using field-measured spectra to remove noise. The average radiance and reflectance values of selected wheat plots from each trial site are shown in Fig. 4.3.

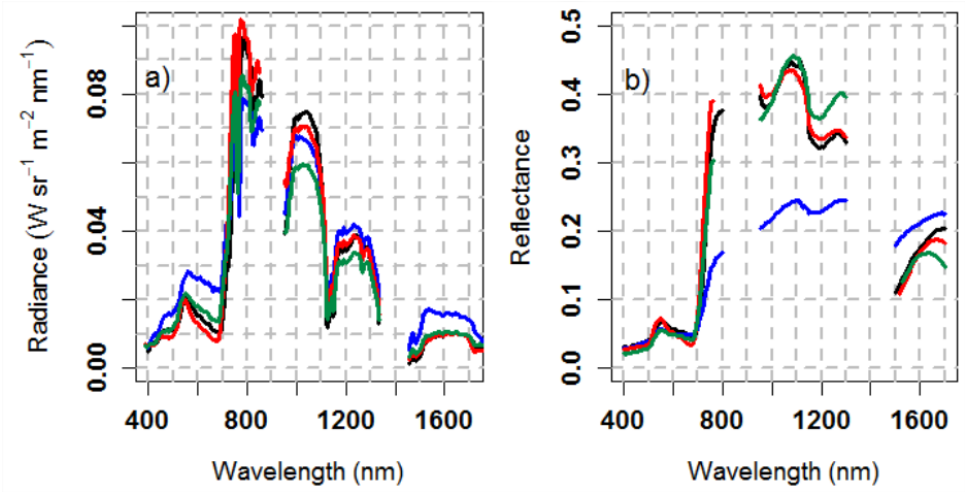

Fig. 4.3. Mean radiance in W·sr^{-1}·m^{-2}·nm^{-1} (a) and reflectance spectra (b) retrieved from hyperspectral cameras at EC (in blue), CA (in black), SA-1(in red) and SA-2 (in Green).

4.2.4 Fluorescence retrieval and calculation of narrow-band indices from the airborne hyperspectral imagery

The atmospheric O_2-A oxygen absorption band at 760.5 nm was used for the fluorescence retrieval via the *in-filling* method. In particular, the Solar Induced Fluorescence (SIF) was quantified from the radiance spectra (Fig. 4.3a) using the Fraunhofer Line Depth (FLD) principle (Plascyk, 1975) as described in Zarco-Tejada *et al*. (2013; 2016). The SIF signal calculated using the in filling method was based on two spectral bands *in* and *out* the O_2-A feature, as described in Meroni *et al*. (2010). The FLD2 method used L_{in} (L762 nm) in this study extracted the radiance and L_{out} (L750 nm) from the airborne imagery, and the irradiance E_{in} (E762 nm) and E_{out} (E750 nm) from irradiance spectra concurrently measured at the time of the flights. Measurements

were made using an ASD Field Spectrometer (FieldSpec Handheld Pro, ASD Inc., CO, USA) with a cosine corrector-diffuser probe for the entire 400-1000 nm spectral region. A modelling study by Damm et al. (2011) quantified the effects of the spectral sampling interval, spectral resolution, signal to noise ratio (SNR) and the spectral shift on the accuracy of the fluorescence retrieval using the O_2-A feature. They demonstrated the feasibility of the SIF retrieval via the FLD methods with broader spectral bandwidths (i.e., 5-7 nm FWHM) when high spectral sampling (below 2.5 nm) and SNR higher than 300:1were available. These results agree with the fluorescence retrievals shown in Zarco-Tejada et al. (2012) and later in Damm *et al.* (2015) with APEX. According to these works, the hyperspectral configuration used in this study is suitable for the SIF retrievals (1.85 nm sampling interval, 6.4 nm bandwidths and SNR of 300:1 with spatial binning).

Narrow-band indices were calculated from the average reflectance per plot using the 260 spectral bands acquired by the micro-hyperspec VNIR, and from the 164 spectral bands acquired by the micro-hyperspec NIR cameras (Fig. 4.3b). In the SWIR region, the atmospheric water absorption spectral region (1330–1490 nm) was masked before analysis. Table 4.2 groups the vegetation indices (VIs) calculated from the micro-hyperspec VNIR into four categories related to: 1) structure, 2) chlorophyll concentration, 3) chlorophyll fluorescence, and 4) nitrogen indices (NIs) using NIR and SWIR spectral domains.

4.2.5 Modelling method

Radiative transfer simulations were carried out with PROSPECT (Jacquemoud and Baret, 1990) linked to the SAILH model (Baret *et al*., 1992). Biophysical canopy parameters by means of numerical model inversion were estimated using look-up tables (LUT). The input variables and their ranges in PROSPECT and SAILH models are shown in Table 4.3. The viewing geometry, defined by the solar zenith and azimuth, and the viewing angles needed to simulate canopy reflectance were extracted for each flight date. In order to minimize the impact of the viewing geometry at each flight date and time, a step of five degrees around the solar zenith angle during the flights was applied to the PROSPECT-SAILH radiative transfer model inversions.

Table 4.2. Summary of the vegetation indices using the VNIR (400-800 nm region) and NIR (900-1700 nm region) hyperspectral airborne imagery.

Indices	Equation	Reference
Structural indices		
Normalized Diff. Veg. Index	$NDVI=(R_{800}-R_{670})/(R_{800}+R_{670})$	Rouse *et al*. (1973)
Opt. Soil-Adjusted Veg. Index	$OSAVI=(1+0.16)(R_{800}-R_{670})/(R_{800}+R_{670}+0.16)$	Rondeaux *et al*. (1996)
Renormalized Diff. Veg. Index	$RDVI=(R_{800}-R_{670})/(R_{800}+R_{670})^{0.5}$	Roujean and Breon (1995)
MCARI/MTVI2	MCARI/MTVI2	Eitel *et al*. (2007)
Chorophyll *a*+*b* indices		
Transf. Chl. Absorp. Rfl. Index	$TCARI = 3[(R_{700}-R_{670})-0.2(R_{700}-R_{550})(R_{700}/R_{670})]$	Haboudane *et al*. (2002)
TCARI/OSAVI	TCARI/OSAVI	Haboudane *et al*. (2002)
Mod. Chl. Absorp. Rfl. Index	$MCARI = [(R_{700}-R_{670})-0.2(R_{700}-R_{550})](R_{700}/R_{670})$	Daughtry *et al*. (2000)
Pig. Spec. Simpl. Ratio Chl. b	$PSSR_b = R_{800}/R_{635}$	Blackburn (1998)
Gitelson and Merzlyak Indices	$GM1=R_{750}/R_{550}$; $GM2=R_{750}/R_{700}$	Gitelson and Merzlyak (1997)
Vogelmann Index	$VOG=R_{740}/R_{720}$	Vogelmann *et al*. (1993)
Red-edge CI	$CI=R_{750}/R_{710}$	Zarco-Tejada *et al*. (2001)
Chlorophyll fluorescence (SIF)		
SIF	FLD2=d-Rb; where $d=L_{762}$; $R=(L_{762}-L_{750})/(E_{762}-E_{750})$ and $b=E_{762}$	Moya *et al*. (2004); Plascyk and Gabriel (1975)
Nitrogen indices (NIs)		
Double-peak C. N	$DCNI=(R_{720}-R_{700})(R_{700}-R_{670})/(R_{720}-R_{670})+0.3)$	Chen *et al*. 2010
$TCARI_{1510\ nm}$	$TCARI_{1510}=3[(R_{700}-R_{1510})-0.2(R_{700}-R_{550})](R_{700}/R_{1510})$	Herrmann *et al*. 2010
$TCARI/OSAVI_{1510\ nm}$	$TCARI_{1510}/OSAVI_{1510}=TCARI_{1510}/[(1+L)(R_{800}-R_{1510})/(R_{800}+R_{1510}+L)]$	Herrmann *et al*. 2010
$MCARI_{1510\ nm}$	$MCARI_{1510}=[(R_{700}-R_{1510})-0.2(R_{700}-R_{550})](R_{700}/R_{1510})$	Herrmann *et al*. 2010
GnyLi	$GnyLi=(R_{900}*R_{1050})(R_{955}*R_{1220})/(R_{900}*R_{1050})+(R_{955}*R_{1220})$	Gnyp *et al*. 2014
Norm. Diff. N. Index	$NDNI=\log(1/R_{1510})-\log(1/R_{1680})/(\log(1/R_{1510})+\log(1/R_{1680})$	Serrano *et al*. 2002
$N_{1645,1715}$	$N_{1645,1715}=(R_{1645}-R_{1715})/(R_{1645}+R_{1715})$	Pimstein *et al*. 2011
$N_{870,1450}$	$N_{870,1450}=(R_{870}-R_{1450})/(R_{870}+R_{1450})$	Pimstein *et al*. 2011
$N_{850,1510}$	$N_{850,1510}=(R_{850}-R_{1510})/(R_{850}+R_{1510})$	This study

In this study two standard model inversions and one inversion method by steps were performed. The range of variation for C_{ab} was determined on the basis of prior field information. In the standard model inversion method, the chlorophyll a+b, water and dry matter content were estimated at the same time, while in the inversion method by steps, the estimation of biophysical canopy parameters required consecutive steps (e.g.; as in Wang *et al*., 2015). The spectral range between 400 and 800 nm measured with the micro-hyperspec VNIR camera was used in the standard model inversion method (named here as INV-1), while the entire spectral region (400 to 1700 nm) from both hyperspectral VNIR and NIR-100 cameras was used in the full-range inversion (here called INV-2) and in the inversion model by steps. In the inversion by steps, the main input parameters were calculated using specific spectral ranges where the biophysical parameters have the greatest influence on the reflectance and transmittance. The procedure was conducted as follows: 1) leaf angle distribution function (LADF) was estimated over the entire spectral domain (400-1750 nm) with variables C_{ab}, C_w and C_m according to Table 4.3. LADF was firstly retrieved by model inversion, given its key

role on canopy structure; 2) the mesophyll structure parameter (N-struct) and leaf area index (LAI) were simultaneously determined over the range 960–1300 nm once the LADF had been fixed to the value retrieved in the first step, and with variable C_{ab}, C_w and C_m according to Table 4.3; 3) C_{ab} was determined over the range 455–690 nm, with C_w and C_m according to Table 4.3, fixing LADF, LAI and N determined in previous steps; 4) C_w and C_m were concurrently retrieved over 900–1700 nm, where water and dry matter have the largest absorption effects (Baret and Fourty, 1997; Feret *et al*., 2008; Fourty *et al*., 1996; Jacquemoud *et al*., 2009, 1996).

Table 4.3. Ranges of the main variables used in the PROSPECT-SAILH radiative transfer model inversions.

Model	Symbol	Quantity	Ranges	Step	Unit
PROSPECT	N-struct	Leaf structure parameter	1.25-1.85	0.1	…
	C_{ab}	Chlorophyll a +b content	10-70	0.5	µg cm^{-2}
	C_w	Equivalent water thickness	0.001-0.05	0. 0005	g cm^{-2}
	C_m	Dry matter content	0.001-0.05	0. 0005	g cm^{-2}
	C_s	Brown pigment content	0	…	…
	Sl	Hot-spot parameter	0.001	…	…
SAILH	LAI	Leaf area index	2-5	0.1	…
	LADF	Leaf inclination distribution function	1,2,3 and 4*	…	…
	TV	Solar zenith angle	45º,60º,85º	5	deg
	Phi	Viewing zenith angle	0º	…	deg
	PSR	Relative azimuth angle	0º	…	deg

* Canopy types proposed to define LADF: planophile (1), erectophile (2), plagiophile (3) and spherical (4).

The accuracy of the estimated parameters (LADF, N-struct, LAI, C_{ab}, C_w and C_m) via model inversion was evaluated by the RMSE calculated between the simulated and measured canopy spectral reflectance. For each standard model inversion, a total of 500000 inversions were carried in forward mode, whereas a total of 200000 inversions were used for the inversion method by steps. Finally, the coefficient of determination (r^2) was calculated to investigate the relationship between the retrieved biophysical parameters (C_{ab}, C_w and C_m) obtained by PROSPECT-SAILH model inversion and the ground-truth physiological measurements.

4.2.6 Statistical analysis

Stepwise multiple regression analysis using forward mode and leave-one-out-cross-validation (LOOCV) techniques were employed to select the best model to quantify N concentration using i) biophysical parameters derived from the different model inversion methods described above, ii) using narrow-band spectral indices calculated

from the VNIR and NIR-100 hyperspectral imagery; and iii) evaluating the performance of the models with the addition of chlorophyll fluorescence quantified from the hyperspectral imagery. Therefore, statistical tests were employed to assess the robustness of each regression model built for nitrogen quantification with and without including solar-induced fluorescence emission retrieved from hyperspectral imagery. A residual analysis model was used to assess the independence of the residual, and the Shapiro-Wilk test for homoscedasticity to verify the normal distribution. The F-test was used to test the significance of the linear regression model, and Student's t-test for the significance of individual regression coefficients. Independent data sets were used for the statistical analysis, using a training data set to build a multiple regression, and an independent second data set to assess the performance of each model under rainfed and irrigated conditions. The training data set comprised the plots located in EC, CA and SA-1, in which the main physiological measurements were made. The test data set was built by SA-1 and SA-2 plots and separated under rainfed and irrigated conditions.

The mean absolute error (MAE), root mean square error (RMSE), mean percentage error (MPE), mean absolute percentage error (MAPE) and coefficient of determination (r^2) between the measured leaf nitrogen content and predicted values were used as skill scores to validate the performance of each model. The statistical analysis was conducted in R software (R Core Team, 2015).

4. 3 Results

4.3.1 Field measurements

Mean values of the field physiological measurements and chlorophyll fluorescence retrieved from the airborne imagery for each field site under rainfed and irrigated conditions are shown in Table 4.4. The results revealed wide variations in the crop physiological status on all sites. As expected, the irrigated plots displayed overall better water and nutritional status than the rainfed plots. There were differences among the rainfed plots; average values of mean N concentration, assimilation rate (A), G_s, and SIF were lower in EC and SA-2 compared to CA and SA-1 (Table 4.4). The irrigated plots at SA-1, which were at an earlier stage of growth, and at SA-2, displayed an overall better water and nutritional status. These data confirmed the water and nutrient stress conditions in rainfed plots and a large variability among plots.

Table 4.4. Average N concentration (%), chlorophyll content derived from SPAD (C_{ab}; $\mu g \cdot cm^{-2}$), net assimilation (A; $\mu mol \cdot m^{-2} \cdot s^{-1}$), stomatal conductance (Gs; $mmol \cdot m^{-2} \cdot s^{-1}$), leaf-water potential (ψL; MPa) and chlorophyll fluorescence (SIF in in $Watt \cdot sr^{-1} \cdot m^{-2} \cdot nm^{-2}$), under rainfed and irrigated conditions at EC, CA, SA-1 and SA-2. The standard deviation is also shown.

	N Conc.	C_{ab} (SPAD)	A	G_s	ψ_L	SIF
Rainfed						
EC	2.50±0.46	23.4±3.7	7.7± 2.1	61.27±2	-2.3±0.2	3.74±0.62
CA	3.28±0.34	28.0±3.6	11.3±2.1	71±24.8	-2.5±0.4	4.22±0.25
SA-1	4.17±0.19	35.0±3.2	17.0±3.3	185.8±56.1	-2.4±0.2	4.88±0.57
SA-2	2.63±0.32	26.0±2.4	10.0±2.5	121.8±40.5	-2.7±0.2	4.01±0.40
Irrigated						
CA	3.37±0.04	28.5±2.3	14.7±4.1	270.6±65.4	-2.1±0.1	4.38±0.17
SA-1	4.29±0.28	35.8±4.1	24.4±2.4	354.6±109.4	-1.7±0.2	5.71±0.29
SA-2	2.95±0.31	29.3±3.9	18.3±2.4	283.2±65.2	-2.2±0.1	5.14±0.28

4.3.2 Nitrogen concentration and narrow-band hyperspectral indices

The solar induced fluorescence emission and narrow-band reflectance indices calculated from hyperspectral imagery were assessed against field measurements of nitrogen content, chlorophyll content measured with SPAD, and net assimilation (Table 4.5). The results showed that the NIR/SWIR-based NIs were marginally better predictors of nitrogen content than the VNIR indices, with the $MCARI_{1510}$ and the NDNI (Fig. 4.4a) indices yielding the best correlation with nitrogen content (r^2=0.69; p-value ≤ 0.005) as compared to MCARI (r^2=0.63) and $PSSR_b$ (r^2=0.63). The NIs that were modified to replace the 670nm band by the 1510 nm band due to its relationship with nitrogen absorption ($TCARI_{1510}$, $MCARI_{1510}$, $TCARI/OSAVI_{1510}$) performed higher at quantifying canopy nitrogen content than their corresponding VNIR-based indices. The $N_{1645/1715}$ using exclusively reflectance in the SWIR domain showed significant relationship with N content (r^2=0.64, p-value<0.005) but still marginally inferior to $MCARI_{1510}$ and NDNI. Table 4.5 also shows that the indices most sensitive to canopy structure yielded significant relationships with nitrogen content (r^2=0.57; p-value <0.005; NDVI). However, the structural indices exhibited saturation over dense canopy, as shown in Fig. 4.4b for NDVI which tends to saturate due to the higher canopy density at high nitrogen levels. Among the chlorophyll indices used in this study, $PSSR_b$ (Fig. 4.4c) obtained the best results for chlorophyll content estimation (r^2=0.57, p-value ≤ 0.0005), yielding better results than NIs. The airborne-quantified chlorophyll fluorescence was also sensitive to nitrogen content (r^2=0.51; p-value ≤

0.005) and to the assimilation rate (r^2=0.74; p-value ≤ 0.005; Fig. 4.4d), confirming other studies that demonstrated the link between airborne-retrieved chlorophyll fluorescence and the photosynthetic activity.

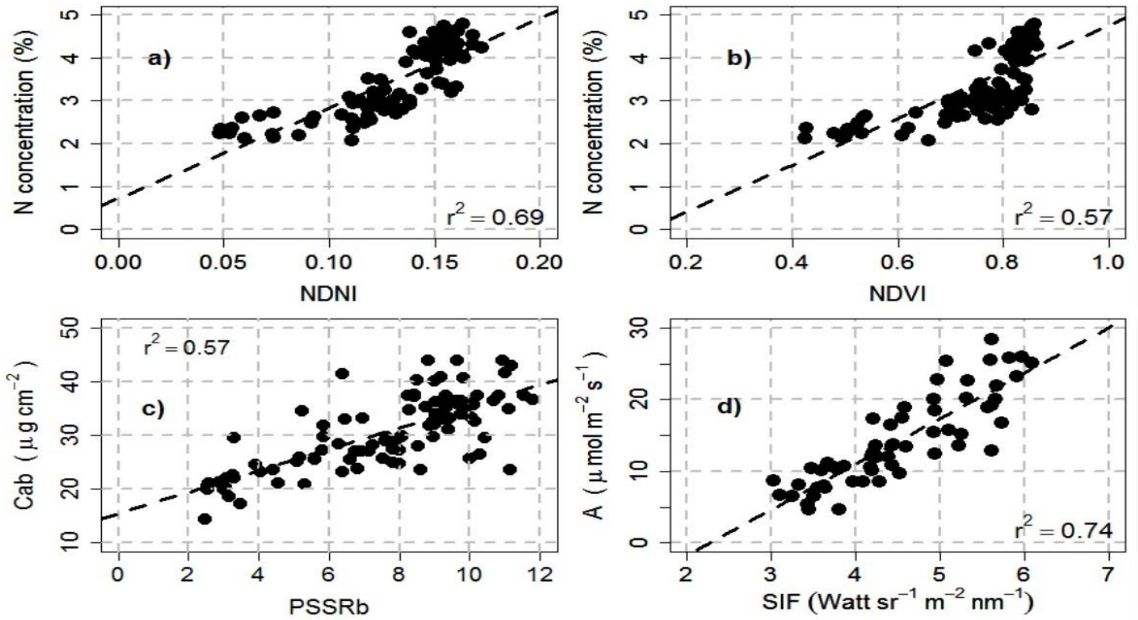

Fig. 4.4. Relationships between N concentration (in %) vs. NDNI (a) and NDVI (b), C_{ab} vs. $PSSR_b$ (c) and A vs. airborne-quantified SIF (d). For all relationships the significance level was p ≤0.0005.

4.3.3 Nitrogen concentration and plant traits estimated by model inversion

The coefficient of determination (r^2) calculated between chlorophyll content (C_{ab}), water content (C_w) and dry matter content (C_m) estimated by PROSPECT-SAILH model inversion and leaf-level physiological measurements (nitrogen concentration, net assimilation rate and chlorophyll content) are shown in Table 4.6. These results correspond with the method proposed in Wang *et al*. (2015) that used biophysical parameters retrieved by model inversion to evaluate the retrieval of leaf N concentration. In the present study, C_{ab} estimated by model inversion by steps correlated with N concentration (r^2=0.71; p-value ≤ 0.0005; Fig. 4.5a), field-measured leaf C_{ab} (r^2=0.81; p-value ≤ 0.0005; Fig. 4.5b) and with the assimilation rate (r^2=0.59; p-value ≤ 0.0005; Fig. 4.5c). Using this model-inversion approach by steps, the relationship between estimated and measured C_{ab} content adjusted well with the 1:1 line for the entire dataset (Fig. 4.5b), yielding a RMSE=2.04 µg·cm^{-2} and MAPE=5.44%. The two standard model-inversion methods (INV-1 and INV-2) displayed quite different behavior; C_{ab} was correctly estimated for plots with N concentration and C_{ab} values that were higher than 3.5% and 30 µg·cm^{-2} respectively, while the retrievals failed for the

plots with nitrogen and C_{ab} values below these (see outliers in Fig. 4.5b). The two standard model inversion approaches thus yielded weaker results in their estimates of nitrogen content (RMSE ≥ 6.33 µg·cm^{-2} and MAPE ≥ 17.68 %) than the model inversion by steps.

Table 4.5. Coefficient of determination (r^2) and level of significance for the narrow-band hyperspectral indices and the solar induced chlorophyll fluorescence (SIF; Watt·m^{-2}·sr^{-1}· nm^{-1}) quantified from hyperspectral imagery against N concentration, chlorophyll content derived from SPAD values (C_{ab}-SPAD; µg·cm^{-2}) and net assimilation (A; µmol·m^{-2}·s^{-1}).

	N concentration		C_{ab}-SPAD		Net assimilation (A)	
Indices	**r^2**	**p-value**	**r^2**	**p-value**	**r^2**	**p-value**
Structural Indices						
NDVI	0.57	< 2.2e-16	0.53	< 2.2e-16	0.55	1.61E-08
OSAVI	0.56	< 2.2e-16	0.49	< 2.2e-16	0.53	3.23E-08
RDVI	0.56	< 2.2e-16	0.48	< 2.2e-16	0.53	3.92E-08
MCARI/MTVI2	0.40	2.14E-13	0.25	2.14E-13	0.46	5.61E-07
Chlorophyll a+b indices						
TCARI	0.54	< 2.2e-16	0.51	< 2.2e-16	0.60	1.02E-09
TCARI/OSAVI	0.45	1.78E-15	0.30	8.64E-10	0.51	8.59E-08
MCARI	0.63	< 2.2e-16	0.55	< 2.2e-16	0.57	4.78E-09
PSSRb	0.63	< 2.2e-16	0.57	< 2.2e-16	0.66	3.72E-11
GM1	0.36	8.32E-12	0.39	2.90E-13	0.47	3.62E-07
GM2	0.52	< 2.2e-16	0.47	2.22E-16	0.26	4.79E-04
VOG1	0.35	4.65E-10	0.32	1.75E-10	0.66	3.72E-11
CI	0.31	1.31E-11	0.35	1.48E-11	0.47	3.62E-07
Nitrogen Indices						
DCNI	0.56	< 2.2e-16	0.50	< 2.2e-16	0.59	1.77E-09
$TCARI_{1510}$	0.56	< 2.2e-16	0.44	1.78E-15	0.59	1.57E-09
$TCARI/OSAVI_{1510}$	0.52	2.35E-18	0.41	7.47E-14	0.63	2.26E-10
$MCARI_{1510}$	0.69	< 2.2e-16	0.56	< 2.2e-16	0.43	1.86E-06
GnyLi	0.31	3.41E-10	0.31	2.36E-10	0.51	7.98E-08
NDNI	0.69	< 2.2e-16	0.49	< 2.2e-16	0.61	5.75E-10
N_{1645}	0.64	< 2.2e-16	0.52	< 2.2e-16	0.59	1.57E-09
$N_{850-1450}$	0.64	< 2.2e-16	0.55	< 2.2e-16	0.63	2.26E-10
$NI_{850/1510}$	0.65	< 2.2e-16	0.53	< 2.2e-16	0.61	5.75E-10
Fluorescence						
SIF	0.51	< 2.2e-16	0.35	1.37E-11	0.74	1.19E-11

Leaf equivalent water thickness retrieval by model inversion was significantly related to N concentration (r^2=0.66; p-value ≤ 0.0005), while dry matter content showed significant (yet lower coefficients of determination than for C_w) yielding r^2=0.23 (step inversion method) and r^2=0.49 (INV-1 method) (in both cases p-value ≤ 0.0005). In this case, the coefficient of determination was significantly affected by outliers, inducing an artificial increase in the correlation coefficients for INV-1 as compared to the step

inversion method. In summary, the three leaf biochemical parameters C_{ab}, C_w and C_m estimated by radiative transfer model inversion from the hyperspectral imagery were significantly related to leaf N concentration (p-value ≤ 0.0005 in all three cases), but C_{ab} and C_w yielded higher relationship with N than C_m.

Table 4.6. Coefficient of determination (r^2) between estimated leaf C_{ab}, C_m and C_w parameters by PROSPECT-SAILH model inversion by steps and by standard inversion methods (INV-1 and INV-2) vs. N concentration, leaf-measured C_{ab} with SPAD, and net assimilation (A).

	N concentration	**C_{ab} (SPAD)**	**Net Assimilation (A)**
Chlorophyll content a+b (C_{ab})			
By step	0.71**	0.81**	0.59**
INV-1	0.012	0.008	0.001
INV-2	0.004	0.002	0
Equivalent water thickness (C_w)			
By step	0.66**	0.56**	0.53**
INV-1	0.017	0.008	0.008
INV-2	0.27**	0.25**	0.19*
Dry-matter content (C_m)			
By step	0.23**	0.1	0.18**
INV-1	0.49**	0.32**	0.30**
INV-2	0.38*	0.24**	0.23**

** p-value < 0.0005; * p-value < 0.02

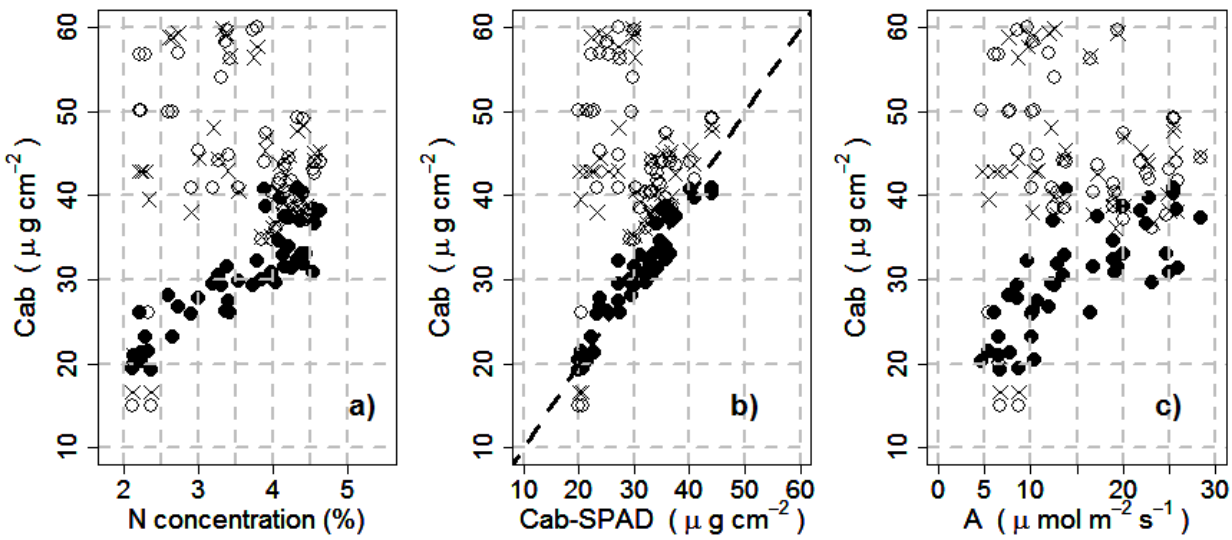

Fig. 4.5. Chlorophyll content (Cab, µg·cm^{-2}) estimated by model inversions vs. N concentration (in %) (a), chlorophyll content derived from SPAD (C_{ab}-SPAD; µg·cm $^{-2}$) (b), and leaf assimilation rate (A, µmol·m^{-2}·s^{-1}) (c). Black points correspond to inversion by steps, black crosses using the INV-1 method and open black circles using the INV-2 model.

4.3.4 Leaf N estimation from the airborne hyperspectral imagery accounting for chlorophyll fluorescence

The stepwise multiple regression and LOOCV methods built to estimate N concentration using the leaf biochemical constituents C_{ab}, C_w and C_m obtained by model inversion, were assessed accounting for the contribution of adding chlorophyll fluorescence. The statistical models built using all input parameters, with and without including SIF as predictor of nitrogen are shown in Table 4.7. The homoscedasticity and the normal distribution requirements were satisfied and passed the statistical test (F-Test). According to the t-test, the regression coefficients for C_{ab} and SIF were significant at the 5% significance level. In contrast, C_m and C_w parameters were non-significant in some of the regression models (see Table 4.7).

Table 4.7. Statistical tests for the validity of the regression models used to estimate N concentration.

	F-test		**Shapiro-Wilk**	**p-value (t-test)**			
	p-value	**W**	**p-value**	**C_{ab}**	**C_w**	**C_m**	**SIF**
Without Fluorescence							
N=*f*(C_{ab})	2.4E-13	0.98	0.55	2.4E-13			
N=*f*(C_{ab},C_w)	2.9E-16	0.98	0.64	6.2E-06	0.0003		
N=*f*(C_{ab},C_m)	7.5E-17	0.98	0.46	7.6E-14		8.2E-5	
N=*f*(C_{ab},C_w,C_m)	6.4E-17	0.98	≥0.05	8.7E-06	0.5911	0.0906	
With Fluorescence							
N=*f*(C_{ab}, SIF)	8.2E-27	0.97	0.35	7.8E-10	1.1E-14		
N=*f*(C_{ab},C_w,SIF)	1.4E-28	0.96	0.17	1.0E-06	0.0059		2.7E-13
N=*f*(C_{ab},C_m,SIF)	1.1E-27	0.97	0.23	1.9E-10		0.0519	7.2E-12
N=*f*(C_{ab},C_w,C_m,SIF)	1.2E-28	0.97	0.2	0.0013	0.0429	0.5395	1.8E-12

The ability of each model to predict N concentration was assessed using the LOOCV scores described earlier, showing the results in Table 4.8. Based on these statistical scores, the multiple linear regression models using SIF as predictive variable considerably improved the accuracy of N estimation ($r^2_{LOOCV} \geq 0.92$; $MAE_{LOOCV} \leq 0.19$ and $RMSE_{LOOCV} \leq 0.23$). As a comparison, regression models without including fluorescence (SIF) reached significantly lower predictive power ($r^2_{LOOCV} \leq 0.77$; $MAE_{LOOCV} \geq 0.33$ and $RMSE_{LOOCV} \geq 0.40$). The contribution of each variable is shown by standardized coefficients (β_0; Table 4.8). These results show that in models that include SIF as predictor, its contribution to the retrieval of N was higher than the rest of the predictors, being almost double than the contribution of C_{ab}. In the models that did not

use SIF as predictor, the estimated C_{ab} by model inversion contributed the highest to N estimation.

According to r^2, RMSE, MAE and MAPE, the most accurate estimation was achieved by the regression model when the predictors were C_{ab}, C_w, C_m and SIF, yielding r^2_{LOOCV} = 0.93, $RMSE_{LOOCV}$ = 0.20, MAE_{LOOCV} = 0.18 and the lowest MAPE (Table 4.8). Nevertheless, the rest of models with less number of parameters (therefore simpler) obtained accuracies only marginally lower (e.g. r^2=0.93 & RMSE=0.20 for the most complex model using C_{ab}, C_w, C_m and SIF as compared to r^2=0.92 & RMSE=0.23 for the model using C_{ab} and SIF). Fig. 4.6 shows the scatter plots between the measured and predicted N concentration using the model without (top plots) and with SIF as predictor (bottom plots). The models using SIF showed lower RMSE and better performance than the rest of the models that did not employ fluorescence as predictor.

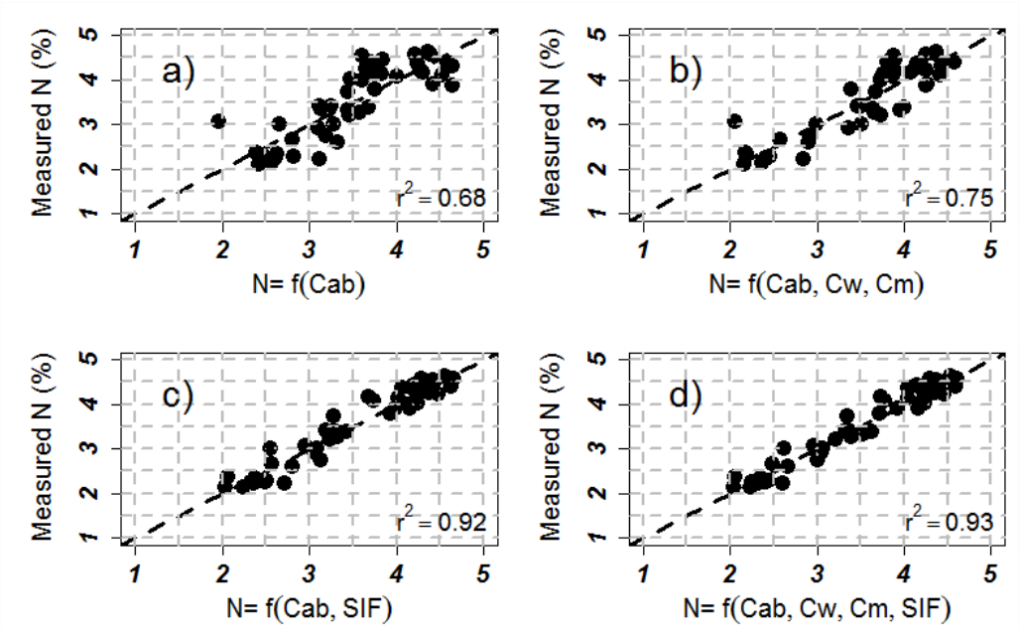

Fig. 4.6. Measured vs. estimated N concentration using the best regression LOOCV models without fluorescence (a,b) and with fluorescence (c,d) as a function of C_{ab} (a), C_{ab}, C_w and C_m (b), C_{ab} and SIF (c) and C_{ab}, C_w and C_m and SIF (d). The dashed line is the 1:1 line.

Table 4.8. Performance of the regression models built to estimate N concentration using r^2, RMSE, ME, MAE, MAPE and standardized coefficients as performance indicators.

Regression Models	r^2	RMSE	MAE	MAPE	Standard. coefficients (β0)			
					C_{ab}	C_w	C_m	SIF
Without Fluorescence								
N=*f*(C_{ab})	0.68	0.47	0.39	12.0%	0.84	…	….	…
N=*f*(C_{ab}, C_w)	0.74	0.41	0.34	9.9%	0.54	0.41	…	…
N=*f*(C_{ab}, C_m)	0.77	0.40	0.33	9.7%	0.77	…	-0.31	…
N=*f*(C_{ab}, C_w, C_m)	0.75	0.41	0.34	10.0%	0.70	0.11	-0.24	…
With Fluorescence								
N=*f*(C_{ab}, SIF)	0.92	0.23	0.19	5.9%	0.43	…	…	0.63
N=*f*(C_{ab}, C_w, SIF)	0.92	0.22	0.18	5.6%	0.34	0.17	…	0.57
N=*f*(C_{ab}, C_m, SIF)	0.92	0.23	0.19	5.9%	0.44	…	-0.10	0.57
N=*f*(C_{ab}, C_w, C_m, SIF)	0.93	0.20	0.18	5.5%	0.30	0.23	0.05	0.58

Based on these results, the proposed models combining leaf biochemical constituents with and without SIF were evaluated as predictors for N concentration separately for rainfed and irrigated conditions. All models showed greater accuracies in predicting N concentration under rainfed (stress) conditions than under irrigated (non-water stress) conditions (e.g. best model performance yielded r^2=0.93 (rainfed) vs. r^2=0.88; (irrigated) (Table 4.9). As Figure 4.7 shows, the plots were aligned over the 1:1 line for both cases of rainfed (Fig. 4.7a) and irrigated conditions (Fig. 4.7b). Under rainfed conditions, the models with SIF as predictor yielded significantly higher scores ($r^2 \geq 0.89$, RMSE $\leq$ 0.26 and MAPE $\leq$ 6.8 %) than models without SIF as predictor ($r^2 \geq$ 0.78, RMSE $\leq$ 0.37 and MAPE $\leq$ 9.46 %).

Under irrigated conditions, the models that used SIF as predictor also showed the best performance. The model built with C_{ab} and SIF displayed better accuracy in predicting nitrogen concentration (r^2 = 0.65, RMSE = 0.42 and MAPE $\leq$ 10.6 %) than the model with C_{ab} only (r^2 = 0.48, RMSE = 0.51 and MAPE $\leq$ 12.56 %), indicating that the contribution of SIF was highly significant under both irrigated and non-irrigated conditions.

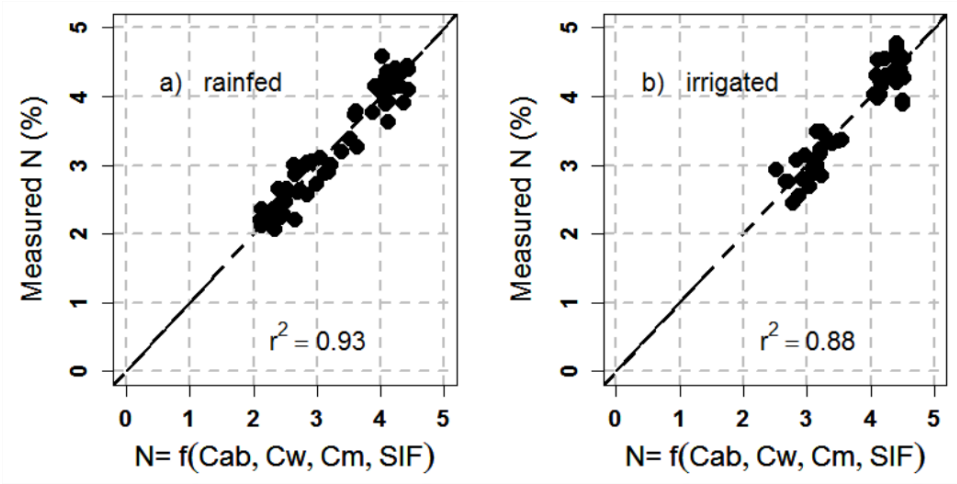

Fig. 4.7. Measured vs. estimated N concentration for rainfed (a) and irrigated conditions (b) using the model built with C_{ab}, C_m and C_w biochemical constituents (estimated by model inversion) including fluorescence. The solid line is the 1:1 line**.**

Table 4.9. Statistics for r^2, RMSE, ME, MAE, MPE and MAPE between measured and predicted N concentration under rainfed and irrigated conditions.

	r^2	RMSE	MAE	MPE	MAPE
Rainfed conditions					
Without Fluorescence					
N = *f*(C_{ab})	0.78	0.37	0.29	-1.44%	9.46%
N = *f*(C_{ab}, C_m)	0.81	0.34	0.27	-1.12%	8.50%
N = *f*(C_{ab}, C_w)	0.86	0.36	0.23	-0.92%	7.54%
N = *f*(C_{ab}, C_w, C_m)	0.86	0.29	0.23	-0.84%	7.24%
With Fluorescence					
N=*f*(C_{ab}, SIF)	0.89	0.26	0.21	-0.65%	6.89%
N = *f*(C_{ab}, C_m, SIF)	0.89	0.26	0.22	-0.64%	6.86%
N = *f*(C_{ab}, C_w, SIF)	0.92	0.23	0.18	-0.45%	5.68%
N = *f*(C_{ab}, C_w, C_m, SIF)	0.93	0.22	0.18	-0.45%	5.65%
Irrigated conditions					
Without Fluorescence					
N = *f*(C_{ab})	0.48	0.51	0.44	-2.03%	12.56%
N = *f*(C_{ab}, C_m)	0.59	0.45	0.37	-1.65%	10.50%
N = *f*(C_{ab}, C_w)	0.76	0.35	0.29	-0.89%	8.05%
N = *f*(C_{ab}, C_w, C_m)	0.77	0.34	0.28	-0.85%	7.68%
With Fluorescence					
N=*f*(C_{ab}, SIF)	0.65	0.42	0.36	-1.41%	10.6%
N = *f*(C_{ab}, C_m, SIF)	0.77	0.34	0.27	-0.93%	7.89%
N = *f*(C_{ab}, C_w, SIF)	0.84	0.28	0.34	-0.58%	6.77%
N = *f*(C_{ab}, C_w, C_m, SIF)	0.88	0.25	0.20	-0.47%	5.63%

These modelling methods enabled the quantification of N concentration from the hyperspectral imagery to show its spatial distribution in the context of precision agriculture and plant phenotyping experiments. Fig. 4.8 shows the spatial distribution of

N concentration using C_{ab}, C_w, C_m and SIF as predictors (Fig. 4.8) over plots under rainfed (Fig. 4.8b) and irrigated conditions (Fig. 4.8c) at the SA field site during the 2016 campaign. Higher values of nitrogen concentration (blue color) from the rainfed plots indicate a better physiological status, while low N values (red color) indicate stress levels as consequence of the rainfed conditions. In comparison with irrigated conditions, the N map clearly showed the lower values obtained in the rainfed fields, with average values of 3.1± 0.18%; under irrigated conditions the average N concentration was higher (4.2± 0.3%). This methodology enables an operational quantification of canopy N concentration at the field level using high resolution hyperspectral remote sensing imagery and radiative-transfer model inversion methods.

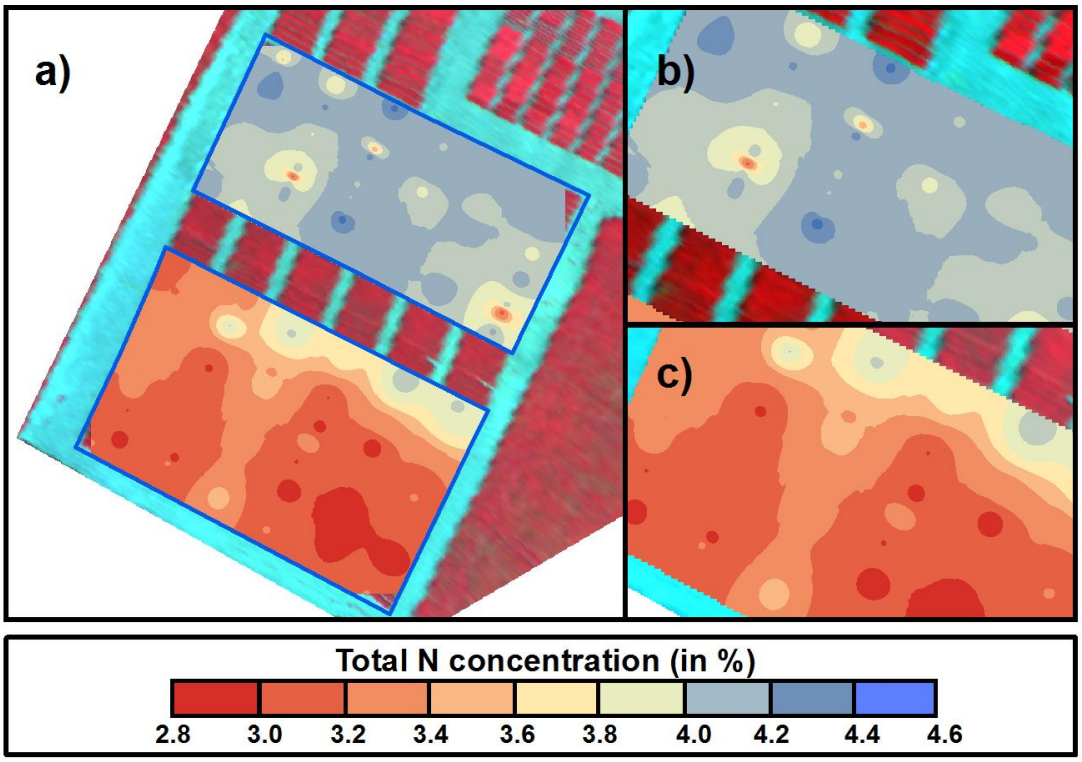

Fig. 4.8. Map showing the spatial distribution of N concentration estimated using the model built with chlorophyll a+b (C_{ab}), water content (C_w), dry matter content (C_m) and solar induced chlorophyll fluorescence (SIF) estimated from hyperspectral imagery (a) and used as predictors under irrigated (b) and rainfed (c) conditions at SA field site during the 2016 airborne campaign.

4. 4 Discussion

Several studies have focused on the estimation of canopy N concentration using remote sensing techniques. The main problem encountered is that N does not absorb radiation with distinct features to enable its direct quantification with reflectance data. Instead, proxies physiologically related to N which are potentially retrievable from

remote sensing spectra are proposed as the only feasible way of detecting nitrogen levels under nutrient-deficiency conditions. An example is the widely used SPAD meter, a hand held instrument that measures chlorophyll content and generally accepted to track N concentration at the leaf level (Ravier *et al*., 2017). Most of the studies that assess the retrieval of N through non-destructive methods have been traditionally based on empirical models with spectral indices (i.e. spectral proxies) calculated from the visible (VIS) and near-infrared (NIR) regions (Clevers and Kooistra, 2012; Li *et al*., 2014), while only a few studies focused on radiative transfer model inversions and the relationships between retrieved parameters (i.e. biophysical parameters and biochemical constituents as proxies) and nitrogen (Thorp *et al*., 2012; Wang *et al*., 2015). The present study evaluated these standard hyperspectral remote sensing techniques for the estimation of N concentration using narrow-band indices combining the VNIR and the SWIR region, but focusing on the potential contribution of a new indicator such as the radiance-based fluorescence SIF for improving the performance of N estimation. According to the results obtained by the regression models built with C_{ab}, C_w, C_m and SIF from the stepwise multiple regression and LOOCV methods, the solar induced chlorophyll fluorescence quantified from the hyperspectral imagery significantly increased the performance for the estimation of N. This result confirms the findings of other studies that suggested a close link between fluorescence emission and nitrogen (Corp *et al*., 2003; Schächtl *et al*., 2005; Cendrero-Mateo *et al*., 2016). The contribution of SIF to predict N concentration was higher than that of C_{ab} and leaf biochemical parameters such as dry matter and equivalent water thickness. In fact, models containing fluorescence emission among their predictors produced the most reliable nitrogen estimation when compared to models without SIF. The results indicated that SIF retrieval by the FLD method from high resolution hyperspectral imagery demonstrated its value for monitoring N concentration under both rainfed and irrigated conditions in the context of precision agriculture and plant phenotyping studies. The solar induced chlorophyll fluorescence provides a potential new tool to estimate canopy N concentration, due to their close link with photosynthetic parameters such as the maximum rate of carboxylation and with plant functioning. These results agree with recent studies that showed the ability of such methods to evaluate crop physiological status under conditions of water stress, compared to hyperspectral narrow-band indices (Herrmann *et al*., 2010; Ranjan *et al*., 2012; Gonzalez-Dugo *et al*., 2015; Zarco-Tejada *et al*., 2016). This study also demonstrates that the biophysical parameters retrieved

from a radiative transfer model at canopy scale are needed for better N concentration estimation due to the more robust quantification of the parameters as compared to single narrow-band hyperspectral indices. This agrees with Wang *et al*. (2015) who demonstrated that the combination of biophysical parameters (leaf chlorophyll, dry matter and water content) retrieved via PROSPECT model inversion provided a reliable tool to estimate N at leaf scale. They found a higher correlation between leaf nitrogen content and dry matter and water content than with chlorophyll. Our results indicate that, in the absence of chlorophyll fluorescence as predictor, chlorophyll a+b was the parameter most related with nitrogen. This result is in agreement with other studies that indicate that the chlorophyll is the most widely used proxy for N estimation (Herrmann *et al*., 2010; Homolová *et al*., 2013). In this regard, this study displayed that C_w and C_m contributions for predicting nitrogen concentration were lower than C_{ab} and SIF in both rainfed and irrigated conditions. However, it was observed that under irrigated conditions the models showed lower accuracy at predicting N concentration, especially when C_{ab} was the only predictor. Under the conditions of this experiment, the lower performance obtained for irrigated vs. rainfed conditions was likely due to the smaller range of variability found for the predictors in the irrigated than in the rainfed plots. The results of this study showed that the contribution of SIF (which can be also derived from VNIR cameras) is superior than the contribution of the NIR-SWIR camera used here to estimate dry matter and equivalent water thickness. Considering the cost, complexity of operation, and the lower resolution generally obtained by SWIR cameras, the interest of retrieving SIF and chlorophyll content from a single VNIR camera outperforms the SWIR under the conditions and objectives of the present study.

This work also demonstrates that the model inversion by steps yields more reliable retrievals than traditional inversions, which used the entire VNIR up to 1700 nm region to retrieve all parameters simultaneously. This result shows that model inversions conducted by steps reduced the ill-posed inverse problems (Combal *et al*., 2003; Wang *et al*., 2007; Yebra and Chuvieco, 2009; Li and Wang, 2011) and improves the parameter retrievals. Our results also confirm findings by Li and Wang (2011) regarding this issue.

Another important result obtained in this study shows that the regression models built with parameters obtained by model-inversion yielded superior results than simple linear models based on spectral indices (Herrmann *et al*., 2010; Pimstein *et al*., 2011;

Bao *et al*., 2013; Mahajan *et al*., 2014; Gnyp *et al*., 2014). This conclusion was true even when using narrow-band indices centered at 1510 and 850 nm, which are highly correlated with N concentration. Regarding hyperspectral indices, our results confirmed findings reported by Herrmann *et al*. (2010) that the use of the SWIR domain significantly improved the estimation of nitrogen concentration when compared to the visible and near-infrared region of the spectrum. In our case, the use of the SWIR spectral range to determine NIs provided better quantification of N concentration than when only the VNIR region was used, in particular when using indices from bands centered at 1510 nm (Herrmann *et al*., 2010; Serrano *et al*., 2002). Among all indices, the NIs that combined 1510 nm and VNIR bands yielded the highest agreement with N concentration (i.e. r^2=0.69 for $MCARI_{1510}$ and r^2=0.65 for $NI_{1850/1510}$). However, these simple relationships obtained between N concentration and chlorophyll indices are affected by structure and the underlying soil. By contrast, the structural indices (e.g. NDVI) tend to saturate their values under dense canopies and with high nitrogen levels (Fig. 4.4b). Nevertheless, none of the hyperspectral index combinations outperformed the results obtained by model inversion when adding fluorescence (i.e. C_{ab}+C_m+C_w+SIF), which was by far the best model for N estimation.

An additional important topic is that the methodology used here for the airborne retrieval of chlorophyll fluorescence from radiance imagery is based on the work presented in previous studies (i.e.: Damm *et al*., 2015; Zarco-Tejada *et al*., 2016), confirming that the use of hyperspectral imagery acquired at broader spectral bands (i.e. with FWHM 2-7 nm) retains sufficient chlorophyll fluorescence signal to yield the most significant relationships against field-measured assimilation rates among all other image-derived indicators.

An issue observed in this work is the potential limitations of the plot sizes normally used by plant breeders during their experimental designs. The plot dimension should be compatible with the spatial resolution of the imagery acquired by remote sensing. When the plots are too small, soil and background effects may play a critical role due to the mixing of the different components (i.e. soil and shadows) with the vegetation. This issue is important in the case in of the coarser resolution generally obtained by SWIR cameras. New sensors carried on board drones and low altitude manned aircraft can potentially obtain high- and ultra-high resolutions, which are compatible with the standard phenotyping and plant breeding experiments. Nevertheless, plant breeding

experimental design should be compatible with the spatial resolutions of the remote sensing sensors to be flown over the study sites. In this way, a line of at least 1/2 to 1 pixel as edge around the center of the plot is recommended.

4. 5 Conclusion

The present study demonstrates that the airborne-quantified solar induced chlorophyll fluorescence (SIF) is a critical predictor for the estimation of N concentration under semi-arid and arid conditions when combined with chlorophyll a+b content and leaf parameters dry matter (C_m) and equivalent water thickness (C_w) plant traits retrieved by radiative transfer model inversion. When the models were built with airborne-quantified SIF, N estimation performance improved under both rainfed (water-stress) and irrigated conditions. Additionally, the models that combined SIF and chlorophyll a+b content performed better than standard empirical methods based on simple linear relationships with narrow-band hyperspectral indices. In addition, this work demonstrates that SWIR-based indices centered at 1510 nm yield more reliable agreements with N concentration (r^2=0.69) than traditional chlorophyll indices (TCARI/OSAVI r^2=0.45) proposed as proxy for N quantification.

References

Bao, Y., Xu, K., Min, J., Xu, J., 2013. Estimating wheat shoot nitrogen content at vegetative stage from in situ hyperspectral measurements. Crop Sci. 53, 2063–2071. https://doi.org/10.2135/cropsci2013.01.0012

Baret, F., Fourty, T., 1997. Estimation of leaf water content and specific leaf weight from reflectance and transmittance measurements. Agronomie 17, 455–464. https://doi.org/10.1051/agro:19970903.

Baret, F., Jacquemoud, S., Guyot, G., Leprieur, C., 1992. Modeled analysis of the biophysical nature of spectral shifts and comparison with information content of broad bands. Remote Sens. Environ. 41, 133–142. https://doi.org/10.1016/0034-4257(92)90073-S.

Berni, J., Zarco-Tejada, P.J., Suarez, L., Fereres, E., 2009. Thermal and Narrowband Multispectral Remote Sensing for Vegetation Monitoring From an Unmanned Aerial Vehicle. IEEE Trans. Geosci. Remote Sens. 47, 722–738. https://doi.org/10.1109/TGRS.2008.2010457

Blackburn, G.A., 1998. Spectral indices for estimating photosynthetic pigment concentrations : a test using senescent tree leaves. Int. J. Remote Sens. 19, 657–675. https://doi.org/10.1080/014311698215919

Calderón, R., Navas-Cortés, J.A., Lucena, C., Zarco-Tejada, P.J., 2013. High-resolution airborne hyperspectral and thermal imagery for early detection of Verticillium wilt

of olive using fluorescence, temperature and narrow-band spectral indices. Remote Sens. Environ. 139, 231–245. https://doi.org/10.1016/j.rse.2013.07.031

Calderón, R., Navas-Cortés, J.A., Zarco-Tejada, P.J., 2015. Early detection and quantification of Verticillium Wilt in olive using hyperspectral and thermal imagery over large areas. Remote Sens. 7, 5584–5610. https://doi.org/10.3390/rs70505584

Cendrero-Mateo, M.P., Moran, M.S., Papuga, S.A., Thorp, K.R., Alonso, L., Moreno, J., Ponce-Campos, G., Rascher, U., Wang, G., 2016. Plant chlorophyll fluorescence: Active and passive measurements at canopy and leaf scales with different nitrogen treatments. J. Exp. Bot. 67, 275–286. https://doi.org/10.1093/jxb/erv456

Chen, P., Haboudane, D., Tremblay, N., Wang, J., Vigneault, P., Li, B., 2010. New spectral indicator assessing the efficiency of crop nitrogen treatment in corn and wheat. Remote Sens. Environ. 114, 1987–1997. https://doi.org/10.1016/j.rse.2010.04.006

Clevers, J.G.P.W., Kooistra, L., 2012. Using hyperspectral remote sensing data for retrieving canopy chlorophyll and nitrogen content. IEEE J. Sel. Top. Appl. Earth Obs. Remote Sens. 5, 574–583. https://doi.org/10.1109/JSTARS.2011.2176468

Combal, B., Baret, F., Weiss, M., Trubuil, A., Macé, D., Pragnère, A., Myneni, R., Knyazikhin, Y., Wang, L., 2003. Retrieval of canopy biophysical variables from bidirectional reflectance using prior information to solve the ill-posed inverse problem. Remote Sens. Environ. 84, 1–15. https://doi.org/10.1016/S0034-4257(02)00035-4

Corp, L.A., McMurtrey, J.E., Middleton, E.M., Mulchi, C.L., Chappelle, E.W., Daughtry, C.S.T., 2003. Fluorescence sensing systems: In vivo detection of biophysical variations in field corn due to nitrogen supply. Remote Sens. Environ. 86, 470–479. https://doi.org/10.1016/S0034-4257(03)00125-1

Croft, H., Chen, J.M., Luo, X., Bartlett, P., Chen, B., Staebler, R.M., 2017. Leaf chlorophyll content as a proxy for leaf photosynthetic capacity. Glob. Chang. Biol. 23, 3513–3524. https://doi.org/10.1111/gcb.13599

Damm, A., Erler, A., Hillen, W., Meroni, M., Schaepman, M.E., Verhoef, W., Rascher, U., 2011. Modeling the impact of spectral sensor configurations on the FLD retrieval accuracy of sun-induced chlorophyll fluorescence. Remote Sens. Environ. 115, 1882–1892. https://doi.org/10.1016/j.rse.2011.03.011

Damm, A., Guanter, L., Paul-Limoges, E., van der Tol, C., Hueni, A., Buchmann, N., Eugster, W., Ammann, C., Schaepman, M.E., 2015. Far-red sun-induced chlorophyll fluorescence shows ecosystem-specific relationships to gross primary production: An assessment based on observational and modeling approaches. Remote Sens. Environ. 166, 91–105. https://doi.org/10.1016/j.rse.2015.06.004

Daughtry, C., 2000. Estimating Corn Leaf Chlorophyll Concentration from Leaf and Canopy Reflectance. Remote Sens. Environ. 74, 229–239. https://doi.org/10.1016/S0034-4257(00)00113-9

Eitel, J.U.H., Long, D.S., Gessler, P.E., Smith, A.M.S., 2007. Using in-situ measurements to evaluate the new RapidEye^{TM} satellite series for prediction of wheat nitrogen status. Int. J. Remote Sens. 28, 4183–4190. https://doi.org/10.1080/01431160701422213

Feret, J.B., François, C., Asner, G.P., Gitelson, A.A., Martin, R.E., Bidel, L.P.R., Ustin, S.L., le Maire, G., Jacquemoud, S., 2008. PROSPECT-4 and 5: Advances in the leaf optical properties model separating photosynthetic pigments. Remote Sens. Environ. 112, 3030–3043. https://doi.org/10.1016/j.rse.2008.02.012

Ferwerda, J.G., Skidmore, A.K., Mutanga, O., 2005. Nitrogen detection with hyperspectral normalized ratio indices across multiple plant species. Int. J. Remote Sens. 26, 4083–4095. https://doi.org/10.1080/01431160500181044

Fourty, T., Baret, F., Jacquemoud, S., Schmuck, G., Verdebout, J., 1996. Leaf optical properties with explicit description of its biochemical composition: Direct and inverse problems. Remote Sens. Environ. 56, 104–117. https://doi.org/10.1016/0034-4257(95)00234-0

Genty, B., Briantais, J.M., Baker, N.R., 1989. The relationship between the quantum yield of photosynthetic electron transport and quenching of chlorophyll fluorescence. Biochim. Biophys. Acta - Gen. Subj. 990, 87–92. https://doi.org/10.1016/S0304-4165(89)80016-9

Gitelson, A. A., Merzlyak, M.N., 1997. Remote estimation of chlorophyll content in higher plant leaves. Int. J. Remote Sens. 18, 2691–2697. https://doi.org/10.1080/014311697217558

Gnyp, M.L., Bareth, G., Li, F., Lenz-Wiedemann, V.I.S., Koppe, W., Miao, Y., Hennig, S.D., Jia, L., Laudien, R., Chen, X., Zhang, F., 2014. Development and implementation of a multiscale biomass model using hyperspectral vegetation indices for winter wheat in the North China Plain. Int. J. Appl. Earth Obs. Geoinf. 33, 232–242. https://doi.org/10.1016/j.jag.2014.05.006

Gonzalez-Dugo, V., Durand, J.-L., Gastal, F., 2010. Water deficit and nitrogen nutrition of crops. A review. Agron. Sustain. Dev. 30, 529–544. https://doi.org/10.1051/agro/2009059

Gonzalez-Dugo, V., Hernandez, P., Solis, I., Zarco-Tejada, P.J., 2015. Using high-resolution hyperspectral and thermal airborne imagery to assess physiological condition in the context of wheat phenotyping. Remote Sens. 7, 13586–13605. https://doi.org/10.3390/rs71013586

Gueymard, C., 1995. SMARTS, a simple model of the atmospheric radiative transfer of sunshine: Algorithms and performance assessment. Technical report no. FSEC-PF-270-95. Cocoa, FL: Florida Solar Energy Center

Gueymard, C.A., Myers, D., Emery, K., 2002. Proposed reference irradiance spectra for solar energy systems testing. Sol. Energy 73, 443–467. https://doi.org/10.1016/S0038-092X(03)00005-7

Haboudane, D., Miller, J.R., Pattey, E., Zarco-Tejada, P.J., Strachan, I.B., 2004. Hyperspectral vegetation indices and novel algorithms for predicting green LAI of

crop canopies: Modeling and validation in the context of precision agriculture. Remote Sens. Environ. 90, 337–352. https://doi.org/10.1016/j.rse.2003.12.013

Haboudane, D., Miller, J.R., Tremblay, N., Zarco-Tejada, P.J., Dextraze, L., 2002. Integrated narrow-band vegetation indices for prediction of crop chlorophyll content for application to precision agriculture. Remote Sens. Environ. 81, 416–426. https://doi.org/10.1016/S0034-4257(02)00018-4

Herrmann, I., Karnieli, A., Bonfil, D.J., Cohen, Y., Alchanatis, V., 2010. SWIR-based spectral indices for assessing nitrogen content in potato fields. Int. J. Remote Sens. 31, 5127–5143. https://doi.org/10.1080/01431160903283892

Homolová, L., Malenovský, Z., Clevers, J.G.P.W., García-Santos, G., Schaepman, M.E., 2013. Review of optical-based remote sensing for plant trait mapping. Ecol. Complex. 15, 1–16. https://doi.org/10.1016/j.ecocom.2013.06.003

Houborg, R., Cescatti, A., Migliavacca, M., Kustas, W.P., 2013. Satellite retrievals of leaf chlorophyll and photosynthetic capacity for improved modeling of GPP. Agric. For. Meteorol. 117, 10–23. https://doi.org/10.1016/j.agrformet.2013.04.006

Jacquemoud, S., Baret, F., 1990. PROSPECT: A model of leaf optical properties spectra. Remote Sens. Environ. 34, 75–91. https://doi.org/10.1016/0034-4257(90)90100-Z.

Jacquemoud, S., Ustin, S.L., Verdebout, J., Schmuck, G., Andreoli, G., Hosgood, B., 1996. Estimating leaf biochemistry using the PROSPECT leaf optical properties model. Remote Sens. Environ. 56, 194–202. https://doi.org/10.1016/0034-4257(95)00238-3.

Jacquemoud, S., Verhoef, W., Baret, F., Bacour, C., Zarco-Tejada, P.J., Asner, G.P., François, C., Ustin, S.L., 2009. PROSPECT + SAIL models: A review of use for vegetation characterization. Remote Sens. Environ. 113, S56–S66. https://doi.org/10.1016/j.rse.2008.01.026.

Jin, X., Yang, G., Tan, C., Zhao, C., 2015. Effects of nitrogen stress on the photosynthetic CO2 assimilation, chlorophyll fluorescence, and sugar-nitrogen ratio in corn. Sci. Rep. 5, 9311. https://doi.org/10.1038/srep09311.

Khamis, S., Lamaze, T., Lemoine, Y., Foyer, C., 1990. Adaptation of the Photosynthetic Apparatus in Maize Leaves as a Result of Nitrogen Limitation : Relationships between Electron Transport and Carbon Assimilation. Plant Physiol. 94, 1436–1443. https://doi.org/10.1104/pp.94.3.1436.

Kjeldahl, J., 1883. Neue Methode zur Bestimmung des Stickstoffs in organischen. J. Anal. Chem. 366–382. https://doi.org/10.1007/BF01338151.

Kokaly, R., 1999. Spectroscopic Determination of Leaf Biochemistry Using Band-Depth Analysis of Absorption Features and Stepwise Multiple Linear Regression. Remote Sens. Environ. 67, 267–287. https://doi.org/10.1016/S0034-4257(98)00084-4.

Lemaire, G., Jeuffroy, M.-H., Gastal, F., 2008. Diagnosis tool for plant and crop N status in vegetative stage: Theory and practices for crop N management. Eur. J. Agron. 28, 614–624. https://doi.org/10.1016/j.eja.2008.01.005.

Li, F., Mistele, B., Hu, Y., Chen, X., Schmidhalter, U., 2014. Reflectance estimation of canopy nitrogen content in winter wheat using optimised hyperspectral spectral indices and partial least squares regression. Eur. J. Agron. 52, 198–209. https://doi.org/10.1016/j.eja.2013.09.006.

Li, P., Wang, Q., 2011. Retrieval of leaf biochemical parameters using PROSPECT inversion: A new approach for alleviating ill-posed problems. IEEE Trans. Geosci. Remote Sens. 49, 2499–2506. https://doi.org/10.1109/TGRS.2011.2109390.

Lichtenthaler, H.K., Lang, M., Sowinska, M., Heisel, F., Miehé, J.A., 1996. Detection of Vegetation Stress Via a New High Resolution Fluorescence Imaging System. J. Plant Physiol. 148, 599–612. https://doi.org/10.1016/S0176-1617(96)80081-2.

Lu, C., Zhang, J., 2000. Photosynthetic CO2 assimilation, chlorophyl fluorescence and photoinhibition as affected by nitrogen deficiency in maize plants. Plant Sci. 151, 135–143.

Mahajan, G.R., Sahoo, R.N., Pandey, R.N., Gupta, V.K., Kumar, D., 2014. Using hyperspectral remote sensing techniques to monitor nitrogen, phosphorus, sulphur and potassium in wheat (Triticum aestivum L.). Precis. Agric. 15, 499–522. https://doi.org/10.1007/s11119-014-9348-7.

Mahajan, G.R., Pandey, R.N., Sahoo, R.N., Gupta, V.K., Datta, S.C., Kumar, D., 2016. Monitoring nitrogen, phosphorus and sulphur in hybrid rice (Oryza sativa L.) using hyperspectral remote sensing. Precis. Agric. 1-26.https://doi.org/10.1007/s11119-016-9485-2.

Meroni, M., Busetto, L., Colombo, R., Guanter, L., Moreno, J., Verhoef, W., 2010. Performance of Spectral Fitting Methods for vegetation fluorescence quantification. Remote Sens. Environ. 114, 363–374. https://doi.org/10.1016/j.rse.2009.09.010

Moya, I., Camenen, L., Evain, S., Goulas, Y., Cerovic, Z.G., Latouche, G., Flexas, J., Ounis, A., 2004. A new instrument for passive remote sensing: 1. Measurements of sunlight-induced chlorophyll fluorescence. Remote Sens. Environ. 91, 186–197. https://doi.org/10.1016/j.rse.2004.02.012.

Nobel, P.S., 2009. Photochemistry of Photosynthesis. Physicochem. Environ. Plant Physiol. 229–275. https://doi.org/10.1016/B978-0-12-374143-1.00005-3.

Pimstein, A., Karnieli, A., Bansal, S.K., Bonfil, D.J., 2011. Exploring remotely sensed technologies for monitoring wheat potassium and phosphorus using field spectroscopy. F. Crop. Res. 121, 125–135. https://doi.org/10.1016/j.fcr.2010.12.001.

Plascyk, J.A., Gabriel, F.C., 1975. The Fraunhofer line discriminator MKII an airborne instrument for precise and standardized ecological luminescence measurement. IEEE Trans. Instrum. Meas. 24, 306–313. https://doi.org/10.1109/TIM.1975.4314448.

Quemada, M., Gabriel, J.L., Zarco-Tejada, P., 2014. Airborne hyperspectral images and ground-level optical sensors as assessment tools for maize nitrogen fertilization. Remote Sens. 6, 2940–2962. https://doi.org/10.3390/rs6042940.

Ranjan, R., Chopra, U.K., Sahoo, R.N., Singh, A.K., Pradhan, S., 2012. Assessment of plant nitrogen stress in wheat (Triticum aestivum L.) through hyperspectral indices. Int. J. Remote Sens. 33, 6342–6360. https://doi.org/10.1080/01431161.2012.687473

Rascher, U., Alonso, L., Burkart, A., Cilia, C., Cogliati, S., Colombo, R., Damm, A., Drusch, M., Guanter, L., Hanus, J., Hyvärinen, T., Julitta, T., Jussila, J., Kataja, K., Kokkalis, P., Kraft, S., Kraska, T., Matveeva, M., Moreno, J., Muller, O., Panigada, C., Pikl, M., Pinto, F., Prey, L., Pude, R., Rossini, M., Schickling, A., Schurr, U., Schüttemeyer, D., Verrelst, J., Zemek, F., 2015. Sun-induced fluorescence - a new probe of photosynthesis: First maps from the imaging spectrometer HyPlant. Glob. Chang. Biol. 21, 4673–4684. https://doi.org/10.1111/gcb.13017

Ravier, C., Quemada, M., Jeuffroy, M.-H., 2017. Use of a chlorophyll meter to assess nitrogen nutrition index during the growth cycle in winter wheat. F. Crop. Res. 214, 73–82. https://doi.org/10.1016/j.fcr.2017.08.023

R Core Team. R: A language and environment for statistical computing. R Foundation for Statistical Computing, 2015. Vienna, Austria. http://www.R-project.org/

Rondeaux, G., Steven, M., Baret, F., 1996. Optimization of soil-adjusted vegetation indices. Remote Sens. Environ. 55, 95–107. https://doi.org/10.1016/0034-4257(95)00186-7

Roujean, J.L., Breon, F.M., 1995. Estimating PAR absorbed by vegetation from bidirectional reflectance measurements. Remote Sens. Environ. 51, 375–384. https://doi.org/10.1016/0034-4257(94)00114-3

Rouse, J.W., Hass, R.H., Schell, J.A., Deering, D.W., 1973. Monitoring vegetation systems in the great plains with ERTS. Third Earth Resour. Technol. Satell. Symp. 1, 309–317. https://doi.org/citeulike-article-id:12009708

Sadras, V.O., 2004. Yield and water-use efficiency of water- and nitrogen-stressed wheat crops increase with degree of co-limitation. Eur. J. Agron. 21, 455–464. https://doi.org/10.1016/j.eja.2004.07.007

Schächtl, J., Huber, G., Maidl, F.-X., Sticksel, E., Schulz, J., Haschberger, P., 2005. Laser-Induced Chlorophyll Fluorescence Measurements for Detecting the Nitrogen Status of Wheat (Triticum aestivum L.) Canopies. Precis. Agric. 6, 143–156. https://doi.org/10.1007/s11119-004-1031-y

Schlerf, M., Atzberger, C., 2006. Inversion of a forest reflectance model to estimate structural canopy variables from hyperspectral remote sensing data. Remote Sens. Environ. 100, 281–294. https://doi.org/10.1016/j.rse.2005.10.006

Serrano, L., Penuelas, J., Ustin, S.L., 2002. Remote sensing of nitrogen and lignin in Mediterranean vegetation\rfrom AVIRIS data:\rDecomposing biochemical from structural signals. Remote Sens. Environ. 81, 355–364

Smith, G.M., Milton, E.J., 1999. The use of the empirical line method to calibrate remotely sensed data to reflectance. Int. J. Remote Sens. 20, 2653–2662. https://doi.org/10.1080/014311699211994

Stroppiana, D., Boschetti, M., Brivio, P.A., Bocchi, S., 2009. Plant nitrogen concentration in paddy rice from field canopy hyperspectral radiometry. F. Crop. Res. 111, 119–129. https://doi.org/10.1016/j.fcr.2008.11.004

Thorp, K.R., Wang, G., West, A.L., Moran, M.S., Bronson, K.F., White, J.W., Mon, J., 2012. Estimating crop biophysical properties from remote sensing data by inverting linked radiative transfer and ecophysiological models. Remote Sens. Environ. 124, 224–233. https://doi.org/10.1016/j.rse.2012.05.013

Tremblay, N., Wang, Z., Cerovic, Z.G., 2012. Sensing crop nitrogen status with fluorescence indicators. A review. Agron. Sustain. Dev. 32, 451–464. https://doi.org/10.1007/s13593-011-0041-1

Uddling, J., Gelang-Alfredsson, J., Piikki, K., Pleijel, H., 2007. Evaluating the relationship between leaf chlorophyll concentration and SPAD-502 chlorophyll meter readings. Photosynth. Res. 91, 37–46. https://doi.org/10.1007/s11120-006-9077-5

Vogelmann, J.E., Rock, B.N., Moss, D.M., 1993. Red edge spectral measurements from sugar maple leaves. Int. J. Remote Sens. 14, 1563–1575. https://doi.org/10.1080/01431169308953986

Walker, A.P., Beckerman, A.P., Gu, L., Kattge, J., Cernusak, L.A., Domingues, T.F., Scales, J.C., Wohlfahrt, G., Wullschleger, S.D., Woodward, F.I., 2014. The relationship of leaf photosynthetic traits - Vcmax and Jmax - to leaf nitrogen, leaf phosphorus, and specific leaf area: A meta-analysis and modeling study. Ecol. Evol. 4, 3218–3235. https://doi.org/10.1002/ece3.1173

Wang, W., Yao, X., Yao, X., Tian, Y., Liu, X., Ni, J., Cao, W., Zhu, Y., 2012. Estimating leaf nitrogen concentration with three-band vegetation indices in rice and wheat. F. Crop. Res. 129, 90–98. https://doi.org/10.1016/j.fcr.2012.01.014

Wang, Y., Li, X., Nashed, Z., Zhao, F., Yang, H., Guan, Y., Zhang, H., 2007. Regularized kernel-based BRDF model inversion method for ill-posed land surface parameter retrieval. Remote Sens. Environ. 111, 36–50. https://doi.org/10.1016/j.rse.2007.03.007

Wang, Z., Skidmore, A.K., Darvishzadeh, R., Heiden, U., Heurich, M., Wang, T., 2015. Leaf Nitrogen Content Indirectly Estimated by Leaf Traits Derived from the PROSPECT Model. IEEE J. Sel. Top. Appl. Earth Obs. Remote Sens. 8, 3172–3182. https://doi.org/10.1109/JSTARS.2015.2422734

Weis, E., Berry, J.A., 1987. Quantum efficiency of Photosystem II in relation to “energy”-dependent quenching of chlorophyll fluorescence. BBA - Bioenerg. 894, 198–208. https://doi.org/10.1016/0005-2728(87)90190-3

Yang, X., Tang, J., Mustard, J.F., Lee, J., Rossini, M., Rascher, U., Alonso, L., Burkart, A., Cilia, C., Cogliati, S., Colombo, R., Damm, A., Drusch, M., Guanter, L., Hanus, J., Hyvärinen, T., Julitta, T., Jussila, J., Kataja, K., Kokkalis, P., Kraft, S., Kraska, T., Matveeva, M., Moreno, J., Muller, O., Panigada, C., Pikl, M., Pinto, F., Prey, L., Pude, R., Rossini, M., Schickling, A., Schurr, U., Schüttemeyer, D., Verrelst, J., Zemek, F., Houborg, R., Cescatti, A., Migliavacca, M., Kustas, W.P., Genty, B., Briantais, J.M., Baker, N.R., 2015. Satellite retrievals of leaf

chlorophyll and photosynthetic capacity for improved modeling of GPP. Agric. For. Meteorol. 990, 10–23. https://doi.org/10.1111/gcb.13017

Yebra, M., Chuvieco, E., 2009. Linking ecological information and radiative transfer models to estimate fuel moisture content in the Mediterranean region of Spain: Solving the ill-posed inverse problem. Remote Sens. Environ. 113, 2403–2411. https://doi.org/10.1016/j.rse.2009.07.001

Zarco-Tejada, P.J., Berjón, A., López-Lozano, R., Miller, J.R., Martín, P., Cachorro, V., González, M.R., De Frutos, A., 2005. Assessing vineyard condition with hyperspectral indices: Leaf and canopy reflectance simulation in a row-structured discontinuous canopy. Remote Sens. Environ. 99, 271–287. https://doi.org/10.1016/j.rse.2005.09.002

Zarco-Tejada, P.J., Berjon, A., Miller, J.R., 2004. Stress Detection in Crops with Hyperspectral Remote Sensing and Physical Simulation Models. Airborne Imaging Spectrosc. Work. 1–5.

Zarco-Tejada, P.J., Catalina, A., González, M.R., Martín, P., 2013. Relationships between net photosynthesis and steady-state chlorophyll fluorescence retrieved from airborne hyperspectral imagery. Remote Sens. Environ. 136, 247–258. https://doi.org/10.1016/j.rse.2013.05.011

Zarco-Tejada, P.J., González-Dugo, V., Berni, J.A.J., 2012. Fluorescence, temperature and narrow-band indices acquired from a UAV platform for water stress detection using a micro-hyperspectral imager and a thermal camera. Remote Sens. Environ. 117, 322–337. https://doi.org/10.1016/j.rse.2011.10.007

Zarco-Tejada, P.J., González-Dugo, M. V., Fereres, E., 2016. Seasonal stability of chlorophyll fluorescence quantified from airborne hyperspectral imagery as an indicator of net photosynthesis in the context of precision agriculture. Remote Sens. Environ. 179, 89–103. https://doi.org/10.1016/j.rse.2016.03.024

Zarco-Tejada, P.J., Miller, J.R., Noland, T.L., Mohammed, G.H., Sampson, P.H., 2001. Scaling-up and model inversion methods with narrowband optical indices for chlorophyll content estimation in closed forest canopies with hyperspectral data. IEEE Trans. Geosci. Remote Sens. 39, 1491–1507. https://doi.org/10.1109/36.934080

Chapter 5

ELSEVIER

Remote Sensing of Environment

Journal Metrics
CiteScore: 7.16
Impact Factor: 6.457
5-Year Impact Factor: 7.737

Radiative transfer Vcmax estimation from hyperspectral imagery and SIF retrievals to assess photosynthetic performance in rainfed and irrigated plant phenotyping trials

Carlos Camino[1], Victoria González-Dugo[1], Pilar Hernández[1], Pablo J. Zarco-Tejada[2, 3, 1*]

1. Instituto de Agricultura Sostenible (IAS), Consejo Superior de Investigaciones Científicas (CSIC), Córdoba, Spain
2. School of Agriculture and Food, Faculty of Veterinary and Agricultural Sciences (FVAS), University of Melbourne, Melbourne, Victoria, Australia
3. Department of Infrastructure Engineering, Melbourne School of Engineering (MSE), University of Melbourne, Melbourne, Victoria, Australia

Accepted in Remote sensing of Environmental, 6 May 2019

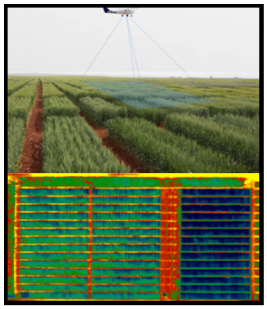

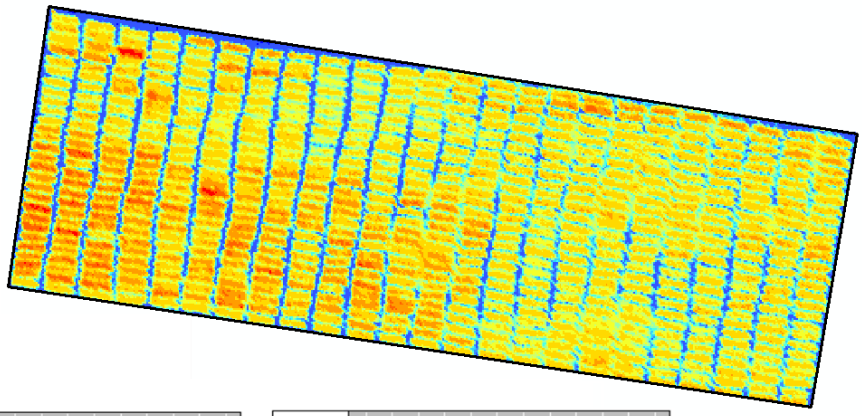

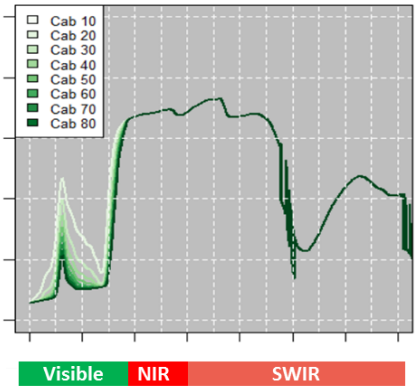

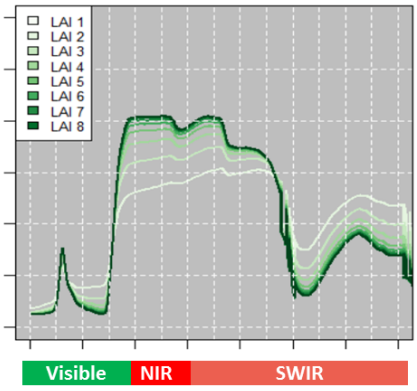

Chapter 5: Radiative transfer Vcmax estimation from hyperspectral imagery and SIF retrievals to assess photosynthetic performance in rainfed and irrigated plant phenotyping trials

Resumen

Los parámetros fotosintéticos de la planta pueden indicar tolerancia al estrés y el rendimiento de un cultivo, lo que origina que su evaluación precisa sea crítica en los ensayos de fenotipado. La tasa máxima de carboxilación (Vcmax) es un parámetro clave para estimar la asimilación de CO_2 (A), ya que controla la tasa de fijación de CO_2. Este estudio demuestra la utilidad de combinar fluorescencia clorofílica (SIF) cuantificada a partir de imágenes hiperespectrales mediante inversión del modelo Soil-Canopy Observation of Photosynthesis and Energy (SCOPE) para estimar Vcmax, aprovechando las resoluciones espectrales disponibles para su aplicación en el contexto de agricultura de precisión. Vcmax se cuantificó en tres ensayos experimentales de fenotipado de trigo durante las campañas de 2015-2018 en condiciones de secano y de riego. Las campañas aerotransportadas se llevaron a cabo con dos cámaras hiperespectrales cubriendo las regiones espectrales de 400–850 nm (resolución de 20 cm) y 950–1750 nm (resolución de 70 cm), y con una cámara térmica (resolución de 25 cm) sensible a la región espectral entre 8–14 µm. La validación entre Vcmax estimado por el modelo y medido en el campo fue estadísticamente significativa (r^2 = 0.77; valor de $p \leq 2.2e-16$) permitiendo que Vcmax se asociara de manera adecuada con A, tanto en condiciones de riego como en condiciones de secano (r^2 = 0.65 y 0.5, respectivamente). Por el contrario, los indicadores estándar de detección remota (NDVI, C_{ab}, $PSSR_b$) no obtuvieron correlaciones significativas con la asimilación en parcelas regadas, mientras que el índice térmico CWSI obtuvo una correlación baja en parcelas de secano. Vcmax mostró sensibilidad superior en condiciones de riego, ya que no se vio afectado por las distorsiones causadas con densidades alta, como sí se observó en otros índices. La estimación de Vcmax mediante detección remota, así como la metodología mostrada en este estudio, son directamente aplicables para el fenotipado de plantas de alto rendimiento, así como para aplicaciones de agricultura de precisión.

Abstract

Plant photosynthetic traits may be indicative of stress tolerance and performance in the field, making their accurate assessment critical in phenotyping trials. The maximum rate of carboxylation (Vcmax) is a key parameter for estimating CO_2 assimilation (A), as it controls the CO_2 fixation rate. This study demonstrates the utility of combining airborne-based solar-induced chlorophyll fluorescence (SIF) and hyperspectral imagery through the inversion of the Soil-Canopy Observation of Photosynthesis and Energy (SCOPE) model to estimate Vcmax, using sensor resolutions available in precision agriculture technologies. Vcmax was quantified in three wheat phenotyping experimental fields during the 2015-2018 growing seasons, comprising both rainfed and irrigated conditions. Airborne campaigns were carried out with two hyperspectral sensors, covering the 400–850 nm (20 cm resolution) and 950–1750 nm (70 cm resolution) spectral regions, and with a thermal camera (25 cm resolution) in the 8–14 µm region. Validation between model-estimated and field-measured Vcmax was statistically significant (r^2= 0.77; p-value ≤ 2.2e-16), and Vcmax was reliably associated with net assimilation both in irrigated and rainfed conditions (r^2=0.65 and 0.5, respectively). By contrast, simulated chlorophyll content (C_{ab}) and airborne-derived structural and chlorophyll indicators (NDVI and $PSSR_b$) lacked significant correlations with assimilation rate in irrigated plots, while the relationship between assimilation rate and the crop water stress index (CWSI) was not significant in rainfed plots. The superior sensitivity of remotely-sensed Vcmax under irrigated conditions was likely related to its robustness to distortions from high canopy densities observed in other indices. The remote sensing retrieval of Vcmax, and the methodology demonstrated in this study is directly relevant for high-throughput plant phenotyping and for precision agriculture applications.

5.1 Introduction

CO_2 assimilation (A) occurs in the chloroplasts and involves light biochemical reactions (Quebbeman and Ramirez, 2016). Environmental conditions such as light intensity and temperature, biophysical processes such as CO_2 transport through the leaf and stomata, and leaf biochemistry determine the assimilation rate (Sharkey et al., 2007). At the leaf level, the photosynthetic capacity is defined by the maximum rate of carboxylation (Vcmax) and the maximum rate of electron transport (Jmax). Vcmax is the maximum rate of Ribulose-1,5 Bisphosphate (RuBP) carboxylation, which controls CO_2 fixation (Farquhar et al., 1980). Jmax is the maximum rate of electron transport, which limits the supply of ATP and NADPH during the carboxylation and the regeneration of RuBP in the Calvin-Benson cycle (Quebbeman and Ramirez, 2016). Wullschleger (1993) demonstrated that Jmax should follow Vcmax across plant species, a relationship not affected by nitrogen content within leaves (Walker et al., 2014).

The most common biochemical photosynthesis model for estimating the CO_2 assimilation at leaf level is the Farquhar–von Caemmerer–Berry (FvCB) model (Farquhar et al., 1980). The FvCB model and its subsequent variants (Caemmerer and Farquhar, 1981; Farquhar and Wong, 1984; Collatz et al., 1992; Harley et al., 1992) relate the kinetic properties of Ribulose-1,5-Bisphosphate Carboxylase-Oxygenase (RuBisCo) to photosynthetic capacity (Caemmerer, 2000). The FvCB model is typically embedded in terrestrial biosphere models (TBM), which have been used to estimate photosynthetic carbon uptake (Norton et al., 2017), gross primary productivity (Sellers, 1987; Koffi et al., 2015) and the leaf respiration (Sitch et al., 2003; Oleson et al., 2013). In recent years, progress has been made to quantify photosynthetic capacity from hyperspectral satellite imagery, enabling the development of TBMs at new spatial scales. In the context of a plant phenotyping study, Silva-Perez et al. (2018) demonstrated the use of hyperspectral reflectance to estimate Vcmax and other physiological traits in wheat crops. However, imagery was obtained at the leaf level, where the remote sensing signal was not affected by canopy structure, as it is for larger-scale applications. For images at the canopy level, standard reflectance indices such as the normalized difference vegetation index (NDVI) (Rouse et al., 1973) have been widely used for detecting vigor, growth, yield and senescence patterns from airborne and near-field scales in maize and wheat crops (Cairns et al., 2012; Kipp et al., 2014). However, NDVI has well-known disadvantages associated with its saturation at high

biomass levels, its sensitivity to canopy background variations, and the inability to track short-term physiological changes due to its strong relationship with tissue structure (Huete, 1988; Huete et al., 2002). Despite these disadvantages, NDVI is still one of the most widely used indicators for the remote assessment of canopy characteristics by plant breeders.

Several studies have demonstrated that canopy temperature can be related to physiological processes (Gonzalez-Dugo et al., 2015) or even used as an indirect proxy for the detection of nutritional deficiencies (Rodriguez et al., 2006). The thermal-based Crop Water Stress Index (CWSI) developed by Idso et al. (1978) and Jackson et al. (1981) is inversely related to transpiration and stomatal conductance, and therefore a potentially good proxy for estimating photosynthesis rates under stress conditions. However, a range of environmental factors may affect stomatal closure and its relationship with the canopy temperature, such as changes in radiation exposure, nutrient deficiency or soil water deficit (Radin et al., 1985; Jones et al., 1995; Zweifel et al., 2002)

In the last twenty years the quantification of sun-induced chlorophyll fluorescence (SIF) through hyperspectral imaging has provided a new tool for monitoring crop photosynthetic activity and vegetation functioning (Frankenberg et al., 2011; Houborg et al., 2013; Zarco-Tejada et al., 2016; Norton et al., 2017). Chlorophyll fluorescence is closely related to the electron transport rate and hence to the photosynthetic activity (Genty et al., 1989; Weis and Berry, 1987). Chlorophyll fluorescence may therefore be a key indicator for detecting nutrient limitation in crops (Camino et al., 2018). Chlorophyll fluorescence may also be used to estimate Vcmax since both are linked with chlorophyll content (Houborg et al., 2013; Croft et al., 2017) and therefore photosynthetic activity (Rascher et al., 2015; Yang et al., 2015).

Recent studies have successfully estimated Vcmax from satellite SIF retrievals (Guan et al., 2016; Zhang et al., 2014, 2018) using the Soil Canopy Observation, Photochemistry and Energy fluxes (SCOPE) model (Guanter et al., 2014; Koffi et al., 2015; Zhang et al., 2014, 2018). Nevertheless, further progress is needed for the assessment of Vcmax under both water and nutrient-limited conditions (i.e. under stress) and in the context of plant phenotyping experiments with high-resolution imagery. In some cases, SIF retrievals have been performed using cost effective

hyperspectral imagers with broader spectral resolutions (i.e. 2–7 nm FWHM) (Damm et al., 2015; Zarco-Tejada et al., 2016; Camino et al., 2018). Although offsets in the fluorescence retrievals may occur due to the broader spectral resolutions used in these imagers, the consequences may be negligible for most precision agriculture applications since emphasis is on relative spatio-temporal variability of stress rather than absolute fluorescence emission levels.

The remote assessment of plant photosynthesis requires careful attention to the influence of stress. Photosynthesis is strongly affected by stress, with assimilation affected by water deficit (Chaves, 1991) and carboxylation capacity sensitive to leaf nitrogen levels (Walker et al. 2014). However, under drought conditions, water deficit may alter the nitrogen balance as growth rate diminishes (Gonzalez-Dugo et al., 2010). In bread wheat, populations display heritable variation in photosynthetic traits, amenable to artificial selection (Carmo-Silva et al. 2017). As a result, remotely sensed chlorophyll fluorescence may be useful for phenotyping photosynthetic traits desirable for breeding. In this study we quantify Vcmax as a proxy for photosynthetic activity in wheat phenotyping trials using airborne hyperspectral-based SIF retrievals through SCOPE model inversions. Specifically, we evaluated airborne estimates of Vcmax under both well-watered and water-limited regimes.

5.2 Material and Methods

5.2.1 Study area

Experiments took place at three field trial sites for bread wheat (Triticum aestivum L.) and durum wheat (Triticum turgidum L. var. durum) in Southern Spain in 2015, 2016 and 2018 (Fig. 5.1). The regional climate is Mediterranean, characterized by mild winters, warm and dry summers and with annual rainfall averages around 600 mm. The first trial site was located in Ecija (37°32′17″N, 5°06′57″W), which was managed under rainfed conditions in 2015 and 2018. The plot size was 12.5 m^2 (10 m×1.25 m) with a spacing of 1 m x 1.25 m between plots (Fig. 5.1a and 5.1d).

The second site trial was located in Carmona (37°30′29″N, 5°34′42″W) in 2015, which was managed under both rainfed and irrigated conditions. Severe drought at the Carmona experimental site during the spring of 2015 (precipitation < 30 mm in preceding months of the airborne campaign) prompted irrigation in rainfed plots the week before the flights to partially recover the experiment and to avoid damage. At

Carmona, 882 individual plots (7.5×1.25 m) were divided across two blocks according to water regime. There was a space of 1.50 m x 0.25 m between plots (Fig. 5.1b). Forty-nine varieties of durum or bread wheat were replicated three times per block.

The third trial site was located in Santaella (37°31′34″N, 4°50′40″W), which was also managed under rainfed and irrigated conditions in 2016. Twenty varieties of durum wheat and 20 varieties of bread wheat were replicated three times across a total of 120 plots (Fig. 5.1c). The plot size was 15 m^2 (10×1.5 m) with a spacing of 2.50 m x 0.50 m between plots.

At all trial sites, plots consisted of five rows of wheat with a spacing of 0.25 cm per row. Physiological measurements and spectral reflectance were taken from the three central rows. The remaining two rows were excluded from analysis. The soil in the three trial sites was dominated by vertisols (FAO classification), which ranged in texture from clay, clay loam to silt. Slope across sites ranged from 2 to 4%. Vertisols are often poor in organic matter and associated with nitrogen and phosphorus deficiencies. Fertilization with diammonium phosphate and urea was carried out in early November to ensure fertility levels.

The wheat growth stage during the airborne campaigns corresponded to i) stem elongation stage, and ii) the grain filling (milking stage) (Table 5.1). All flights were performed under clear sky conditions. Average meteorological conditions during each flight (ERA-Interim atmospheric reanalysis data; http://www.ecmwf.int) are presented in Table 1.

Table 5.1. Flight dates and field measurements collected during the airborne campaigns. The meteorological conditions at the time of the flights are included.

Year	Site	Flight dates	Growth Stage	Airborne imagery	Field measurements	Meteorological conditions		
						T_a	RH	R_{in}
2015	Ecija	28/05	Grain filling	T + VNIR + NIR	ψ_L, A, C_{ab} , N	295.1	38.0	944.2
	Carmona	30/05	Grain filling	T + VNIR + NIR	ψ_L, A, C_{ab}, N	296.8	38.8	935.8
2016	Santaella	17/03	Stem elongation	T + VNIR + NIR	ψ_L, A, C_{ab} , N	289.6	49.2	558.2
	Santaella	26/04	Grain filling	T + VNIR + NIR	ψ_L, A, C_{ab} , N	297.5	42.5	933.3
2018	Ecija	18/04	Stem elongation	T + VNIR + NIR	A, C_{ab}, N, Curve A/C_i	297.1	43.6	924.8

T= thermal, VNIR = hyperspectral visible and infrared region, NIR = hyperspectral near-short wave infrared region, ψ_L= leaf water potential (MPa), A = net assimilation rate ($\mu \cdot mol \cdot m^{-2} \cdot s^{-1}$), C_{ab} = chlorophyll content ($\mu g \cdot cm^{-2}$), N= nitrogen concentration (%), Curve A/Ci = response curves of A to the intercellular CO_2 concentration,

T_a= air temperature (K), RH= relative humidity (%) and R_{in}= Incoming shortwave radiation ($W \cdot m^{-2}$).

5.2.2 Field physiological measurements and leaf gas exchange curves

A summary of the physiological variables measured for each site and sampling date is included in Table 5.1. Field measurements of assimilation rate (A; $\mu mol \cdot m^{-2} \cdot s^{-1}$) and leaf water potential (ψL; MPa) were made at the same time (±1 hour) as acquisition of high-resolution airborne imagery over the experimental field sites. These measurements were performed on leaves at the top of the canopy at noontime, under clear skies and with photosynthetically active radiation (PAR) values ranging from 1700 to 2200 $\mu mol \cdot m^{-2} \cdot s^{-1}$. To assess the physiology and nutritional status of the wheat plots under different water regimes, some additional leaf measurements were made at the trial sites (Table 5.1). Leaf photosynthesis was measured with a photosynthesis measurement system (LC pro- SD, ADC Bioscientific Ltd., Herts, UK) on two leaves per plot. The LCpro-SD plant leaf photosynthesis chamber has a flow rate accuracy of ± 2% of its range. Leaf water potential (ψL) was measured on two sunlit leaves per plot with a pressure chamber (Model 600 Pressure Chamber Instrument, PMI Instrument Company, Albany, NY, USA). Chlorophyll content was measured on 10–15 leaves per plot using a hand-held chlorophyll meter (SPAD-502, Minolta Corp., Ramsey, NJ, USA). The SPAD-502 chlorophyll meter has an accuracy of ± 1 SPAD units. In 2018, leaf chlorophyll content was measured with the Dualex instrument (FORCE-A, Orsay, France), which has an accuracy of 5%. The SPAD and Dualex readings were converted to chlorophyll content (µg·cm-2) according to Uddling et al. (2007). Total N concentration (%) was determined by the Kjeldahl method (Kjeldahl, 1883) in random samples of 20-25 leaves from the top of the canopy in select plots. This value was demonstrated to be a good proxy of the crop nutritional status (Farruggia et al., 2004).

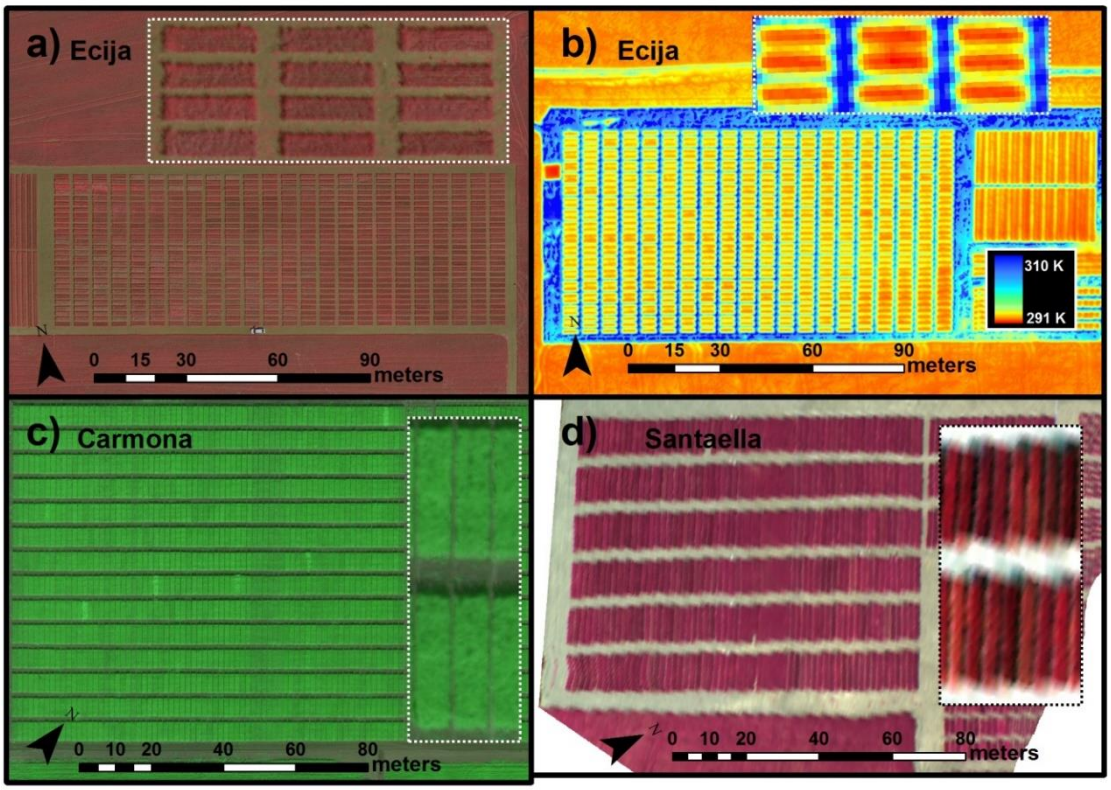

Fig. 5.1. Overview of the field trial sites at Ecija (a and b), Carmona (c) and Santaella (d). Figures a and c were obtained with a CIR camera (a: 800 (R), 670 (G) and 550 (B) nm; c: true color). Figure b shows a sample of the thermal imagery. Figure d was obtained with a VNIR hyperspectral imager (composite: 706 (R), 679 (G) and 520 (B) nm).

The response of assimilation to intercellular CO_2 concentration was measured using the portable LCpro-SD photosynthesis measurement system during the field campaign at Ecija in 2018. To assess variability in CO_2 response curves, six wheat varieties (W_I to W_{VI}) displaying contrasting nutritional and physiological statuses were selected across the trial site (Fig. 5.2). Varieties were selected based on patterns in chlorophyll content, nitrogen, and assimilation rate (red asterisks in Fig. 5.2). The photosynthetic photon flux density was kept constant at 1900 $\mu mol \cdot m^{-2} \cdot s^{-1}$ during measurements. Prior to sampling, selected leaves were adapted to the chamber light conditions, humidity and temperature for about 5 minutes. CO_2 concentration was then ramped in steps of 100 ppm, with each step lasting a minimum of 1 minute and a maximum of 3 minutes.

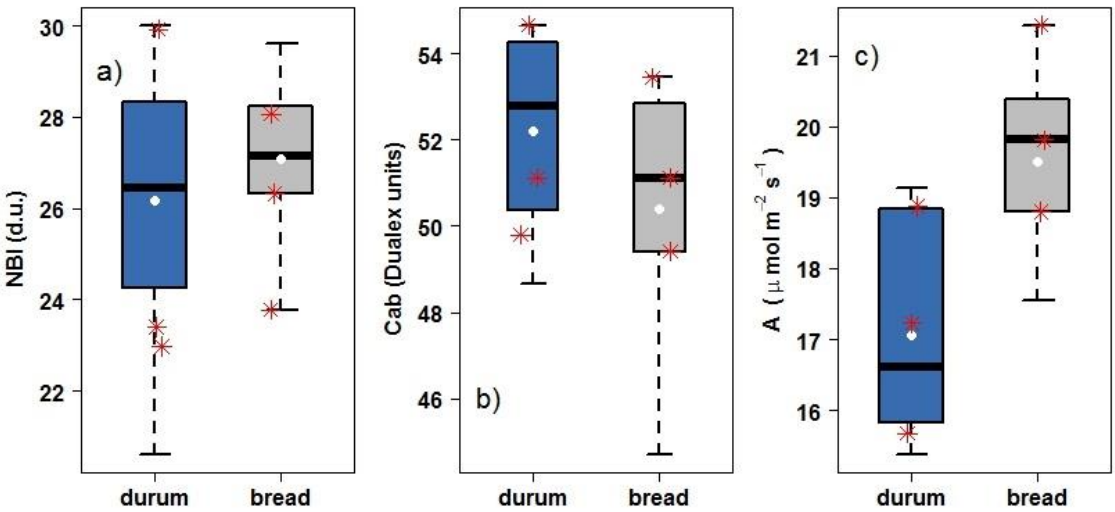

Fig. 5.2. Leaf physiological measurements on durum wheat plots (in blue) and bread wheat plots (in grey) carried out during the field campaign in Ecija 2018 under rainfed conditions: a) the nitrogen balance index (NBI) in dimensionless units (d.u.), b) chlorophyll content (C_{ab}) in Dualex units (both measurements were collected with the hand-held Dualex device) and c) assimilation rate (A) in $\mu mol \cdot m^{-2} \cdot s^{-1}$, measured with the plant leaf photosynthesis chamber. The red asterisks indicate wheat plots selected for A/Ci curves. In the box plots, the black line within the box is the median, and the top and bottom of the box represent the 75th and 25th quartiles, respectively. The whiskers represent the upper and lower range. The average values are shown with a white point over each box plot.

Leaf Vcmax was estimated from assimilation-intercellular CO_2 concentration (A-Ci) curves (Fig. 5.3) using the C_3 FvCB photosynthesis model (Farquhar et al., 1980). Photosynthetic response [CO_2] curves developed by Sharkey et al. (2007) were used to estimate Vcmax according to the FvCB model. Following this method, field measurements with intercellular CO_2 partial pressure between 20 to 30 Pa were excluded to reduce errors associated with the interface between the RuBisCo-limited and RuBP-regeneration-limited state.

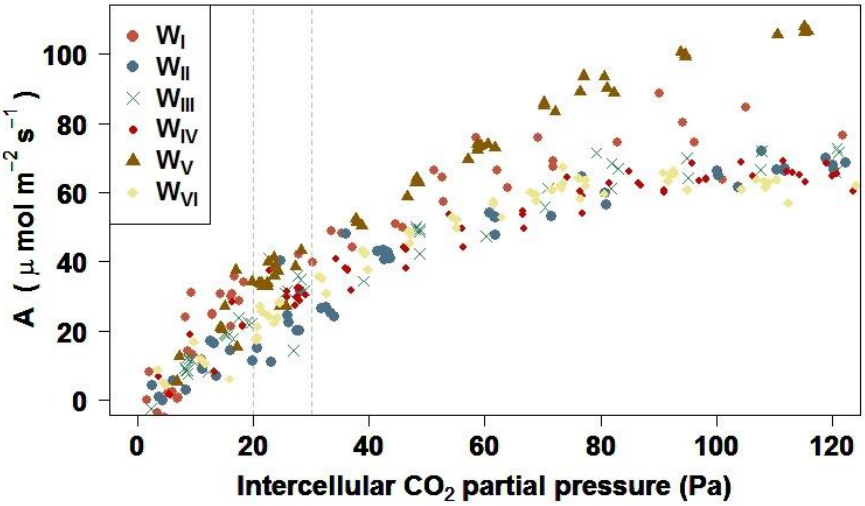

Fig. 5.3. Relationship obtained between assimilation rate (A; μmol·m^{-2}·s-1) and intercellular CO_2 partial pressure (Pa). Each colour is associated with different wheat varieties (W_n). The dashed lines represent the RuBisCo-limited (left) and RuBP-regeneration-limited (right) state according to Sharkey et al. (2007).

Kinetic parameters for respiration (R_d) and the mesophyll conductance (g_m) were estimated for each wheat variety following the nonlinear curve fitting procedures outlined in Sharkey et al. (2007). The temperature dependence of the Michaelis-Menten constant of RuBisCo (K_c) for CO_2, inhibition constant (K_o), photorespiratory compensation point (Γ*), Rd, g_m, Vcmax, rate of photosynthetic electron transport (J) and triose phosphate use (TPU) were estimated using exponential functions of temperature responses described in Harley et al. (1992b). The scaling constant (c), enthalpies of activation (ΔH_a), deactivation (ΔH_d) and entropy (ΔS) were taken from Sharkey et al. (2017) in Table 1.

The retrievals of Vcmax were adjusted to 25ºC using the FvCB model. Only measurements where leaf temperatures were ±0.5ºC of the average were used in generating these estimates. Atmospheric pressure and intercellular concentration of oxygen (O_i) for all collected wheat varieties were set to 21 kPa and 99.75 kPa, respectively. Rd and g_m values used to estimate Vcmax are provided in Table 5.2.

Table 5.2. Input parameters and constants (adjusted to 25ºC), maximum carboxylation rate (Vcmax), photosynthetic electron transport rate (J) and triose phosphate use (TPU) obtained from the A/Ci curves shown in Fig. 3 for six wheat varieties using exclusively measures with a leaf temperature equal to the average ± 0.5ºC. The kinetic parameters include the Michaelis constant of RuBisCo for carbon dioxide (K_c), the inhibition constant (K_o), and the photorespiratory compensation point (Γ*). Day respiration (R_d) and the mesophyll conductance (g_m) were used for adjusting estimates to 25ºC. Temperature responses were estimated using the equations described in Harley et al. (1992b). The specific kinetic constants [scaling constant (c), enthalpies of activation (ΔHa), deactivation (ΔHd) and entropy (ΔS)] were taken from Sharkey et al. (2007).

Parameters	W_I	W_{II}	W_{III}	W_{IV}	W_V	W_{VI}
Temperature leaf (ºC)	32.6±0.2	24.12±0.5	25.2±0.2	26.2±0.2	26.42±0.5	23.5±0.5
Constants for fitting						
K_c (Pa)	61.87	24.73	27.84	31.05	31.82	23.09
K_o (kPa)	21.08	16.12	16.69	17.23	17.35	15.80
Γ*(Pa)	4.79	3.63	3.77	3.89	3.92	3.56
Constant for adjusting to 25ºC						
R_d (mmol·m^{-2}·s^{-1})	1.601	0.947	1.013	1.078	1.094	0.910
g_m (mmol m-2 s^{-1}·Pa^{-1})	1.611	0.943	1.014	1.083	1.100	0.904
Outputs adjusting to 25ºC						
Vcmax (µmol·m^{-2}·s^{-1})	109	118	106	109	101	104
J (µmol·m^{-2}·s^{-1})	201	292	275	259	227	299
TPU (µmol·m^{-2}·s^{-1})	18.6	24.1	23.1	21.2	2.5	25.0

5.2.3 Airborne campaigns

Five airborne campaigns were conducted using an aircraft operated by the Laboratory for Research Methods in Quantitative Remote Sensing (QuantaLab), Consejo Superior de Investigaciones Científicas (IAS-CSIC, Spain). Flights occurred at 250 m above ground level (AGL) with heading on the solar plane. Images were acquired concurrently with field data acquisitions (Table 5.1) between 12:00 and 13:00h (local time) under clear sky conditions and free of coarse aerosol (i.e.: dust mineral, biomass burning). To minimize differences due to sun angle effects, the flights were performed at solar zenith angle between 45º and 60º, which varied according to the day, place and the exact flight time. The viewing zenith angle was 0º for all flights. Images were collected with a micro-hyperspectral imager (Micro-Hyperspec VNIR model, Headwall Photonics, Fitchburg, MA, USA), a Micro-Hyperspec NIR-100 (Headwall Photonics) and a thermal infrared camera (FLIR SC655, FLIR Systems, Wilsonville, OR, USA). The Micro Hyperspec VNIR was configured to acquire 260 spectral bands with a light dispersion of 1.85 nm/pixel with 12-bit radiometric resolution in the 400–885 nm spectral region, yielding a 6.4 nm full width at half maximum (FWHM) with an entrance slit width of 25-µm. The acquisition and storage module obtained 50 frames per second at 25 ms integration time. The 8-mm focal length lens yielded an IFOV of

0.93 mrad and an angular FOV of 50º with a spatial resolution of 20 cm (Fig. 5.1c). The micro-hyperspec NIR-100 sensor was configured for 165 spectral bands at 16-bit radiometric resolution covering the 950–1750 nm spectral region, yielding 6.05 nm FWHM with a spatial resolution of 70 cm. Radiometric calibration of the VNIR and NIR 100 cameras was performed with an integrating sphere (CSTM-USS-2000C LabSphere, North Sutton, NH, USA) using four levels of illumination and six integration times.

Hyperspectral imagery was atmospherically corrected using incoming irradiance measured with a field spectrometer (FieldSpec Handheld Pro, ASD Inc., Longmont, Colorado, USA) for the VNIR sensor, and simulated by the SMARTS model (Gueymard, 1995; Gueymard et al., 2002) for the NIR-100 sensor. In addition, the view and illumination angle effects were corrected using a bidirectional reflectance distribution function (BRDF) in the VNIR and NIR-100 hyperspectral imagery. Irradiance measurements were interpolated and convoluted to the bandwidth of each sensor. To simulate incoming irradiance, aerosol optical measurements (Table 5.3) were acquired at flight time with a Microtops II handheld multichannel sunphotometer (Solar Light, Philadelphia, USA) connected to a GPS-12 model (Garmin, Olathe, KS). The aerosol measurements carried out with the sunphotometer instrument at flight-time confirmed the absence of dust mineral, biomass burning (AOD500nm $\leq$ 0.25 and Ångström exponent (AE) $\geq$ 0.6, according to Cuevas et al. (2015)) and other extinction aerosols which could affect the reflectance and radiance spectrum during the airborne campaign. A portable weather station (Transmitter PTU30, Vaisala, Helsinki, Finland) was used for simultaneous readings of the relative humidity, temperature and pressure at the time of hyperspectral and thermal acquisitions. Ortho-rectification of hyperspectral imagery was performed following Zarco-Tejada et al. (2016). Sample average radiance and reflectance spectra of wheat plots obtained with the VNIR hyperspectral sensor at the Ecija trial site in 2018 are shown in Fig. 5.4.

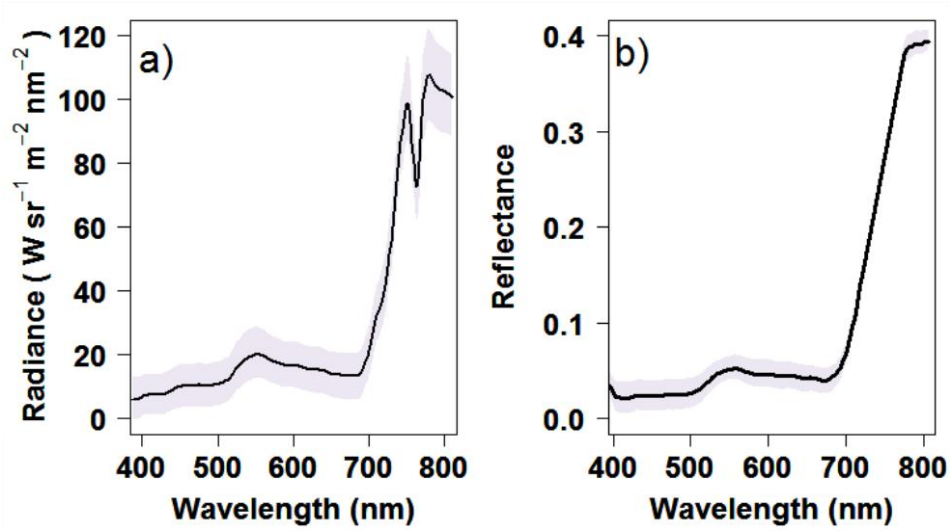

Fig. 5.4. Mean radiance (W·sr^{-1}·m^{-2}·nm^{-1}) (a) and reflectance spectra (b) retrieved from the VNIR hyperspectral camera at the Ecija site in 2018. The black lines correspond to the average spectra of all wheat plots. Shaded areas comprise the ± 1 standard deviation of the average radiance and reflectance profiles.

The FLIR SC655 thermal camera used in this study had a resolution of 640 × 480 pixels with a 13.1 mm focal length at 16 bits, providing an angular FOV of 45 × 33.7º and a ground resolution of 25 cm at the flight altitude (Figure 5.1d). Thermal imagery was calibrated using ground temperature data collected with a handheld infrared thermometer (LaserSight, Optris, Germany) on each flight date.

Table 5.3. Average values of aerosol optical depth (AOD) at 500 nm, the Ångström exponent (AE) at 440 -936 nm, air mass and the precipitable water vapour column (in cm) measured using a hand-held sun photometer (MicroTops-II) instrument. The sun photometer measurements were performed at each trial site during the airborne campaigns of 2015-2018.

Year	Site	Flight dates	$AOD_{500\ nn}$	$AE_{440\text{-}936nm}$	Air mass	H_2O atm (in cm)
2015	Ecija	28/05	0.09	0.84	1.30	1.05
	Carmona	30/05	0.07	0.75	1.28	1.30
2016	Santaella	17/03	0.13	0.69	1.31	1.06
	Santaella	26/04	0.09	0.65	1.27	1.22
2018	Ecija	18/04	0.12	0.61	1.25	0.98

5.2.4 Fluorescence retrievals, narrow-band indices and the CWSI from the high-resolution hyperspectral and thermal imagery

According to the method developed by Camino et al. (2018b), an automatic segmentation based on quartile breaks was applied to the high-resolution hyperspectral imagery for minimizing the effect of the soil background inside wheat plots. The average radiance and reflectance spectra (Fig. 5.4) were extracted from the high-resolution hyperspectral imagery using the segmented areas, which corresponded with the central region of each wheat plot. Using the same scheme as for the hyperspectral imagery, the watershed segmentation method was applied to high-resolution thermal imagery for separating the vegetation from the soil background.

Solar induced fluorescence (SIF) was quantified from radiance spectra (Fig. 4a) by the in-filling method using the Fraunhofer Line Depth (FLD) principle (Plascyk and Gabriel, 1975). The FLD method compares canopy radiance to incoming irradiance at the 760.5 nm atmospheric O_2-A oxygen absorption Fraunhofer Line, as described in Moya et al. (2004) and Meroni et al. (2010). We compared the radiance values Lin (L762 nm) and Lout (L750 nm) extracted from the VNIR hyperspectral imagery, to incoming irradiances Ein (E762 nm) and Eout (E750 nm) measured at the time of the flights. Reasonable SIF retrieval via the FLD method using broader spectral bandwidths (i.e., 5–7 nm FWHM) has been demonstrated in a simulation study (Damm et al., 2011) and experimentally (Zarco-Tejada et al., 2012, 2016; Damm et al., 2015; Hernandez-Clemente et al., 2017). The configuration of the hyperspectral imager during the airborne campaigns carried out in this study (1.85 nm sampling interval, 6.4 nm bandwidths and SNR of 300:1 with spatial binning) is comparable to that of Zarco-Tejada et al. (2012), and observations with the Airborne Prism EXperiment (APEX) sensor in Damm et al. (2015). In addition, NDVI and the pigment-specific simple ratio chlorophyll b index ($PSSR_b$) proposed by Blackburn (1998) were calculated from the average reflectance values for each experimental plot (Fig. 5.4b).

The Crop Water Stress Index (CWSI) was calculated from the thermal imagery according to the methodology proposed by Idso et al. (1981, Eq. 5.1). For the assessment of CWSI, the average canopy temperature (Tc) retrieved from the top of the wheat canopy at sunlit conditions and the air temperature (Ta) registered at the flight time were used.

$$CWSI = \frac{(Tc - Ta) - (Tc - Ta)_{LL}}{(Tc - Ta)_{UL} - (Tc - Ta)_{LL}} \quad (5.1)$$

$(Tc\text{-}Ta)_{LL}$ represents the canopy-air temperature differential of a canopy transpiring at the maximum rate and $(Tc\text{-}Ta)_{UL}$ represents this temperature differential when transpiration is completely halted. The Non-Water-Stress-Baseline (NWSB) was used to derive $(Tc\text{-}Ta)_{LL}$, defined as the relationship between the Tc-Ta of a well-irrigated wheat plot at a given vapour pressure deficit (VPD). The NWSB used in this study (Tc-Ta=3.38-3.25·VPD) was obtained by Idso (1982), while the upper limit was calculated according to the methodology proposed by Idso *et al*. (1981).

5.2.5 Modelling methods

Vcmax, standardized to a reference temperature at 25 °C (hereinafter referred to Vcmax), was estimated by inversion of the SCOPE model v1.70 (van der Tol et al., 2009a) using biophysical parameter retrievals and SIF quantification for each wheat plot. SCOPE is a vertical (1-D) integrated radiative transfer and energy balance model.

The SCOPE model is focused on the relationship between chlorophyll fluorescence and photosynthesis at the leaf level as a function of environmental conditions (van der Tol et al., 2009b). Photosynthesis and chlorophyll fluorescence simulations are carried out in SCOPE with meteorological forcing inputs (incoming shortwave and long-wave radiation, air temperature, humidity, wind speed and CO_2 concentration) and four kinds of parameters: i) leaf parameters including leaf mesophyll structure (N-struct), leaf chlorophyll content (C_{ab}), dry matter content (C_m), leaf equivalent water thickness (C_w), senescent material (C_s) and anthocyanins (C_{ant}); ii) vegetation structural parameters, including the leaf area index (LAI), leaf angle distribution, leaf size and canopy height (hc); iii) optical parameters, including vegetation emissivity and soil reflectance in the visible, near infrared and thermal bands; and iv) physiological parameters, including stomatal conductance (m) and maximum carboxylation capacity. A summary of the relevant SCOPE inputs for this study is given in Table 5.4.

The canopy geometry effects on the outgoing spectrum and on the heterogeneity of net radiation are treated stochastically with 60 elementary layers, with a maximum LAI of 0.1 each, 13 discrete leaf zenith inclinations and 36 leaf azimuth classes for shaded and sunlit leaves. The fluorescence contributions from individual leaves are integrated over the canopy layer to calculate top of canopy (TOC) fluorescence in the viewing

direction of the hyperspectral sensor based on absorbed fluxes over the photosynthetic active radiation (PAR) region (400–700 nm). The chlorophyll fluorescence at leaf level is computed as a product of the FvCB photosynthesis model, stomatal resistance (Cowan, 1978), the Ball–Berry stomatal conductance model (Ball et al., 1987), the coupled photosynthesis-stomatal model (Collatz et al., 1991), and the emission of chlorophyll fluorescence. The SCOPE model combines the Collatz et al. (1991) model and the Farquhar et al. (1980) photosynthesis model for retrieving the Vcmax, taking into account the stomatal conductance and assimilation rate. For further details see van der Tol et al. (2009b) and van der Tol et al. (2014).

Table 5.4. Range of the PROSPECT-SAILH and SCOPE parameters used in this study.

Parameters	Definition	Unit	Range	Step
PROSPECT				
Leaf biophysical				
N-struct	Leaf structure mesophyll parameter	[-]	1.25–1.85	0.1
C_{ab}	Chlorophyll a +b content	$\mu g \cdot cm^{-2}$	10–70	0.5
C_w	Equivalent water thickness	$g \cdot cm^{-2}$	0.001–0.05	0. 0005
C_m	Dry matter content	$g \cdot cm^{-2}$	0.001–0.05	0. 0005
C_s	Senescence factor	[-]	0	…
S_l	Hot-spot parameter	[-]	0[(d)]	…
FLUSPECT (integrated into SCOPE model)				
C_{ant}	Anthocyanin content	$\mu g \cdot cm^{-2}$	3,5,10	…
SAILH				
Canopy				
LAI	Leaf area index	$m^2 \cdot m^{-2}$	2–5	0.1
LADF	Leaf inclination distribution function	[-]	1,2,3 and 4[(a)]	…
TV	Solar zenith angle	deg	45,60,85	5
Ph_i	Viewing zenith angle	deg	0	…
PSR	Relative azimuth angle	deg	0	…
SCOPE				
Leaf biochemistry				
Vcmax	Maximum carboxylation capacity	$\mu mol \cdot m^{-1} \cdot s^{-1}$	0–260	10
m	Ball-Berry stomatal conductance	[-]	8	…
Rdparam	Parameter for dark respiration	[-]	0.015	…
K_v	Extinction coefficient for vertical Vcmax profile	[-]	0.64	…
K_c	Cowan's water use efficiency	[-]	700	…
ρ(thermal)	Leaf thermal reflectance	[-]	0.01	…
τ(thermal)	Leaf thermal transmittance	[-]	0.01	…
ρ_s(thermal)	Soil thermal reflectance	[-]	0.06	…
Stressfactor	Stress multiplier for Vcmax	[-]	1	…
kNPQs	Rate thermal dissipation	[-]	0	…
qLs	Fraction active photosystems	[-]	1	…
fqe	Fraction of photons partitioned to PSII	[-]	0.02	…
Canopy				
l_w	Leaf width	m	0.1	…
$LIDF_a$	Leaf inclination distribution of leaves	[-]	-1–1	0.05
$LIDF_b$	Variation in leaf inclination	[-]	-1–1	0.05
hc	Canopy height	m	1.2	…
Micrometeorological				
p	Air pressure	hPa	988–997[(b)]	…
u	Wind speed	m^{-1}	2.2–2.8[(c)]	…
Oa	O_2 concentration in the air	per mille	209	…
ea	Atmospheric vapor pressure	hPa	15	…
Ca	CO_2 concentration in the air	ppm	392.2	…
Ta	Air temperature	ºC	18–25[(b)]	…
R_{in}	Incoming shortwave radiation	$W \cdot m^{-2}$	500–950[(b)]	…
R_{li}	Incoming longwave radiation	$W \cdot m^{-2}$	70–150[(b)]	…

a) Canopy types proposed to define LADF: planophile (1), erectophile (2), plagiophile (3) and spherical (4)
b) Meteorological variables retrieved from hourly ERA-Interim reanalysis dataset for each trial sites.
c) Wind speed at 2-meter from a weather station located close to each trial sites.
d) Leaves were under sunlit conditions without shadowing effects on the bidirectional reflectance

5.2.5.1 Ancillary climatic reanalysis data

The meteorological inputs required for SCOPE simulations were extracted from ERA-Interim atmospheric reanalysis data (Dee *et al*., 2011) produced by the European Centre for Medium-Range Weather Forecasts (ECMWF). The ERA-Interim is the latest global atmospheric reanalysis produced by the ECMWF (http://www.ecmwf.int). Surface parameters extracted from 3-hourly time step ERA-Interim reanalysis included 2-meter air temperature, air pressure, water vapour pressure, incoming shortwave and long-wave downward radiation, and 10-meter wind speeds. The data from ERA-Interim atmospheric reanalysis was spatially interpolated from their native spatial grid (0.75° by 0.75°) to a finer 0.25° by 0.25º resolution using nearest-neighbour resampling. To assess the meteorological variables retrieved from ERA-Interim atmospheric reanalysis, data were compared with observations from the nearest meteorological stations in the regional agro-climatic network (Consejería de Agricultura y Pesca, Junta de Andalucía). Errors associated with convective processes at surface level were reduced using wind speed at 2 meters from this network.

5.2.5.2 Leaf biophysical and structural parameters

The leaf and canopy parameters needed for SCOPE simulations were estimated using a PROSPECT-SAILH model inversion scheme by steps from the reflectance in the 400–1700 nm spectral region. A look-up table (LUT) of 200,000 simulations was built to minimize the *ill-posed inversion* problem (Combal *et al*., 2003; Li and Wang, 2011; Yebra and Chuvieco, 2009). The range of variation for C_{ab} was determined based on prior field information. The main input parameters were calculated using specific spectral ranges (Table 5.3) where the biophysical parameters are known to have the greatest influence on reflectance and transmittance spectra. The iterative-optimization numerical (I-optN) approach was used to invert the PROSPECT-SAILH model for the estimation of leaf traits and canopy parameters from reflectance across the observed spectrum. The I-optN method estimates the set of parameters, symbolized by the vector θ = [LADF, LAI, N, C_{ab}, C_m, C_w] which minimizes Δ^2 (Eq. 5.2). The method calculates the root mean square error (RMSE) between the simulated reflectance and the hyperspectral image reflectance by successive input parameter iteration.

$$\Delta^2 = \sum_{\mathrm{n}} \left[\rho_{\lambda,\mathrm{obs}} - \rho_{\lambda,sim}\right]^2 \qquad (5.2)$$

Where $\rho_{\lambda,obs}$ is the image (canopy level) spectral reflectance, and $\rho_{\lambda,sim}$ is the modelled canopy spectral reflectance with a set of parameters defined in the LUT for each wavelength n. The procedure was conducted in several steps: 1) a leaf angle distribution function (LADF) was estimated over the VNIR and SWIR spectral range (400–1750 nm) with variables C_{ab}, C_w and C_m. LADF was first retrieved by model inversion, given its key role in canopy structure; 2) the mesophyll structural parameter (N-struct) and the leaf area index (LAI) were simultaneously determined over the range 960–1300 nm using the LADF from step 1, and variable C_{ab}, C_w and C_m inputs; 3) C_{ab} was then calculated using reflectances in the 455–690 nm range, where chlorophyll absorption has the strongest effect, with fixed LADF, LAI and N estimated in previous steps; 4) Finally, C_m and C_w were estimated over 900–1700 nm, where dry and water matter have the largest absorption effects (Baret and Fourty, 1997b; Feret et al., 2008; Fourty et al., 1996; Jacquemoud et al., 2009, 1996), fixing C_{ab}, LADF, LAI and N obtained previously.

5.2.5.3 SCOPE iterative-optimization for LIDFs and Rin parameters

After meteorological, leaf, and canopy parameters had been obtained, the SCOPE model was run using an I optN approach with a LUT table of 27,500 simulations for optimizing the LADF and the broadband incoming shortwave radiation (R_{in}). The LADF retrievals derived from PROSPECT-SAILH were optimized with SCOPE iterative-optimization using the radiance spectrum, varying the leaf inclination angle distribution function (LIDF) parameters. The $LIDF_a$ and $LIDF_b$ parameters mathematically describe the LAD function estimated using PROSPECT-SAILH inversions, where $LIDF_a$ determines the average leaf inclination and $LIDF_b$ describes the variation in leaf inclination, controlling the distribution's bimodality.

The I-optN method minimizes a cost function (Eq. 5.3) to estimate the set of parameters symbolized by the vector $\theta = [R_{in}, LIDF_a, LIDF_b]$. In this step, the I-optN method was based on the calculation of the RMSE between the *at-sensor* canopy spectral radiance and the SCOPE-simulated spectra by successive input parameter iterations over the spectral region used for the SIF retrievals (740–780 nm).

$$\Delta^2 = \sum_n \left[L_{\lambda,obs} - L_{\lambda,sim}\right]^2 \qquad (5.3)$$

Where $L_{\lambda obs}$ is the measured canopy spectral radiance, and $L_{\lambda sim}$ is the canopy spectral radiance modeled by SCOPE with the set of parameters defined in the LUT for

a given wavelength n. The LUT was built varying R_{in} and LIDFs, but keeping the Vcmax constant at 80 µmol·m^{-2}·s^{-1} and the remaining default values fixed, as shown in Table 5.4. R_{in} varied 100 W·m^{-2} with a step of 5-10 W·m^{-2} from the incoming shortwave radiation from the ERA-Interim reanalysis for each trial site. The leaf inclination distribution factors ($LIDF_a$ and $LIDF_b$) varied according to the LADF obtained from PROSPECT-SAILH inversions, using a total of 500 variations. Among the canopy structural variables, $LIDF_a$, representing the inclination distribution of leaves, had the greatest effect on SIF variability. In fact, $LIDF_a$ had a large influence on modeled reflectance with a contribution of over 20% of the variation between 720–1150 nm, while the LAI parameter governed over ≥ 50 % of variation in reflectance at wavelengths longer than 1400 nm. The remaining structural inputs used in SCOPE (leaf width, LIDFb, and canopy height) had a marginal impact on the modeled reflectance (Verrelst et al., 2015). Recent studies (Koffi et al., 2015; Verrelst et al., 2016, 2015) have demonstrated the importance of R_{in}, since the fluorescence spectrum is proportional to the absorbed PAR.

5.2.5.4 Vcmax estimation from SCOPE model inversion

Once the leaf, canopy and meteorological parameters were obtained following the I-optN approaches using the PROSPECT-SAILH and SCOPE simulations, the relationships between Vcmax and canopy fluorescence (Vcmax=f(SIF); Fig 5.5b) were established for all wheat plots. For this purpose, the SCOPE model was run in forward mode with the Vcmax range set to 0–260 µmol·m^{-2}·s^{-1}, divided into 27 intervals. As an additional step, the simulated radiance spectra from SCOPE at 1 nm resolution in the 640–800 spectral windows was convoluted using the Whittaker Shannon interpolation, as described in Butzer et al. (2011). Fig. 5.5a shows the comparison between the radiance retrieved with the VNIR hyperspectral sensor, the original radiance simulated by SCOPE at 1nm, and the simulated SCOPE radiance spectra convoluted to match the airborne hyperspectral data. The spectral convolution of the radiance simulated by SCOPE was critical to match the broader resolution of the hyperspectral imager, and therefore to obtain comparable SIF values. Fig. 5.5b shows the effect of the convoluted radiance signal when applied to the SCOPE simulations, observing the relationship between SIF and Vcmax.

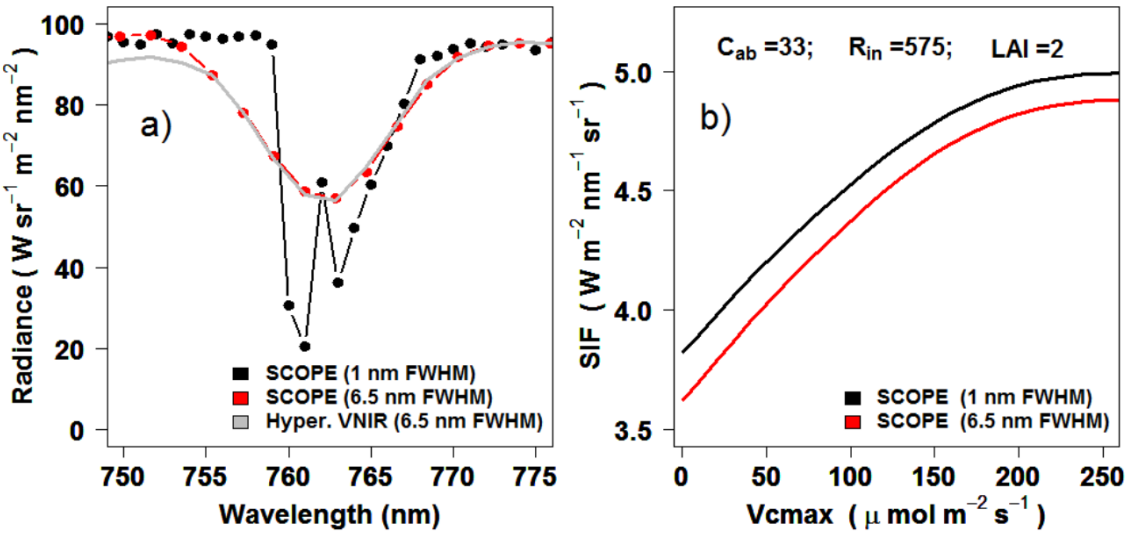

Fig. 5.5. Radiance spectra obtained by the VNIR hyperspectral sensor (in grey), the radiance simulated by SCOPE model at 1 nm (in black) and the convoluted SCOPE-simulated radiance using Whittaker and moving average filters (in red) (a). For the same wheat plot, the SCOPE-simulated SIF (black line) and the SIF obtained after convolution (red line) are shown as a function of Vcmax (μmol·m^{-2}·s^{-1}) (b) for simulations with C_{ab}=33 μg·cm^{-2}, LAI=2 and R_{in} = 575 W·m^{-2}.

5.3 Results

5.3.1 Nutrient and water-stress variability in rainfed and irrigated study sites

Field-based leaf physiological measurements (net assimilation, N concentration and water potential), Vcmax estimated by SCOPE inversions, C_{ab} estimated by PROSPECT-SAILH inversions, and CWSI for the entire experiment comprising rainfed and irrigated plots are shown in Fig. 5.6. There were large differences in the crop photosynthesis, water and nitrogen status between water regimes. As expected, irrigated plots had better water and nutritional status compared to rainfed plots overall. Irrigated plots had higher assimilation rates, N concentrations, Vcmax, and C_{ab} (Fig 5.6a, b, d and e) than rainfed plots. ANOVA analysis confirmed statistically significant differences between the means of the two water stress regimes for all field physiological measurements (all p-values ≤ 0.0036).

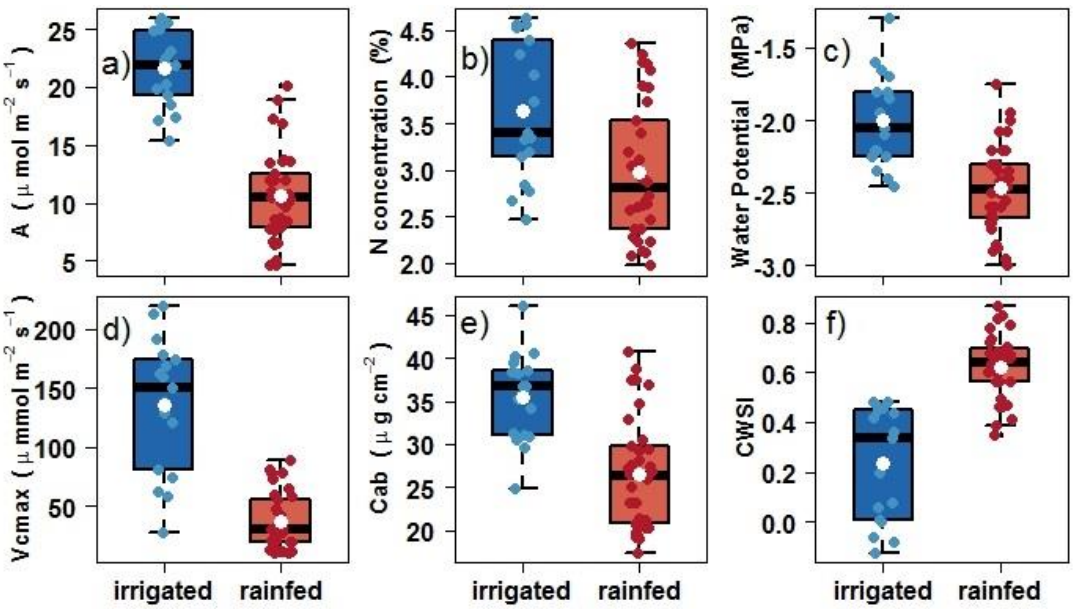

Fig. 5.6. Leaf- and canopy-level physiological data acquired in plots under rainfed (red) and irrigated (blue) conditions: a) assimilation rate (μmol·m^{-2}·s^{-1}); b) leaf N concentration (%); c) water potential (MPa); d) Vcmax estimated by SCOPE (μmol·m-2·s^{-1}); e) chlorophyll content estimated by PROSPECT-SAILH (μg·cm^{-2}); and f) CWSI calculated from high-resolution thermal imagery. In the box plots, the horizontal black line represents the median and the top and bottom of the box is the 75th and 25th quartile, respectively. The whiskers represent the upper and lower range. The average values are shown with a white point over the box plot.

There was a significant correlation between CWSI and water potential in rainfed plots (r^2 = 0.30, p-value = 0.7e-4), although the correlation was stronger for irrigated plots (r^2 = 0.72, p-value = 1.7e-5). The high variability in N concentration for both treatments (Fig. 5.6b) suggests that rainfed plots were also affected by N deficit. Assimilation rate was significantly correlated with the N concentration (r^2 = 0.51 and 0.56 for irrigated and rainfed, respectively) indicating that the N concentration also affected the photosynthetic capacity in both water regimes.

5.3.2 Effects of the biochemical and environmental parameters on SIF and Vcmax estimation

The sensitivity of the convoluted radiance signal simulated with SCOPE to chlorophyll content, LAI and the broadband incoming shortwave radiation are shown in Figure 5.7. Variation in C_{ab} had a relatively small effect on radiance at the spectral region typically used to quantify chlorophyll fluorescence (750–775 nm), particularly as compared to LAI and R_{in} (Fig 5.7b and c). In general, for the same value of C_{ab}, the radiance significantly increased with the increase of LAI and R_{in} in the O_2-A region. However, large differences were observed as a function of R_{in} variation, reaching more

than 30 W·sr^{-1}·m^{-2}·nm^{-2}. These results showed that R_{in} was a key micrometeorological variable in driving SIF variability simulated by the SCOPE model.

Figure 5.8 shows the relationship between SCOPE-simulated SIF and Vcmax, as a function of LAI, C_{ab} and R_{in}. At constant radiation (R_{in} = 800 W·m^{-2}) and LAI (2), fluorescence increased with increasing values of C_{ab} and Vcmax. The largest increase in the SIF retrievals occurred for Vcmax between 10–60 µmol·m^{-2}·s^{-1}. For larger Vcmax values (≥150 µmol·m^{-2}·s^{-1}), SIF retrievals remained steady, with a tendency to increase with C_{ab}.

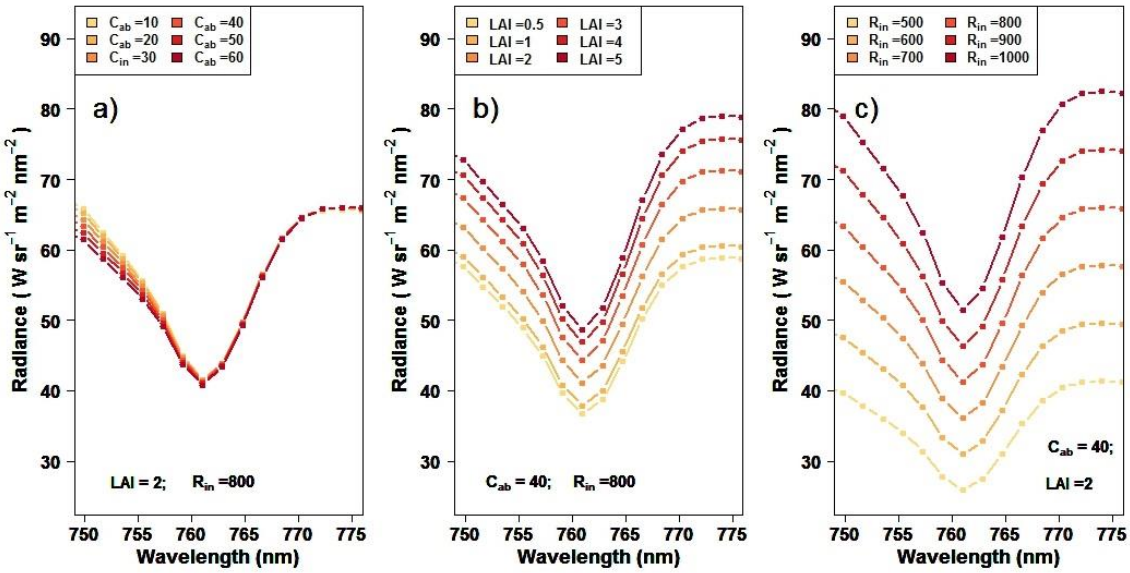

Fig. 5.7. Sensitivity of SCOPE radiance profiles convoluted to match the FWHM of the hyperspectral imager used in the study, as a function of chlorophyll content (C_{ab}) in µg·cm^{-2} (a), leaf area index (LAI) (b) and the broadband incoming shortwave radiation (R_{in}) in W·m^{-2} (c) for Vcmax = 80 µmol·m^{-2}·s^{-1}. CO_2 and O_2 concentration at the interface of the canopy were set to 382.17 ppm and 200 ×103 ppm, respectively.

At constant C_{ab}, there were dramatic changes in the relationship between simulated SIF and Vcmax with increased with LAI and R_{in} (Fig. 5.8b and c). SIF significantly increased with LAI, nearly doubling with an increase in LAI from 1 to 5 (Fig 5.8b). Unsurprisingly, SIF increased proportionally to R_{in} (Fig 5.8c).

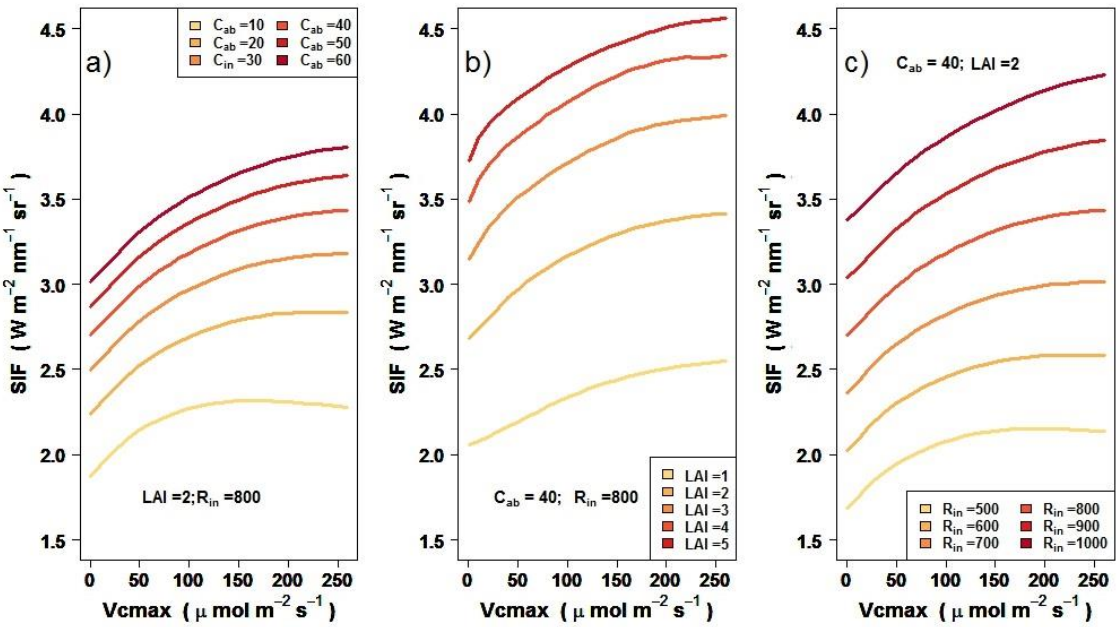

Fig. 5.8. Relationships between SIF estimated from SCOPE radiance simulations and Vcmax (µmol·m^{-2}·s^{-1}) as a function of chlorophyll content (Cab) in µg·cm^{-2} (a), LAI (b) and the broadband incoming shortwave radiation (R_{in}) in W·m^{-2} (c).

5.3.3 Validation of Vcmax estimated by SCOPE using leaf photosynthesis measurements.

The relationship between the SCOPE-estimated Vcmax and the field-measured Vcmax is shown in Fig. 5.9a. There was an almost 1:1 linear relationship (r^2= 0.77; p-value ≤ 2.2e-16 and RMSE = 2.61 µmol·m^{-2}·s^{-1}) between measured and estimated Vcmax, using the FvCB approach on the six wheat varieties from the airborne campaign in 2018. The relationship between the measured Vcmax and the net photosynthetic rates also displayed a significant relationship for both types of Vcmax estimates (r^2=0.68; p-value ≤ 0.005) (Fig. 5.9b).

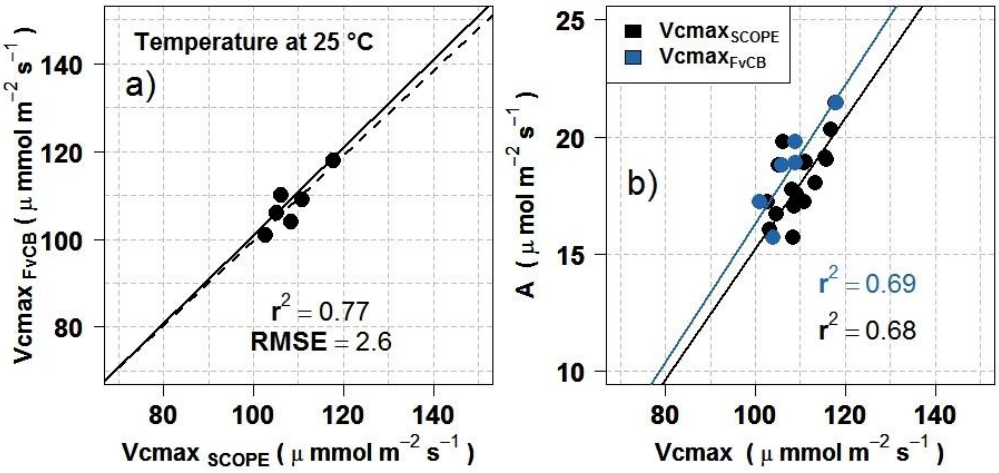

Fig. 5.9. a) Relationship between carboxylation maximum capacity (Vcmax; µmol·m^{-2}·s^{-1}) retrieved from the hyperspectral image through the SCOPE model inversion vs. field measured Vcmax through Farquhar–von Caemmerer–Berry (FvCB) model using the curve A/Ci (wheat Ecija plots, 2018). The black line is the fit line and the dashed line is the one-to-one line; b) relationships between the average net assimilation (A; µmol·m^{-2}·s^{-1}) measured using the photosynthesis chamber at flight time and the simulated Vcmax (in black dots) and the Vcmax calculated from FvCB model (in blue dots).

The relationship between Vcmax simulated by SCOPE model inversion and SIF quantified from the hyperspectral imagery at the different trial sites yielded a significant non-linear relationship (r^2= 0.84; p-value ≤ 2.2e-16; Fig. 5.10). Irrigated plots had high SIF values (≥ 4.92 W·sr^{-1}·m^{-2}·nm^{-2}) that were related to large values of Vcmax, mainly over 100 µmol·m^{-2}·s^{-1}. Under the severe water stress conditions in most rainfed plots, Vcmax was lower than 90 µmol·m^{-2}·s^{-1}. However, for some rainfed plots (Ecija 2018), which were in an early growth stage and under moderate water stress, Vcmax and SIF retrievals were larger than 90 µmol·m^{-2}·s^{-1} and 5 W·sr^{-1}·m^{-2}·nm^{-2} for Vcmax and SIF, respectively.

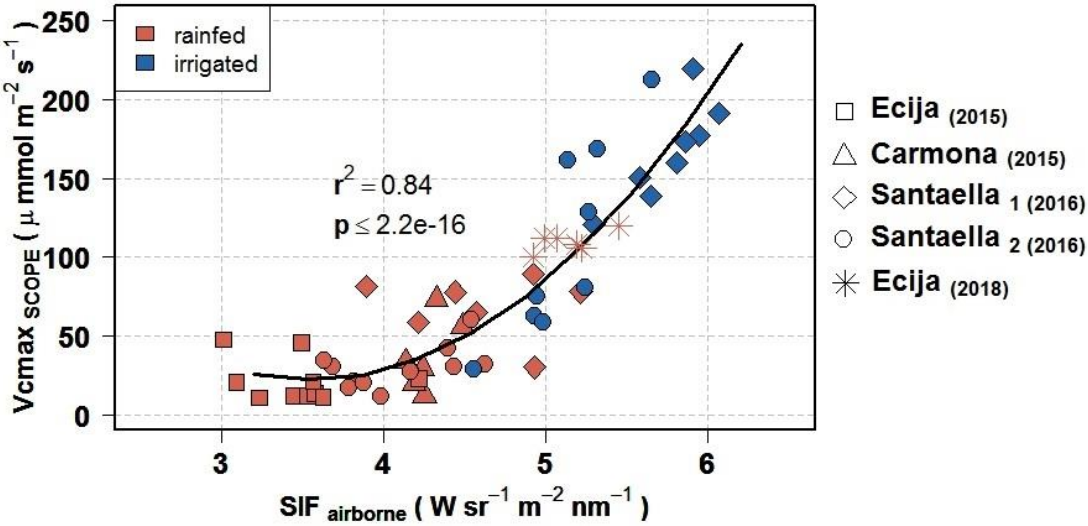

Fig. 5.10. Relationship between carboxylation maximum capacity (Vcmax, µmol·m^{-2}·s^{-1}) estimated by hyperspectral imagery through SCOPE model inversion and SIF quantified from the hyperspectral imagery, displaying rainfed (red) and irrigated (blue) conditions. Each symbol corresponds with a single plot measurement.

5.3.4 Relationships between Vcmax and assimilation under irrigation and rainfed conditions

The relationships between net assimilation and SCOPE-estimated Vcmax, CWSI, leaf C_{ab}, and NDVI are shown in Fig 5.11 and Fig 5.12 for each water regime. The SCOPE-estimated Vcmax was significantly correlated with the assimilation rate (r^2=0.50, p-value=2.91e-6) under rainfed conditions. This relationship was stronger under irrigated conditions (r^2=0.65, p-value=9.31e-5). The slightly weaker correlation obtained in rainfed plots could be associated with nutrient and water limitations, as well as an increased influence of background effects under stress conditions. In this context, variation in Vcmax was reduced and values were smaller (< 90 µmol·m^{-2}·s^{-1}), relative to irrigated conditions.

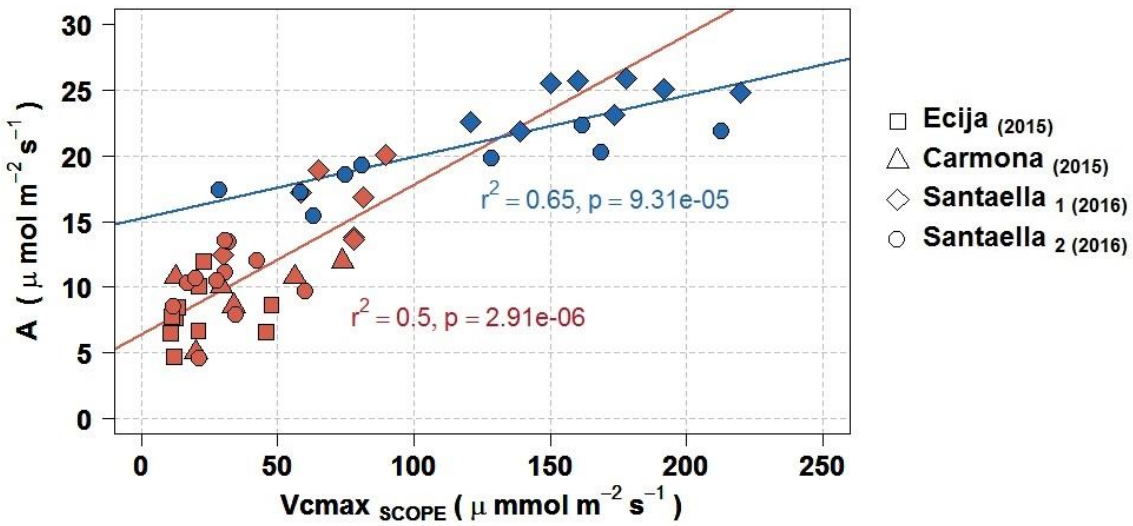

Fig. 5.11. Relationship between average assimilation (A; µmol·m^{-2}·s^{-1}) measured in leaves and Vcmax (µmol· m^{-2}·s^{-1}) estimated by hyperspectral imagery through SCOPE model inversion under rainfed (red; n=33) and irrigated (blue, n=18) conditions. The average net assimilation per plot was obtained using two leaves from the top of the canopy and a portable photosynthesis chamber.

Net assimilation was significantly related to C_{ab} (r^2=0.56; p-value =3.93e-7), NDVI (r^2=0.46; p-value =1.19e-5) and $PSSR_b$ (r^2=0.56; p-value =4.21e-7) under rainfed conditions (Fig 5.12b, c and d). Under rainfed conditions, chlorophyll indicators (C_{ab} and $PSSR_b$) had better correspondence to net assimilation than remote sensing estimates of Vcmax (r^2=0.50). By contrast, the relationship between the assimilation rate and the thermal-based CWSI (Fig. 5.12a) was weak (r^2 = 0.14, p-value < 0.03), suggesting that the chronic water-stress may have resulted in an associated nutrient deficiency that limited assimilation rates. Indeed, net assimilation under rainfed conditions was more related to nitrogen and pigment indicators rather than to CWSI. Furthermore, after the supplemental irrigation in the Carmona plots in 2015, photosynthetic rates remained low despite partially recovered water status. For these plots, CWSI reached values close to 0.4, while assimilation rates were maintained below 15 µmol·m^{-2}·s^{-1}.

Under well-irrigated conditions, the relationships between net assimilation and C_{ab}, NDVI and $PSSR_b$ showed weak, nonsignificant relationships (r^2 < 0.13; p-value = 0.83 for leaf C_{ab} content; p-value = 0.41 for $PSSR_b$; p-value = 0.15 for NDVI, Fig. 5.12). It is likely that these relationships exhibited scaling problems due to saturation effects associated with high canopy densities in irrigated plots. By contrast, the relationship between net assimilation and CWSI was strongly correlated for irrigated plots (r^2 = 0.73, p-value = 1.30e-5). The estimation of Vcmax as a function of SIF retrievals

enabled the calculation of the spatial distribution of Vcmax and the net assimilation in the wheat experimental plots (Fig. 5.13). Pixel-level estimates of Vcmax and assimilation for rainfed and irrigated wheat varieties were retrieved using the regression between SIF and Vcmax shown in Fig. 5.10 and Fig 5.11 respectively.

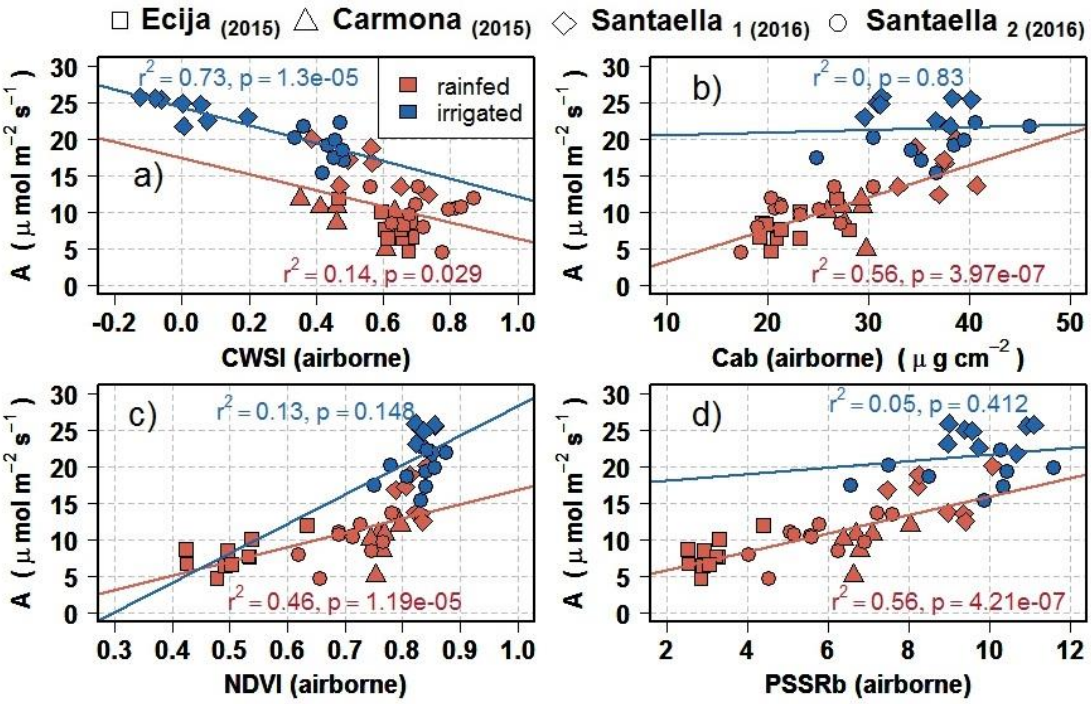

Fig. 5.12. Relationships between net average net assimilation (A, µmol·m^{-2}·s^{-1}) and (a) CWSI, (b) chlorophyll content (C_{ab}; µg·cm^{-2}) estimated by PROSPECT-SAILH model inversion, (c) NDVI, and (d) $PSSR_b$ calculated from the hyperspectral imagery under rainfed (red points; n=33) and irrigated (blue points, n=18) conditions. Average net assimilation per plot was obtained from two leaves at the top of the canopy with a portable photosynthesis chamber.

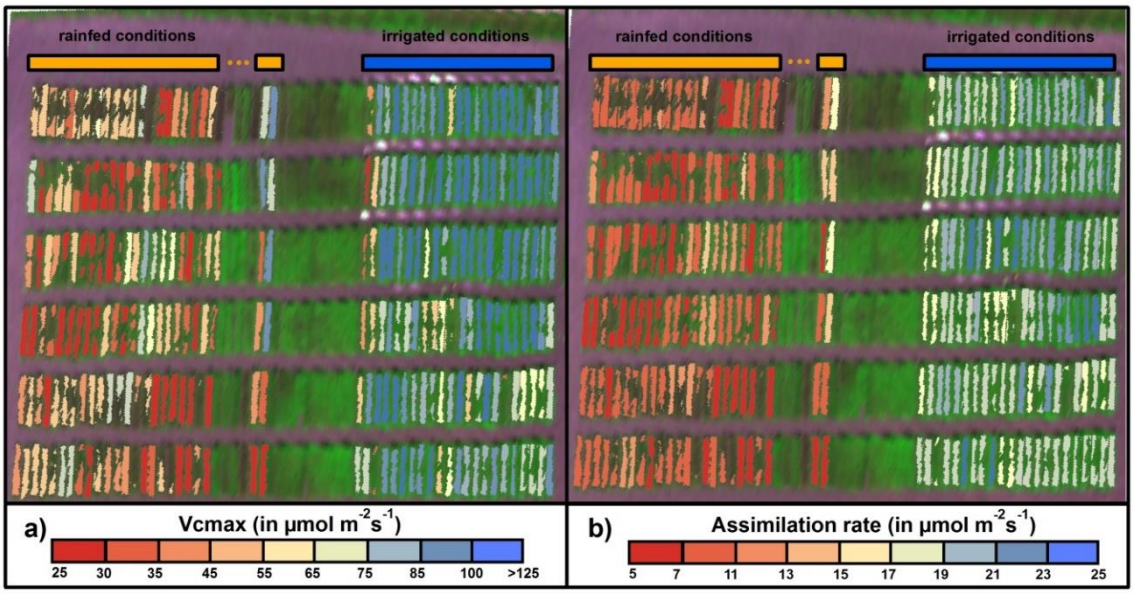

Fig. 5.13. Maps of Vcmax (µmol·m^{-2}·s^{-1}) simulated using the SCOPE model (a) and assimilation rate (A; µmol·m^{-2}·s^{-1}) predicted from Vcmax (b), under irrigated and rainfed conditions at SA field site during 2016 airborne campaign.

5.4 Discussion

Several studies have shown the utility of remotely-sensed SIF as an indicator of the photosynthetic activity at across spatial resolutions (Meroni et al., 2009; Porcar-Castell et al., 2014; Rascher et al., 2015). SIF retrieved from satellite imagery has improved estimations of gross primary productivity at ecosystem to global scales (Frankenberg et al., 2011; Guanter et al., 2014; Smith et al., 2018). However, SIF-GPP relationships require appropriate modelling methods to compensate for structural effects of vegetation canopies (Levula et al., 2019), spatial and temporal scales (Hu et al., 2018), seasonal changes in photosynthetic pigments (Campbell et al., 2018), environmental conditions (Verma et al., 2017) and other confounding factors. In this regard, He et al. (2017) showed that the sun-satellite view observation geometry could produce unwanted SIF variations, affecting the accuracy of GPP. Due to its close link to photosynthetic activity, SIF also has great potential for use in precision agriculture and plant breeding programs. At both global (satellite) and local (airborne and drone) scales, remote estimation of the maximum rate of carboxylation, Vcmax is thought to be a suitable proxy for photosynthesis. Zhang et al. (2014) demonstrated that estimation of Vcmax from space-based SIF retrievals combined with SCOPE simulations in corn and soybean crops was feasible. Nevertheless, further work was needed to understand if these methods are applicable to remote sensing instruments readily available in the context of routine precision agriculture operations and in plant breeding programs. In particular, it

is necessary to test whether SIF and Vcmax retrievals are feasible with the technical constraints of the spectral resolution available for operational and commercial remote sensing work, the high spatial resolution required, and the general aim of detecting subtle physiological changes across varieties and under water and nutrient stress levels.

The work presented here demonstrates that the Vcmax estimated from airborne hyperspectral imagery through SCOPE model inversion was able to detect physiological changes induced by differing irrigation regimes and crop varieties. The relationships between net photosynthetic rates and both measured Vcmax and simulated Vcmax (Fig 5.9b) at the Ecija site were significantly correlated ($r^2 \geq 0.68$ and p-value ≤ 0.005). The sample size used in the validation of SCOPE-simulated Vcmax was low due to the time-consuming nature of obtaining CO_2 response curves. Nevertheless, a larger dataset ($n > 50$) was used to demonstrate the relationship between Vcmax retrieved from SCOPE and plant physiological traits (Fig 5.11 and Fig 5.12). It demonstrates that Vcmax estimates are related to the physiological changes associated to water status. Issues related to the coarser spectral resolution of hyperspectral instruments used in precision agriculture and plant breeding programs were evaluated with respect to SIF retrieval, and its impact on Vcmax estimation, as validated by field measurements of plant traits and net assimilation. In particular, the small plot sizes normally used by plant breeders during their wheat selection trials may limit the accuracy of remotely-sensed SIF. The planting-row designs with 25-cm row spacing used in this study could affect the retrievals of narrow-band and high-resolution hyperspectral (25 cm) and thermal (20 cm) imagery. When the plots are too small, soil and background effects may contaminate the signal due to the mixing of the soil and vegetation reflectance. Therefore, segmentation algorithms should be implemented to reduce soil background effects on estimates of plant physiological traits at canopy level, especially in early growth stages where these effects could significantly reduce the accuracy of retrievals. This issue is especially relevant for coarse-resolution sensors such as the SWIR camera (70 cm) and the thermal sensors. Spatial resolution issues should be considered during the experimental design in breeding programs where the remote sensing sensors are expected to be used.

The SCOPE-simulated radiance data which was convoluted to match the spectral resolution of the airborne hyperspectral imager used in our study was critical for obtaining SIF and Vcmax parameters within expected ranges. Analysis confirmed that the canopy structure and the incoming shortwave radiation were the main driving variables for modeled SIF emissions (Verrelst et al., 2015, 2016). In particular, R_{in} had a dominant influence on SIF, as expected based on the pivotal role of PAR load on fluorescence emission. As explained in Van der Tol et al. (2014), PAR and Vcmax are the main contributors to the fluorescence yield in SCOPE. The effects of chlorophyll content, LAI and R_{in} on the relationship between SIF and Vcmax were also included in the sensitivity analysis reported in our manuscript, showing the large impact of C_{ab} on the SIF Vcmax relationships (Fig. 5.8a), which is in agreement with Koffi et al. (2015).

Estimates of Vcmax from wheat plot image spectra through SCOPE model inversion were within the ranges reported by other studies for wheat crops (10–219 $\mu mol \cdot m\ m^{-2} \cdot s^{-1}$; Wullschleger, 1993; Silva-Pérez et al., 2017). The relationship between the estimated Vcmax and chlorophyll fluorescence (r^2= 0.84; Fig. 5.10) differed greatly between irrigated and water-stressed plots. As shown in Fig 5.10, the SIF and Vcmax are modulated by water status. In this regard, Zheng et al. (2017) showed that photosynthesis at noon is mainly limited by Vcmax, further indicating that Vcmax may be a suitable proxy for evaluating plant stress levels. For irrigated conditions, the relationship was almost linear and displayed a steeper slope with larger Vcmax values ($\geq$100 $\mu mol \cdot m^{-2} \cdot s^{-1}$). Under water deficit the relationship was weak. As crops reduce stomatal and mesophyll conductance in response to stress, the CO_2 concentration within the chloroplast drops, causing a reduction in the photosynthesis capacity (Vcmax). Under low CO_2 concentrations, plant carboxylation rates are limited by RuBisCo rather than Vcmax (Sharkey et al., 2007). Consequently, under severe water stress, both Vcmax and SIF retrievals were suppressed, which is in agreement with the findings by Zheng et al. (2017).

Due to the intensive field-work required to estimate the relationships between A and Ci, the number of observations used to estimate Vcmax in the field was small. Nevertheless, our data suggests that simulated Vcmax corresponded well with in situ measurements. The results were satisfactory (r^2=0.77; p-value $\leq$ 2.2e-16 and RMSE = 2.6 $\mu mol \cdot m^{-2} \cdot s^{-1}$) despite the limited number of leaf Vcmax samples, suggesting that Vcmax could reasonably be estimated from SCOPE and convoluted SIF retrievals using

hyperspectral imaging technology suitable for precision agriculture. Simulated Vcmax yielded a significant relationship with assimilation rate at the Ecija site in 2018 under non severe water stress conditions (r^2=0.68; p-value ≤ 0.005). These results are in accordance with results obtained by Zhang et al. (2014, 2018) in soybean and corn crops. The relationships observed between Vcmax and the net photosynthesis (Fig. 5.11) supports the hypothesis that airborne-quantified Vcmax is a feasible indicator of crop functioning under contrasting water regimes. Moreover, we showed (Fig. 5.12) that in the absence of water stress, Vcmax was a stronger predictor of photosynthetic capacity than standard indicators such as C_{ab}, and NDVI and $PSSR_b$. These indicators likely performed poorly due to scaling problems related to the high canopy densities in irrigated plots. As a result, non-significant relationships were also found between net assimilation and these indices (all p-value ≥0.15). In dense biomass canopies, the NIR reflectance increases greatly, reducing the sensitivity of the normalized ratios such as NDVI or $PSSR_b$ to plant biochemical content (Thenkabail et al., 2000; Gitelson, 2004).

Under rainfed conditions, i.e. in the presence of water stress, Vcmax, C_{ab} and reflectance indices were related to CO_2 assimilation rate, but thermal CWSI was not. Under water stress, stomatal closure reduces the CO_2 concentration inside the chloroplast, decreasing the photochemical activity and also photo-inhibition processes (Flexas and Medrano, 2002). Thus, leaf photochemistry decreases, resulting in a reduction of the chlorophyll fluorescence and RuBisCo activity. The fact that reflectance-based indicators (C_{ab}, $PSSR_b$, and NDVI) became significantly associated to A, under water stress, suggests that the saturation effects from canopy biomass were not present in rainfed plots. In this study, partial recovery of the water status (as happened in Carmona field in 2015) after sever water stress did not result in elevated assimilation rates. This suggests that instantaneous assessment of water status might not track photosynthetic performance if severe water stress has affected the photosynthetic apparatus.

From an operational perspective, the remote estimation of Vcmax from high-resolution hyperspectral imagery through SCOPE model inversion methods provides a powerful tool to accurately assess crop assimilation rates in large plant breeding programs and in precision agriculture studies. Moreover, its robustness across both irrigated and water-stressed plots was demonstrated when compared against standard

reflectance-based remote sensing indicators widely used for crop screening and high-throughput phenotyping

5.5 Conclusions

The work presented in this manuscript demonstrates the estimation of maximum rate of carboxylation (Vcmax) using SCOPE model inversion with airborne-quantified SIF from hyperspectral imagery. Estimates suitably tracked photosynthetic rates and clearly distinguished physiological differences in irrigated and rainfed conditions. Under water stress, all plant trait indicators performed similarly (Vcmax, NDVI, C_{ab} and $PSSR_b$) and were well related to assimilation rates. Nevertheless, estimated Vcmax outperformed standard remote sensing indices for the quantification of crop photosynthesis under irrigated conditions (i.e. in the absence of water stress). The methodology demonstrated in this study is directly relevant for high-throughput plant phenotyping and for precision agriculture applications.

Reference

Ball, J.T., Woodrow, I.E., Berry, J.A., 1987. A Model Predicting Stomatal Conductance and its Contribution to the Control of Photosynthesis under Different Environmental Conditions BT - Progress in Photosynthesis Research: Volume 4 Proceedings of the VIIth International Congress on Photosynthesis Providence, Rhode Island, USA, August 10–15, 1986, in: Biggins, J. (Ed.), . Springer Netherlands, Dordrecht, pp. 221–224. https://doi.org/10.1007/978-94-017-0519-6_48

Baret, F., Fourty, T., 1997. Estimation of leaf water content and specific leaf weight from reflectance and transmittance measurements. Agronomie 17, 455–464. https://doi.org/10.1051/agro:19970903

Blackburn, G.A., 1998. Spectral indices for estimating photosynthetic pigment concentrations : a test using senescent tree leaves. Int. J. Remote Sens. 19, 657–675. https://doi.org/10.1080/014311698215919

Butzer, P.L., Ferreira, P.J.S.G., Higgins, J.R., Saitoh, S., Schmeisser, G., Stens, R.L., 2011. Interpolation and Sampling: E.T. Whittaker, K. Ogura and Their Followers, Journal of Fourier Analysis and Applications. https://doi.org/10.1007/s00041-010-9131-8

Caemmerer, S. Von, Farquhar, G.D., 1981. Some relationships between the biochemistry of photosynthesis and the gas exchange of leaves. Planta 153, 376–387. https://doi.org/10.1007/BF00384257

Caemmerer, S. Von, 2000. Biochemical models of leaf photosynthesis. Tech. Plant Sci. 53, 1689–1699. https://doi.org/10.1017/CBO9781107415324.004

Cairns, J.E., Sanchez, C., Vargas, M., Ordoñez, R., Araus, J.L., 2012. Dissecting Maize Productivity: Ideotypes Associated with Grain Yield under Drought Stress and Well-watered Conditions. J. Integr. Plant Biol. 54, 1007–1020. https://doi.org/10.1111/j.1744-7909.2012.01156.x

Camino, C., González-Dugo, V., Hernández, P., Sillero, J.C., Zarco- Tejada, P.J., 2018a. Improved nitrogen retrievals with airborne-derived fluorescence and plant traits quantified from VNIR-SWIR hyperspectral imagery in the context of precision agriculture. Int. J. Appl. Earth Obs. Geoinf. 70, 105–117. https://doi.org/10.1016/j.jag.2018.04.013

Camino, C., Zarco-Tejada, P.J., Gonzalez-Dugo, V., 2018b. Effects of heterogeneity within tree crowns on airborne-quantified SIF and the CWSI as indicators of water stress in the context of precision agriculture. Remote Sens. 10. https://doi.org/10.3390/rs10040604

Campbell, P.K., Huemmrich, K.F., Middleton, E.M., Ward, L.A., 2018. Diurnal and Seasonal Variations in Chlorophyll Fluorescence Associated with Photosynthesis at Leaf and Canopy Scales 1–36. https://doi.org/10.3390/rs11050488

Carmo-Silva, E., Andralojc, P.J., Scales, J.C., Driever, S.M., Mead, A., Lawson, T., Raines, C.A., Parry, M.A.J., 2017. Phenotyping of field-grown wheat in the UK highlights contribution of light response of photosynthesis and flag leaf longevity to grain yield. J. Exp. Bot. 68, 3473–3486. https://doi.org/10.1093/jxb/erx169

Chaves, M.M., Chaves, M.M., 1991. Effects of water deficits on carbon assimilation. J. Exp. Bot. 42, 1–16. https://doi.org/10.1093/jxb/42.1.1

Collatz, G., Ribas-Carbo, M., and Berry, J.A., 1992. Coupled photosynthesis-stomatal conductance model for leaves of C4 plants. Aus. J. Plant Physiol., 1 9, 519–538.

Collatz, G.J., Ball, J.T., Grivet, C., Berry, J.A., 1991. Physiological and environmental regulation of stomatal conductance, photosynthesis and transpiration: a model that includes a laminar boundary layer. Agric. For. Meteorol. 54, 107–136. https://doi.org/10.1016/0168-1923(91)90002-8

Combal, B., Baret, F., Weiss, M., Trubuil, A., Macé, D., Pragnère, A., Myneni, R., Knyazikhin, Y., Wang, L., 2003. Retrieval of canopy biophysical variables from bidirectional reflectance using prior information to solve the ill-posed inverse problem. Remote Sens. Environ. 84, 1–15. https://doi.org/10.1016/S0034-4257(02)00035-4

Cowan, I.R., 1978. Stomatal Behaviour and Environment, in: Preston, R.D., Woolhouse, H.W.B.T.-A. in B.R. (Eds.), . Academic Press, pp. 117–228. https://doi.org/https://doi.org/10.1016/S0065-2296(08)60370-5

Croft, H., Chen, J.M., Luo, X., Bartlett, P., Chen, B., Staebler, R.M., 2017. Leaf chlorophyll content as a proxy for leaf photosynthetic capacity. Glob. Chang. Biol. 23, 3513–3524. https://doi.org/10.1111/gcb.13599

Cuevas, E., Camino, C., Benedetti, A., Basart, S., Terradellas, E., Baldasano, J.M., Morcrette, J.J., Marticorena, B., Goloub, P., Mortier, A., Berjón, A., Hernández, Y., Gil-Ojeda, M., Schulz, M., Berjón, A., Hernández, Y., Gil-Ojeda, M., Schulz, M., 2015. The MACC-II 2007-2008 reanalysis: atmospheric dust evaluation and characterization over northern Africa and the Middle East. Atmos. Chem. Phys. 15, 3991–4024. https://doi.org/10.5194/acpd-14-27797-2014

Damm, A., Erler, A., Hillen, W., Meroni, M., Schaepman, M.E., Verhoef, W., Rascher, U., 2011. Modeling the impact of spectral sensor configurations on the FLD retrieval accuracy of sun-induced chlorophyll fluorescence. Remote Sens. Environ. 115, 1882–1892. https://doi.org/10.1016/j.rse.2011.03.011

Damm, A., Guanter, L., Paul-Limoges, E., van der Tol, C., Hueni, A., Buchmann, N., Eugster, W., Ammann, C., Schaepman, M.E., 2015. Far-red sun-induced chlorophyll fluorescence shows ecosystem-specific relationships to gross primary production: An assessment based on observational and modeling approaches. Remote Sens. Environ. 166, 91–105. https://doi.org/10.1016/j.rse.2015.06.004

Dee, D.P., Uppala, S.M., Simmons, A.J., Berrisford, P., Poli, P., Kobayashi, S., Andrae, U., Balmaseda, M.A., Balsamo, G., Bauer, P., Bechtold, P., Beljaars, A.C.M., van de Berg, L., Bidlot, J., Bormann, N., Delsol, C., Dragani, R., Fuentes, M., Geer, A.J., Haimberger, L., Healy, S.B., Hersbach, H., Hólm, E. V., Isaksen, L., Kållberg, P., Köhler, M., Matricardi, M., Mcnally, A.P., Monge-Sanz, B.M., Morcrette, J.J., Park, B.K., Peubey, C., de Rosnay, P., Tavolato, C., Thépaut, J.N., Vitart, F., 2011. The ERA-Interim reanalysis: Configuration and performance of the data assimilation system. Q. J. R. Meteorol. Soc. 137, 553–597. https://doi.org/10.1002/qj.828

Farquhar, G.D., von Caemmerer, S., Berry, J.A., 1980. A biochemical model of photosynthetic CO2 assimilation in leaves of C3 species. Planta 149, 78–90. https://doi.org/10.1007/BF00386231

Farquhar, G.D., Wong, S.C., 1984. An Empirical Model of Stomatal Conductance. Funct. Plant Biol. 11, 191–210.

Farruggia, A., Gastal, F., Scholefield, D., 2004. Assessment of the nitrogen status of grassland. Grass Forage Sci. 59, 113–120. https://doi.org/10.1111/j.1365-2494.2004.00411.x

Feret, J.B., François, C., Asner, G.P., Gitelson, A.A., Martin, R.E., Bidel, L.P.R., Ustin, S.L., le Maire, G., Jacquemoud, S., 2008. PROSPECT-4 and 5: Advances in the leaf optical properties model separating photosynthetic pigments. Remote Sens. Environ. 112, 3030–3043. https://doi.org/10.1016/j.rse.2008.02.012

Flexas, J., Medrano, H., 2002. Drought-inhibition of photosynthesis in C3plants: Stomatal and non-stomatal limitations revisited. Ann. Bot. 89, 183–189. https://doi.org/10.1093/aob/mcf027

Fourty, T., Baret, F., Jacquemoud, S., Schmuck, G., Verdebout, J., 1996. Leaf optical

properties with explicit description of its biochemical composition: Direct and inverse problems. Remote Sens. Environ. 56, 104–117. https://doi.org/10.1016/0034-4257(95)00234-0

Frankenberg, C., Butz, A., Toon, G.C., 2011. Disentangling chlorophyll fluorescence from atmospheric scattering effects in O2 A-band spectra of reflected sun-light. Geophys. Res. Lett. 38, 1–5. https://doi.org/10.1029/2010GL045896

Genty, B., Briantais, J.M., Baker, N.R., 1989. The relationship between the quantum yield of photosynthetic electron transport and quenching of chlorophyll fluorescence. Biochim. Biophys. Acta - Gen. Subj. 990, 87–92. https://doi.org/10.1016/S0304-4165(89)80016-9

Gitelson, A.A., 2004. Wide Dynamic Range Vegetation Index for Remote Quantification of Biophysical Characteristics of Vegetation. J. Plant Physiol. 161, 165–173. https://doi.org/10.1078/0176-1617-01176

Gonzalez-Dugo, V., Durand, J.-L., Gastal, F., 2010. Water deficit and nitrogen nutrition of crops. A review. Agron. Sustain. Dev. 30, 529–544https://doi.org/10.1051/agro/2009059

Gonzalez-Dugo, V., Hernandez, P., Solis, I., Zarco-Tejada, P.J., 2015. Using high-resolution hyperspectral and thermal airborne imagery to assess physiological condition in the context of wheat phenotyping. Remote Sens. 7, 13586–13605. https://doi.org/10.3390/rs71013586

Guan, K., Berry, J.A., Zhang, Y., Joiner, J., Guanter, L., Badgley, G., Lobell, D.B., 2016. Improving the monitoring of crop productivity using spaceborne solar-induced fluorescence. Glob. Chang. Biol. 22, 716–726. https://doi.org/10.1111/gcb.13136

Guanter, L., Zhang, Y., Jung, M., Joiner, J., Voigt, M., Berry, J.A., Frankenberg, C., Huete, A.R., Zarco-Tejada, P., Lee, J.-E., Moran, M.S., Ponce-Campos, G., Beer, C., Camps-Valls, G., Buchmann, N., Gianelle, D., Klumpp, K., Cescatti, A., Baker, J.M., Griffis, T.J., 2014. Global and time-resolved monitoring of crop photosynthesis with chlorophyll fluorescence. Proc. Natl. Acad. Sci. 111, E1327–E1333. https://doi.org/10.1073/pnas.1320008111

Gueymard, C., 1995. Professional Paper A Simple Model of the Atmospheric Radiative Transfer of Sunshine: Algorithms and performance assessment. Florida Sol. Energy Cent.

Gueymard, C.A., Myers, D., Emery, K., 2002. Proposed reference irradiance spectra for solar energy systems testing. Sol. Energy 73, 443–467. https://doi.org/10.1016/S0038-092X(03)00005-7

Harley, P.C., Loreto, F., Di Marco, G., Sharkey, T.D., 1992a. Theoretical Considerations when Estimating the Mesophyll Conductance to CO2 Flux by Analysis of the Response of Photosynthesis to CO2. Plant Physiol. 98, 1429–1436. https://doi.org/10.1104/pp.98.4.1429

Harley, P.C., Thomas, R.B., Reynolds, J.F., Strain, B.R., 1992b. Modelling photosynthesis of cotton grown in elevated CO2. Plant. Cell Environ. 15, 271–282. https://doi.org/10.1111/j.1365-3040.1992.tb00974.x

He, L., Chen, J.M., Liu, J., Mo, G., Joiner, J., 2017. Angular normalization of GOME-2 Sun-induced chlorophyll fluorescence observation as a better proxy of vegetation productivity. Geophys. Res. Lett. 44, 5691–5699. https://doi.org/10.1002/2017GL073708

Hernández-Clemente, R., North, P.R.J., Hornero, A., Zarco-Tejada, P.J., 2017. Assessing the effects of forest health on sun-induced chlorophyll fluorescence using the FluorFLIGHT 3-D radiative transfer model to account for forest structure. Remote Sens. Environ. 193, 165–179. https://doi.org/10.1016/j.rse.2017.02.012

Houborg, R., Cescatti, A., Migliavacca, M., Kustas, W.P., Yang, X., Tang, J., Mustard, J.F., Lee, J., Rossini, M., Rascher, U., Alonso, L., Burkart, A., Cilia, C., Cogliati, S., Colombo, R., Damm, A., Drusch, M., Guanter, L., Hanus, J., Hyvärinen, T., Julitta, T., Jussila, J., Kataja, K., Kokkalis, P., Kraft, S., Kraska, T., Matveeva, M., Moreno, J., Muller, O., Panigada, C., Pikl, M., Pinto, F., Prey, L., Pude, R., Rossini, M., Schickling, A., Schurr, U., Schüttemeyer, D., Verrelst, J., Zemek, F., Houborg, R., Cescatti, A., Migliavacca, M., Kustas, W.P., Genty, B., Briantais, J.M., Baker, N.R., 2013. Satellite retrievals of leaf chlorophyll and photosynthetic capacity for improved modeling of GPP. Agric. For. Meteorol. 117, 10–23. https://doi.org/10.1016/j.agrformet.2013.04.006

Hu, J., Liu, L., Guo, J., Du, S., Liu, X., 2018. Upscaling solar-induced chlorophyll fluorescence from an instantaneous to daily scale gives an improved estimation of the gross primary productivity. Remote Sens. 10. https://doi.org/10.3390/rs10101663

Huete, A., Didan, K., Miura, T., Rodriguez, E.P., Gao, X., Ferreira, L.G., 2002. MODIS_MOD13_NDVI_referenc 83, 195–213. https://doi.org/10.1016/S0034-4257(02)00096-2

Huete, A.R., 1988. A soil-adjusted vegetation index (SAVI). Remote Sens. Environ. 25, 295–309. https://doi.org/10.1016/0034-4257(88)90106-X

Idso, S.B., Jackson, R.D., Reginato, R.J., 1978. Extending the " Degree Day " Concept of Plant Phenological Development to Include Water Stress Effects Author (s): Sherwood B . Idso , Ray D . Jackson , Robert J . Reginato Published by : Ecological Society of America Stable URL : http://www.jstor.org/s. Ecology 59, 431–433. https://doi.org/10.2307/1936570

Idso, S.B., 1982. Non-water-stressed baselines: A key to measuring and interpreting plant water stress. Agric. Meteorol. 27, 59–70. https://doi.org/10.1016/0002-1571(82)90020-6

Idso, S.B., Jackson, R.D., Pinter, P.J., Reginato, R.J., Hatfield, J.L., 1981. Normalizing the stress-degree-day parameter for environmental variability. Agric. Meteorol. 24, 45–55. https://doi.org/10.1016/0002-1571(81)90032-7

Jackson, R.D., Idso, S.B., Reginato, R.J., Pinter, J.P.J., 1981. Canopy temperature as a crop water stress indicator. Water Resour. Res. 17, 1133–1138. https://doi.org/10.1029/WR017i004p01133

Jacquemoud, S., Ustin, S.L., Verdebout, J., Schmuck, G., Andreoli, G., Hosgood, B., 1996. Estimating leaf biochemistry using the PROSPECT leaf optical properties model. Remote Sens. Environ. 56, 194–202. https://doi.org/10.1016/0034-4257(95)00238-3

Jacquemoud, S., Verhoef, W., Baret, F., Bacour, C., Zarco-Tejada, P.J., Asner, G.P., François, C., Ustin, S.L., 2009. PROSPECT + SAIL models: A review of use for vegetation characterization. Remote Sens. Environ. 113, S56–S66. https://doi.org/10.1016/j.rse.2008.01.026

Jones, H.G., Hall, D.O., Corlett, J.E., Massacci, A., 1995. Drought Enhances Stomatal Closure in Response to Shading in Sorghum (Sorghum bicolor) and in Millet (Pennisetum americanum). Funct. Plant Biol. 22, 1–6.

Kipp, S., Mistele, B., Baresel, P., Schmidhalter, U., 2014. High-throughput phenotyping early plant vigour of winter wheat. Eur. J. Agron. 52, 271–278. https://doi.org/10.1016/j.eja.2013.08.009

Kjeldahl, J., 1883. Neue Methode zur Bestimmung des Stickstoffs in organischen. J. Anal. Chem. 366–382. https://doi.org/10.1007/BF01338151

Koffi, E.N., Rayner, P.J., Norton, A.J., Frankenberg, C., Scholze, M., 2015. Investigating the usefulness of satellite-derived fluorescence data in inferring gross primary productivity within the carbon cycle data assimilation system. Biogeosciences 12, 4067–4084. https://doi.org/10.5194/bg-12-4067-2015

Levula, J., Sabater, N., Mammarella, I., Vesala, T., Atherton, J., Drolet, G., Wade, T., MacLellan, C., Nichol, C., Middleton, E., Porcar-Castell, A., 2019. Diurnal and Seasonal Solar Induced Chlorophyll Fluorescence and Photosynthesis in a Boreal Scots Pine Canopy. Remote Sens. 11, 273. https://doi.org/10.3390/rs11030273

Li, P., Wang, Q., 2011. Retrieval of leaf biochemical parameters using PROSPECT inversion: A new approach for alleviating ill-posed problems. IEEE Trans. Geosci. Remote Sens. 49, 2499–2506. https://doi.org/10.1109/TGRS.2011.2109390

Meroni, M., Busetto, L., Colombo, R., Guanter, L., Moreno, J., Verhoef, W., 2010. Performance of Spectral Fitting Methods for vegetation fluorescence quantification. Remote Sens. Environ. 114, 363–374. https://doi.org/10.1016/j.rse.2009.09.010

Meroni, M., Rossini, M., Guanter, L., Alonso, L., Rascher, U., Colombo, R., Moreno, J., 2009. Remote sensing of solar-induced chlorophyll fluorescence: Review of

methods and applications. Remote Sens. Environ. 113, 2037–2051. https://doi.org/10.1016/j.rse.2009.05.003

Moya, I., Camenen, L., Evain, S., Goulas, Y., Cerovic, Z.G., Latouche, G., Flexas, J., Ounis, A., 2004. A new instrument for passive remote sensing: 1. Measurements of sunlight-induced chlorophyll fluorescence. Remote Sens. Environ. 91, 186–197. https://doi.org/10.1016/j.rse.2004.02.012

Norton, A.J., Rayner, P.J., Koffi, E.N., Scholze, M., 2017. Assimilating solar-induced chlorophyll fluorescence into the terrestrial biosphere model BETHY-SCOPE: Model description and information content. Geosci. Model Dev. Discuss. 1–26. https://doi.org/10.5194/gmd-2017-34

Oleson, K.W., Dai, Y., et al., 2013. Technical description of version 4.5 of the Community Land Model (CLM). NCAR Technical Note NCAR/TN-503+STR 420. https://doi.org/10.5065/D6RR1W7M

Plascyk, J.A., Gabriel, F.C., 1975. The Fraunhofer line discriminator MKII an airborne instrument for precise and standardized ecological luminescence measurement. IEEE Trans. Instrum. Meas. 24, 306–313. https://doi.org/10.1109/TIM.1975.4314448

Porcar-Castell, A., Tyystjärvi, E., Atherton, J., Van Der Tol, C., Flexas, J., Pfündel, E.E., Moreno, J., Frankenberg, C., Berry, J.A., 2014. Linking chlorophyll a fluorescence to photosynthesis for remote sensing applications: Mechanisms and challenges. J. Exp. Bot. 65, 4065–4095. https://doi.org/10.1093/jxb/eru191

Quebbeman, J.A., Ramirez, J.A., 2016. Optimal allocation of leaf-level nitrogen: Implications for covariation of Vcmax and Jmax and photosynthetic downregulation. J. Geophys. Res. G Biogeosciences 121, 2464–2475. https://doi.org/10.1002/2016JG003473

Radin, J.W., Mauney, J.R., Guinn, G., 1985. Effects of N fertility on plant water relations and stomatal responses to water stress in irrigated cotton. Crop Sci. 25, 110–115. https://doi.org/10.2135/cropsci1985.0011183X002500010028x

Rascher, U., Alonso, L., Burkart, A., Cilia, C., Cogliati, S., Colombo, R., Damm, A., Drusch, M., Guanter, L., Hanus, J., Hyvärinen, T., Julitta, T., Jussila, J., Kataja, K., Kokkalis, P., Kraft, S., Kraska, T., Matveeva, M., Moreno, J., Muller, O., Panigada, C., Pikl, M., Pinto, F., Prey, L., Pude, R., Rossini, M., Schickling, A., Schurr, U., Schüttemeyer, D., Verrelst, J., Zemek, F., 2015. Sun-induced fluorescence - a new probe of photosynthesis: First maps from the imaging spectrometer HyPlant. Glob. Chang. Biol. 21, 4673–4684. https://doi.org/10.1111/gcb.13017

Rodriguez, D., Fitzgerald, G.J., Belford, R., Christensen, L.K., 2006. Detection of nitrogen deficiency in wheat from spectral reflectance indices and basic crop eco-physiological concepts. Aust. J. Agric. Res. 57, 781–789. https://doi.org/10.1071/AR05361

Rouse, J.W., Hass, R.H., Schell, J.A., Deering, D.W., 1973. Monitoring vegetation systems in the great plains with ERTS. Third Earth Resour. Technol. Satell. Symp. 1, 309–317. https://doi.org/citeulike-article-id:12009708

Sellers, P.J., 1987. Canopy Reflectance, Photosynthesis,and Transpiration. II. The Role of Biophysics in the Linearity of Their Interdependence. Remote Sens. Environ. 21, 143–183.

Sharkey, T.D., Bernacchi, C.J., Farquhar, G.D., Singsaas, E.L., 2007. Fitting photosynthetic carbon dioxide response curves for C3 leaves. Plant, Cell Environ. 30, 1035–1040. https://doi.org/10.1111/j.1365-3040.2007.01710.x

Silva-Pérez, V., Furbank, R.T., Condon, A.G., Evans, J.R., 2017. Biochemical model of C3 photosynthesis applied to wheat at different temperatures. Plant Cell Environ. 40, 1552–1564. https://doi.org/10.1111/pce.12953

Silva-Perez, V., Molero, G., Serbin, S.P., Condon, A.G., Reynolds, M.P., Furbank, R.T., Evans, J.R., 2018. Hyperspectral reflectance as a tool to measure biochemical and physiological traits in wheat. J. Exp. Bot. 69, 483–496. https://doi.org/10.1093/jxb/erx421

Sitch, S., Smith, B., Prentice, I.C., Arneth, a., Bondeau, a., Cramer, W., Kaplan, J.O., Levis, S., Lucht, W., Sykes, M.T., Thonicke, K., Venevsky, S., 2003. Evaluation of ecosystem dynamics, plant geography and terrestrial carbon cycling in the LPJ dynamic global vegetation model. Glob. Chang. Biol. 9, 161–185. https://doi.org/10.1046/j.1365-2486.2003.00569.x

Smith, W.K., Biederman, J.A., Scott, R.L., Moore, D.J.P., He, M., Kimball, J.S., Yan, D., Hudson, A., Barnes, M.L., Macbean, N., Fox, A.M., Litvak, M.E., 2018. Chlorophyll Fluorescence Better Captures Seasonal and Interannual Gross Primary Productivity Dynamics Across Dryland Ecosystems of Southwestern North America. Geophys. Res. Lett. 748–757. https://doi.org/10.1002/2017GL075922

Thenkabail, P.S., Smith, R.B., De Pauw, E., 2000. Hyperspectral vegetation indices and their relationships with agricultural crop characteristics. Remote Sens. Environ. 71, 158–182. https://doi.org/10.1016/S0034-4257(99)00067-X

Uddling, J., Gelang-Alfredsson, J., Piikki, K., Pleijel, H., 2007. Evaluating the relationship between leaf chlorophyll concentration and SPAD-502 chlorophyll meter readings. Photosynth. Res. 91, 37–46. https://doi.org/10.1007/s11120-006-9077-5

van der Tol, C., Verhoef, W., Rosema, A., 2009a. A model for chlorophyll fluorescence and photosynthesis at leaf scale. Agric. For. Meteorol. 149, 96–105. https://doi.org/10.1016/j.agrformet.2008.07.007

van der Tol, C., Verhoef, W., Timmermans, J., Verhoef, A., Su, Z., 2009b. An integrated model of soil-canopy spectral radiances, photosynthesis, fluorescence, temperature and energy balance. Biogeosciences 6, 3109–3129. https://doi.org/10.5194/bg-6-3109-2009

van der Tol, C., Berry, J.A., Campbell, P.K.E., Rascher, U., 2014. Models of fluorescence and photosynthesis for interpretingmeasurements of solar-induced chlorophyll fluorescence. J. Geophys. Res. Biogeosciences 119, 2312–2327. https://doi.org/10.1002/2014JG002713.

Verma, M., Schimel, D., Evans, B., Frankenberg, C., Beringer, J., Drewry, D.T., Magney, T., Marang, I., Hutley, L., Moore, C., Eldering, A., 2017. Effect of environmental conditions on the relationship between solar-induced fluorescence and gross primary productivity at an OzFlux grassland site. J. Geophys. Res. Biogeosciences 122, 716–733. https://doi.org/10.1002/2016JG003580

Verrelst, J., Rivera, J.P., van der Tol, C., Magnani, F., Mohammed, G., Moreno, J., 2015. Global sensitivity analysis of the SCOPE model: What drives simulated canopy-leaving sun-induced fluorescence? Remote Sens. Environ. 166, 8–21. https://doi.org/10.1016/j.rse.2015.06.002

Verrelst, J., van der Tol, C., Magnani, F., Sabater, N., Rivera, J.P., Mohammed, G., Moreno, J., 2016. Evaluating the predictive power of sun-induced chlorophyll fluorescence to estimate net photosynthesis of vegetation canopies: A SCOPE modeling study. Remote Sens. Environ. 176, 139–151. https://doi.org/10.1016/j.rse.2016.01.018

Walker, A.P., Beckerman, A.P., Gu, L., Kattge, J., Cernusak, L.A., Domingues, T.F., Scales, J.C., Wohlfahrt, G., Wullschleger, S.D., Woodward, F.I., 2014. The relationship of leaf photosynthetic traits - Vcmax and Jmax - to leaf nitrogen, leaf phosphorus, and specific leaf area: A meta-analysis and modeling study. Ecol. Evol. 4, 3218–3235. https://doi.org/10.1002/ece3.1173

Weis, E., Berry, J.A., 1987. Quantum efficiency of Photosystem II in relation to ’energy’-dependent quenching of chlorophyll fluorescence. BBA - Bioenerg. 894, 198–208. https://doi.org/10.1016/0005-2728(87)90190-3

Wullschleger, S.D., 1993. Biochemical Limitations to Carbon Assimilation in C 3 Plants—A Retrospective Analysis of the A/C i Curves from 109 Species. J. Exp. Bot. 44, 907–920. https://doi.org/10.1093/jxb/44.5.907

Yang, X., Tang, J., Mustard, J.F., Lee, J., Rossini, M., 2015. Geophysical Research Letter Supplementary information for “Solar-induced chlorophyll fluorescence correlates with canopy photosynthesis on diurnal and seasonal scales in a temperate deciduous forest” 2977–2987. https://doi.org/10.1002/2015GL063201.Received

Yebra, M., Chuvieco, E., 2009. Linking ecological information and radiative transfer models to estimate fuel moisture content in the Mediterranean region of Spain: Solving the ill-posed inverse problem. Remote Sens. Environ. 113, 2403–2411. https://doi.org/10.1016/j.rse.2009.07.001

Zarco-Tejada, P.J., González-Dugo, V., Berni, J.A.J., 2012. Fluorescence, temperature and narrow-band indices acquired from a UAV platform for water stress detection

using a micro-hyperspectral imager and a thermal camera. Remote Sens. Environ. 117, 322–337. https://doi.org/10.1016/j.rse.2011.10.007

Zarco-Tejada, P.J., González-Dugo, M. V., Fereres, E., 2016. Seasonal stability of chlorophyll fluorescence quantified from airborne hyperspectral imagery as an indicator of net photosynthesis in the context of precision agriculture. Remote Sens. Environ. 179, 89–103. https://doi.org/10.1016/j.rse.2016.03.024

Zhang, Y., Guanter, L., Berry, J.A., Joiner, J., van der Tol, C., Huete, A., Gitelson, A., Voigt, M., Köhler, P., 2014. Estimation of vegetation photosynthetic capacity from space-based measurements of chlorophyll fluorescence for terrestrial biosphere models. Glob. Chang. Biol. 20, 3727–3742. https://doi.org/10.1111/gcb.12664

Zhang, Y., Guanter, L., Joiner, J., Song, L., Guan, K., 2018. Spatially-explicit monitoring of crop photosynthetic capacity through the use of space-based chlorophyll fluorescence data. Remote Sens. Environ. 210, 362–374. https://doi.org/10.1016/j.rse.2018.03.031

Zheng, T., Chen, J., He, L., Arain, M.A., Thomas, S.C., Murphy, J.G., Geddes, J.A., Black, T.A., 2017. Inverting the maximum carboxylation rate (Vcmax) from the sunlit leaf photosynthesis rate derived from measured light response curves at tower flux sites. Agric. For. Meteorol. 236, 48–66. https://doi.org/10.1016/j.agrformet.2017.01.008

Zweifel, R., Bohm, J.P., Hasler, R., 2002. Midday stomatal closure in Norway spruce--reactions in the upper and lower crown. Tree Physiol. 22, 1125–1136. https://doi.org/10.1093/treephys/22.15-16.1125

Chapter 6: Conclusions

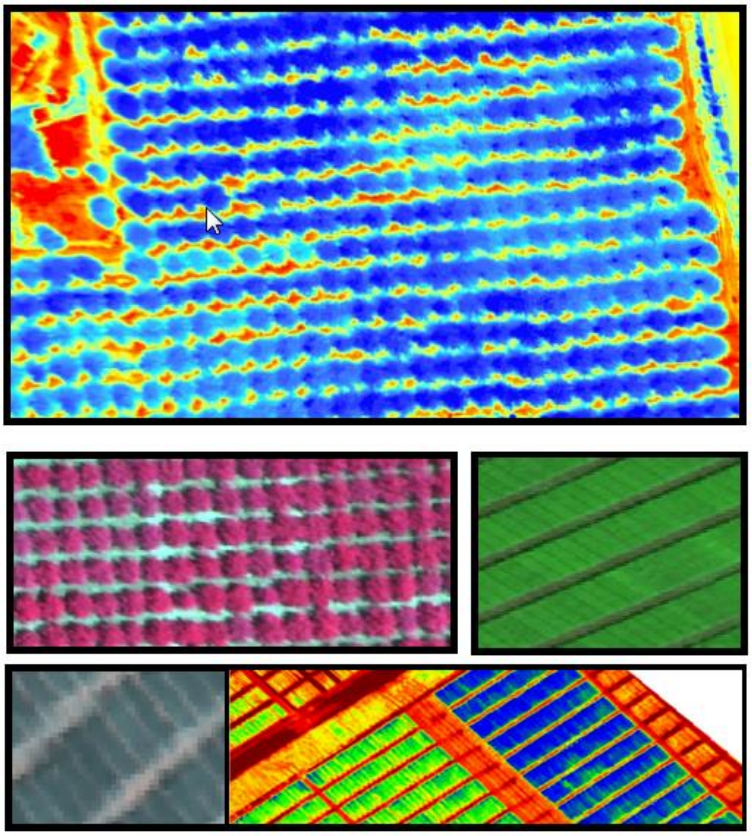

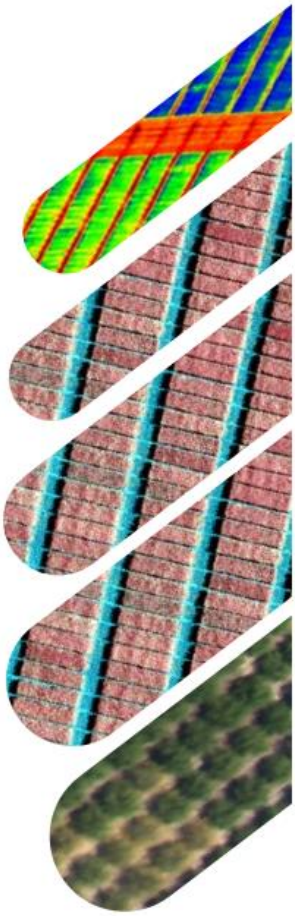

Chapter 6: Conclusions

6. 1 Conclusions of the main chapters

From the research article: Camino C., Zarco-Tejada P. J. & González Dugo V. *Effects of Heterogeneity within Tree Crowns on Airborne-Quantified SIF and the CWSI as Indicators of Water Stress in the Context of Precision Agriculture*. Remote Sensing, 2018, 10(4), 604; https://doi.org/10.3390/rs10040604.

I. Airborne-derived SIF retrievals and thermal-based CWSI extracted from tree-crowns were highly degraded due to the effects of structure, leaf density, sunlit/shaded areas and background soil effects, masking changes in fluorescence and CWSI amplitude caused by the physiological condition.

II. The crown segmentation methods applied to target pure crown-level vegetation pixels improved the relations between SIF and field-measured leaf assimilation rate.

III. The normalization scheme for SIF using the maximum fluorescence signal emitted by control well-watered almond trees confirmed the feasibility of using normalized SIF as an indicator of photosynthetic activity throughout the season.

IV. CWSI retrievals were highly modulated by the spatial heterogeneity of canopy temperature within tree-crowns, affecting the relationship with stomatal conductance measured at leaf level. In particular, pixels more affected by soil background shifted the CWSI values beyond the maximum theoretical CWSI limit.

V. The automatic object-based tree crown detection algorithm, based on quartile breaks, minimized the impact of canopy structure and reduced the soil background effects, enabling accurate estimations of plant photosynthetic traits.

From the research article: Camino C., González-Dugo V., Hernández P., Sillero J.C. & Zarco-Tejada P. J. *Improved nitrogen retrievals with airborne-derived fluorescence and plant traits quantified from VNIR-SWIR hyperspectral imagery in the context of precision agriculture*. International Journal of Applied Earth Observation and Geoinformation, Volume 70, August 2018, Pages 105-117. https://doi.org/10.1016/j.jag.2018.04.013.

I. The airborne-quantified solar induced chlorophyll fluorescence is a critical predictor for the estimation of N concentration under irrigated and rainfed Mediterranean conditions.

II. The chlorophyll a+b content and leaf parameters dry matter and equivalent water thickness retrieved from a radiative transfer model at canopy scale are needed for better N concentration estimation.

III. Regression models with the airborne-quantified SIF and plant physiological traits improved the N quantification under both rainfed (water-stress) and irrigated conditions.

IV. Multiple regression models for estimating N concentration yielded better results than standard empirical methods based on simple linear relationships with narrow-band hyperspectral indices.

V. The nitrogen indices retrieved from the SWIR domain significantly improved the estimation of nitrogen concentration, as compared to pigment and structural indices based on visible and NIR spectral regions. In particular, SWIR-based NIs centered at 1510 nm yield more reliable agreements with N concentration.

From the research article: Camino C., González Dugo V., Hernández P. & Zarco-Tejada P. J. *Radiative transfer Vcmax estimation from hyperspectral imagery and SIF retrievals to assess photosynthetic performance in rainfed and irrigated plant phenotyping trials*. Submitted to Remote Sensing of Environment, 2018.

I. This work showed a feasible remote sensing methodology for the estimation of Vcmax from airborne-based SIF retrievals combined with SCOPE simulations using high-resolution hyperspectral imagery at canopy scales.

II. The maximum rate of carboxylation retrievals derived from SCOPE model inversion enabled to successfully capture the photosynthetic capacity in irrigated and rainfed conditions through the use of high-resolution hyperspectral imagery.

III. The estimation of Vcmax outperformed standard remote sensing indices (eg. NDVI) and C_{ab} for the quantification of crop photosynthesis under irrigated conditions.

IV. Standard remote sensing indicators (NDVI, C_{ab}, $PSSR_b$) yielded non-significant correlations with assimilation in irrigated plots while the CWSI yielded non-significant correlation in rainfed plots. The superior sensitivity of remotely-sensed Vcmax under irrigated conditions was likely due to the fact that the structural effects typical of high canopy densities did not affect Vcmax as much as standard remote sensing indicators.

V. The estimation of Vcmax as a function of SIF retrievals enabled the calculation of the spatial distribution of Vcmax and the net assimilation in high-throughput plant phenotyping and for precision agriculture applications.

6. 2 General conclusions

The main goal of this research was to assess the contribution of the airborne-retrieved solar-induced SIF and thermal-based indicators to the retrieval of nitrogen and plant photosynthetic traits under contrasted water stress regimes in different crops. This PhD thesis demonstrates that the use of radiative transfer models using hyperspectral imagery in the visible, near-infrared and short-wave infrared spectral region is a reliable method to estimate vegetation plant traits and to monitor nutritional status and photosynthesis activity. In particular, RTMs have been shown superior to empirical models based on single narrow-band hyperspectral indices.

This PhD thesis shows a successful approach for the retrieval of plant photosynthetic traits through chlorophyll fluorescence emission coupled with terrestrial biosphere models. In particular, this thesis investigates an approach via SCOPE model that coupled RTMs, photosynthesis biochemical models and balance energy models to investigate the effects of canopy structure and plant traits using chlorophyll fluorescence estimation at the top of the canopy and high-resolution airborne hyperspectral imagery.

The work conducted during this PhD thesis demonstrate that chlorophyll fluorescence is an important factor for improving the quantification of nitrogen concentration and for estimating the maximum rate of carboxylation (Vcmax) using passive remote sensing techniques in plant phenotyping experiments. These results highlight the critical importance of the remotely-sensed SIF as an indicator of Vcmax using hyperspectral imagery and physical-based models.

In this research also we also confirm that CWSI is a reliable tool for monitoring water stress using high-resolution thermal imagery under different water regimes. This PhD thesis highlights that the thermal imaging for detecting water stress offers the potential to retrieve thermal-based indicators from airborne imaging to map spatial variability of water status. In particular, our results provide a detailed quantification of

the spatial variability of the tree temperature within tree crowns, providing an automatic procedure for improving the accuracy for monitoring water status in orchard tree crops.

The results presented in this PhD thesis, also highlight that the large effects driven by the canopy structure and soil background should be taken in account when estimating chlorophyll fluorescence and the thermal-based CWSI indicator from high-resolution hyperspectral and thermal airborne imagery. This PhD thesis demonstrates the large impact played by the canopy and tree crown structure, yielding more robust relationships with stomatal conductance and assimilation rate when pure vegetation pixels were targeted. The visible, near infrared and short-wave infrared regions were studied for assessing N concentration in several water regimes. The work conducted in this research demonstrates the narrow-band indices based on NIR/SWIR regions improved the quantification of nitrogen concentration, compared to narrow-band indices calculated from the visible and near-infrared region of the spectrum.

6. 3 Further research

The research conducted during this thesis leads to establishing further research in the fields of high-throughput plant phenotyping and in precision agriculture. Future research topics include the following:

- Future research is required on developing advanced methods for better quantification of the partitioning between excitation / fluorescence energy and thermal dissipation as part of photosynthesis processes in the context of nitrogen quantification.
- Continue the research on thermal infrared and fluorescence imaging in the context of crop water stress to understand the links between plant photosynthesis traits, nitrogen status and chlorophyll fluorescence emission under water stress conditions
- Assess the robustness and the transferability of the methodologies developed in this PhD thesis for the quantification of biochemical parameters and plant photosynthesis traits to other crops and environmental conditions.
- Improve scaling up methods through radiative transfer modelling for the quantification of N and Vcmax using airborne-based SIF retrievals in crops with complex structural characteristics.

- Develop new remote sensing methods through high-resolution hyperspectral imagery for detecting new spectral bands sensitive to nitrogen content and other macronutrients using near-infrared and short-wave infra-red regions, including artificial intelligence methods such as machine learning algorithms.

APPENDIX: Scientific production

Appendix: Scientific production

Other scientific contributions derived from this Doctoral Thesis are listed below

Publications in international journals

P. J. Zarco-Tejada, **C. Camino**, P. S. A. Beck, R. Calderon, A. Hornero, R. Hernández-Clemente, T. Kattenborn, M. Montes-Borrego, L. Susca, M. Morelli, V. González-Dugo, P. R. J. North, B. B. Landa, D. Boscia, M. Saponari and J. A. Navas-Cortes. Previsual symptoms of Xylella fastidiosa infection revealed in spectral plant-trait alterations. Nature Plants, volume 4, pages 432–439 (2018). https://doi.org/10.1038/s41477-018-0189-7.

S. Gálvez, R. Mérida-García, **C. Camino**, P. Borrill, M. Abrouk, R. H. Ramírez-González, S. Biyiklioglu, F. Amil-Ruiz, The IWGSC, G. Dorado, H. Budak,V. González-Dugo, P. J. Zarco-Tejada, R. Appels, Cristobal Uauy, Pilar Hernandez. *Hotspots in the genomic architecture of field drought responses in wheat as breeding targets.* Funct. Integr. Genomics. https://doi.org/10.1007/s10142-018-0639-3

Publications in national journals

R. Calderon, **C. Camino**, P.S.A. Beck, A. Hornero, R. Hernández-Clemente, T. Kattenborn, M. Montes-Borrego, L. Susca, M. Morelli, V. Gonzalez-Dugo, P.R.J. North, B.B. Landa, D. Boscia, M. Saponari, P.J. Zarco-Tejada and J.A. Navas-Cortes. Detección pre-visual de la infección por Xylella fastidiosa en olivo a partir de imágenes hiperespectrales y térmicas. Phytoma, Diciembre 2018

Oral communications at conferences

P. S. A. Beck, **C. Camino**, R. Calderón Madrid, A. Hornero Luque, R. Hernández-Clemente, T. Kattenborn, M. Montes Borrego, D. Susca, M. Morelli, V. González-Dugo, P. North, C. J. Carstens, B. B. Landa, D. Boscia, M. Saponari, G. Strona, J. A. Navas-Cortes, P. J. Zarco-Tejada Anticipating and understanding new Xylella fastidiosa epidemics across European landscapes; insights from remote sensing and network analysis. ICPP 2018. Abstracts of Concurrent Session. October 2018, Volume 108, Number 10S Pages S1.240-S1.319. https://doi.org/10.1094/PHYTO-108-10-S1.240

C. Camino, P. J. Zarco-Tejada and V. González-Dugo. *Assessment of the spatial variability of CWSI within almond tree- crowns and its effects on the relationship with stomatal conductance*. Geoscience and Remote Sensing (IGARSS), IEEE International Symposium, 22-25 July, 2018, Valencia Spain.

C. Camino, V. González-Dugo R. Mérida-García, P. Hernández and P. J. Zarco-Tejada. Retrieval of wheat nitrogen content using airborne hyperspectral VNIR-SWIR imagery through radiative transfer models and chlorophyll fluorescence quantification. 10th EARSeL SIG Imaging Spectroscopy Workshop, 19-21 April 2017, Zurich. Switzerland.

Poster communications at conferences and courses

C. Camino, V. González-Dugo, M. López-López, P. J. Zarco-Tejada. Crown segmentation effects on the relation between field-measured assimilation and chlorophyll fluorescence quantified from high-spatial resolution hyperspectral imagery. 5th International Symposium Recent Advances in Quantitative Remote Sensing, 18-22 September 2017, Torrent (Valencia), Spain.